



Trajectory-aided GNSS land navigation : application to train positioning

Guoliang Zhu

► To cite this version:

Guoliang Zhu. Trajectory-aided GNSS land navigation : application to train positioning. Operations Research [math.OC]. Université de Technologie de Troyes, 2014. English. NNT: 2014TROY0007 . tel-03356028v2

HAL Id: tel-03356028

<https://theses.hal.science/tel-03356028v2>

Submitted on 27 Sep 2021

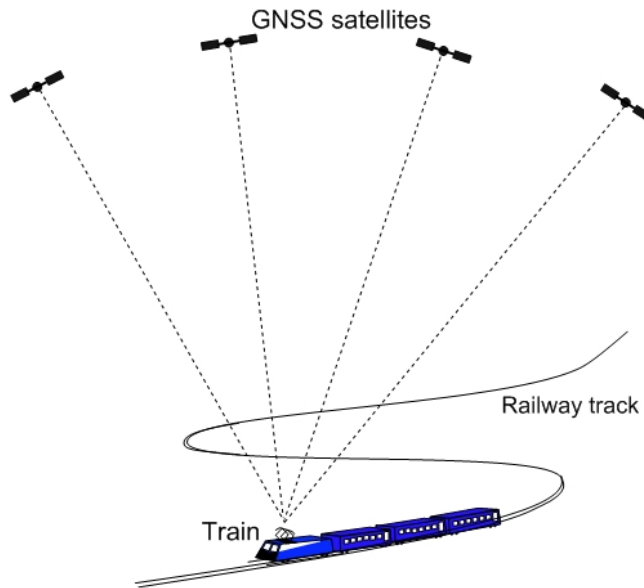
HAL is a multi-disciplinary open access archive for the deposit and dissemination of scientific research documents, whether they are published or not. The documents may come from teaching and research institutions in France or abroad, or from public or private research centers.

L'archive ouverte pluridisciplinaire **HAL**, est destinée au dépôt et à la diffusion de documents scientifiques de niveau recherche, publiés ou non, émanant des établissements d'enseignement et de recherche français ou étrangers, des laboratoires publics ou privés.

Thèse
de doctorat
de l'UTT

Guoliang ZHU

Trajectory-aided GNSS Land Navigation: Application to Train Positioning



Spécialité :
Optimisation et Sûreté des Systèmes

2014TROY0007

Année 2014

THESE

pour l'obtention du grade de

DOCTEUR de l'UNIVERSITE DE TECHNOLOGIE DE TROYES

Spécialité : OPTIMISATION ET SURETE DES SYSTEMES

présentée et soutenue par

Guoliang ZHU

le 27 février 2014

Trajectory-aided GNSS Land Navigation: Application to Train Positioning

JURY

M. R LENGELLÉ	PROFESSEUR DES UNIVERSITES	Président
M. P. BONNIFAIT	PROFESSEUR DES UNIVERSITES	Rapporteur
M. L. FILLATRE	PROFESSEUR DES UNIVERSITES	Directeur de thèse
Mme M. MALVEZZI	RICERCATORE CONFERMATO	Examinateur
M. I. NIKIFOROV	PROFESSEUR DES UNIVERSITES	Directeur de thèse
M. J. RODRIGUEZ	DIRECTEUR DE RECHERCHE IFFSTAR-ESTAS	Rapporteur

Personnalité invitée

M. P. DAVID	CHEF DE PROJET SNCF
-------------	---------------------

Remerciements

I wish to express my gratitude to all those who helped and encouraged me during my doctoral studies.

I would like firstly to express my deep gratitude to my supervisors, Professor Lionel FILLATRE and Professor Igor NIKIFOROV who accompanied me throughout the three and a half years. I can not thank them enough for their availability, their unwavering support, their scientific enthusiasm and encouragement that helped me to complete my work, especially in the most difficult moments.

I express my gratitude to the members of the jury who participate in the discussion of this thesis : Professor Philippe BONNIFAIT at the UTC, Professor Joaquin RODRIGUEZ at the IFSTTAR as a reviewer, Professor Regis LENGELLE at the UTT, Assistant Professor Monica MALVEZZI at the University of Siena as an examiner and Mr. Philippe DAVID at the SNCF as a member of the jury.

All my work was done within the LM2S laboratory at the UTT. I would also like to thank all team members for their hospitality, their sympathy and their constructive ideas. A big thank you to the secretaries of the pôle ROSAS : Ladies Marie-José ROUSSELET, Veronique BANSE and Bernadette ANDRE ; the secretaries of the doctoral school : Ladies Isabelle LECLERCQ, Pascale DENIS and Thérèse KAZARIAN.

I want to thank my friends with whom I shared pleasant moments during these years in Troyes : Hui SHANG, Fei ZHU, Zhenmin YUE, Kun JIA, Jian ZHANG, Tian WANG and Lei QIN. I would like to thank my parents who have always supported me, gave me confidence and encouraged me and without whom nothing would have been possible.

Finally, I would like to thank the China Scholarship Council and the University of Technology of Troyes for the financial support for three and a half years.

Résumé

Over these years, GNSS technology has attracted many attentions around world and it has been widely applied in navigation for aviation, ground vehicle and marine application. On the other hand, advanced railway operating systems have been widely used to guarantee the safety and efficiency of the railway network. The efficiency of these systems is based on the availability of reliable train positioning. Hence, applying GNSS technology in the train positioning is a very promising research area, since it has such important benefits as lower initial costs and lower maintenance. In this thesis, several algorithmic solutions are proposed for train positioning by using GNSS signals and the railway centerline stored in the onboard computer database. At first, the train travelled distance and speed are estimated by using GNSS signals and an "ideal" railway centerline. The "ideal" model of railway centerline is composed of straight line segments, transition curves and arcs of circles, defined by parametric equations. The impact of the railroad curvature on the train speed and distance estimation is studied. Secondly, the train travelled distance and speed are estimated by using GNSS signals and a "non-ideal" railway centerline. The "non-ideal" model of railway centerline is defined by a polygonal line with some level of uncertainty. The impact of the track geometric model imprecision on the train speed and distance estimation is studied. Finally, the train travelled distance and speed are estimated by integrating the GNSS measurements with a track database. The impact of the GNSS measurements and the track database errors on the train speed and distance estimation is studied.

Mots-clés : Train positioning, GNSS, Parameter estimation, Least square method, Linear regression model, Non-linear regression model, Integrated system, Data fusion

Table des matières

I General Introduction	1
I.1 Train Positioning	1
I.1.1 Significance of Train Positioning	1
I.1.2 Key Issues in Train Positioning	3
I.1.3 Train GNSS Positioning	4
I.1.3.1 Overview of GNSS	4
I.1.3.2 Coordinate System Definitions	6
I.1.3.3 Coordinate Transformations	8
I.1.3.4 GNSS Classic (3D) Navigation	9
I.1.3.5 GNSS Train (1D) Navigation	13
I.1.4 Previous Research and Literature Review	14
I.2 Problems Studied in This Thesis	20
I.3 Estimation Theory (parametric approach)	21
I.4 Contributions	29
I.5 Thesis Structure	31
II Distance and Speed Estimation Based on GNSS and an "Ideal" Train Track	33
II.1 Introduction	33

II.2 Track Geometry Design	33
II.3 Description of "Ideal" Train Track Models	37
II.4 Speed Estimation for a Constant Speed Case	41
II.4.1 Exact Pseudo-range Measurement Model and Estimation	41
II.4.2 Impact of The Curve Radius on The Estimation Error	42
II.4.3 Numerical Simulations	44
II.5 Distance and Speed Estimation for a Variable Speed Case	46
II.5.1 Exact Pseudo-range Measurement Model and Estimation	47
II.5.2 Impact of The Curve Radius on The Estimation Error	49
II.5.3 Numerical Simulations	50
II.6 Conclusions	54
III Distance and Speed Estimation Based on GNSS and a "Non-ideal" Train Track	55
III.1 Introduction	55
III.2 Description of "Non-ideal" Train Track Models	55
III.3 Speed Estimation for a Constant Speed Case	56
III.3.1 Imprecise Pseudo-range Measurement Model and Estimation . .	57
III.3.2 Impact of The Track Geometry Imprecision on The Estimation Error	58
III.3.3 Numerical Simulations	60
III.4 Distance and Speed Estimation for a Variable Speed Case	62
III.4.1 Imprecise Pseudo-range Measurement Model and Estimation . .	63

III.4.2 Impact of The Track Geometry Imprecision on The Estimation Error	65
III.4.3 Numerical Simulations	69
III.5 Conclusions	71
 IV Distance and Speed Estimation Based on Integrating GNSS with The Track Database	 73
IV.1 Introduction	73
IV.2 Description of Track Database Models	73
IV.2.1 Continuous Track Database Models	74
IV.2.2 Discrete Track Database Models	75
IV.3 Speed Estimation Based on a Model of Integrated System for a Constant Speed Case	78
IV.3.1 Model of GNSS/Track Database Integrated System	78
IV.3.2 Numerical Simulations	80
IV.4 Speed and Distance Estimation Based on a Model of Integrated System for a Variable Speed Case	82
IV.4.1 Model of GNSS/Track Database Integrated System	83
IV.4.2 Numerical Simulations	86
IV.5 Conclusions	89
 V Conclusions and Future Researches	 91
V.1 Conclusions	91
V.2 Future Researches	93
 Annexe A Basic Notions in Estimation Theory	 95

Annexe B Mathematical Derivations	99
Annexe C Expressions of Jacobian Matrix	111
Annexe D Integrated System Models	113
Annexe E Résumé de Thèse en Français	123
E.1 Introduction	123
E.1.1 Importance du positionnement du train	123
E.1.2 Questions clés dans le positionnement du train	124
E.1.3 Problèmes étudiés dans cette thèse	125
E.1.4 Contributions	125
E.2 Estimation de la distance, vitesse du train à base de GNSS et une voie ferroviaire "idéale"	127
E.2.1 Description du modèle "idéal" de voie ferroviaire	127
E.2.2 Estimation de la vitesse pour le cas d'une vitesse constante	128
E.2.2.1 Modèle exact de mesure de pseudo-distance et l'estimation	129
E.2.2.2 Impact du rayon de courbure de la voie ferroviaire sur l'erreur d'estimation	129
E.2.2.3 Simulations numériques	130
E.2.3 Estimation de la distance, vitesse pour le cas d'une vitesse variable	131
E.2.3.1 Modèle exact de mesure de pseudo-distance et l'estimation	132
E.2.3.2 Impact du rayon de courbure de la voie ferroviaire sur l'erreur d'estimation	133

E.2.3.3	Simulations numériques	133
E.2.4	Conclusions	134
E.3	Estimation de la distance, vitesse du train à base de GNSS et une voie ferroviaire "non-idéale"	135
E.3.1	Description du modèle "non-idéal" de voie ferroviaire	135
E.3.2	Estimation de la vitesse pour le cas d'une vitesse constante	136
E.3.2.1	Modèle imprécis de mesure de pseudo-distance et l'estimation.	137
E.3.2.2	Impact de l'incertitude des données sur l'erreur d'estimation	137
E.3.2.3	Simulations numériques	138
E.3.3	Estimation de la distance, vitesse pour le cas d'une vitesse variable	139
E.3.3.1	Modèle imprécis de mesure de pseudo-distance et l'estimation.	139
E.3.3.2	Impact de l'incertitude des données sur l'erreur d'estimation	140
E.3.3.3	Simulations numériques	140
E.3.4	Conclusions	141
E.4	Estimation de la distance, vitesse du train à base de l'intégration GNSS avec la base de données	142
E.4.1	Description de la base de données d'une voie ferroviaire	142
E.4.2	Estimation de la vitesse à base du système intégré pour le cas d'une vitesse constante	143
E.4.2.1	Modèle du système intégré	143
E.4.2.2	Simulations numériques	144

E.4.3 Estimation de la distance, vitesse à base du système intégré pour le cas d'une vitesse variable	146
E.4.3.1 Modèle du système intégré	146
E.4.3.2 Simulations numériques	147
E.4.4 Conclusions	148
E.5 Conclusions et recherches futures	149
E.5.1 Conclusions	149
E.5.2 Recherches futures	150
Bibliographie	153

Nomenclature

<i>Notation</i>	<i>Meaning</i>
ATC	Automatic Train Control.
ATP	Automatic Train Protection.
CDF	Cumulative Distribution Function.
DLR	German Aerospace Center.
ESA	European Space Agency.
EU	European Union.
GEO	Geostationary (satellite).
GLONASS	Global'naya Navigatsionnaya Sputnikovaya Sistema (Global Navigation Satellite System).
GNSS	Global Navigation Satellite System.
GPS	Global Positioning System.
INS	Inertial Navigation System.
LS	Least Square.
MEO	Medium Earth Orbit (satellite).
MLE	Maximum Likelihood Estimator.
MSE	Mean Squared Error.
NAVSTAR	Navigation System with Timing and Ranging.
PDF	Probability Density Function.
PMF	Probability Mass Function.
US	United States.

Basic symbols

(a, b)	Open interval.
I_m	Identity matrix of order m .
$[a, b]$	Closed interval.
\mathbb{R}	Set of real numbers.
\mathbb{R}^n	The n-dimensional space of Euclidean geometry.
$\det A$	Determinant of matrix A .
$\ X\ _2 = \sqrt{\sum_{i=1}^n x_i^2}$	Euclidean norm of $X \in \mathbb{R}^n$.
\mathbb{N}	Set of natural numbers.
$\text{tr } A$	Trace of matrix A .
\mathbb{I}_x	Indicator function of event x .
$\mathbf{1}_n$	A vector of dimension n whose each element is one.

Symbols for probability

$(\xi_n)_{n \geq 1}$	A sequence of random variables.
$F(x)$	Cumulative distribution function.
cov	Covariance.
\mathbb{E}	Expectation.
\mathcal{F}	Fisher information.
\mathcal{L}	Probability law.
\mathcal{N}	Normal (or Gaussian) law.
$\mathbb{P}(B)$	Probability of the event B .
var	Variance.
$g(x), f(x)$	Probability density, pdf.
$g_\theta(x), f_\theta(x)$	Parameterized probability density, pdf.
$\mathcal{P} = \{P_\theta, \theta \in \Theta\}$	Parametric family of probability distributions.

Symbols for train GNSS positioning

R	Railway curve radius.
T	Time period.
Δt	GNSS sampling interval.
ℓ	Curvilinear abscissa.
i	Current number of satellite, $1 \leq i \leq n$.
k	Current time instant - discrete time.
t	Current time instant - continuous time.

Liste des tableaux

I.1 Example with four satellites.	12
II.1 Segments of the tested simulation scenario.	44
IV.1 Segments of the tested simulation scenario.	81
E.1 Segments de la trajectoire testée.	130

Liste des figures

I.1	Architecture of a typical train positioning system.	2
I.2	GPS constellation.	5
I.3	The relationship between geodetic and ECEF coordinate system.	7
I.4	ENU coordinate system.	8
I.5	Train 1D GNSS positioning.	10
I.6	Methods of train positioning.	15
I.7	Illustration of the parameter estimation.	22
II.1	Track gauge.	34
II.2	Cant h_t and cant angle φ_t	34
II.3	A transition curve connecting between the straight line and circular curve.	35
II.4	The definition of circular curve radius R	36
II.5	Track gradient.	36
II.6	A vertical curve between two adjacent gradients.	37
II.7	Train track composed of three segments on the local tangent plane.	38
II.8	Determination of transition curve length.	39
II.9	Example of transition curve.	39
II.10	The centerline curvature of the tested simulation scenario.	44
II.11	The simulated train trajectory on the local horizontal plane.	44

II.12	The estimated speed mean error for $R = 100$ m.	45
II.13	The estimated speed second order moment for $R = 100$ m.	45
II.14	The estimated speed mean error for $R = 1000$ m.	45
II.15	The estimated speed second order moment for $R = 1000$ m.	45
II.16	Typical train motion diagram.	46
II.17	The centerline curvature of the tested simulation scenario.	50
II.18	The simulated train trajectory on the local horizontal plane.	50
II.19	The mean error of the estimated distance, speed and acceleration for $R = 100$ m and $q = 20$	51
II.20	The second order moment of the estimated distance, speed and acceleration for $R = 100$ m and $q = 20$	52
II.21	The mean error of the estimated distance, speed and acceleration for $R = 1000$ m and $q = 20$	52
II.22	The second order moment of the estimated distance, speed and acceleration for $R = 1000$ m and $q = 20$	53
II.23	The second order moment of the estimated distance, speed and acceleration for $R = 100$ m and $q = 5$	53
III.1	Train track model.	56
III.2	The estimated speed mean error for $\delta_j = 0$	61
III.3	The estimated speed second order moment for $\delta_j = 0$	61
III.4	The estimated speed mean error for $\delta_j \in [-0.01, 0.01]^2$	61
III.5	The estimated speed second order moment for $\delta_j \in [-0.01, 0.01]^2$	61
III.6	The estimated speed mean error for $\delta_j \in [-0.05, 0.05]^2$	61
III.7	The estimated speed second order moment for $\delta_j \in [-0.05, 0.05]^2$	61

III.8	Typical train motion diagram.	62
III.9	The mean error of the estimated distance, speed and acceleration for the centerline uncertainty of $\xi_j = 0$ and $q = 20$	69
III.10	The second order moment of the estimated distance, speed and acceleration for the centerline uncertainty of $\xi_j = 0$ and $q = 20$	70
III.11	The mean error of the estimated distance, speed and acceleration for the centerline uncertainty of $\xi_j \in [-2, 2]^2$ and $q = 20$	70
III.12	The second order moment of the estimated distance, speed and acceleration for the centerline uncertainty of $\xi_j \in [-2, 2]^2$ and $q = 20$	71
IV.1	Train track composed of three segments on the local tangent plane. . .	74
IV.2	The measurement errors in the track database.	76
IV.3	The centerline curvature of the tested simulation scenario.	81
IV.4	The simulated train trajectory on the local horizontal plane.	81
IV.5	The mean error of the estimated speed for $R = 1000$ m and $\sigma_{\text{PD}} = \sigma_{\text{DB}} = 2$ m.	82
IV.6	The second order moment of the estimated speed for $R = 1000$ m and $\sigma_{\text{PD}} = \sigma_{\text{DB}} = 2$ m.	82
IV.7	The mean error of the estimated speed for $R = 100$ m and $\sigma_{\text{PD}} = \sigma_{\text{DB}} = 2$ m.	82
IV.8	The second order moment of the estimated speed for $R = 100$ m and $\sigma_{\text{PD}} = \sigma_{\text{DB}} = 2$ m.	82
IV.9	Typical train motion diagram.	83
IV.10	The centerline curvature of the tested simulation scenario.	87
IV.11	The simulated train trajectory on the local horizontal plane.	87

IV.12 The mean error of the estimated distance, speed and acceleration for $R = 1000$ m, $\sigma_{\text{PD}} = \sigma_{\text{DB}} = 2$ m and $q = 20$	87
IV.13 The second order moment of the estimated distance, speed and acceleration for $R = 1000$ m, $\sigma_{\text{PD}} = \sigma_{\text{DB}} = 2$ m and $q = 20$	88
IV.14 The mean error of the estimated distance, speed and acceleration for $R = 100$ m, $\sigma_{\text{PD}} = \sigma_{\text{DB}} = 2$ m and $q = 20$	88
IV.15 The second order moment of the estimated distance, speed and acceleration for $R = 100$ m, $\sigma_{\text{PD}} = \sigma_{\text{DB}} = 2$ m and $q = 20$	89
 E.1 La voie ferroviaire composée de trois segments au plan tangent local. . .	128
E.2 Courbure calculée pour la trajectoire.	130
E.3 La trajectoire testée au plan tangent local.	130
E.4 L'erreur moyenne de la vitesse estimée pour $R = 100$ m.	131
E.5 Le moment d'ordre deux de la vitesse estimée pour $R = 100$ m.	131
E.6 Schéma de mouvement de train.	131
E.7 Courbure calculée pour la trajectoire.	134
E.8 La trajectoire testée au plan tangent local.	134
E.9 L'erreur moyenne de la distance, de la vitesse et de l'accélération pour $R = 100$ m et $q = 20$	134
E.10 Le moment d'ordre deux de la distance, de la vitesse et de l'accélération pour $R = 100$ m et $q = 20$	134
E.11 Le modèle "non-idéal" de voie ferroviaire.	136
E.12 L'erreur moyenne de la vitesse estimée pour $\delta_j \in [-0.05, 0.05]^2$	138
E.13 Le moment d'ordre deux de la vitesse estimée pour $\delta_j \in [-0.05, 0.05]^2$. .	138

E.14 L'erreur moyenne de la distance, de la vitesse et de l'accélération pour l'incertitude de $\xi_j \in [-2, 2]^2$ et $q = 20$	141
E.15 Le moment d'ordre deux de la distance, de la vitesse et de l'accélération pour l'incertitude de $\xi_j \in [-2, 2]^2$ et $q = 20$	141
E.16 Les erreurs de mesure dans la base de données.	143
E.17 Courbure calculée pour la trajectoire.	145
E.18 La trajectoire testée au plan tangent local.	145
E.19 L'erreur moyenne de la vitesse estimée pour $R = 100$ m et $\sigma_{\text{PD}} = \sigma_{\text{DB}} = 2$ m.	145
E.20 Le moment d'ordre deux de la vitesse estimée pour $R = 100$ m et $\sigma_{\text{PD}} = \sigma_{\text{DB}} = 2$ m.	145
E.21 Courbure calculée pour la trajectoire.	148
E.22 La trajectoire testée au plan tangent local.	148
E.23 L'erreur moyenne de la distance, de la vitesse et de l'accélération pour $R = 100$ m, $\sigma_{\text{PD}} = \sigma_{\text{DB}} = 2$ m et $q = 20$	148
E.24 Le moment d'ordre deux de la distance, de la vitesse et de l'accélération pour $R = 100$ m, $\sigma_{\text{PD}} = \sigma_{\text{DB}} = 2$ m et $q = 20$	148

Chapitre I

General Introduction

This thesis mainly concerns the train positioning by using GNSS signals. In this chapter we introduce the significance, key issues, literature review of train positioning, then present a brief review of estimation theory (parametric approach), in the end, provide the studied problems, contributions and structure of this thesis.

I.1 Train Positioning

I.1.1 Significance of Train Positioning

In recent years, due to large capacity, high speed, high reliability and low energy consumption, railway transportation plays a more and more important role in mass transit. To guarantee the railway network works safely and efficiently, advanced railway operating system such as Automatic Train Protection/Automatic Train Control (ATP/ATC) systems and European Rail Traffic Management System/European Train Control System (ERTMS/ETCS) has been widely used in modern railway management (Sun et al. - 2011).

The efficiency of the railway operating system is fundamental for the safety of the railway operating system, it is based on the availability of a reliable train positioning. Moreover, other safety critical functions like level crossing control and work site protection can also benefit from a reliable train positioning. A high reliability of the train position and speed estimation is of importance, since an error on the train position may lead to a potential overestimation of the distance available for braking. Hence, some parameters such as the travelled distance, position and speed of train should be estimated with a high level of accuracy (Malvezzi et al. - 2008) and integrity (Nikiforov

et Choquette - 2003). Moreover, accurate measurement of position, speed and acceleration can increase the railway line capacity (The maximum number of trains which can be moved in each direction over a specified section of track in a 24 hour period.) without adding extra infrastructure (Mirabadi et al. - 1996). So it can provides not only benefits on performance but also on cost.

Conventional positioning methods in railway systems are based on trackside located technical equipment, i.e. axle counters, track circuits, etc (Becker et al. - 2006b,c). The positioning information of an axle counter is available at a special point when the train is passing the counter. These equipments can provide train positioning information with an accuracy of several hundred meters, which is sufficient for existing protection systems but reduces the performance with respect to railway line capacity. These devices are installed on all ground sections, so they require enormous installations and maintenance efforts and exhibit a poor adaptability towards innovation or changing operational requirements. For modern railway management, it's necessary to develop a train positioning system, integrating innovative technologies with the main focus on GNSS positioning, since GNSS can provide the flexibility to change the requirements and has also benefits such as lower initial costs (all necessary equipments can be installed on the locomotive) and lower maintenance. Fig. I.1 shows the architecture of a

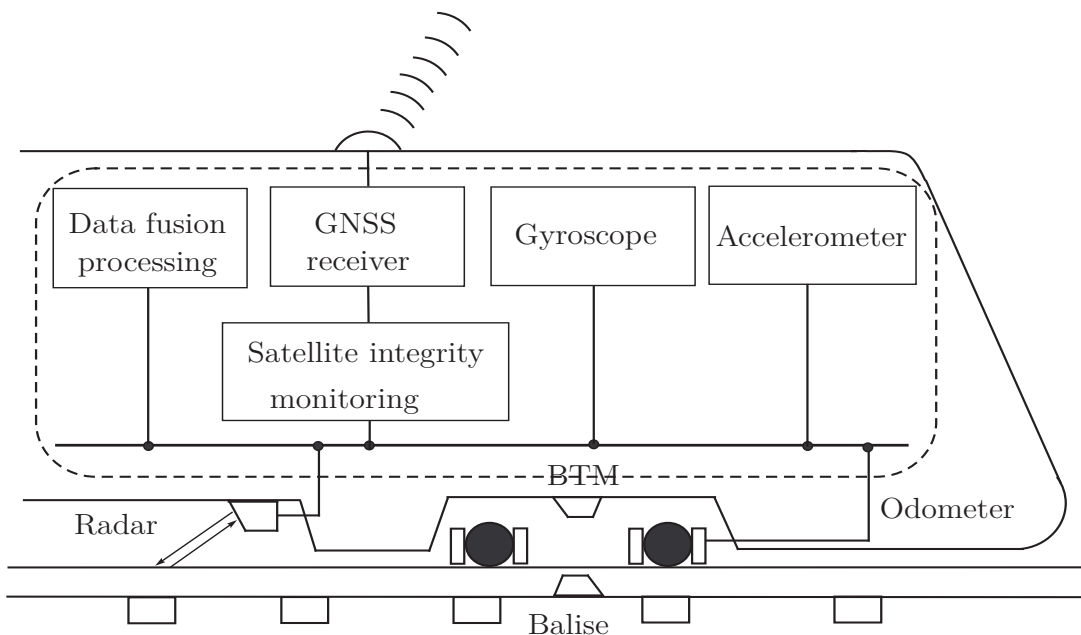


Figure I.1 – Architecture of a typical train positioning system.

typical positioning system, includes GNSS receivers, odometer, Balise Tracking Module (BTM), aided positioning sensors, e.g., gyroscope, accelerometer, Doppler radar, etc, and a core data process unit with information fusion (Liu et al. - 2012).

Given all that, driven by technical and economical reasons, a vehicle-based train positioning system to assure safe and precise operation at low costs needs to be made efforts to develop.

I.1.2 Key Issues in Train Positioning

For safety critical rail applications, special attention needs to be drawn to the accuracy, integrity, continuity and availability of the positioning information (Ochieng et al. - 1999; Hartwig et al., 2006; Group - 2003).

- Accuracy

Accuracy refers to the closeness of the estimated position and speed to the true value. Different accuracy of these estimated parameters can be reached by using different positioning systems.

- Integrity

Integrity relates to the level of trust that can be placed in the information provided by the navigation system. It includes the ability of the navigation system to provide timely and valid warnings to users when the system must not be used for positioning.

- Continuity

Continuity is the capability of a navigation system to provide required accuracy and integrity during an intended period of operation.

- Availability

Availability stands for the percentage of time when the service of the navigation system is available.

Among the above mentioned requirements, the accuracy and integrity are the two most essential aspects for rail application because the train needs high accuracy position

and the integrity directly relates to the safety.

I.1.3 Train GNSS Positioning

I.1.3.1 Overview of GNSS

A satellite navigation is a system of satellites that provide autonomous geo-spatial positioning with global coverage, which can be termed a global navigation satellite system or GNSS. GNSS implies several existing systems like Global Positioning System (GPS), GLONASS, Galileo or Beidou. In addition, these systems are supplemented by Space-based Augmentation Systems (SBAS) or Ground-based Augmentation Systems (GBAS). Examples of SBAS are the United States (US) Wide-area Augmentation System (WASS), the European Geostationary Navigation Overlay System (EGNOS), or the Japanese Multi-functional Transport Satellite (MTSAT) Space-based Augmentation System (MSAS). These systems augment the existing Medium Earth Orbit (MEO) satellite constellations with Geostationary (GEO) or geosynchronous satellites. The GNSS system is composed of three segments (Wasle - 2007) :

- Space segment

In order to provide a continuous global positioning capability, a constellation with a sufficient number of satellites must be developed for each GNSS to ensure that at least four satellites are simultaneously visible at every site.

- Control segment

The control segment (also referred to as ground segment) is responsible for steering the whole system. The task includes the deployment and maintenance of the system, tracking of the satellites for the determination and prediction of orbital and clock parameters, monitoring of auxiliary data, and upload of the data message to the satellites. It is also responsible for a possible encryption of data and the protection of services against unauthorized users.

- User segment

The user segment can be classified into user categories, receiver types and various information services. User categories are subdivided into military and civilian users as

well as authorized and unauthorized users. Civilian and unauthorized users do not have access to all signals or services of the GNSS. The receiver types depend on the market today. One characterization is based on the type of observable, i.e., the kind of pseudo-ranges. Another criterion is the ability to track one, two or even more frequencies. Several governmental and private information services have been established to provide GNSS status information and data to the users. The information contains constellation status reports, scheduled outages, and orbital data.

Until now, there have been only two fully operational systems, GPS and GLONASS. The other two systems, Galileo and Beidou, are still being deployed.

GPS

The Navigation System with Timing and Ranging (NAVSTAR) GPS was developed by the United States Department of Defense for military applications in 1973. Then the system was made available for civilian use in 1983. As of August 2008, GPS comprises a constellation of 31 MEO satellites. The present nominal constellation consists of 24 operational satellites deployed in six evenly spaced planes with an inclination of 55° and with four satellites per plane. The orbits are arranged so that at least six satellites are within line of sight from almost everywhere on Earth's surface, and at least four satellites are visible at least 15° above the horizon (Gao - 2008). Fig. I.2 shows the orbits and the constellation.



Figure I.2 – GPS constellation.

GLONASS

The GLONASS is the Russian counterpart to GPS and is operated by the Russian military. Development of GLONASS began in the Soviet Union in 1976. Beginning on 12 October 1982, numerous rocket launches added satellites to the system until the constellation was completed in 1995. By 2010, GLONASS had achieved 100% coverage of Russia's territory and in October 2011, the full orbital constellation of 24 satellites was restored, enabling full global coverage.

Galileo

Galileo is a GNSS currently being built by the European Union (EU) and European Space Agency (ESA). On 21 October 2011, the first two of four operational satellites were launched to validate the system. Full completion of the 30-satellite Galileo system (27 operational and three active spares) is expected by 2019.

BeiDou

The BeiDou Navigation Satellite System is a Chinese satellite navigation system. BeiDou-1 which is the first BeiDou system, consists of three satellites and offers limited coverage and applications, since 2000. The second generation of the system, known as BeiDou-2 or Compass, will be a global satellite navigation system consisting of 35 satellites, and is under development as of January 2013. It became operational in China in December 2011, with 10 satellites in use, and began offering services to customers in the Asia-Pacific region in December 2012. It is planned to begin serving global customers upon its completion in 2020.

I.1.3.2 Coordinate System Definitions

Three coordinate systems are important to our research. These include the geodetic coordinate system, the Earth-Centered, Earth-Fixed (ECEF) coordinate system and the local East, North, Up (ENU) coordinate system.

Geodetic Coordinate System

The geodetic coordinate system is widely used in GNSS-based navigation. It's not a usual Cartesian coordinate system but a system that characterizes a coordinate point M

near the Earth's surface in terms of longitude, latitude and height (or altitude), denoted by λ , ϕ and h (see Fig. I.3). The longitude λ measures the rotational angle between the prime meridian and the measured point M . The latitude ϕ measures the angle between the equatorial plan and the normal of the reference ellipsoid that passes through the measured point M . The height (or altitude) h is the local vertical distance between the measured point M and the reference ellipsoid.

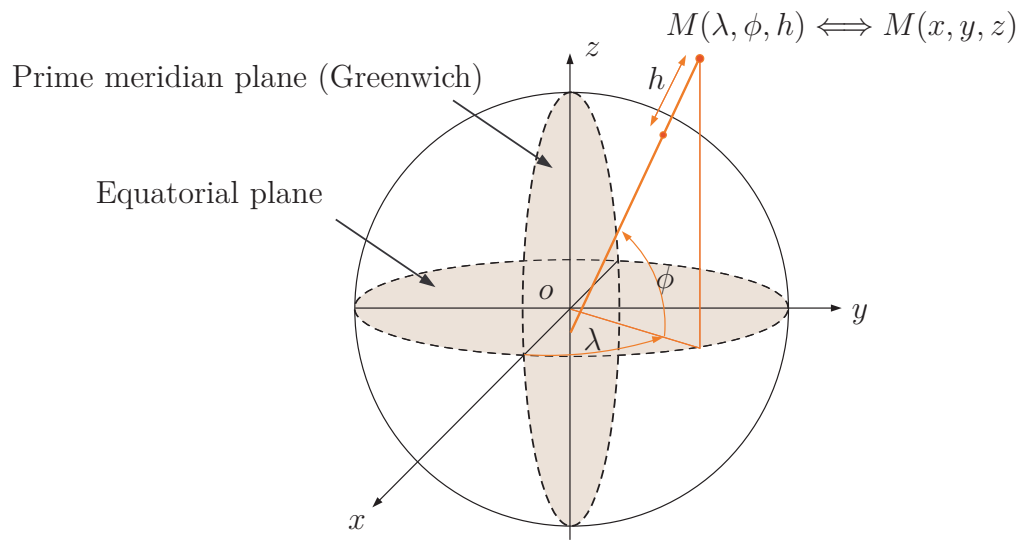


Figure I.3 – The relationship between geodetic and ECEF coordinate system.

ECEF Coordinate System

The ECEF is a coordinate frame fixed to the Earth, what means it rotates with the Earth around its spin axis. The origin and axes of the ECEF coordinate system are defined as follows (also see Fig. I.3) :

1. The origin o is located at the center of the Earth.
2. The z -axis is along the spin axis of the Earth, pointing to the North pole.
3. The x -axis intersects the sphere of the Earth at 0° latitude and 0° longitude.
4. The y -axis is orthogonal to the z - and x -axes with the usual right-hand rule.

ENU Coordinate System

The ENU coordinate system is a local system fixed to the Earth's surface. It is formed from a plane tangent to the Earth's surface fixed to a specific location, hence it's also known as the "local tangent plane". In this plane, the unit vector x_l points to

the East, the unit vector y_l points to the North and the unit vector z_l points Upward, as shown in Fig. I.4.

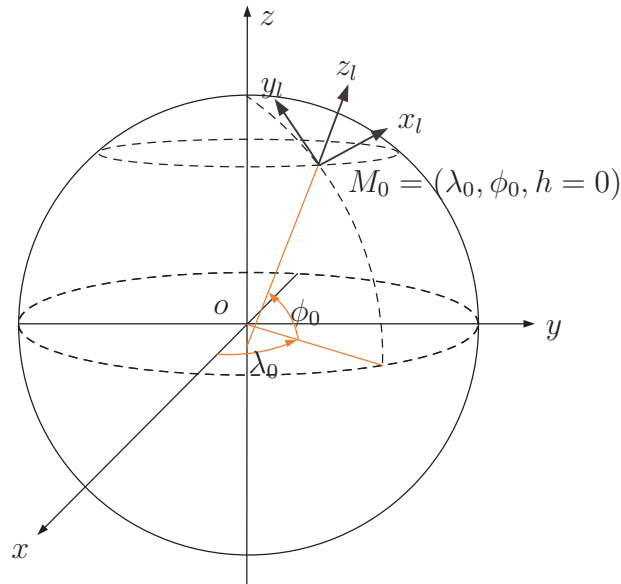


Figure I.4 – ENU coordinate system.

I.1.3.3 Coordinate Transformations

The transformation relationships among these three coordinate systems are introduced in this section.

Geodetic Coordinate System and ECEF Coordinate System

As shown in Fig. I.3, the transformation of the coordinates of a point M for the geodetic coordinate system to the ECEF coordinate system is given by (Tsui - 2007) :

$$\begin{cases} x = (N + h) \cos \phi \cos \lambda \\ y = (N + h) \cos \phi \sin \lambda, \\ z = [N(1 - e^2) + h] \sin \phi \end{cases} \quad (\text{I.1})$$

where $N = \frac{a}{\sqrt{1 - e^2 \sin^2 \phi}}$ is the radius of curvature in the prime vertical (which is the vertical plane normal to the astronomical meridian). a and e are the semi-major axis and the eccentricity of the Earth, respectively.

The reverse problem that computes $M(\lambda, \phi, h)$ from $M(x, y, z)$ requires an iteration for ϕ and h . Directly $\lambda = \arctan(y/x)$. Then the procedure is given as follows :

Initialization : $h = 0$, $N = a$, $p = \sqrt{x^2 + y^2}$.

Iteration : $\sin \phi = \frac{z}{N(1-e^2)+h}$, $\phi = \arctan(\frac{z+e^2N \sin \phi}{p})$, $N(\phi) = \frac{a}{\sqrt{1-e^2 \sin^2 \phi}}$, $h = \frac{p}{\cos \phi} - N$.

Stop the iteration if $|h_i - h_{i-1}| \leq \varsigma$, where ς is a small positive constant.

ECEF Coordinate System and ENU Coordinate System

The transformation of the coordinates of a point $M_0(\lambda_0, \phi_0, h = 0)$ from the ECEF coordinate system to the ENU coordinate system is given by (see Fig. I.4) :

$$\begin{pmatrix} x_l \\ y_l \\ z_l \end{pmatrix} = \begin{pmatrix} -\sin \lambda_0 & \cos \lambda_0 & 0 \\ -\sin \phi_0 \cos \lambda_0 & -\sin \phi_0 \sin \lambda_0 & \cos \phi_0 \\ -\cos \phi_0 \cos \lambda_0 & \cos \phi_0 \sin \lambda_0 & \sin \phi_0 \end{pmatrix} \begin{pmatrix} x - N_0 \cos \phi_0 \cos \lambda_0 \\ y - N_0 \cos \phi_0 \sin \lambda_0 \\ z - N_0(1 - e^2) \sin \phi_0 \end{pmatrix}, \quad (\text{I.2})$$

where N_0 is calculated exactly as in equation (I.1) but with $M_0(\lambda_0, \phi_0, h = 0)$ instead of $M(\lambda, \phi, h)$.

The convert from the ENU coordinate system to the ECEF coordinate system is obtained by inverting the transformation :

$$\begin{pmatrix} x \\ y \\ z \end{pmatrix} = \begin{pmatrix} N_0 \cos \phi_0 \cos \lambda_0 \\ N_0 \cos \phi_0 \sin \lambda_0 \\ N_0(1 - e^2) \sin \phi_0 \end{pmatrix} + \begin{pmatrix} -\sin \lambda_0 & \cos \lambda_0 & 0 \\ -\sin \phi_0 \cos \lambda_0 & -\sin \phi_0 \sin \lambda_0 & \cos \phi_0 \\ -\cos \phi_0 \cos \lambda_0 & \cos \phi_0 \sin \lambda_0 & \sin \phi_0 \end{pmatrix}^T \begin{pmatrix} x_l \\ y_l \\ z_l \end{pmatrix}. \quad (\text{I.3})$$

I.1.3.4 GNSS Classic (3D) Navigation

Two ways of GNSS navigation have been discussed by many authors : point positioning or relative positioning (B.Hofmann-Wellenhof et al. - 1992; El-Rabbany - 2002; Misra et Enge - 2011; Ahn - 2013; Nikiforov - 2013). In this section, the first method is described in details. The navigation solution is based on accurate measuring the distance (range) from several satellites with known locations to a user (see Fig. I.5). Let us assume that there are n satellites located in three-space at the known positions $X_i = (x_i, y_i, z_i)^T$, $i = 1, \dots, n$, and a user at $X_u = (x, y, z)^T$. The pseudo-range r_i from

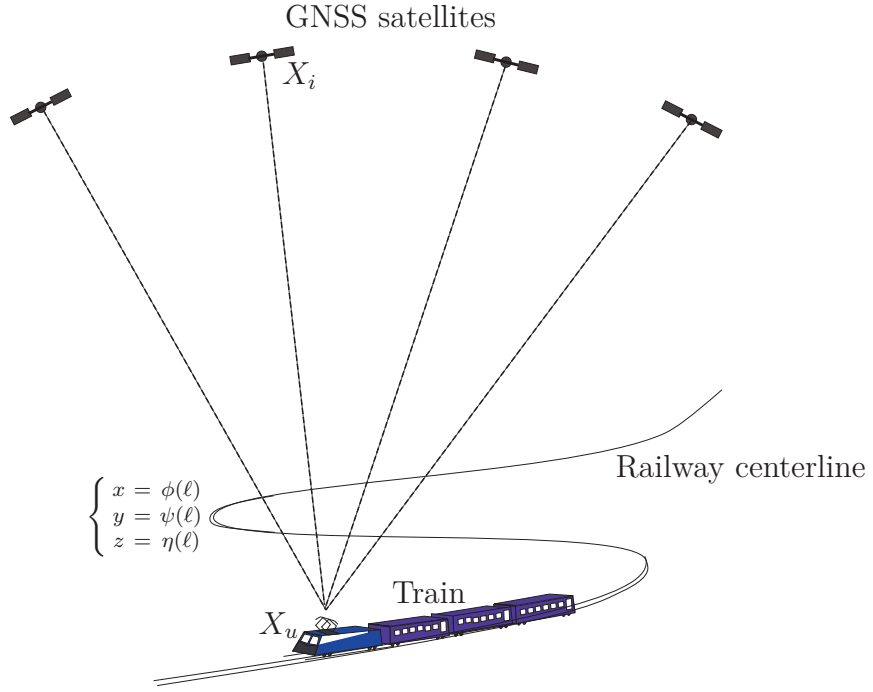


Figure I.5 – Train 1D GNSS positioning.

the i -th satellite to the user can be written as

$$\begin{cases} r_1 = d_1(x, y, z) + cb_r + \varepsilon_1 \\ r_2 = d_2(x, y, z) + cb_r + \varepsilon_2 \\ \vdots \quad \vdots \quad \vdots \\ r_n = d_n(x, y, z) + cb_r + \varepsilon_n \end{cases} \quad (\text{I.4})$$

where $d_i(x, y, z) = \|X_i - X_u\|_2$, $i = 1, \dots, n$, is the true distance from the i -th satellite to the user, b_r is a user clock bias, $c \simeq 2.9979 \cdot 10^8 \text{ m/s}$ is the speed of light and ε_i is the pseudo-range noise. Let us introduce the following vectors : $R = (r_1, \dots, r_n)^T$ and $X = (X_u^T, cb_r)^T$. By linearizing the pseudo-range equation with respect to the state vector X around the working point $X_0 = (X_{u0}^T, cb_0)^T$, we get the measurement equation

$$\begin{pmatrix} y_1 \\ y_2 \\ \vdots \\ y_n \end{pmatrix} = \begin{pmatrix} r_1 - r_{10} \\ r_2 - r_{20} \\ \vdots \\ r_n - r_{n0} \end{pmatrix} \simeq \begin{pmatrix} h_{1x} & h_{1y} & h_{1z} & 1 \\ h_{2x} & h_{2y} & h_{2z} & 1 \\ \vdots & \vdots & \vdots & \vdots \\ h_{nx} & h_{ny} & h_{nz} & 1 \end{pmatrix} \cdot \begin{pmatrix} x - x_0 \\ y - y_0 \\ z - z_0 \\ cb_r - cb_0 \end{pmatrix} + \begin{pmatrix} \varepsilon_1 \\ \varepsilon_2 \\ \vdots \\ \varepsilon_n \end{pmatrix}, \quad (\text{I.5})$$

where $r_{i0} = d_{i0} + cb_0$, $d_{i0} = d_i(x_0, y_0, z_0) = \|X_i - X_{u0}\|_2$, $i = 1, \dots, n$ and the coefficients of the Jacobian matrix H_0 of size $(n \times 4)$ are given by

$$h_{ix} = \frac{\partial d_i}{\partial x}(x_0, d_{i0}) = \frac{x_0 - x_i}{d_{i0}}, h_{iy} = \frac{\partial d_i}{\partial y}(y_0, d_{i0}) = \frac{y_0 - y_i}{d_{i0}}, h_{iz} = \frac{\partial d_i}{\partial z}(z_0, d_{i0}) = \frac{z_0 - z_i}{d_{i0}}.$$

The above linearized measurement equations (I.5) can be written as follows

$$Y = R - R_0 \simeq H_0(X - X_0) + \Xi, \quad (\text{I.6})$$

where H_0 is a full rank matrix of size $(n \times 4)$ defined in equation (I.5), $R_0 = (r_{10}, \dots, r_{n0})^T$, $\Xi = (\varepsilon_1, \dots, \varepsilon_n)^T$. If we assume that $n \geq 5$, $\mathbb{E}(\Xi) = 0$ and $\text{cov}(\Xi) = \sigma^2 I_n$, the iterative least square (LS) algorithm provides us with an optimal solution. First, we compute the LS estimate \widehat{X} by using the measurement vector R and the initial working point X_0 :

$$\widehat{X} = X_0 + (H_0^T H_0)^{-1} H_0^T (R - R_0). \quad (\text{I.7})$$

Then, the working point is set to be $X_0 = \widehat{X}$ for the next iteration. Usually only two or three steps are necessary to reach the convergence of the iterative process. The stopping rule is defined as follows:

$$\text{stop the iterations if } \|\widehat{X} - X_0\|_2 = \|(H_0^T H_0)^{-1} H_0^T (R - R_0)\|_2 \leq \varsigma, \quad (\text{I.8})$$

where ς is a small positive constant. When the convergence has been reached, the residual vector e is given by the following equation

$$e = R - R_0. \quad (\text{I.9})$$

Now we assess the quality of this estimator. First, substituting the right side of equation (I.6) into equation (I.7) yields to

$$\widehat{X} = X + (H_0^T H_0)^{-1} H_0^T \Xi. \quad (\text{I.10})$$

Then the expectation and variance of this estimator are calculated as follows

$$\begin{aligned} \mathbb{E}(\widehat{X} - X) &= \mathbb{E}[(H_0^T H_0)^{-1} H_0^T \Xi] = 0, \\ \text{var}(\widehat{X}) &= \mathbb{E}[(\widehat{X} - X)(\widehat{X} - X)^T] = \mathbb{E}[(H_0^T H_0)^{-1} H_0^T \Xi \Xi^T H_0 (H_0^T H_0)^{-1}] = \sigma^2 (H_0^T H_0)^{-1}. \end{aligned} \quad (\text{I.11})$$

The first expression shows that the estimator is unbiased. It is also interesting to compare the variance of this estimator with the Cramér-Rao lower bound in the class $\mathcal{K}_0 = \{\widehat{X} : \mathbb{E}(\widehat{X} - X) = 0\}$ of unbiased estimator. In the following Section I.3, it will be shown that the variance of this estimator $\text{var}(\widehat{X})$ achieves the Cramér-Rao lower bound, i.e.,

$$\text{var}(\widehat{X}) \geq \frac{1}{n} \mathcal{F}^{-1}(X) = \sigma^2 (H_0^T H_0)^{-1}. \quad (\text{I.12})$$

Hence, the estimator is unbiased and efficient.

The accuracy of the instant absolute positioning is correlated with the geometry of the satellite constellation in the sky. The satellite geometry effect can be measured by a parameter called the Dilution of Precision (DOP), which can be calculated from the variance-covariance of the coordinates and time. Let us consider the covariance matrix in the ENU coordinate system and we have :

$$\text{cov}(\widehat{\boldsymbol{X}}) = \begin{pmatrix} \sigma_E^2 & \sigma_{EN} & \sigma_{Eh} & \sigma_{Et} \\ \sigma_{NE} & \sigma_N^2 & \sigma_{Nh} & \sigma_{Nt} \\ \sigma_{hE} & \sigma_{hN} & \sigma_h^2 & \sigma_{ht} \\ \sigma_{tE} & \sigma_{tN} & \sigma_{th} & \sigma_t^2 \end{pmatrix}.$$

Let σ be the Standard Deviation (SD) of pseudo-range error. In practice we have several forms of the DOP :

- The vertical dilution of precision (VDOP) : $\text{VDOP} = \frac{\sigma_h}{\sigma}$.
- The horizontal dilution of precision (HDOP) : $\text{HDOP} = \frac{\sqrt{\sigma_N^2 + \sigma_E^2}}{\sigma}$.
- The position dilution of precision (PDOP) : $\text{PDOP} = \frac{\sqrt{\sigma_N^2 + \sigma_E^2 + \sigma_h^2}}{\sigma}$.
- The time dilution of precision (TDOP) : $\text{TDOP} = \frac{\sigma_t}{\sigma}$.
- The geometric dilution of precision (GDOP) : $\text{GDOP} = \frac{\sqrt{\sigma_N^2 + \sigma_E^2 + \sigma_h^2 + \sigma_t^2}}{\sigma}$.

The lower the value of the DOP, the better the positioning accuracy.

Example I.1.1. Let pseudo-range SD be $\sigma = 1$ m. Three satellites are equally spaced on the horizon, at minimum elevation angle, with the fourth satellite directly overhead, as listed in Tab. I.1. Typical example values of the above covariance matrix for this

Satellite location				
Satellite number	1	2	3	4
Elevation (deg)	5	5	5	90
Azimuth (deg)	0	120	240	0

Tableau I.1 – Example with four satellites.

geometry are

$$\begin{pmatrix} 0.672 & 0.000 & 0.000 & 0.000 \\ 0.000 & 0.672 & 0.000 & 0.000 \\ 0.000 & 0.000 & 1.600 & -0.505 \\ 0.000 & 0.000 & -0.505 & 0.409 \end{pmatrix}.$$

The value of the DOP for this example are :

$$\text{VDOP} = \sqrt{1.600} = 1.26,$$

$$\text{HDOP} = \sqrt{0.672 + 0.672} = 1.16,$$

$$PDOP = \sqrt{0.672 + 0.672 + 1.600} = 1.72,$$

$$TDOP = \sqrt{0.409} = 0.64,$$

and

$$GDOP = \sqrt{0.672 + 0.672 + 1.600 + 0.409} = 1.83.$$

I.1.3.5 GNSS Train (1D) Navigation

Since trains travel on pre-defined track, 3D navigation becomes 1D navigation problem that fixes the train position along the track. Let us assume that the train track is defined by the following parametric equations in three-space :

$$\begin{cases} x = \phi(\ell) \\ y = \psi(\ell) \\ z = \eta(\ell) \end{cases}$$

where $\ell \in [0, +\infty)$ is the travelled distance. This situation is also illustrated in Fig. I.5. Hence, the measurement model defined by equation (I.4) can be rewritten as follows :

$$\begin{cases} r_1 = d_1(\phi(\ell), \psi(\ell), \eta(\ell)) + cb_r + \varepsilon_1 \\ r_2 = d_2(\phi(\ell), \psi(\ell), \eta(\ell)) + cb_r + \varepsilon_2 \\ \vdots \quad \vdots \quad \vdots \quad \vdots \\ r_n = d_n(\phi(\ell), \psi(\ell), \eta(\ell)) + cb_r + \varepsilon_n. \end{cases} \quad (\text{I.13})$$

By linearizing the pseudo-range equation with respect to the state vector $\tilde{X} = (\ell, cb_r)^T$ around the working point $\tilde{X}_0 = (\ell_0, cb_0)^T$, we get the measurement equation

$$\begin{pmatrix} y_1 \\ y_2 \\ \vdots \\ y_n \end{pmatrix} = \begin{pmatrix} r_1 - r_{10}(\ell_0) \\ r_2 - r_{20}(\ell_0) \\ \vdots \\ r_n - r_{n0}(\ell_0) \end{pmatrix} \simeq \begin{pmatrix} \tilde{h}_1 & 1 \\ \tilde{h}_2 & 1 \\ \vdots & \vdots \\ \tilde{h}_n & 1 \end{pmatrix} \cdot \begin{pmatrix} \ell - \ell_0 \\ cb_r - cb_0 \end{pmatrix} + \begin{pmatrix} \varepsilon_1 \\ \varepsilon_2 \\ \vdots \\ \varepsilon_n \end{pmatrix}, \quad (\text{I.14})$$

where $r_{i0}(\ell_0) = d_{i0}(\ell_0) + cb_0$, $d_{i0}(\ell_0) = d_i(\phi(\ell_0), \psi(\ell_0), \eta(\ell_0))$, $i = 1, \dots, n$ and the coefficients of the Jacobian matrix \tilde{H}_0 of size $(n \times 2)$ are given by

$$\tilde{h}_i = \frac{\partial d_i}{\partial \ell}(\ell_0) = \frac{a_\phi(\ell_0)(\phi(\ell_0) - x_i) + a_\psi(\ell_0)(\psi(\ell_0) - y_i) + a_\eta(\ell_0)(\eta(\ell_0) - z_i)}{d_i(\ell_0)},$$

where $a_\phi(\ell) = \frac{d\phi(\ell)}{d\ell}$, $a_\psi(\ell) = \frac{d\psi(\ell)}{d\ell}$, $a_\eta(\ell) = \frac{d\eta(\ell)}{d\ell}$. By analogy with the case of 3D navigation (see equation (I.6)), the above linearized measurement equation (I.14) can be rewritten as follows

$$Y = R - R_0 \simeq \tilde{H}_0(\tilde{X} - \tilde{X}_0) + \Xi, \quad (\text{I.15})$$

where \widetilde{H}_0 is a full rank matrix of size $(n \times 2)$ defined in equation (I.14). The solution $(\hat{\ell}, \hat{b}_r)$ for the 1D navigation is obtained by using a nonlinear LS algorithm by analogy with the 3D solution (I.8)-(I.9).

As discussed in the case of 3D navigation, we also assess the quality of this estimator. Substituting the right side of equation (I.15) into the LS estimator yields to

$$\widehat{\widetilde{X}} = \widetilde{X} + (\widetilde{H}_0^T \widetilde{H}_0)^{-1} \widetilde{H}_0^T \Xi. \quad (\text{I.16})$$

Then the expectation and variance of this estimator are calculated as follows

$$\begin{aligned} \mathbb{E}(\widehat{\widetilde{X}} - \widetilde{X}) &= \mathbb{E}\left[(\widetilde{H}_0^T \widetilde{H}_0)^{-1} \widetilde{H}_0^T \Xi\right] = 0, \\ \text{var}(\widehat{\widetilde{X}}) &= \mathbb{E}\left[\left(\widehat{\widetilde{X}} - \widetilde{X}\right)\left(\widehat{\widetilde{X}} - \widetilde{X}\right)^T\right] = \mathbb{E}\left[(\widetilde{H}_0^T \widetilde{H}_0)^{-1} \widetilde{H}_0^T \Xi \Xi^T \widetilde{H}_0 (\widetilde{H}_0^T \widetilde{H}_0)^{-1}\right] \quad (\text{I.17}) \\ &= \sigma^2 (\widetilde{H}_0^T \widetilde{H}_0)^{-1}. \end{aligned}$$

The first expression shows that the estimator is unbiased. It is also interesting to compare the variance of this estimator with the Cramér-Rao lower bound in the class $\mathcal{K}_0 = \left\{ \widehat{\widetilde{X}} : \mathbb{E}(\widehat{\widetilde{X}} - \widetilde{X}) = 0 \right\}$ of unbiased estimator. In the following Section I.3, it will also be shown that the variance $\text{var}(\widehat{\widetilde{X}})$ achieves the Cramér-Rao lower bound, i.e.,

$$\text{var}(\widehat{\widetilde{X}}) \geq \frac{1}{n} \mathcal{F}^{-1}(\widetilde{X}) = \sigma^2 (\widetilde{H}_0^T \widetilde{H}_0)^{-1}. \quad (\text{I.18})$$

Hence, the estimator is unbiased and efficient.

I.1.4 Previous Research and Literature Review

The following subsection gives a summary of projects and methods of train positioning.

Several research projects have developed systems for the railways navigation by using GNSS, e.g. GaLoRoi (Juliette - 2011), GRAIL (zu Hörste et al. - 2008), DemoOrt (Becker et al. - 2006a), SATNAB (Illgen et al. - 2000), LOCOPROL (Mertens et al. - 2003), APOLO (Hartwig et al. - 2006) and GADEROS (Urech et al. - 2003) or using different sensors, e.g. the Sistema di Controllo Maricia Treno (SCMT) system in Italy.

Several methods of train positioning have been proposed and can be divided into the following four categories : GNSS-based train positioning, Sensor-based train positioning, Global Navigation Satellite System/Inertial Navigation System (GNSS/INS)-based train positioning and GNSS/Sensor-based train positioning, which are illustrated in Fig. I.6.

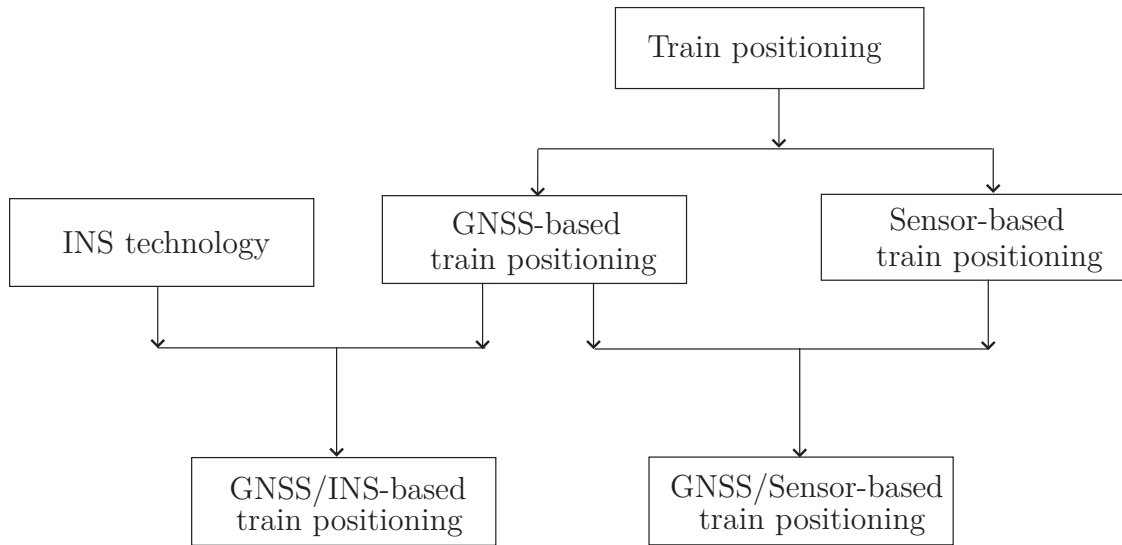


Figure I.6 – Methods of train positioning.

GNSS-based Train Positioning

Nikiforov et Choquette (2003); Foulardirad et Nikiforov (2003); Lacresse et al. (2003); Lacresse (2004); Lacresse et al. (2005) discuss the problem of train positioning integrity monitoring using GNSS (or DGNSS) under the LOCOPROL project and several GNSS integrity methods have been studied thoroughly in order that GNSS can be safely used in rail operations. Recently, they provide several algorithmic solutions which are devoted to the trajectory-aided train positioning by using a GNSS receiver. The aim is to estimate some desired parameters such as the travelled distance, speed with a high level of accuracy (Zhu et al. - 23-26 Apr. 2013, 27-28 Jun. 2013, 3-6 Sept. 2013, Apr. 2013).

Zheng (2007, 2008); Zheng et Cross (2012) develops a system that integrates GNSS with different accuracy of track database for safety-critical railway control systems. The feature of this system is its ability to take into account uncertainties in both GNSS

observables and the spatial railway network data. The impact of accuracy of the track database on positioning accuracy is studied. When the GNSS is integrated with the track database, the accuracy, integrity and availability are improved. Specifically, in the open areas where the satellite visibility is good, compared to the standalone GNSS, the integration system improves the accuracy both in the along track direction and in the across track direction. In the tough environment where the visibility of satellites is low, the improvements of accuracy and the external reliability by the integration system are more apparent than they are in the open areas due to the poor performance of the standalone GNSS in the tough areas. The integration system also increases the availability of the GNSS by using reducing its required satellites. It makes the position to be able to be calculated only if two satellites are available, the RAIM be calculated only if three satellites are visible and only four satellites are required for FDE.

GADEROS is a project aimed at demonstrating the use of GNSS integrity and safety of life characteristics for defining a satellite-based system to perform train location for safe railway application, which is to be integrated into ERTMS/ETCS architecture. The demonstration on a low density traffic line provides real-life implementation of train location based on a GNSS receiver with integrity and augmentation.

Lüddeken et Rahmig (2011) introduce a method of improving track-selectivity of positioning taking into account further GNSS observation data instead of additional sensors and thus providing an alternative way of precise and reliable positioning at switches. It is shown that the integration of the direction-dependent standard deviation of GNSS position measurement and the GNSS course observation results in an improved multi-hypothesis based map-matching algorithm. Its positioning accuracy enables a selection of the correct track after having passed a switch at the latest at the clearance point.

Sensor-based Train Positioning

Malvezzi et al. (2001) develop the odometry algorithm for the Italian ATP system named SCMT, exploiting only data coming from two encoders measuring axle angular speed, which is installed on train circulating in Italian railways. A number of algorithms based on fuzzy logic (Allotta et al. - 2002; Malvezzi et al. - 2001) and neural networks (Colla et al. - 23-25 Apr. 2003, 3-6 Jun. 2003) have been developed to estimate the

train speed and position.

In the specific application, wheel angular speed sensors give a reliable and accurate estimation of train speed but only the adhesion conditions between the wheel and the rail are good. In presence of wheel sliding (when train is accelerating or braking), Malvezzi et al. (2008, 2011) improved both safety and performance only by adding a simple monoaxial accelerometer for the estimation of train longitudinal acceleration. The results show that the proposed algorithm gives a better estimation of train speed with respect to the SCMT algorithm. The integration of the sensor measuring train acceleration in the odometric device leads to a significant improvement in the precision of both velocity and travelled distance estimation.

Vettori et al. (12-15 Sept. 2011) also develop an estimation algorithm for railway vehicles based on odometers and an INS based on Inertial Navigation Unit (IMU). The objective is to increase the accuracy of the odometric estimation, especially in critical adhesion conditions. The results show a significant improvement of odometric algorithm performance, compared with the conventional SCMT algorithm.

GNSS/INS-based Train Positioning

Simsky et al. (8-10 Dec. 2004) develop a prototype train-borne positioning system within the framework of the LOCOLOC/LOCOPROL projects. The primary objective of both projects is to develop and demonstrate a complete very low-cost failsafe train positioning system based on GNSS. The algorithms are based on the previous knowledge of the track, which makes the positioning problem one-dimensional : only along-track position is to be computed. This significantly increases availability and redundancy of GNSS satellites and hence the integrity of the solution increases to the level required for safety-critical operation. Doppler speed radar is used to provide reference for GNSS-computed velocity and a loosely coupled GNSS/INS system is used to provide the position reference. It has been demonstrated that the LOCOPROL positioning technology of failsafe railway positioning based on the 1D algorithm satisfies both accuracy and safety requirements for low-density traffic lines. It has been shown that the developed 1D algorithm provides adequate confidence intervals for computed position and speed.

Liu et al. (2010, 2012) build a GNSS/INS integrated positioning system architecture,

in which the Cubature Kalman Filter (CKF) is employed to solve the problem of nonlinearity and computation efficiency, and the integrity design is realized by the Principal Component Analysis (PCA) based Fault Detection and Diagnosis (FDD). To compare the positioning performance of CKF with other approaches, practical GNSS/INS measurements from Qinghai-Tibet line are adopted for CKF, Unscented Kalman Filter (UKF) and Particle Filter (PF) positioning solutions. The position errors in east and north direction are calculated. The results demonstrate that the CKF approach earns a high accuracy and efficiency ability than traditional UKF and PF solutions, the integrity performance of the train positioning system could be improved by the PCA based FDD strategies.

Filip et al. (2000, 2002, 2004); Filip (2007); Filip et al. (2008) design a GNSS/INS based train position locator for railway signalling at Czech Railways. The experiments demonstrated that the GNSS/INS based Train Position Locator (TPL) is able to determine one dimensional position of the train with the accuracy of about 0.5 m on the track section with length of about 1 km under absence of Signal In Space (SIS). Further it was demonstrated that after the train passed the same track section (also under SIS absence) including the switch (against the switch blade), there was possible to determine with high probability on which of the parallel tracks the train was located. It should be noted that during these experiments the intentionally generated wheel slips introduced large odometry errors to the distance travelled measurements exceeding of 150 m. It means that there was possible to detect the errors and correct them.

GNSS/Sensor-based Train Positioning

The objective of the GaLoRoi project is the development of a certifiable safety relevant satellite based on-board train localisation unit to be used on low traffic density railway lines. The safe and precise on-board localisation unit control but also for train integrity monitoring, train and fleet management, green driving and furthermore for track inspection. GaLoRoi allows migrating for conventional localisation techniques towards a satellite based technology. A safe localisation will be enabled by a satellite independent device (eddy current sensor) supported by the EGNOS Safety of Life service.

The German Aerospace Center (DLR)'s Institute of Transportation Systems (ITS)

works on the development of a demonstrator for the train borne, self-supporting navigation for safety relevant applications in the project "DemoOrt" in cooperation with the Technical University Braunschweig, the University Karlsruhe and Bombardier Transportation - Rail Control Solutions. The objective is the integration of different navigation systems into an innovative platform, to demonstrate a self-supporting navigation of the rail vehicle. The concept, consisting of a GNSS-receiver, an eddy-current sensor and a digital map, performs the calculation of the positioning information with high accuracy, reliability, integrity and availability. The platform guarantees the positioning of a rail vehicle with the required high precision and availability. It has been tested and demonstrated on a track near Karlsruhe in Germany and a narrow gauge line in the High Tatras in Slovakia (Hartwig et al., 2006).

The Railway User Navigation Equipment (RUNE) project demonstrates the use of GNSS integrity and safety of life service characteristics for defining a satellite-based system to perform train location for safe railway applications. The RUNE technical solution is based on GNSS receivers : navigation data will come from GPS with differential EGNOS corrections to enable autonomous and reliable determination of train position, velocity under practically all environmental conditions. The system also offers another technological approach for the train location function : the use of GNSS signals with inertial sensors and on-board odometers (Albanese et al. - 16-18 Mar. 2005).

Bedrich et Gu (2004) describes a mobile telematics prototype system called INTEGRAIL aims at achieving significant improvements for the rail traffic operator with regard to cost, redundancy and reliability of the present train speed measurement systems, which are based on odometers, by adding satellite navigation information and the integrity information offered by EGNOS. The basic objective of the INTEGRAIL development is to demonstrate the profitable use of GNSS for advanced rail traffic management. INTEGRAIL is the first step towards providing train position, velocity and heading by means of satellite navigation to safety-critical rail applications. At this stage it allows already for the more profitable exploitation of low-density rail lines. Eventually, INTEGRAIL provides a GNSS-based odometry interface within the already emerging ERTMS standard to serve high-speed lines as well.

Among the mentioned projects, most of them sought to develop a train location system by using GNSS and sensors. GaLoRoi allows migrating for conventional locali-

sation techniques towards a satellite based technology, but the localisation unit is used only on low density railway lines. DemoOrt is the integration of different navigation systems, nowadays GPS, in future the European system GALILEO, into an innovative platform. The project SATNAB deals with the concepts of location with only one satellite, digital map assisted by a rubidium oscillator. GADEROS integrates the GALILEO integrity and augmentation within the train position locator. A few projects develop a onboard train location system by using only GNSS signals. Developing a train location system based on GNSS seems to be very promising.

I.2 Problems Studied in This Thesis

The algorithms described in this thesis are devoted to the train positioning by a low-cost GNSS receiver, using pseudo-distance measurements from satellites. Two approaches of the train travelled distance, speed and acceleration estimation can be considered. The first approach is based on the 3D track geometry model (this is the so-called 1D navigation). In the case of 1D navigation, as discussed in Section I.1.3.5, the GNSS receiver needs measurements from two satellites or more to estimate the train position and clock bias. The information about the train track is stored in the onboard train database. With this information and the knowledge concerning geometric design of train track model, a realistic train track can be made. The second approach does not use any information about the track geometry model (hence, it is a conventional 2D or 3D navigation). The first approach can potentially provide the users with the best precision but some preliminary investigations should be done prior its incorporation. Hence, the following crucially important questions need to be considered :

1. What is the impact of such a track geometric model imprecision on the estimation of train speed, acceleration and distance ?
2. What is the impact of the railroad curvature or railway curve radius on the train speed, acceleration and distance estimation ?
3. Will a change of acceleration cause imprecise estimation of the train speed, acceleration and distance ?

The proposed methods of statistical estimation permit us to study the above mentioned questions. Estimation is the process of obtaining a set of unknowns of interest from a set of uncertain measurements, according to a definite optimization criterion. The estimation method used in our research is the LS algorithm, which uses the measurement model. The LS algorithm is the most common estimation procedure in GNSS navigation and its optimization criterion is based on minimizing the sum of the square residual. The LS estimator coincides with the Maximum Likelihood Estimator (MLE).

I.3 Estimation Theory (parametric approach)

The goal of this section is to provide a brief overview of estimation methods that have been used in our research. Some basic concepts of convergence of random variables are given in Appendix A.

Problem Statement

The problem of unknown parameter estimation arises when the statistician wishes to estimate some unknown parameters θ of the parameterized distribution P_θ . Therefore, the statistician has to define a function of observations (or statistics) which is used instead of the parameter θ as its approximation

$$\hat{\theta} = \hat{\theta}_n(y_1, y_2, \dots, y_n).$$

We will use the symbol $\hat{\cdot}$ to denote a function of observations (or statistics), which is usually called "estimator" (or estimation) of θ . It is assumed that we dispose of a parameterized family of distributions $\mathcal{P} = \{P_\theta, \theta \in \Theta\}$. We also have a set of possible values Θ for the parameter θ . This idea is illustrated in the following figure.

Maximum Likelihood Method

Let us now discuss one classical method of estimation : maximum likelihood method. It can be interpreted as realisations of the principle of substitution (see details in Appendix A). First of all, let us start with the definition of Kullback-Leibler "distance" and its property.

Definition 1. Let F and G be two distributions. It is assumed that F and G admit the densities, denoted by $f(x)$ and $g(x)$, respectively. The Kullback-Leibler "distance"

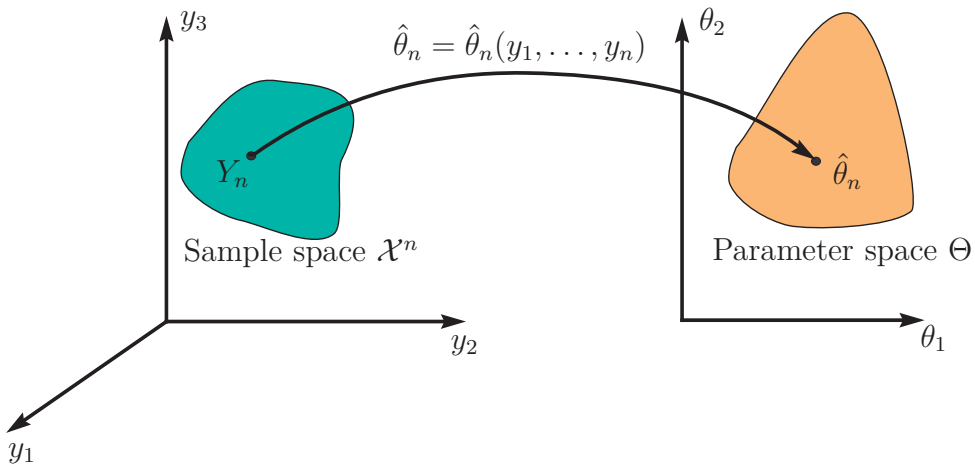


Figure I.7 – Illustration of the parameter estimation.

between F and Q is given by

$$\rho(g, f) = \int \log \frac{g(x)}{f(x)} g(x) dx.$$

Lemma 1 (Kullback-Leibler property). *The Kullback-Leibler "distance" is always non-negative. Then*

$$\rho(g, f) = \int \log \frac{g(x)}{f(x)} g(x) dx \geq 0$$

and $\rho(g, f) = 0$ iff $f(x) = g(x)$ almost everywhere.

Let us consider a parametric family $\mathcal{P} = \{P_\theta\}_{\theta \in \Theta}$. It is assumed that P_θ and Q admit the densities, denoted by $f_\theta(x)$ and $g(x)$, respectively. By using the method of minimum distance with the Kullback-Leibler "distance" $d(P_\theta, Q) = \rho(g, f_\theta)$ between the distribution Q and one element P_θ from the family \mathcal{P} , an estimator $\hat{\theta}$ can be defined as a value of θ which minimize the following expression :

$$\min_{\theta \in \Theta} \rho(g, f_\theta) = \min_{\theta \in \Theta} \int \log \frac{g(x)}{f_\theta(x)} g(x) dx$$

or which maximize :

$$\max_{\theta \in \Theta} \int \log f_\theta(x) g(x) dx.$$

Definition 2. *The observations ξ_1, \dots, ξ_n are assumed to come from P_θ , where $P_\theta \in \mathcal{P}$. The maximum likelihood estimator is given by*

$$\hat{\theta} = \arg \max_{\theta \in \Theta} \int \log f_\theta(x) d\hat{G}_n(x) = \arg \max_{\theta \in \Theta} \frac{1}{n} \sum_{i=1}^n \log f_\theta(y_i).$$

Definition 3. The mapping $\theta \mapsto f_\theta(Y_n) = \prod_{i=1}^n f_\theta(y_i)$, considered as a function of θ , is called the likelihood function and $\theta \mapsto \log f_\theta(Y_n) = \sum_{i=1}^n \log f_\theta(y_i)$ is called the log-likelihood function.

Bias (or Bias Function) of an Estimator

In statistics, the bias (or bias function) of an estimator is the difference between this estimator's expected value and the true value of the parameter being estimated. The mean of the sampling distribution of the estimator $\hat{\theta}$ is used to define the bias of the estimator. Hence, it can be defined as follows :

Definition 4. The bias of the estimator $\hat{\theta}$ is $b(\theta) = \mathbb{E}_\theta(\hat{\theta} - \theta)$. The estimator for which $b(\theta) = 0$ is called unbiased. Sometimes, it is useful to define an asymptotic notion of bias. Let us denote by $\hat{\theta}_n$ the estimator using first n observations. The asymptotic bias is defined as follows $b(\theta) = \lim_{n \rightarrow \infty} \mathbb{E}_\theta(\hat{\theta}_n - \theta)$.

Cramér-Rao Inequality

It is also interesting to compare the variance of the estimator with the Cramér-Rao lower bound in the class $\mathcal{K}_0 = \{\hat{\theta} : \mathbb{E}(\hat{\theta} - \theta) = 0\}$ of unbiased estimator. An unbiased estimator which achieves this lower bound is said to be efficient. Let us here consider the vector case $\theta \in \Theta \subseteq \mathbb{R}^m$ (see the scalar case $\theta \in \Theta \subseteq \mathbb{R}$ in Appendix A). The observations ξ_1, \dots, ξ_n are assumed to come from P_θ , where $P_\theta \in \mathcal{P}$. The likelihood function for these observations is given by

$$L(\xi_1, \dots, \xi_n; \theta) = \sum_{i=1}^n l(\xi_i, \theta), \quad l(\xi, \theta) = \log f_\theta(\xi),$$

where $f_\theta(x)$ is the PDF of P_θ .

Regularity conditions :

R 1 : the function $\theta \mapsto \sqrt{f_\theta(x)}$, for almost all values of x , is continuously differentiable in θ_i ($i = 1, \dots, m$) ;

R 2 : the integrals

$$\mathcal{F}_{i,j}(\theta) = \mathbb{E}_\theta [l'_i(\xi, \theta) l'_j(\xi, \theta)] = \mathbb{E}_\theta \left[\frac{\partial l(\xi, \theta)}{\partial \theta_i} \frac{\partial l(\xi, \theta)}{\partial \theta_j} \right] = \int \frac{\partial l(x, \theta)}{\partial \theta_i} \frac{\partial l(x, \theta)}{\partial \theta_j} f_\theta(x) dx,$$

where $i, j = 1, \dots, m$, exist, the Fisher matrix

$$\mathcal{F}(\theta) = \begin{pmatrix} \mathcal{F}_{1,1}(\theta) & \dots & \mathcal{F}_{1,m}(\theta) \\ \mathcal{F}_{2,1}(\theta) & \dots & \mathcal{F}_{2,m}(\theta) \\ \vdots & \vdots & \vdots \\ \mathcal{F}_{m,1}(\theta) & \dots & \mathcal{F}_{m,m}(\theta) \end{pmatrix}$$

is continuous in θ and its determinant is non-zero : $\det \mathcal{F}(\theta) \neq 0$.

Theorem 1 (Cramér-Rao inequality). *Let $\hat{\theta} \in \mathcal{K}_b$ be an estimator. If the conditions of regularity R 1 and R 2 are satisfied, then*

$$V_\theta(\hat{\theta}) \geq \frac{1}{n}(I_m + B'(\theta))\mathcal{F}^{-1}(\theta)(I_m + B'(\theta))^T$$

where I_m is the identity matrix of order m , $B'(\theta)$ is the square matrix of order m :

$$B'(\theta) = \begin{pmatrix} b'_{1,1}(\theta) & \dots & b'_{1,m}(\theta) \\ b'_{2,1}(\theta) & \dots & b'_{2,m}(\theta) \\ \vdots & \vdots & \vdots \\ b'_{m,1}(\theta) & \dots & b'_{m,m}(\theta) \end{pmatrix}$$

where $b'_{i,j}(\theta) = \frac{\partial b_i}{\partial \theta_j}(\theta)$ and $b(\theta) = (b_1(\theta), \dots, b_m(\theta))^T$, $i, j = 1, \dots, m$.

For the class \mathcal{K}_0 of unbiased estimators, the so-called *Cramér-Rao lower bound* is

$$V_\theta(\hat{\theta}) \geq \frac{1}{n}\mathcal{F}^{-1}(\theta).$$

Fisher Information

In the above discussion, the quality of Fisher information plays a very important role in parameter estimation. Let us now discuss this quality more details on the scalar case.

Definition 5. *Let us consider a parametric family $\mathcal{P} = \{P_\theta\}_{\theta \in \Theta}$. The observations ξ_1, \dots, ξ_n are assumed to come from P_θ , where $P_\theta \in \mathcal{P}$. It is assumed that P_θ admit the PDF $f_\theta(x)$. The Fisher information about θ contained in the sample $\Xi = (\xi_1, \dots, \xi_n)$ is*

$$\mathcal{F}_n(\theta) = \mathbb{E}_\theta \left[\left(\frac{\partial L(\Xi, \theta)}{\partial \theta} \right)^2 \right] = \mathbb{E}_\theta \left[\left(\frac{f'_\theta(\Xi)}{f_\theta(\Xi)} \right)^2 \right] = \int \cdots \int \frac{f'_\theta(X)}{f_\theta(X)} dx_1 \cdots dx_n,$$

where $L(\Xi, \theta) = \sum_{i=1}^n \log f_\theta(\xi_i)$, $X = (x_1, \dots, x_n)^T$ and $f'_\theta(X) = \frac{\partial f_\theta}{\partial \theta}(X)$.

Lemma 2 (Fisher information property). Let us assume that $\xi \sim P_\theta$ is a random variable which is defined on \mathcal{D} . If the domain \mathcal{D} doesn't depend on θ , we have

$$\mathcal{F}_n(\theta) = \mathbb{E}_\theta \left[\left(\frac{\partial L(\Xi, \theta)}{\partial \theta} \right)^2 \right] = -\mathbb{E}_\theta \left(\frac{\partial^2 L(\Xi, \theta)}{\partial \theta^2} \right)$$

Example I.3.1 Let us consider the linear model often arising in the regression analysis :

$$\begin{pmatrix} y_1 \\ y_2 \\ \vdots \\ y_n \end{pmatrix} = \begin{pmatrix} h_{11} & h_{12} & \cdots & h_{1r} \\ h_{21} & h_{22} & \cdots & h_{2r} \\ \vdots & \vdots & \ddots & \vdots \\ h_{n1} & h_{n2} & \cdots & h_{nr} \end{pmatrix} \cdot \begin{pmatrix} \theta_1 \\ \theta_2 \\ \vdots \\ \theta_r \end{pmatrix} + \begin{pmatrix} \varepsilon_1 \\ \varepsilon_2 \\ \vdots \\ \varepsilon_n \end{pmatrix}, \quad (\text{I.19})$$

where $Y = H\theta + \Xi$, the vector Y are the responses, the matrix of regressors H consists of n observations on each of the r independent variables. The vector θ is unknown and must be estimated. The vector Ξ contains random noise terms which are independently distributed with zero mean and variance σ^2 .

Let us suppose that $n > r$ and the columns of the matrix H are linearly independent. The likelihood function of the sample Y for given H is equal to

$$f_\theta(Y) = \frac{1}{(2\pi)^{\frac{n}{2}} \sigma^n} \exp \left\{ -\frac{1}{2\sigma^2} \sum_{i=1}^n \left(y_i - \sum_{j=1}^r \theta_j h_{ij} \right)^2 \right\} = \frac{1}{(2\pi)^{\frac{n}{2}} \sigma^n} \exp \left\{ -\frac{1}{2\sigma^2} \|Y - H\theta\|_2^2 \right\}.$$

Maximum likelihood method is applied to estimate the unknown vector θ :

$$\hat{\theta} = \arg \max_{\theta} f_\theta(Y) = \arg \min_{\theta} N^2(\theta) = \arg \min_{\theta} \|Y - H\theta\|_2^2.$$

Hence, in order to find $\hat{\theta}$ that maximizes the likelihood function, we must find $\hat{\theta}$ that minimizes the Euclidean norm of the squared error $N^2(\theta) = \|Y - H\theta\|_2^2$, that is to say, the maximum likelihood algorithm coincides here with the LS algorithm.

Necessary conditions for extremum : To find the critical point $\hat{\theta}$, we solve the system of n equations with r unknown variables $\theta_1, \dots, \theta_r$:

$$\vec{\text{grad}}N^2(\theta) = 2H^T H\theta - 2H^T Y = 0,$$

where the gradient vector $\vec{\text{grad}}f(X)$ is defined by

$$\vec{\text{grad}}f(X) = \begin{pmatrix} \frac{\partial f(X)}{\partial x_1} \\ \frac{\partial f(X)}{\partial x_2} \\ \vdots \\ \frac{\partial f(X)}{\partial x_n} \end{pmatrix} \text{ for the function } X \mapsto f(X), \text{ with } X = \begin{pmatrix} x_1 \\ x_2 \\ \vdots \\ x_n \end{pmatrix}, \quad (\text{I.20})$$

hence the critical point is

$$\hat{\theta} = (H^T H)^{-1} H^T Y.$$

Sufficient conditions for extremum : To investigate the nature of the critical point $\hat{\theta}$, sufficient conditions for extremum is used. Since the square matrix of second-order partial derivatives is equal to

$$\begin{pmatrix} \frac{\partial^2 N^2(\theta)}{\partial \theta_1^2} & \frac{\partial^2 N^2(\theta)}{\partial \theta_1 \partial \theta_2} & \cdots & \frac{\partial^2 N^2(\theta)}{\partial \theta_1 \partial \theta_r} \\ \frac{\partial^2 N^2(\theta)}{\partial \theta_2 \partial \theta_1} & \frac{\partial^2 N^2(\theta)}{\partial \theta_2^2} & \cdots & \frac{\partial^2 N^2(\theta)}{\partial \theta_2 \partial \theta_r} \\ \vdots & \vdots & \ddots & \vdots \\ \frac{\partial^2 N^2(\theta)}{\partial \theta_r \partial \theta_1} & \frac{\partial^2 N^2(\theta)}{\partial \theta_r \partial \theta_2} & \cdots & \frac{\partial^2 N^2(\theta)}{\partial \theta_r^2} \end{pmatrix} = H^T H, \quad (\text{I.21})$$

accordingly, it is positive definite, the function $\theta \mapsto \|Y - H\theta\|_2^2$ admits a minimum at the critical point $\hat{\theta}$.

Properties of maximum likelihood estimator : Let us now find the statistical properties of this estimator. Because $Y = H\theta + \Xi$, it's evident that

$$\hat{\theta} = (H^T H)^{-1} H^T (H\theta + \Xi) = \theta + (H^T H)^{-1} H^T \Xi.$$

It can be concluded that this estimator is unbiased, because the expectation can be calculated as

$$\mathbb{E}(\hat{\theta} - \theta) = \mathbb{E}[(H^T H)^{-1} H^T \Xi] = 0.$$

The matrix of central moments of second order of this estimator is equal to

$$\text{var}(\hat{\theta}) = \mathbb{E}[(\hat{\theta} - \theta)^T (\hat{\theta} - \theta)] = \mathbb{E}[(H^T H)^{-1} H^T \Xi \Xi^T H (H^T H)^{-1}] = \sigma^2 (H^T H)^{-1}.$$

Now it is also interesting to compare the variance of this estimator with the Cramér-Rao lower bound in the class $\mathcal{K}_0 = \{\hat{\theta} : \mathbb{E}(\hat{\theta} - \theta) = 0\}$ of unbiased estimator :

$$\text{var}(\hat{\theta}) \geq \frac{1}{n} \mathcal{F}^{-1}(\theta) = \mathcal{F}_n^{-1}(\theta), \quad (\text{I.22})$$

where the Fisher matrix

$$\mathcal{F}_n(\theta) = \begin{pmatrix} \mathcal{F}_{n;1,1}(\theta) & \cdots & \mathcal{F}_{n;1,r}(\theta) \\ \mathcal{F}_{n;2,1}(\theta) & \cdots & \mathcal{F}_{n;2,r}(\theta) \\ \vdots & \ddots & \vdots \\ \mathcal{F}_{n;r,1}(\theta) & \cdots & \mathcal{F}_{n;r,r}(\theta) \end{pmatrix}$$

and $\mathcal{F}_{n;i,j}(\theta) = \mathbb{E}_\theta \left[\frac{\partial l(Y, \theta)}{\partial \theta_i} \frac{\partial l(Y, \theta)}{\partial \theta_j} \right]$, $l(Y, \theta) = \log f_\theta(Y)$, the PDF $f_\theta(Y) = \frac{1}{(2\pi)^{\frac{n}{2}} \sigma^n} \exp \left\{ -\frac{1}{2\sigma^2} \|Y - H\theta\|_2^2 \right\}$. It follows that

$$\begin{aligned}\mathcal{F}_n(\theta) &= \frac{1}{\sigma^4} \mathbb{E}_\theta [\vec{\text{grad}} \|Y - H\theta\|_2^2 \vec{\text{grad}}^T \|Y - H\theta\|_2^2] \\ &= \frac{1}{\sigma^4} \mathbb{E}_\theta [(H^T H\theta - H^T Y)(H^T H\theta - H^T Y)^T] \\ &= \frac{1}{\sigma^4} \mathbb{E}_\theta (H^T \Xi \Xi^T H) = \frac{1}{\sigma^2} H^T H,\end{aligned}$$

and for the class \mathcal{K}_0 of unbiased estimators, the Cramér-Rao lower bound is

$$\text{var}(\hat{\theta}) \geq \frac{1}{n} \mathcal{F}^{-1}(\theta) = \sigma^2 (H^T H)^{-1}. \quad (\text{I.23})$$

Hence, the maximum likelihood estimator is unbiased and efficient.

Example I.3.2 Let us consider the nonlinear model often arising in the regression analysis (G.Seber et C.Wild - 1988) : suppose that we have n observations (X_i, y_i) , $i = 1, 2, \dots, n$, from a non-random regressor nonlinear model with a known functional relationship f . Thus

$$y_i = f(X_i; \theta) + \varepsilon_i \quad (i = 1, 2, \dots, n),$$

where X_i is a $k \times 1$ vector, $\varepsilon_i \sim \mathcal{N}(0, \sigma^2)$ is a random noise, each $f(X_i; \theta)$ is differentiable with respect to θ and the vector $\theta \in \Theta \subseteq \mathbb{R}^m$ is unknown and must be estimated. We shall use the notation $Y = (y_1, y_2, \dots, y_n)^T$, $f_i(\theta) = f(X_i; \theta)$ and

$$f(\theta) = (f_1(\theta), f_2(\theta), \dots, f_n(\theta))^T.$$

Let us start by first noting that a working point θ_0 and the true value θ , we have the linear Taylor expansion

$$f(\theta) \simeq f(\theta_0) + H_0 \cdot (\theta - \theta_0),$$

where the coefficients of the Jacobian matrix H_0 of size $(n \times m)$ are

$$h_{ij} = \left. \frac{\partial f_i}{\partial \theta_j} \right|_{\theta=\theta_0}.$$

Hence, the problem of a nonlinear model can be reduced to that of a linear model. The nonlinear model can be rewritten as follows

$$Y - f(\theta_0) \simeq H_0 \cdot (\theta - \theta_0) + \Xi, \quad (\text{I.24})$$

where H_0 is a full rank matrix of size $(n \times m)$, $\Xi = (\varepsilon_1, \dots, \varepsilon_n)^T$. The iterative LS algorithm provides us with an optimal solution. We compute the LS estimate $\hat{\theta}$ by using the responses Y and the working point θ_0 :

$$\hat{\theta} = \theta_0 + (H_0^T H_0)^{-1} H_0^T [Y - f(\theta_0)].$$

Then, the working point is set to be $\theta_0 = \hat{\theta}$ for the next iteration. Usually only two or three steps are necessary to reach the convergence of the iterative process. The stopping rule is defined as follows :

$$\text{stop the iterations if } \|\hat{\theta} - \theta_0\|_2 = \|(H_0^T H_0)^{-1} H_0^T [Y - f(\theta_0)]\|_2 \leq \varsigma, \quad (\text{I.25})$$

where ς is a small positive constant. When the convergence has been reached, the residual vector e is given by the following equation

$$e = Y - f(\theta_0), \quad (\text{I.26})$$

where the working point is equal to the estimation after the final iteration, i.e., $\theta_0 = \hat{\theta}$.

Properties of maximum likelihood estimator : It is very difficult to calculate the bias and variance of the estimator in the nonlinear model. The bias and variance are functions of certain arrays of projected second derivatives called curvature arrays. These arrays are fundamental to the study of nonlinearity. The estimator $\hat{\theta}$ has a bias $b(\theta)$ with a variance-covariance matrix $\text{var}(\hat{\theta})$. Let us first consider the QR decomposition of the $n \times m$ matrix H_0 (assumed to have rank m), namely

$$H_0 = QR_1 = \left(\begin{array}{c|c} Q_m & Q_{n-m} \end{array} \right) \left(\begin{array}{c} R_{11} \\ \hline \mathbf{0} \end{array} \right) = Q_m R_{11}, \quad (\text{I.27})$$

where Q is an orthogonal matrix. R_{11} is a nonsingular upper triangular matrix. If R_{11} is unique, then the matrix Q_m can be calculated as

$$Q_m = H_0 R_{11}^{-1} = H_0 K. \quad (\text{I.28})$$

Then we also have the following quadratic Taylor approximation :

$$f(\theta) \simeq f(\theta_0) + H_0 \cdot (\theta - \theta_0) + \frac{1}{2} (\theta - \theta_0)^T J_0 (\theta - \theta_0),$$

where J_0 is a three-dimensional $n \times m \times m$ array with typical element

$$j_{irs} = \left. \frac{\partial^2 f_i}{\partial \theta_r \partial \theta_s} \right|_{\theta=\theta_0}.$$

The bias $b(\theta)$ in nonlinear estimation is given by

$$b(\theta) = \mathbb{E}(\hat{\theta} - \theta) = -\frac{1}{2}\sigma^2 K \sum_{r=1}^m a'_{rr},$$

where K is available from equation (I.28), and a'_{rr} , $r = 1, \dots, m$ is the m -dimensional vectors, extracted from the $m \times m \times m$ array $A' = [Q_m^T][K^T J_0 K]$. Here, we define square-bracket by the equation

$$[D][W] = \{(Dw_{rs})\},$$

where D is a $q \times n$ matrix, $W = \{(w_{rs})\}$ is a $n \times m \times m$ array made up of a $m \times m$ array of n -dimensional vectors w_{rs} ($r, s = 1, 2, \dots, m$). The right-hand side $\{(Dw_{rs})\}$ is a $q \times m \times m$ array. For the variance, we have

$$\text{var}(\hat{\theta}) = \sigma^2 (H_0^T H_0)^{-1} + \sigma^4 K \left[\sum_{i=1}^{n-m} (A''_{i,\cdot,\cdot})^2 + \frac{1}{2} L \right] K^T, \quad (\text{I.29})$$

where $A''_{i,\cdot,\cdot}$, $i = 1, \dots, n-m$ is the i -th slice of the $(n-m) \times m \times m$ array $A'' = [Q_{n-m}^T][K^T J_0 K]$. L is a $m \times m$ matrix with element $l_{rs} = \text{tr}(A'_{r,\cdot,\cdot} A'_{s,\cdot,\cdot})$. $A'_{r,\cdot,\cdot}$ and $A'_{s,\cdot,\cdot}$ ($r, s = 1, 2, \dots, m$) denote the r -th and s -th slice of array A' , respectively. From (I.29) we can see that the first term, namely $\sigma^2 (H_0^T H_0)^{-1}$, is the variance-covariance matrix of $\hat{\theta}$ when the linear approximation is valid. The second term underlines the effect of the nonlinearity on the variance.

I.4 Contributions

The analysis, described in this thesis, can be divided into three parts.

In the first part, an "ideal" railway centerline, composed of straight line segments, transition curves and arcs of circles, is defined by parametric equation. The goal of this part is to estimate the train travelled distance and speed by using a low-cost GNSS receiver and to study the impact of railway curvature on these estimations. Two cases are studied : a constant and variable speed. For both cases, a LS estimator is designed. For the constant speed case, it is assumed that the train travels along the "ideal" railway centerline with a constant speed. The LS algorithm is designed to estimate the train speed by using the GNSS signals and the railway centerline geometric model. The impact of the railroad curvature on the mean error and on the

second order moment of the estimated speed is estimated. Then it is assumed that the train speed is variable. Assuming that the train acceleration is constant over a short time period, a LS algorithm is designed by using the GNSS signals and the train dynamical model. The algorithm exploits a block of GNSS measurements to succeed in estimating simultaneously the travelled distance, the speed and the acceleration of the train. Using a block of measurements is necessary to overcome the ill-posed nature of the estimation problem. The impact of the railroad curvature on the mean error and on the second order moment of these three estimations is estimated. For both cases, the equations for first two moments of the estimated speed and these three estimations are obtained and compared with the results of Monte-Carlo simulations.

In the second part, a "non-ideal" railway centerline is approximated by a polygonal line with some level of uncertainty. It represents a piecewise linear approximation of the "ideal" model. We also consider two cases : a constant and variable speed. For both cases, a LS estimator is designed. For the constant speed case, the train speed is calculated by using GNSS signals and the "non-ideal" railway centerline. The negative impact of the railway centerline uncertainty on the mean error and on the second order moment of the estimated speed is estimated. For the variable speed case, we also exploit a block of GNSS measurements to estimate the travelled distance, speed and acceleration. The negative impact of the railway centerline uncertainty on the mean error and on the second order moment of these three estimations is estimated. For both cases, the equations for first two moments of the estimated speed and these three estimations are obtained and compared with the results of Monte-Carlo simulations.

At last, we consider that the railway centerline geometry can provide the users with some very reliable *a priori* information on the smooth character of the train trajectory. But this information is available within a track database with measurement errors. The train travelled distance and speed is estimated by integrating the GNSS signals with this database information. Two cases are studied : a constant and variable speed. For both cases, a rigorous mathematical model for the GNSS/track database integrated system is designed. Then the impact of errors in this integrated system on these estimations is studied.

I.5 Thesis Structure

This thesis is organized as follows.

Chapter II describes the method of train travelled distance and speed estimation by using GNSS signals and an "ideal" railway centerline. Then the impact of the railroad curvature on the train speed and distance estimation is studied.

Chapter III describes the method of train travelled distance and speed estimation by using GNSS signals and a "non-ideal" railway centerline. Then the impact of the track geometric model imprecision on the train speed and distance estimation is studied.

Chapter IV describes the method of train travelled distance and speed estimation by integrating the GNSS measurements with the track database. Then the impact of the GNSS measurements and the track database errors on the train speed and distance estimation is studied.

Chapter V concludes the thesis and discusses the future work.

Chapitre II

Distance and Speed Estimation Based on GNSS and an "Ideal" Train Track

II.1 Introduction

In this chapter, the "ideal" model of railway centerline is composed of straight line segments, transition curves and arcs of circles, defined by parametric equations. The goal of this chapter is to estimate the travelled distance and speed of the train by using a low-cost GNSS receiver and to study the impact of railroad curvature on these estimations. Two cases are studied : a constant and variable speed. For both cases, a LS estimator is designed. The mean error and the second order moment are theoretically calculated for these estimations and compared with the results of Monte-Carlo simulations.

II.2 Track Geometry Design

Track geometry is 3D geometry of track layouts and associated measurements used in design, construction and maintenance of railroad tracks (Lindahl - 2001). The subject is used in the context of standard, speed limits and other regulations in the areas of track gauge, alignment, elevation, curvature and track. In this section several important quantities of track geometry will be introduced as follows

- Track gauge
- Track cant
- Transition curve and superelevation ramp

- Horizontal curve radius
- Vertical curve and gradient

Track Gauge

Track gauge is the distance between the inner sides (gauge sides) of the heads of the two load bearing rails that make up a single railway line (see Fig. II.1). Each country uses different gauges for different types of trains. Standard track gauge is 1435 mm.



Figure II.1 – Track gauge.

Track Cant

In curved track, it is designed to raise the outer rail, allowing trains to maneuver through the curve at higher speeds if the surface was flat. The difference in elevation between the outer rail and the inner rail is called cant (also called superelevation) and is arranged to compensate part of the lateral acceleration (see Fig. II.2). A cant angle arises where a cant is arranged. The cant angle is defined as

$$\varphi_t = \arcsin \frac{h_t}{2b_o}, \quad (\text{II.1})$$

where $2b_o = 1.5$ m on standard track gauge.

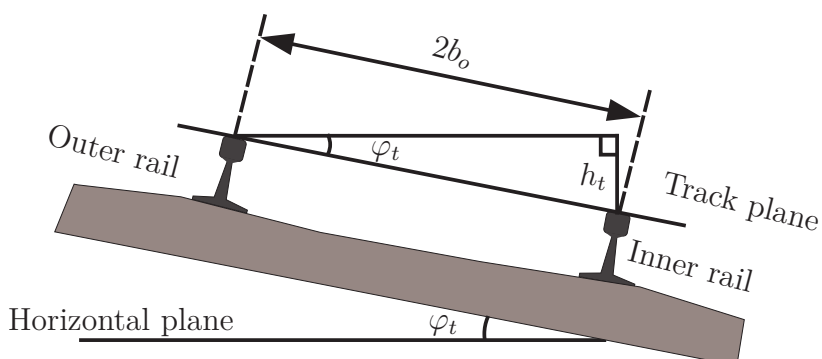


Figure II.2 – Cant h_t and cant angle φ_t .

A maximum value of cant is set for cant because of the following problems which arise if a train is forced to stop or run slowly in a curve :

- passenger discomfort at standstill or low speed ;
- risk of derailment of freight trains in sharp curves due to the combined effect of high lateral and low vertical load on the outer wheel at low speed ;
- possible displacement of wagon loads.

Transition Curve and Superelevation Ramp

In track geometry, the horizontal layout includes the layout of three main track types : tangent track (straight line), curved track and transition curve which connects between a straight line and a curved track (Deakin - 2013a). There are two types of transition curves that are commonly used in railway horizontal alignment : (1) Clothoid ; (2) Cubic parabola. As shown in Fig. II.3, a transition curve AD connects the straight $A'A$ and the circular curve of radius R whose center is O . The transition curve has an infinite radius at A , decreasing gradually to a radius of R at D .

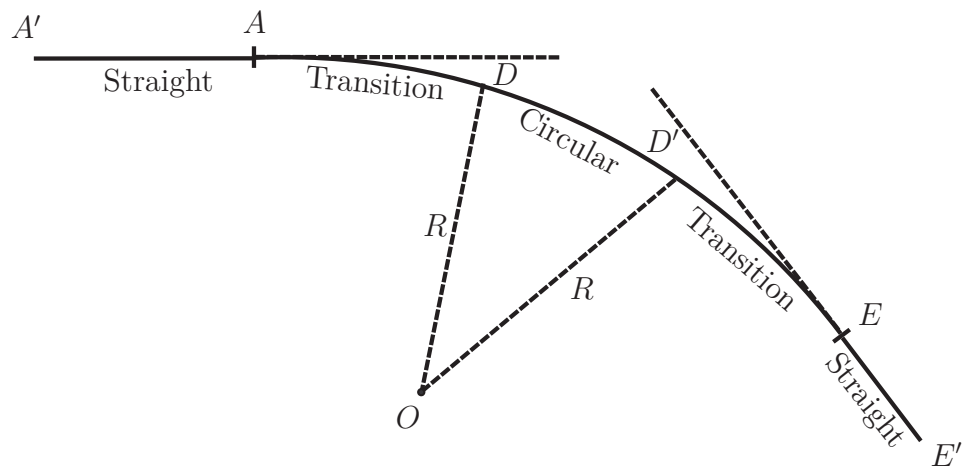


Figure II.3 – A transition curve connecting between the straight line and circular curve.

Transition curves introduce cant via superelevation ramps. A superelevation ramp is a section of the track where the cant changes gradually.

Horizontal Curve Radius

The radius R is the radius of the circle at the center line of the track (see Fig. II.4). The radius is inverse proportional to curvature, $\kappa = \frac{1}{R}$. The shorter the radius, the sharper the curve is. Due to the limitation of maximum speed of train, there is a

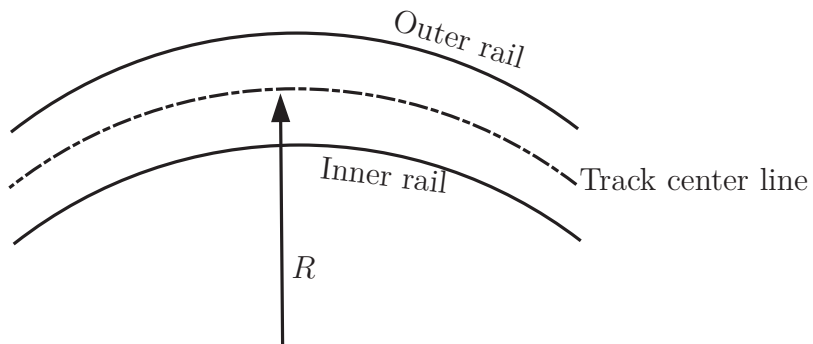


Figure II.4 – The definition of circular curve radius R .

boundary value of minimum curve radius to control the sharpness of all curves along the railway track.

Vertical Curve and Gradient

The topographical conditions usually require some kind of vertical-longitudinal gradients. Track gradient is relative elevation of the two rails along the track, which can be defined by the distance travelled horizontally for a rise of one unit, or in terms of an angle of inclination or a percentage difference in elevation for a given distance of the track (Dingwall - 1998). As shown in Fig. II.5, the gradient is given by

$$\text{grad} = \frac{\Delta h}{d} \quad \text{or} \quad \text{grad} = \tan \alpha. \quad (\text{II.2})$$

In road and railway design, gradients are usually expressed in percentage; e.g., a road of $+g\%$ gradient rises g units vertically in 100 units horizontally (Deakin - 2013b). Gradients rising from left to right are positive and falling left to right are negative.

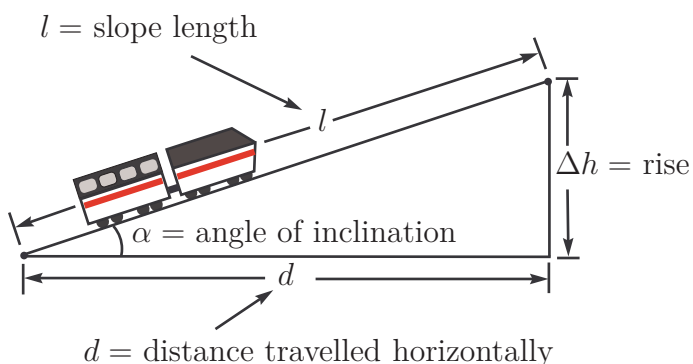


Figure II.5 – Track gradient.

A vertical curve is used to allow vehicles to pass smoothly from one gradient to another. Vertical curves connect two gradients, the gradient to the left of the vertical curve will be denoted by $g_1\%$ and the gradient to the right will be denoted by $g_2\%$. L_t is the length of the curve between the tangent points ta and tb (see Fig. II.6).

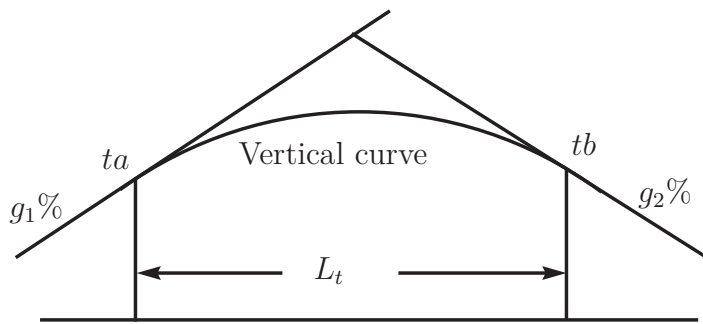


Figure II.6 – A vertical curve between two adjacent gradients.

II.3 Description of "Ideal" Train Track Models

As described in Section II.2, the horizontal alignment of a transportation engineering design is constructed as a combination of straight line segments and arcs of circles. On the straight line segment the vehicle can travel at a constant direction, whereas the circular curves are used so that the vehicle can change the travel direction (Gikas et Stratakos - Mar. 2012). However, to achieve the safety and comfort, a transition curve should be interposed for transition from rectilinear to curvilinear motion. Clothoid curves or cubic parabolas can be used for this purpose. In railway engineering the curve commonly used by many railway authorities is the cubic parabola (Profillidis - 2006; Mo.S.SA; Mundrey - 2007).

In this section, the railway track consists of a series of three typical segments (straight line-cubic parabola-circle arc-cubic parabola-straight line), as shown in Fig. II.3. Hence, we discuss three connected typical segments in the entire train trajectory. It's sufficient to study the impact of railroad curvature on the estimated travelled distance and speed of the train in the following section.

The straight line segment, transition curve and circular arc are described by equations formulated in terms of the curvilinear abscissa ℓ . To seek simplicity, let us assume that the track completely belongs to the local tangent plane. Fig. II.7 shows

three connected typical segments $[\ell_m; \ell_{m+1}]$, $[\ell_{m+1}; \ell_{m+2}]$ and $[\ell_{m+2}; \ell_{m+3}]$ indexed by ℓ_m which is the covered distance corresponding to the m -th segment ($m = 1, 2, \dots$).

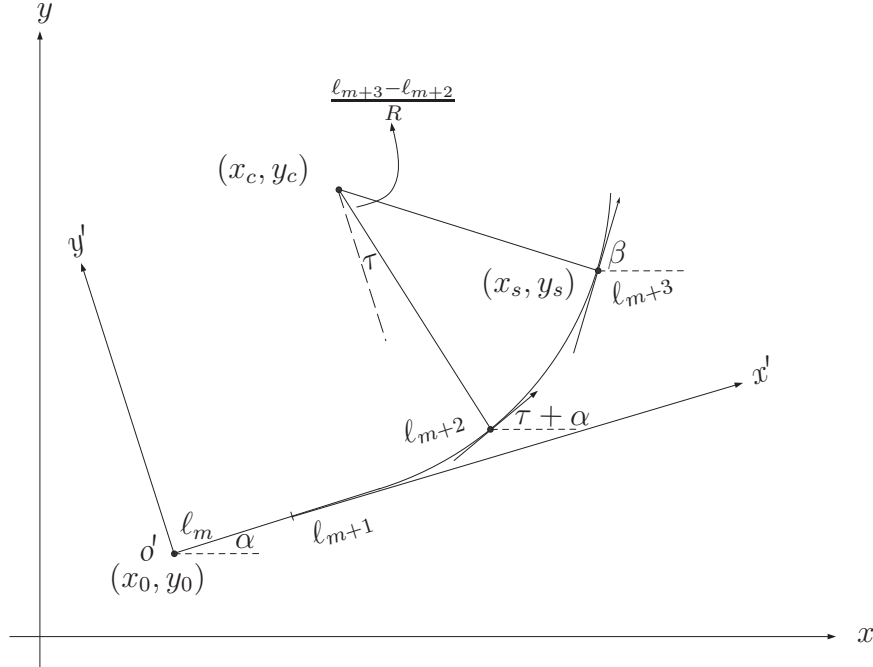


Figure II.7 – Train track composed of three segments on the local tangent plane.

Straight Line Segment

The straight line segment provides a stretch of railway track, on which the train runs at a constant direction. On the straight line, curvature is zero. The equation for the straight line segment ($\ell_m \leq \ell \leq \ell_{m+1}$) which is shown in Fig. II.7 is

$$\begin{cases} x(\ell) = x_0 + (\ell - \ell_m) \cdot \cos \alpha \\ y(\ell) = y_0 + (\ell - \ell_m) \cdot \sin \alpha, \end{cases} \quad (\text{II.3})$$

where (x_0, y_0) is the starting point of the m -th segment, ℓ denotes the curvilinear abscissa and α is the initial azimuth of the m -th segment.

Transition Curve

The transition curve is used for connecting the straight line segments and circular arcs. Its radius of curvature r gradually changes from infinity (straight line) to a particular value R (radius of circular arc). The length of transition curve must be designed so that it minimizes passenger discomfort and maximizes safety (Caulfield - 2012). The transition curve is illustrated in Fig. II.8.

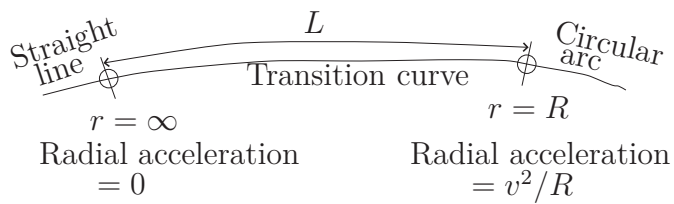


Figure II.8 – Determination of transition curve length.

Let us suppose that a vehicle of mass m travels, at a constant speed v , along a curve of radius r . At any point the radial force is $F = mv^2/r$, so the radial acceleration at any point is $a_r = v^2/r$. Hence, the passenger discomfort and safety risks (which directly depend on the radial force) increase as a_r increases. Design standards recommend the maximum value $0.3\ m^2/s$ for a_r above which passenger discomfort takes place (Caulfield - 2012). The transition curve length L can be determined from a_r by the formula $L = v^3/(a_r R)$ where v is in m/s .

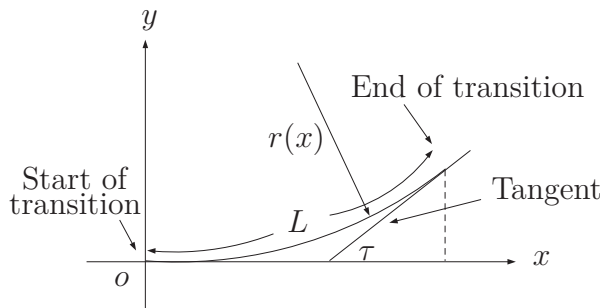


Figure II.9 – Example of transition curve.

Let us draw the transition curve, keeping the tangent track horizontal, as shown in Fig. II.9. With the transition curve length L and the radius R at the end of transition curve, the equation for cubic parabola is given by (Shen et al. - 2013; Sood)

$$y = k_c \cdot x^3 \quad \text{with} \quad k_c = \frac{1}{6RL}. \quad (\text{II.4})$$

For example, when the radius $R = 7000\ m$ and the transition curve length $L = 275\ m$, the coefficient is $k_c = 5.1948 \times 10^{-7}$. Let $L(x)$ be the length of the cubic parabola from the start of transition until the point with abscissa x . The length $L(x)$ is given by

$$L(x) = \int_0^x \sqrt{1 + 9k_c^2 \cdot u^4} du. \quad (\text{II.5})$$

This integral can be calculated by using the following power series :

$$\sqrt{1 + 9k_c^2 \cdot u^4} \simeq 1 + \frac{1}{2} \cdot 9k_c^2 \cdot u^4 + \dots, \quad (\text{II.6})$$

which is valid for $9k_c^2 \cdot u^4 < 1$. The terms after the second one in the right side of equation (II.6) can be neglected. Integrating the power series between 0 and x , we get

$$L(x) = \int_0^x \sqrt{1 + 9k_c^2 \cdot u^4} du \simeq x. \quad (\text{II.7})$$

Hence, in the transition curve equation (II.4), the cartesian abscissa x can be replaced by the curvilinear abscissa $L(x)$. It follows that the equation for the cubic parabola ($\ell_{m+1} < \ell \leq \ell_{m+2}$) in Fig. II.7 is well approximated by

$$\begin{cases} x(\ell) = x_0 + (\ell - \ell_m) \cos \alpha - k_c(\ell - \ell_{m+1})^3 \sin \alpha \\ y(\ell) = y_0 + (\ell - \ell_m) \sin \alpha + k_c(\ell - \ell_{m+1})^3 \cos \alpha. \end{cases} \quad (\text{II.8})$$

The calculation of the radius of curvature is also of interest because it constantly changes on the transition curve. For the cubic parabola, the radius of curvature $r(x)$ at abscissa x is defined by

$$r(x) = \left| \frac{(1 + 9k_c^2 \cdot x^4)^{3/2}}{6k_c \cdot x} \right|, \quad (\text{II.9})$$

where $|\cdot|$ denotes the absolute value. Using equation (II.6) and equation (II.7), $r(x)$ is well approximated by

$$r(x) = \left| \frac{(1 + 9k_c^2 \cdot x^4)^{3/2}}{6k_c \cdot x} \right| \simeq \left| \frac{1}{6k_c \cdot x} \right| \simeq \left| \frac{R \cdot L}{L(x)} \right|. \quad (\text{II.10})$$

Hence, the curvature $1/r(x)$ for a cubic parabola is proportional to the covered length $L(x)$ and $r(L) = R$.

Circular Arc

The vehicle always changes its travel direction on the circular arc. On a curve of radius R , the curvature is $1/R$. The equation for the circular arc ($\ell_{m+2} < \ell \leq \ell_{m+3}$) illustrated in Fig. II.7 is

$$\begin{cases} x(\ell) = x_0 + x'(\ell) \cdot \cos \alpha - y'(\ell) \cdot \sin \alpha \\ y(\ell) = y_0 + x'(\ell) \cdot \sin \alpha + y'(\ell) \cdot \cos \alpha, \end{cases} \quad (\text{II.11})$$

where

$$\begin{cases} x'(\ell) = x_c + R \sin \left(\tau + \frac{\ell - \ell_{m+2}}{R} \right) \\ y'(\ell) = y_c - R \cos \left(\tau + \frac{\ell - \ell_{m+2}}{R} \right) \end{cases} \quad (\text{II.12})$$

is the representation of circular arc on the $x'y'$ -plane, $\tau = \arctan(3k_c L^2)$ is the angle of the tangent at the end of transition curve and

$$\begin{cases} x_c = L \cdot (1 - 9k_c^2 L^4)/2 + \ell_{m+1} - \ell_m \\ y_c = (1 + 15k_c^2 L^4)/6k_c L \end{cases} \quad (\text{II.13})$$

is the center of the circular arc.

II.4 Speed Estimation for a Constant Speed Case

This section assumes that the acceleration is negligible for some short periods. Hence, it is supposed that the train runs along the "ideal" railway track with an unknown constant speed v . The covered distance ℓ_t at time t is equal to the product of speed v and duration t , i.e., $\ell_t = v \cdot t$. Hence, the true train position at time t is defined as : $X_t = (x(\ell_t), y(\ell_t), 0)^T$, $t = 1, 2, \dots$, where $(x(\ell_t), y(\ell_t))$ is the corresponding position on the local tangent plane described in Section II.3.

II.4.1 Exact Pseudo-range Measurement Model and Estimation

Suppose that there are n satellites located at the known positions $X_i^s = (x_i, y_i, z_i)^T$, $i = 1, \dots, n$. The pseudo-range r_i^t from the i -th satellite to the train position X_t at time t can be written as :

$$\begin{cases} r_1^t = d_1^t(v) + cb_r^t + \varepsilon_1^t \\ r_2^t = d_2^t(v) + cb_r^t + \varepsilon_2^t \\ \vdots \quad \vdots \quad \vdots \quad \vdots \\ r_n^t = d_n^t(v) + cb_r^t + \varepsilon_n^t \end{cases} \quad (\text{II.14})$$

where $d_i^t(v) = \|X_t - X_i^s\|_2$, $i = 1, \dots, n$, is the true distance from the i -th satellite to the train. b_r^t is a user clock bias, $c \simeq 2.9979 \cdot 10^8 \text{ m/s}$ is the speed of light and $\varepsilon_i^t \sim \mathcal{N}(0, \sigma^2)$ is a pseudo-range noise, $\Xi^t = (\varepsilon_1^t, \dots, \varepsilon_n^t)^T$ is the vector of pseudo-range noises. Let us introduce the following vector : $R^t = (r_1^t, \dots, r_n^t)^T$. By linearizing the pseudo-range equation with respect to the state vector $V_t = (v_t, cb_r^t)^T$ around the working point

$V_0 = (v_0, cb_0)^T$, we get the measurement equation

$$\begin{pmatrix} y_1^t \\ y_2^t \\ \vdots \\ y_n^t \end{pmatrix} = \begin{pmatrix} r_1^t - r_{1,0}^t \\ r_2^t - r_{2,0}^t \\ \vdots \\ r_n^t - r_{n,0}^t \end{pmatrix} \simeq \begin{pmatrix} h_{1,0}^t & 1 \\ h_{2,0}^t & 1 \\ \vdots & \vdots \\ h_{n,0}^t & 1 \end{pmatrix} \cdot \begin{pmatrix} v_t - v_0 \\ cb_r^t - cb_0 \end{pmatrix} + \begin{pmatrix} \varepsilon_1^t \\ \varepsilon_2^t \\ \vdots \\ \varepsilon_n^t \end{pmatrix}, \quad (\text{II.15})$$

where $r_{i,0}^t = d_{i,0}^t(v_0) + cb_0$, $d_{i,0}^t(v_0) = \|X_{t,0} - X_i^s\|_2$ is the distance from the i -th satellite to the working point and $X_{t,0} = (x(\ell_{t,0}), y(\ell_{t,0}), 0)^T$, $\ell_{t,0} = v_0 \cdot t$ and the coefficients of the Jacobian matrix H_0^t of size $(n \times 2)$ are given by

$$h_{i,0}^t = \frac{(X_{t,0} - X_i^s)^T \cdot \frac{\partial X_t}{\partial v}|_{v=v_0}}{d_{i,0}^t(v_0)}.$$

The above mentioned linearized measurement equation (II.15) can be rewritten in the following matrix form

$$Y^t = R^t - R_0^t \simeq H_0^t \cdot (V_t - V_0) + \Xi^t, \quad (\text{II.16})$$

where H_0^t is a full rank matrix of size $(n \times 2)$ defined in equation (II.15), the vector $V_t = (v_t, cb_r^t)^T$ is unknown and must be estimated. The working point at instant t is equal to the previously calculated estimation : $V_0 = \hat{V}_{t-1}$. The LS estimator is given by

$$\hat{V}_t = \hat{V}_{t-1} + \left[(H_0^t)^T H_0^t \right]^{-1} (H_0^t)^T (R^t - R_0^t). \quad (\text{II.17})$$

II.4.2 Impact of The Curve Radius on The Estimation Error

The goal of this subsection is to study the impact of the railway curve radius R on the first and second moments of the LS estimator \hat{v}_t . To do this, we firstly expand the pseudo-range equation (II.14) to second order with respect to v around the working point v_0 , and then the measurement equation (II.15) can be written in the matrix form :

$$R^t - R_0^t \simeq H_0^t \cdot (V_t - V_0) + \frac{1}{2} J_0^t \cdot (v_t - v_0)^2 + \Xi^t, \quad (\text{II.18})$$

where $J_0^t = (j_{1,0}^t, j_{2,0}^t, \dots, j_{n,0}^t)^T$ and $j_{i,0}^t = \left. \frac{\partial^2 [d_i^t(v)]}{\partial v^2} \right|_{v=v_0}$. Due to the presence of J_0^t , this equation underlines the role of the railway track curve radius in the measurement model.

The current estimation error is $\hat{V}_t - V_t$. After substituting the right side of equation (II.18) into the LS estimator (II.17), we look at the mean of this error which is computed

as

$$\mathbb{E}(\hat{V}_t - V_t) = \mathbb{E} \left\{ B_0^{-1} (H_0^t)^T \left[\frac{1}{2} J_0^t \cdot (v_t - v_0)^2 + \Xi^t \right] \right\}, \quad (\text{II.19})$$

where $B_0 = (H_0^t)^T H_0^t$. If the random vector Ξ^t is close enough to its mean $\mathbb{E}(\Xi^t) = \mathbf{0}_n$, we use the delta method and get

$$\mathbb{E}(\hat{V}_t - V_t) \simeq \frac{1}{2} \bar{B}_0^{-1} (\bar{H}_0^t)^T \bar{J}_0^t \cdot (v_t - v_0)^2, \quad (\text{II.20})$$

where $\bar{B}_0 = (\bar{H}_0^t)^T \bar{H}_0^t$. The matrices \bar{H}_0^t and \bar{J}_0^t are calculated exactly as in equation (II.18) but with the working point $v_0 = v_{t-1}$.

For the second order moment of the estimation error $\hat{V}_t - V_t$, the delta method yields to

$$\mathbb{E}(\hat{V}_t - V_t)(\hat{V}_t - V_t)^T \simeq \frac{1}{4} \bar{B}_0^{-1} (\bar{H}_0^t)^T \bar{J}_0^t (\bar{J}_0^t)^T \bar{H}_0^t \bar{B}_0^{-1} (v_t - v_0)^4 + \sigma^2 \bar{B}_0^{-1}. \quad (\text{II.21})$$

The Delta Method (Oehlert - 1992; Feiveson - 2008)

The delta method is a technique for approximating the moments of functions of random variables. It essentially expands a function of a random variable about its mean, with the Taylor approximation, and then takes the variance.

Scalar Case

Let ξ be a random variable with mean μ_ξ and there exists a function $g(\xi) : \xi \mapsto g(\xi)$, which is differentiable. If we want to approximate the variance of $g(\xi)$, then we can try

$$g(\xi) \simeq g(\mu_\xi) + (\xi - \mu_\xi)g'(\mu_\xi),$$

so that

$$\text{var}(g(\xi)) \simeq \text{var}(\xi)[g'(\mu_\xi)]^2,$$

where $g'() = \frac{dg}{d\xi}$. This is a good approximation only if ξ has a high probability of being close enough to its mean μ_ξ so that the Taylor approximation is still good.

Vector Case

It can be expanded to vector-valued functions of random vectors,

$$\text{var}(g(\xi)) \simeq g'(\mu_\xi) \text{var}(\xi) [g'(\mu_\xi)]^T,$$

and that, in fact, is the basis for deriving the asymptotic variance of maximum-likelihood estimators. In the above, ξ is a $1 \times m$ column vector, $\text{var}(\xi)$ is its $m \times m$ variance-covariance matrix ; $g()$ is a vector function returning a $1 \times n$ column vector ; and $g'()$ is its $n \times m$ of first derivatives. T is the transpose operator. $\text{var}(g(\xi))$ is the resulting $n \times n$ variance-covariance matrix of $g(\xi)$.

II.4.3 Numerical Simulations

The following scenario will be used in the sequel. The segments of the simulated train trajectory stored in the onboard train database are summarized in Tab. II.1. The centerline curvature and the simulated train trajectory are shown by Fig. II.10 and II.11, respectively. From Fig. II.11, it can be seen that two complete train trajectories are composed of straight line segments, transition curves and circular arcs of radius R . Moreover, these two trajectories of $R = 100$ m and $R = 1000$ m have the same travelled distances. The curvature of a transition curve gradually changes between zero and that of a circular arc, i.e. $1/R$ or $-1/R$, as shown in Fig. II.10.

m	Curves	Curvilinear abscissa	Curvature
1	Straight	$[\ell_1, \ell_2]$	0
2	Transition	$(\ell_2, \ell_3]$	$0 \rightarrow \frac{1}{R}$
3	Circular	$(\ell_3, \ell_4]$	$\frac{1}{R}$
4	Transition	$(\ell_4, \ell_5]$	$\frac{1}{R} \rightarrow 0$
5	Straight	$(\ell_5, \ell_6]$	0
6	Transition	$(\ell_6, \ell_7]$	$0 \rightarrow -\frac{1}{R}$
7	Circular	$(\ell_7, \ell_8]$	$-\frac{1}{R}$
8	Transition	$(\ell_8, \ell_9]$	$-\frac{1}{R} \rightarrow 0$
9	Straight	$(\ell_9, \ell_{10}]$	0

Tableau II.1 – Segments of the tested simulation scenario.

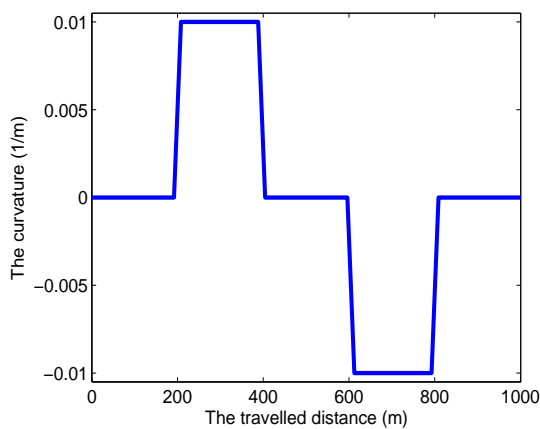


Figure II.10 – The centerline curvature of the tested simulation scenario.

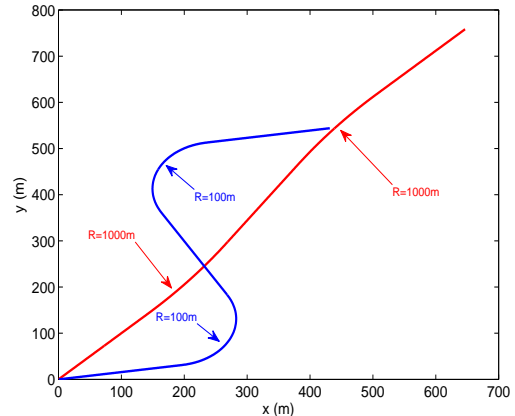


Figure II.11 – The simulated train trajectory on the local horizontal plane.

The standard GNSS constellation has been used with $n = 6$ visible satellites and with pseudo-range SD $\sigma = 2$ m. The satellite positions are supposed to be fixed, because

the satellites motions around the earth can be neglected during the short time period that the train runs on the railway track. That is to say, the impact of elevation angle and azimuth is negligible for our study. The GNSS sampling interval is $\Delta t = 0.5$ s. The true train speed is 20 m/s and the initial working point v_0 has been chosen as 10 m/s. Different values of minimum railway curve radius have been tested : $R = 100$ m and $R = 1000$ m. The comparison of first two moments of the estimated speed given by equation (II.20) and equation (II.21), respectively, with the results of a 10^4 -repetition Monte-Carlo simulation, is shown in Fig. II.12-II.15.

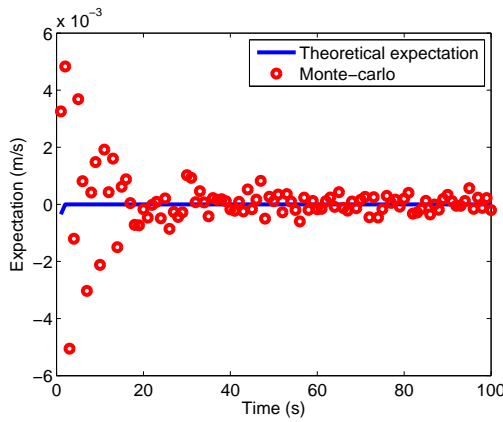


Figure II.12 – The estimated speed mean error for $R = 100$ m.

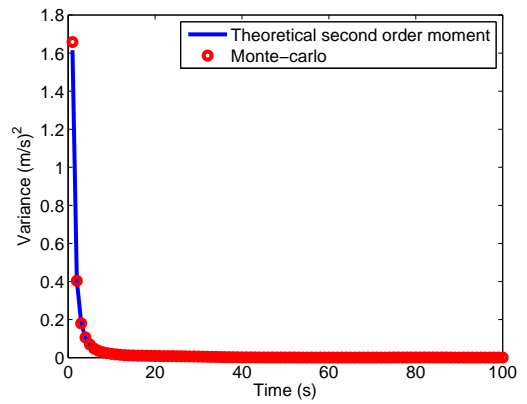


Figure II.13 – The estimated speed second order moment for $R = 100$ m.

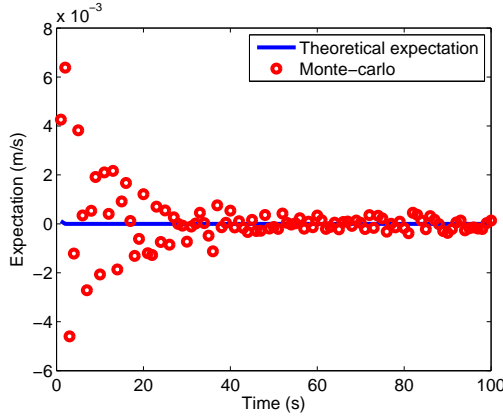


Figure II.14 – The estimated speed mean error for $R = 1000$ m.

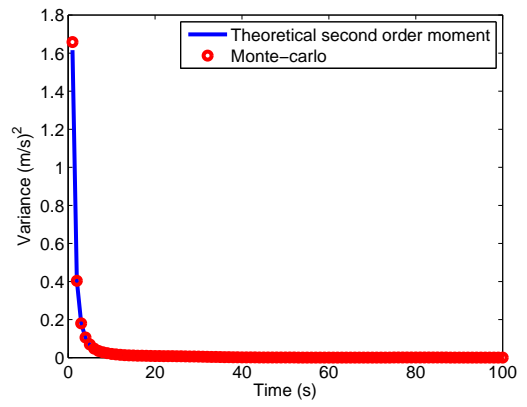


Figure II.15 – The estimated speed second order moment for $R = 1000$ m.

From Fig. II.14, it can be seen that the estimated speed mean error is approaching zero after a short time period due to the nonlinearity of the model. To estimate the

impact of the curvature on the estimated speed, we reduce the railway curve radius from $R = 1000$ m to $R = 100$ m and get a similar result, as shown in Fig. II.12. For the estimated speed second order moment, by comparison with Fig. II.13 and II.15, we can see that it quickly becomes very weak in both cases.

II.5 Distance and Speed Estimation for a Variable Speed Case

The goal of this section is to estimate the travelled distance and speed of the train when its acceleration is not neglected. Hence, it is assumed that the train runs along the "ideal" railway centerline with a variable speed. The train dynamical model is described by an equation formulated in terms of the travelled distance, speed and acceleration (see Fig. II.16).

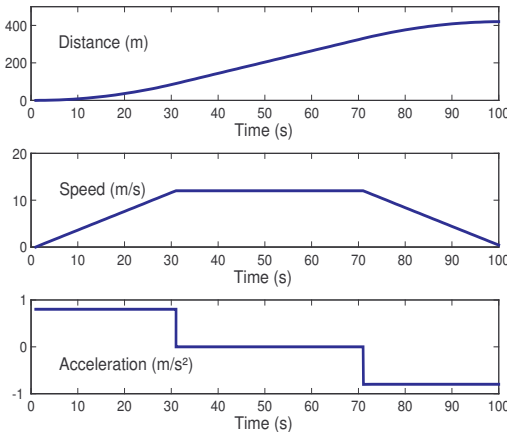


Figure II.16 – Typical train motion diagram.

Let $\Delta t = t_k - t_{k-1}$ be the GNSS sampling interval and t_k denotes the instant of the k -th measurement (GNSS epoch). Let us consider a short time period of length $T = (q + 1) \cdot \Delta t$ where q is a positive integer. Over this time period, the distance ℓ_k covered by the train, its speed v_k and its acceleration a_k at instant t_k ($1 \leq k \leq q$) are given as follows

$$\left\{ \begin{array}{l} \ell_k = \ell_{k-1} + v_{k-1} \cdot \Delta t + \frac{1}{2} a_{k-1} \cdot \Delta t^2 \\ v_k = v_{k-1} + a_{k-1} \cdot \Delta t \\ a_k = a_{k-1}. \end{array} \right. \quad (\text{II.22})$$

Let us consider the block of $q+1$ last GNSS measurements at time instant t_k . Assuming that the acceleration a_k is constant during T (s), the train position is given by

$$X(\ell_{k-q+p}) = [x(\ell_{k-q+p}), y(\ell_{k-q+p}), 0]^T,$$

where $(x(\ell_{k-q+p}), y(\ell_{k-q+p}))$ is the corresponding position on the local tangent plane described in Section II.3, $p = 0, 1, \dots, q$ and the distance is calculated as

$$\ell_{k-q+p} = \begin{pmatrix} 1 & (p-q) \cdot \Delta t & \frac{1}{2}(p-q)^2 \cdot \Delta t^2 \end{pmatrix} \begin{pmatrix} \ell_k \\ v_k \\ a_k \end{pmatrix} = \omega_p \cdot \theta_k, \quad (\text{II.23})$$

where the vector $\theta_k = (\ell_k, v_k, a_k)^T$ is unknown and must be estimated.

II.5.1 Exact Pseudo-range Measurement Model and Estimation

Suppose that there are n satellites located at the known positions $X_i^s = (x_i, y_i, z_i)^T$, $i = 1, \dots, n$. The pseudo-range r_{k-q+p}^i from the i -th satellite to the train position $X(\ell_{k-q+p})$ at time $k - q + p$ can be written as :

$$\begin{cases} r_{k-q+p}^1 = d_{k-q+p}^1(\ell_{k-q+p}) + cb_r^{k-q+p} + \varepsilon_{k-q+p}^1 \\ r_{k-q+p}^2 = d_{k-q+p}^2(\ell_{k-q+p}) + cb_r^{k-q+p} + \varepsilon_{k-q+p}^2 \\ \vdots \quad \vdots \quad \vdots \quad \vdots \\ r_{k-q+p}^n = d_{k-q+p}^n(\ell_{k-q+p}) + cb_r^{k-q+p} + \varepsilon_{k-q+p}^n \end{cases} \quad (\text{II.24})$$

where $p = 0, 1, \dots, q$, $d_{k-q+p}^i(\ell_{k-q+p}) = \|X(\ell_{k-q+p}) - X_i^s\|_2$, $i = 1, \dots, n$, is the true distance from the i -th satellite to the train. b_r^{k-q+p} is a user clock bias, $c \simeq 2.9979 \cdot 10^8 m/s$ is the speed of light and $\varepsilon_{k-q+p}^i \sim \mathcal{N}(0, \sigma^2)$ is the pseudo-range noise at time $k - q + p$. Let us introduce the following vector : $R_{k-q+p} = (r_{k-q+p}^1, \dots, r_{k-q+p}^n)^T$. By linearizing the pseudo-range equation with respect to the state variable ℓ_{k-q+p} around the working point $\ell_{k-q+p,0}$, we get the measurement equation

$$\begin{aligned} \begin{pmatrix} r_{k-q+p}^1 \\ r_{k-q+p}^2 \\ \vdots \\ r_{k-q+p}^n \end{pmatrix} - \begin{pmatrix} d_{k-q+p,0}^1 \\ d_{k-q+p,0}^2 \\ \vdots \\ d_{k-q+p,0}^n \end{pmatrix} &\simeq \begin{pmatrix} h_{k-q+p,0}^1 \\ h_{k-q+p,0}^2 \\ \vdots \\ h_{k-q+p,0}^n \end{pmatrix} \cdot (\ell_{k-q+p} - \ell_{k-q+p,0}) + \begin{pmatrix} cb_r^{k-q+p} \\ cb_r^{k-q+p} \\ \vdots \\ cb_r^{k-q+p} \end{pmatrix} \\ &+ \begin{pmatrix} \varepsilon_{k-q+p}^1 \\ \varepsilon_{k-q+p}^2 \\ \vdots \\ \varepsilon_{k-q+p}^n \end{pmatrix}, \end{aligned} \quad (\text{II.25})$$

where $d_{k-q+p,0}^i = d_{k-q+p}^i(\ell_{k-q+p,0}) = \|X(\ell_{k-q+p,0}) - X_i^s\|_2$ is the distance from the i -th satellite to the working point and the coefficients of the Jacobian matrix $H_{k-q+p,0}$ of size $(n \times 1)$ are given by

$$h_{k-q+p,0}^i = \frac{[X(\ell_{k-q+p,0}) - X_i^s]^T \cdot \left. \frac{\partial X(\ell_{k-q+p})}{\partial \ell_{k-q+p}} \right|_{\ell_{k-q+p,0}}}{\|X(\ell_{k-q+p,0}) - X_i^s\|_2}.$$

The above mentioned linearized measurement equations (II.25) can be rewritten in the following matrix form

$$R_{k-q+p} - D_{k-q+p,0} \simeq H_{k-q+p,0} \cdot (\ell_{k-q+p} - \ell_{k-q+p,0}) + \mathbf{1}_n \cdot cb_r^{k-q+p} + \Xi_{k-q+p}, \quad (\text{II.26})$$

where $\mathbf{1}_n$ is a vector of dimension n whose each element is one. It follows that

$$\begin{pmatrix} R_k \\ \vdots \\ R_{k-q} \end{pmatrix} - \begin{pmatrix} D_{k,0} \\ \vdots \\ D_{k-q,0} \end{pmatrix} \simeq \begin{pmatrix} H_{k,0} \cdot \ell_k + \mathbf{1}_n \cdot cb_r^k \\ \vdots \\ H_{k-q,0} \cdot \ell_{k-q} + \mathbf{1}_n \cdot cb_r^{k-q} \end{pmatrix} - \begin{pmatrix} H_{k,0} \cdot \ell_{k,0} \\ \vdots \\ H_{k-q,0} \cdot \ell_{k-q,0} \end{pmatrix} + \begin{pmatrix} \Xi_k \\ \vdots \\ \Xi_{k-q} \end{pmatrix}. \quad (\text{II.27})$$

To estimate the travelled distance, speed and acceleration simultaneously, substituting equation (II.23) into equation (II.27) yields to

$$\begin{pmatrix} R_k \\ \vdots \\ R_{k-q} \end{pmatrix} - \begin{pmatrix} D_{k,0} \\ \vdots \\ D_{k-q,0} \end{pmatrix} + \begin{pmatrix} H_{k,0} & & & \\ & \ddots & & \\ & & H_{k-q,0} & \\ & & & \end{pmatrix} \begin{pmatrix} \ell_{k,0} \\ \vdots \\ \ell_{k-q,0} \end{pmatrix} \simeq \begin{pmatrix} H_{k,0} \cdot \omega_q & \mathbf{1}_n & & \\ \vdots & & \ddots & \\ H_{k-q,0} \cdot \omega_0 & & \mathbf{1}_n & \end{pmatrix} \begin{pmatrix} \theta_k \\ cb_r^k \\ \vdots \\ cb_r^{k-q} \end{pmatrix} + \begin{pmatrix} \Xi_k \\ \vdots \\ \Xi_{k-q} \end{pmatrix}. \quad (\text{II.28})$$

The pseudo-range measurement model is rewritten in the matrix form as

$$R^k - D_0^k + Y_0^k \simeq H_0^k \cdot \beta_k + \Xi^k, \quad (\text{II.29})$$

where the vector $\beta_k = (\theta_k^T, cb_r^k, \dots, cb_r^{k-q})^T$ is unknown and must be estimated. Finally, using intuitive notations, the pseudo-range measurement model is rewritten in a traditional form

$$Y^k \simeq H_0^k \cdot \beta_k + \Xi^k, \quad (\text{II.30})$$

where $Y^k = R^k - D_0^k + Y_0^k$, so the LS estimator is given by

$$\hat{\beta}_k = \left[\left(H_0^k \right)^T H_0^k \right]^{-1} \left(H_0^k \right)^T Y^k, \quad (\text{II.31})$$

where the working point is equal to the product of factor ω_p and previously calculated estimation $\hat{\theta}_{k-1}$, i.e., $\ell_{k-q+p,0} = \omega_p \cdot \theta_{k,0} = \omega_p \cdot \hat{\theta}_{k-1}$.

II.5.2 Impact of The Curve Radius on The Estimation Error

The goal of this subsection is to study the impact of the railway curve radius R on the first and second moments of these three estimations. To do this, we firstly expand the pseudo-range equation (II.24) to second order with respect to ℓ_{k-q+p} around the point $\ell_{k-q+p,0}$, and then the measurement equation (II.25) can be written in the matrix form :

$$R_{k-q+p} - D_{k-q+p,0} \simeq H_{k-q+p,0} \cdot (\ell_{k-q+p} - \ell_{k-q+p,0}) + \frac{1}{2} J_{k-q+p,0} \cdot (\ell_{k-q+p} - \ell_{k-q+p,0})^2 + \mathbf{1}_n \cdot cb_r^{k-q+p} + \Xi_{k-q+p}, \quad (\text{II.32})$$

where $J_{k-q+p,0} = (j_{k-q+p,0}^1, j_{k-q+p,0}^2, \dots, j_{k-q+p,0}^n)^T$ and $j_{k-q+p,0}^i = \left. \frac{\partial^2 d_{k-q+p}^i}{\partial \ell_{k-q+p}^2} \right|_{\ell_{k-q+p,0}}$. It follows that

$$\begin{aligned} & \begin{pmatrix} R_k \\ \vdots \\ R_{k-q} \end{pmatrix} - \begin{pmatrix} D_{k,0} \\ \vdots \\ D_{k-q,0} \end{pmatrix} + \begin{pmatrix} H_{k,0} & & & \\ & \ddots & & \\ & & \ddots & \\ & & & H_{k-q,0} \end{pmatrix} \begin{pmatrix} \ell_{k,0} \\ \vdots \\ \ell_{k-q,0} \end{pmatrix} \simeq \\ & \begin{pmatrix} H_{k,0} \cdot \omega_q & \mathbf{1}_n & & \\ \vdots & \ddots & & \\ H_{k-q,0} \cdot \omega_0 & & \mathbf{1}_n & \end{pmatrix} \begin{pmatrix} \theta_k \\ cb_r^k \\ \vdots \\ cb_r^{k-q} \end{pmatrix} + \frac{1}{2} \begin{pmatrix} J_{k,0} \cdot (\ell_k - \ell_{k,0})^2 \\ \vdots \\ J_{k-q,0} \cdot (\ell_{k-q} - \ell_{k-q,0})^2 \end{pmatrix} + \begin{pmatrix} \Xi_k \\ \vdots \\ \Xi_{k-q} \end{pmatrix}. \end{aligned} \quad (\text{II.33})$$

The above equation (II.33) can be written as

$$R^k - D_0^k + Y_0^k \simeq H_0^k \cdot \beta_k + \frac{1}{2} J_0^k + \Xi^k. \quad (\text{II.34})$$

Due to the presence of $J_{k-q+p,0}$, this equation underlines the role of the railway track curve radius in the measurement model.

The current estimation error is $\hat{\beta}_k - \beta_k$. After substituting the right side of equation (II.34) into the LS estimator (II.31), we look at the mean of this error which is computed

as

$$\mathbb{E}(\hat{\beta}_k - \beta_k) = \mathbb{E} \left[\left(B^k \right)^{-1} \left(H_0^k \right)^T \left(\frac{1}{2} J_0^k + \Xi^k \right) \right], \quad (\text{II.35})$$

where $B^k = \left(H_0^k \right)^T H_0^k$. Using the delta method, we get

$$\mathbb{E}(\hat{\beta}_k - \beta_k) \simeq \frac{1}{2} \left(\bar{B}^k \right)^{-1} \left(\bar{H}_0^k \right)^T \bar{J}_0^k, \quad (\text{II.36})$$

where $\bar{B}^k = \left(\bar{H}_0^k \right)^T \bar{H}_0^k$. The matrices \bar{H}_0^k and \bar{J}_0^k are calculated exactly as in equation (II.34) but with the working point $\ell_{k-q+p,0} = \omega_p \cdot \theta_{k-1}$.

For the second order moment of the estimation error $\hat{\beta}_k - \beta_k$, the delta method yields to

$$\mathbb{E}(\hat{\beta}_k - \beta_k)(\hat{\beta}_k - \beta_k)^T \simeq \frac{1}{4} \left(\bar{B}^k \right)^{-1} \left(\bar{H}_0^k \right)^T \bar{J}_0^k \left(\bar{J}_0^k \right)^T \bar{H}_0^k \left(\bar{B}^k \right)^{-1} + \sigma^2 \left(\bar{B}^k \right)^{-1}. \quad (\text{II.37})$$

II.5.3 Numerical Simulations

The following scenario will be used in the sequel. The segments of the simulated train trajectory stored in the onboard train database are summarized in Tab. II.1. The centerline curvature and the simulated train trajectory are shown by Fig. II.17 and II.18, respectively.

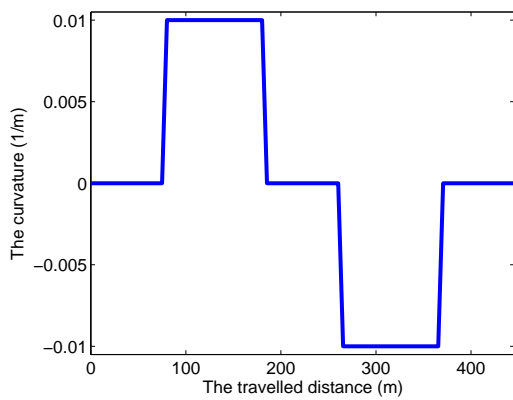


Figure II.17 – The centerline curvature of the tested simulation scenario.

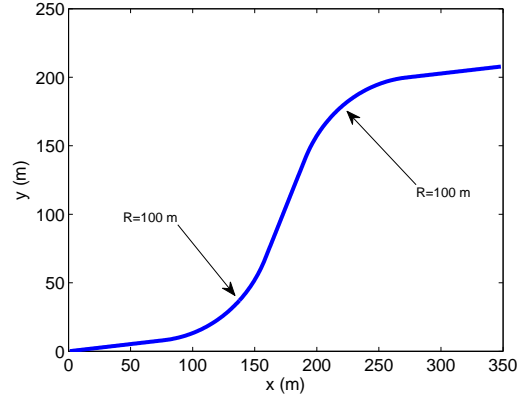


Figure II.18 – The simulated train trajectory on the local horizontal plane.

The standard GNSS constellation with $n = 6$ visible satellites is used. The GNSS sampling interval is $\Delta t = 0.5$ s. The pseudo-range SD is assumed to be of $\sigma = 2$ m. The

true acceleration during the acceleration, free-running and braking period is assumed to be of 0.8 m/s^2 , 0 m/s^2 and -0.8 m/s^2 , respectively.

The train motion diagram is shown in Fig. II.16. The comparison of the theoretical mean error and second order moment of the estimated distance, speed and acceleration given by equation (II.36) and equation (II.37), respectively, with the results of a 10^4 -repetition Monte-Carlo simulation, is shown in Fig. II.19-II.22. Different values of railway curve radius have been tested : $R = 100 \text{ m}$ and $R = 1000 \text{ m}$. As it follows from Fig. II.19-II.22 the theoretical moments of estimated distance, speed and acceleration coincide with their empirical estimations obtained by Monte-Carlo simulation.

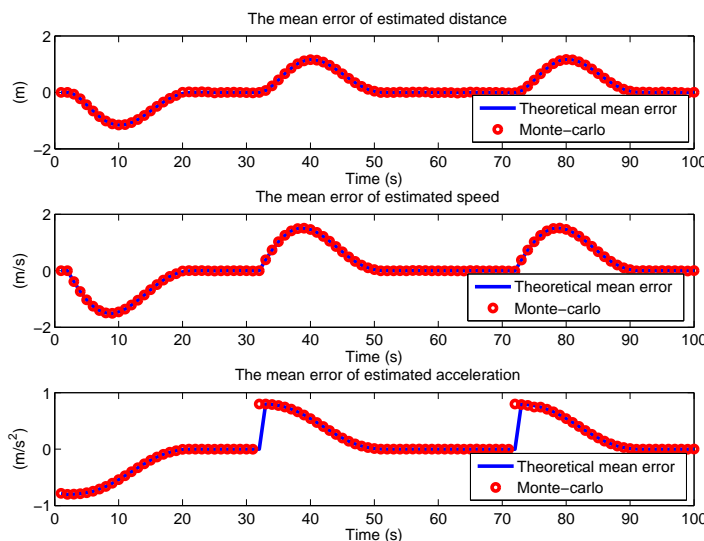


Figure II.19 – The mean error of the estimated distance, speed and acceleration for $R = 100 \text{ m}$ and $q = 20$.

From Fig. II.19 and II.21, we can see that the change of acceleration causes an imprecise estimation of the train travelled distance, speed and acceleration for a short time period. In fact, it's a problem of linear approximation : when the sliding window arrives the moment that the acceleration changes, the working point is far from the true value. Because when we calculate the working point, we assume that the acceleration is constant. When we linearize the pseudo-range vector around the working point, the linear approximation is not valid.

By comparison with Fig. II.20 and II.22, it can also be seen that the second order moment of these estimations is augmented slightly when the railway centerline curve

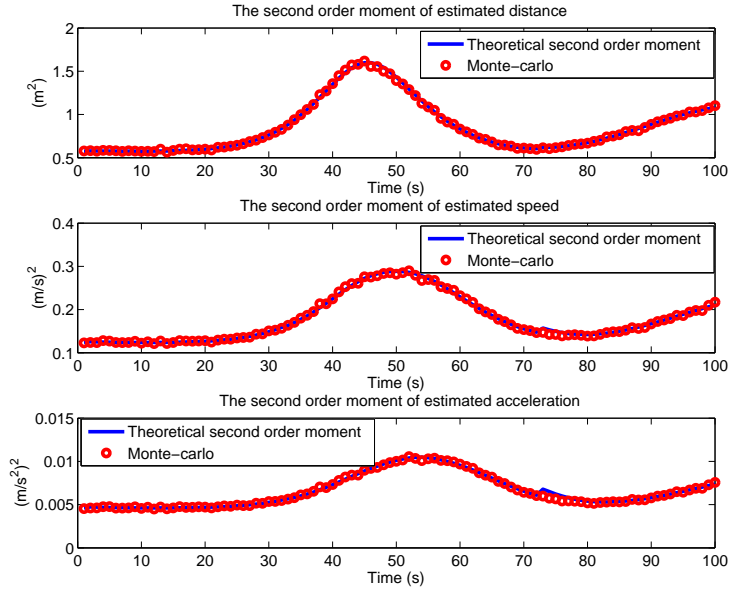


Figure II.20 – The second order moment of the estimated distance, speed and acceleration for $R = 100$ m and $q = 20$.

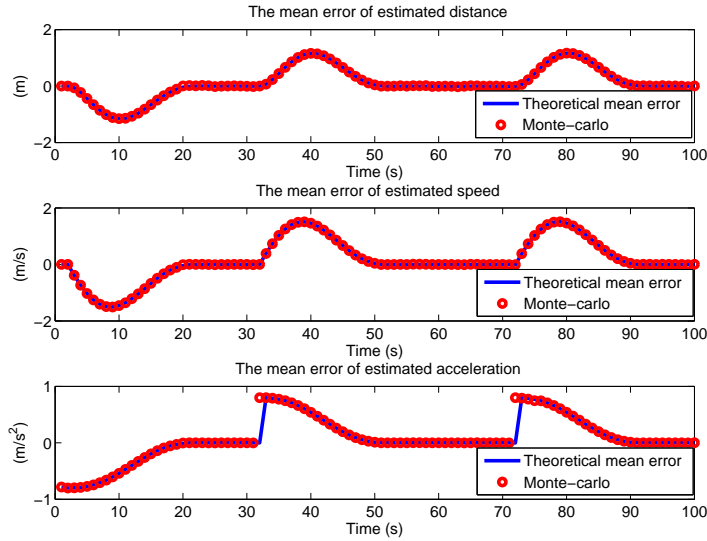


Figure II.21 – The mean error of the estimated distance, speed and acceleration for $R = 1000$ m and $q = 20$.

radius has been reduced from $R = 1000$ m to $R = 100$ m.

The negative impact of the sliding window length q on the precision of the estimated distance, speed and acceleration is limited to short periods after changing the acceleration. Trying to reduce the negative impact of the sliding window length on

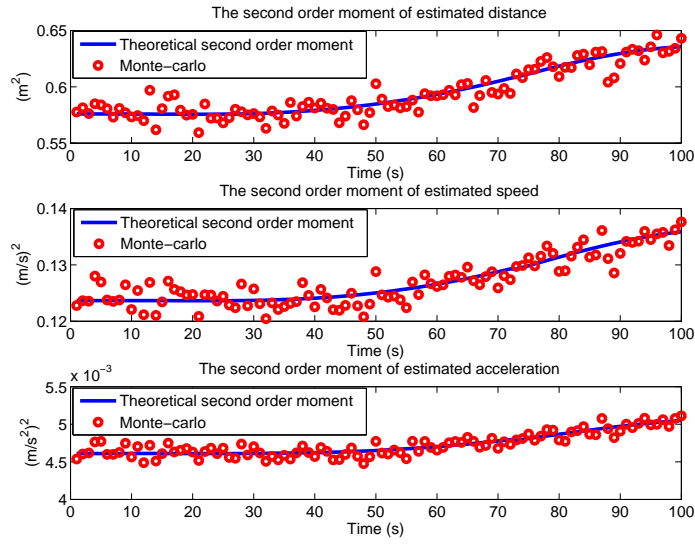


Figure II.22 – The second order moment of the estimated distance, speed and acceleration for $R = 1000$ m and $q = 20$.

the mean errors during the acceleration changing, the sliding window length has been reduced from $q = 20$ to $q = 5$ (see Fig. II.23). It is worth noting this reduction leads to a serious augmentation of the second moment especially for estimated acceleration and speed, as shown in Fig. II.20 and II.23.

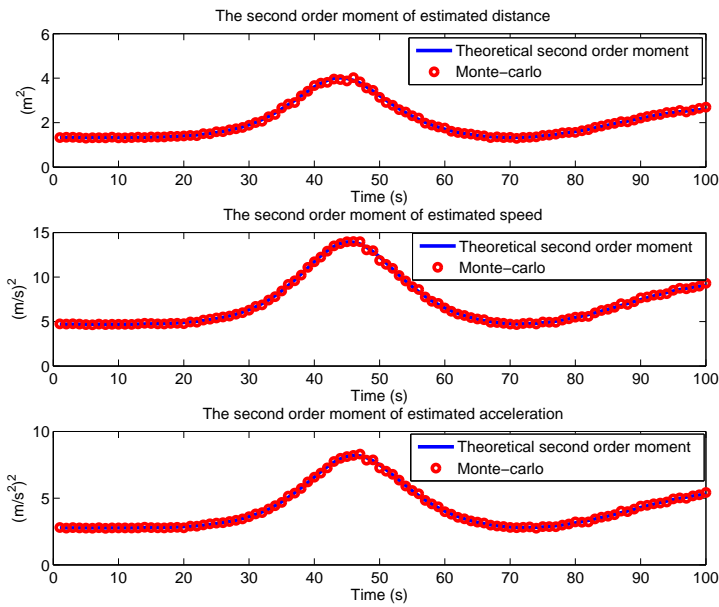


Figure II.23 – The second order moment of the estimated distance, speed and acceleration for $R = 100$ m and $q = 5$.

II.6 Conclusions

In absence of acceleration, the train speed estimation by GNSS is practically unbiased, even with minimum railway curve radius. The estimated speed second order moment quickly becomes very weak. The negative impact of railroad curvature on the train speed estimation by GNSS is nearly negligible.

In the variable speed case, analytic expressions for first two moments of the estimated travelled distance, speed and acceleration have been obtained to estimate the negative impacts of the railway curve radius on the above parameters. It has been shown that the change of acceleration causes an imprecise estimation of the travelled distance, speed and acceleration for a short time period. The mean error is always practically unbiased except for a short time period after the acceleration changes, but the second order moment remains almost unchanged during this period. Small railway centerline curve radius can augment slightly the second order moment of the train distance, velocity and acceleration estimation.

Chapitre III

Distance and Speed Estimation Based on GNSS and a "Non-ideal" Train Track

III.1 Introduction

In this chapter, the "non-ideal" model of railway centerline is defined by a polygonal line with some level of uncertainty in the train onboard database. It represents a piecewise linear approximation of the "ideal" model. The goal of this chapter is to estimate the travelled distance and speed of the train by using a low-cost GNSS receiver and to study the impact of the centerline uncertainty on these estimations. Two cases are studied : a constant and variable speed. For both cases, a LS estimator is designed. The mean error and the second order moment are theoretically calculated for these estimations and compared with the results of Monte-Carlo simulations.

III.2 Description of "Non-ideal" Train Track Models

Let us assume that the railway centerline is approximated by a polygonal line (piecewise linear curve), which represents a connected series of line segments in the ECEF coordinates. More formally, the railway centerline is defined by a sequence of vertices $Z_0, Z_1, Z_2, \dots, Z_n, Z_i \in \mathbb{R}^3$, so that the curve consists of the line segments connecting the consecutive vertices. It is assumed that the errors related with such an approximation of the vector function $\ell \mapsto X(\ell)$, $\ell \in \mathbb{R}$, $X(\ell) \in \mathbb{R}^3$, defining the railway centerline is negligible for our study. Here and in the rest of the paper, ℓ denotes the curvilinear

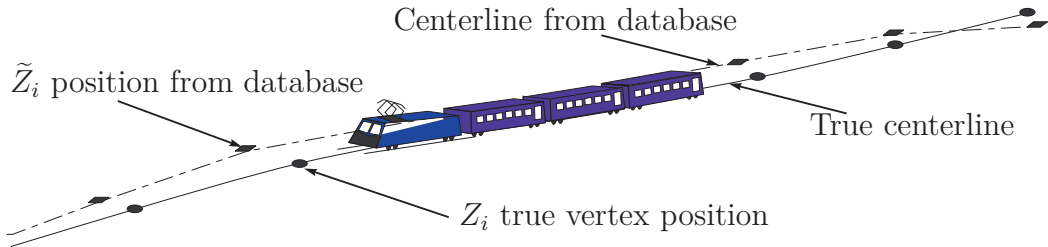


Figure III.1 – Train track model.

abscissa, or the travelled distance, and $\lambda = \|Z_{j+1} - Z_j\|_2 = \text{const}$ is the distance between two adjacent vertices, respectively. Unfortunately, the on-board database uses an imprecise information about the positions of vertices, namely : $\tilde{Z}_0, \tilde{Z}_1, \tilde{Z}_2, \dots, \tilde{Z}_n$. The quantity $\xi_i = Z_i - \tilde{Z}_i$ defines the knowledge uncertainty concerning the train track. This situation is illustrated by Fig. III.1. To simplify the presentation, a two-dimensional train trajectory is considered.

III.3 Speed Estimation for a Constant Speed Case

In this section, it is assumed that the acceleration is negligible for some short periods. Let us suppose that the train runs along the "non-ideal" railway track with an unknown constant speed v . Hence, the true train position is defined as follows :

$$X_k = X_{k-1} + A_{j(k)} \cdot v \cdot \Delta t \quad k = 1, 2, \dots, \quad (\text{III.1})$$

where the distance $v \cdot \Delta t$ is supposed to be small in comparison with the distance λ between two adjacent vertices. $X_k = (x_k, y_k, z_k)^T$ is the train position at the k -th GNSS measurement (GNSS epoch), t_k denotes the instant of the k -th measurement, $\Delta t = t_k - t_{k-1}$ represents the GNSS sampling interval, $A_j = (a_x^j, a_y^j, a_z^j)^T = \frac{1}{\lambda}(Z_{j+1} - Z_j)$ is the directional vector corresponding to the segment number j , $\|A_j\|_2 = 1$. The current segment number $j = j(k)$ is calculated as a function of k by using the following equation

$$j(k) = \min \{j \in \mathbb{N} | j \geq (v \cdot \Delta t \cdot k) / \lambda\}, \quad (\text{III.2})$$

where \mathbb{N} is the set of natural numbers. The train position X_k can be rewritten as

$$X_k = X_0 + v \Delta t \sum_{t=1}^k A_{j(t)}, \quad (\text{III.3})$$

where $X_0 = (x_0, y_0, z_0)^T$ is the starting point.

III.3.1 Imprecise Pseudo-range Measurement Model and Estimation

Suppose that there are n satellites located at the known positions $X_i^s = (x_i, y_i, z_i)^T$, $i = 1, \dots, n$. The pseudo-range r_i^k from the i -th satellite to the train position X_k at time t_k can be written as :

$$\begin{cases} r_1^k &= d_1^k(v) + cb_r^k + \varepsilon_1^k \\ r_2^k &= d_2^k(v) + cb_r^k + \varepsilon_2^k \\ \vdots &\vdots \quad \vdots \quad \vdots \\ r_n^k &= d_n^k(v) + cb_r^k + \varepsilon_n^k \end{cases}$$

where $d_i^k(v) = \left\| X_0 + v\Delta t \sum_{t=1}^k A_{j(t)} - X_i^s \right\|_2$ is the true distance from the i -th satellite to the train. b_r^k is a user clock bias, $c \simeq 2.9979 \cdot 10^8 m/s$ is the speed of light and $\varepsilon_i^k \sim \mathcal{N}(0, \sigma^2)$ is a pseudo-range noise. $\Xi^k = (\varepsilon_1^k, \dots, \varepsilon_n^k)^T$ is the vector of pseudo-range noises. Let us introduce the following vector : $R^k = (r_1^k, \dots, r_n^k)^T$. By linearizing the pseudo-range equation with respect to the state vector $V_k = (v, cb_k)^T$ around the working point $V_0 = (v_0, cb_0)^T$, we get the measurement equation

$$\begin{pmatrix} y_1^k \\ y_2^k \\ \vdots \\ y_n^k \end{pmatrix} = \begin{pmatrix} r_1^k - r_{1,0}^k \\ r_2^k - r_{2,0}^k \\ \vdots \\ r_n^k - r_{n,0}^k \end{pmatrix} \simeq \begin{pmatrix} h_{1,0}^k & 1 \\ h_{2,0}^k & 1 \\ \vdots & \vdots \\ h_{n,0}^k & 1 \end{pmatrix} \cdot \begin{pmatrix} v - v_0 \\ cb_r^k - cb_0 \end{pmatrix} + \begin{pmatrix} \varepsilon_1^k \\ \varepsilon_2^k \\ \vdots \\ \varepsilon_n^k \end{pmatrix}, \quad (\text{III.4})$$

where $r_{i,0}^k = d_{i,0}^k(v_0) + cb_0$, $d_{i,0}^k(v_0) = \left\| X_0 + \left(\sum_{t=1}^k A_{\hat{j}(t)} \right) \cdot v_0 \Delta t - X_i^s \right\|_2$ is the distance from the i -th satellite to the working point and the coefficients of the Jacobian matrix H_0^k of size $(n \times 2)$ are given by

$$h_{i,0}^k = \frac{1}{d_{i,0}^k(v_0)} \left[X_0 + \left(\sum_{t=1}^k A_{\hat{j}(t)} \right) \cdot v_0 \Delta t - X_i^s \right]^T \left(\sum_{t=1}^k A_{\hat{j}(t)} \right) \Delta t.$$

Because the true train speed v is unknown, the current segment number $\hat{j} = \hat{j}(t)$ is calculated as a function of the working point v_0 by using equation (III.2) with $v = v_0$. The above mentioned linearized measurement equation (III.4) can be rewritten in the following matrix form

$$Y^k = R^k - R_0^k \simeq H_0^k \cdot (V_k - V_0) + \Xi^k, \quad (\text{III.5})$$

where H_0^k is a full rank matrix of size $(n \times 2)$ defined in equation (III.4), the vector $V_k = (v, cb_r^k)^T$ is unknown and must be estimated. The working point at step k is equal to the previously calculated estimation : $V_0 = \hat{V}_{k-1}$.

Let us discuss now an unprecise measurement model. Since the true vertex position Z_j is unknown and only its imprecise estimation \tilde{Z}_j is available, the linearized measurement equation (III.5) cannot be used to compute the train speed. To estimate the impact of this uncertainty, let us define the directional vector $\tilde{A}_j = A_j + \delta_j$, where the random vector $\delta_j = (\delta_x^j, \delta_y^j, \delta_z^j)^T$ is assumed to be uniformly distributed in the cube $[-b, b]^3$ with $b > 0$. To measure the imprecise vertex position \tilde{Z}_j , some estimated methods have been used. Due to the instrument errors, this value b depends on which methods have been adopted. For example, if a GNSS receiver is used to collect these vertex positions, b depends on the receiver accuracy.

Finally, the imprecise pseudo-range measurement model (III.6) is defined for the imprecise directional vectors \tilde{A}_j in the following manner

$$R^k - \tilde{R}_0^k \simeq \tilde{H}_0^k \cdot (V_k - V_0) + \Xi^k, \quad (\text{III.6})$$

where \tilde{R}_0^k and \tilde{H}_0^k are calculated exactly as in equation (III.4) but with the vector \tilde{A}_j instead of A_j .

III.3.2 Impact of The Track Geometry Imprecision on The Estimation Error

The goal of this section is to study the impact of the train track uncertainty δ_j on the first and second moments of the LS estimator \hat{v}_k . To seek simplicity, let us assume that the track entirely belongs to the local tangent plane. We follow here the analysis of the regression model uncertainties and their impact on the LS estimators developed in (Hodges et Moore - 1972; Davies et Hutton - 1975; Swindel et Bower - 1972). First, the measurement equation (III.6) can be rewritten as follows :

$$Y^k + \Delta Y^k \simeq (H_0^k + \Delta H^k) \cdot \beta_k + \Xi^k, \quad (\text{III.7})$$

where $Y^k = R^k - R_0^k$ are the responses, H_0^k are the matrix of regressors, the data uncertainties in the regression model are

$$\Delta Y^k = R_0^k - \tilde{R}_0^k = \begin{pmatrix} \Delta y_1^k \\ \Delta y_2^k \\ \vdots \\ \Delta y_n^k \end{pmatrix},$$

whose elements are

$$\Delta y_i^k = -\frac{\partial \tilde{r}_{i,0}}{\partial \delta_j} \Big|_{\delta_j=0} \cdot \delta_j = -\frac{\partial \tilde{r}_{i,0}}{\partial \delta_x^j} \delta_x^j - \frac{\partial \tilde{r}_{i,0}}{\partial \delta_y^j} \delta_y^j,$$

and it is assumed that the second column of the data uncertainties ΔH^k is equal to zero because the impact on the clock bias estimation is of no interest for this study, that is

$$\Delta H^k = \tilde{H}_0^k - H_0^k = \begin{pmatrix} \Delta h_1^k & 0 \\ \Delta h_2^k & 0 \\ \vdots & \vdots \\ \Delta h_n^k & 0 \end{pmatrix},$$

whose elements are

$$\Delta h_i^k = \frac{\partial \tilde{h}_{i,0}}{\partial \delta_j} \Big|_{\delta_j=0} \cdot \delta_j = \frac{\partial \tilde{h}_{i,0}}{\partial \delta_x^j} \delta_x^j + \frac{\partial \tilde{h}_{i,0}}{\partial \delta_y^j} \delta_y^j.$$

The vector $\beta_k = V_k - V_0$ is unknown and must be estimated.

The LS estimator is given by

$$\hat{\beta}_k = \left[(H_0^k + \Delta H^k)^T (H_0^k + \Delta H^k) \right]^{-1} (H_0^k + \Delta H^k)^T (Y^k + \Delta Y^k). \quad (\text{III.8})$$

After expanding $\left[(H_0^k + \Delta H^k)^T (H_0^k + \Delta H^k) \right]^{-1}$ around H_0^k (see appendix of Hodges et Moore (1972)) and computing the expectation of equation (III.8), it has been shown in Section A1 of the Appendix B that the mean error of $\hat{V}_k - V$ can be given by

$$\mathbb{E}(\hat{V}_k - V) = B_0^{-1} [(H_0^k)^T \Sigma_H C - F + G] \beta_k, \quad (\text{III.9})$$

where $B_0 = (H_0^k)^T H_0^k$, the covariance matrix Σ_H of ΔH^k is equal to

$$\Sigma_H = \frac{b^2}{3} \cdot \begin{pmatrix} \left(\frac{\partial \tilde{h}_{1,0}}{\partial \delta_x^j} \right)^2 + \left(\frac{\partial \tilde{h}_{1,0}}{\partial \delta_y^j} \right)^2 & \dots & \frac{\partial \tilde{h}_{1,0}}{\partial \delta_x^j} \frac{\partial \tilde{h}_{n,0}}{\partial \delta_x^j} + \frac{\partial \tilde{h}_{1,0}}{\partial \delta_y^j} \frac{\partial \tilde{h}_{n,0}}{\partial \delta_y^j} \\ \vdots & \ddots & \vdots \\ \frac{\partial \tilde{h}_{1,0}}{\partial \delta_x^j} \frac{\partial \tilde{h}_{n,0}}{\partial \delta_x^j} + \frac{\partial \tilde{h}_{1,0}}{\partial \delta_y^j} \frac{\partial \tilde{h}_{n,0}}{\partial \delta_y^j} & \dots & \left(\frac{\partial \tilde{h}_{n,0}}{\partial \delta_x^j} \right)^2 + \left(\frac{\partial \tilde{h}_{n,0}}{\partial \delta_y^j} \right)^2 \end{pmatrix},$$

the two matrices F and G are calculated as

$$F = \begin{pmatrix} \text{tr}(\Sigma_H) & 0 \\ 0 & 0 \end{pmatrix} \quad \text{and} \quad G = \begin{pmatrix} \text{tr}[H_0^k B_0^{-1} (H_0^k)^T \Sigma_H] & 0 \\ 0 & 0 \end{pmatrix},$$

the first column of a $(n \times 2)$ matrix C is equal to the first column of $H_0^k B_0^{-1}$ and its second column is equal to zero.

Since the random vector ΔY^k acts in the same way as the pseudo-range noise Ξ^k , the two errors can be considered together. After expanding and ignoring the terms of order $(\Delta H^k)^2$ and under the assumption that the errors ΔH^k are reasonably small, it has also been shown in Section A1 of the Appendix B that the second order moment of $\widehat{V}_k - V$ can be given by

$$\mathbb{E}(\widehat{V}_k - V)(\widehat{V}_k - V)^T = B_0^{-1}(H_0^k)^T [\sigma^2 I_n + \Sigma_Y - \beta_1(\Sigma_{\widetilde{H}Y} + \Sigma_{Y\widetilde{H}}) + \beta_1^2 \Sigma_H] H_0^k B_0^{-1}, \quad (\text{III.10})$$

where $\beta_1 = v - v_0$, the covariance matrix Σ_Y of ΔY^k is equal to

$$\Sigma_Y = \frac{b^2}{3} \cdot \begin{pmatrix} \left(\frac{\partial \tilde{r}_{1,0}}{\partial \delta_x^j} \right)^2 + \left(\frac{\partial \tilde{r}_{1,0}}{\partial \delta_y^j} \right)^2 & \dots & \frac{\partial \tilde{r}_{1,0}}{\partial \delta_x^j} \frac{\partial \tilde{r}_{n,0}}{\partial \delta_x^j} + \frac{\partial \tilde{r}_{1,0}}{\partial \delta_y^j} \frac{\partial \tilde{r}_{n,0}}{\partial \delta_y^j} \\ \vdots & \ddots & \vdots \\ \frac{\partial \tilde{r}_{1,0}}{\partial \delta_x^j} \frac{\partial \tilde{r}_{n,0}}{\partial \delta_x^j} + \frac{\partial \tilde{r}_{1,0}}{\partial \delta_y^j} \frac{\partial \tilde{r}_{n,0}}{\partial \delta_y^j} & \dots & \left(\frac{\partial \tilde{r}_{n,0}}{\partial \delta_x^j} \right)^2 + \left(\frac{\partial \tilde{r}_{n,0}}{\partial \delta_y^j} \right)^2 \end{pmatrix}, \quad (\text{III.11})$$

the cross-covariance matrix $\Sigma_{Y\widetilde{H}}$ between ΔY^k and $\Delta \widetilde{H}^k$ is calculate as

$$\Sigma_{Y\widetilde{H}} = -\frac{b^2}{3} \cdot \begin{pmatrix} \frac{\partial \tilde{r}_{1,0}}{\partial \delta_x^j} \frac{\partial \tilde{h}_{1,0}}{\partial \delta_x^j} + \frac{\partial \tilde{r}_{1,0}}{\partial \delta_y^j} \frac{\partial \tilde{h}_{1,0}}{\partial \delta_y^j} & \dots & \frac{\partial \tilde{r}_{1,0}}{\partial \delta_x^j} \frac{\partial \tilde{h}_{n,0}}{\partial \delta_x^j} + \frac{\partial \tilde{r}_{1,0}}{\partial \delta_y^j} \frac{\partial \tilde{h}_{n,0}}{\partial \delta_y^j} \\ \vdots & \ddots & \vdots \\ \frac{\partial \tilde{r}_{n,0}}{\partial \delta_x^j} \frac{\partial \tilde{h}_{1,0}}{\partial \delta_x^j} + \frac{\partial \tilde{r}_{n,0}}{\partial \delta_y^j} \frac{\partial \tilde{h}_{1,0}}{\partial \delta_y^j} & \dots & \frac{\partial \tilde{r}_{n,0}}{\partial \delta_x^j} \frac{\partial \tilde{h}_{n,0}}{\partial \delta_x^j} + \frac{\partial \tilde{r}_{n,0}}{\partial \delta_y^j} \frac{\partial \tilde{h}_{n,0}}{\partial \delta_y^j} \end{pmatrix},$$

the vector $\Delta \widetilde{H}^k$ of dimension n is equal to the first column of ΔH^k , and $\Sigma_{Y\widetilde{H}} = \Sigma_{\widetilde{H}Y}^T$. When the expectation (III.9) of $\widehat{V}_k - V$ is almost zero, this second order moment corresponds to the variance of \widehat{V}_k .

III.3.3 Numerical Simulations

The following scenario will be used in the sequel. The standard GNSS constellation has been used with $n = 6$ visible satellites and $\sigma = 2$ (m). The GNSS sampling interval is $\Delta t = 0.5$ s. The distance between two adjacent vertices has been chosen $\lambda = 50$ (m). Different values of railway centerline uncertainty have been tested : $b = 0$ (no uncertainty); $b = 0.01$ (uncertainty $\simeq \pm 0.5$ m); $b = 0.05$ (uncertainty $\simeq \pm 2.5$ m). The comparison of the theoretical mean error and second order moment given by equation (III.9) and equation (III.10), respectively, with the results of a 10^4 -repetition Monte-Carlo simulation, is shown in Fig. III.2-III.7. From Fig. III.2, III.4 and III.6, we can see that the estimated speed mean error is approaching zero, even with the centerline uncertainties, but the centerline uncertainties considerably augment the estimated speed second order moment by comparison with Fig. III.3, III.5 and III.7.

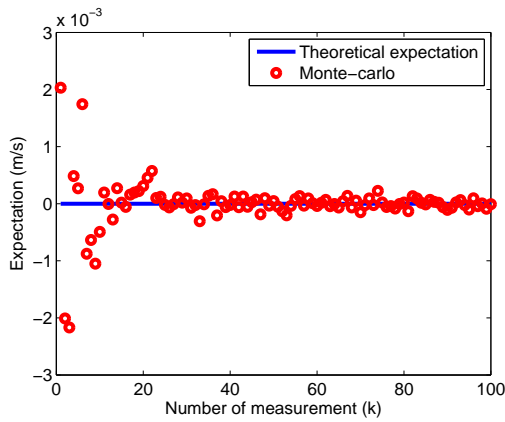


Figure III.2 – The estimated speed mean error for $\delta_j = 0$.

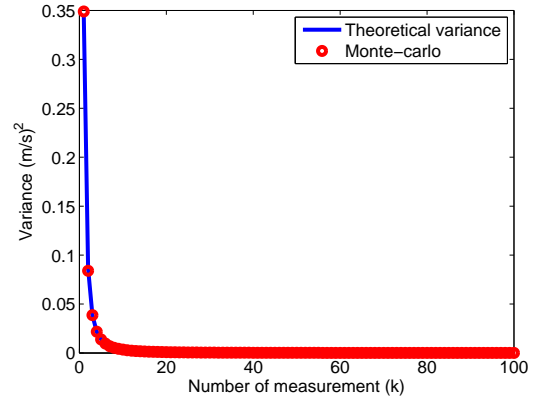


Figure III.3 – The estimated speed second order moment for $\delta_j = 0$.

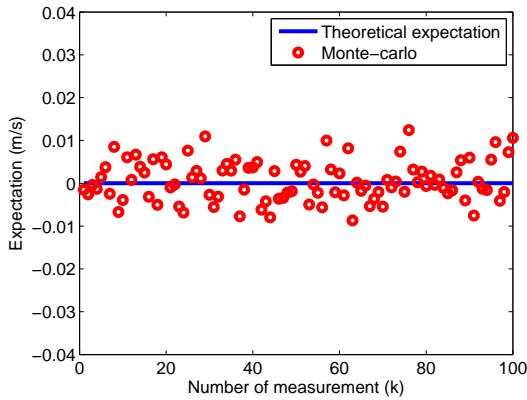


Figure III.4 – The estimated speed mean error for $\delta_j \in [-0.01, 0.01]^2$.

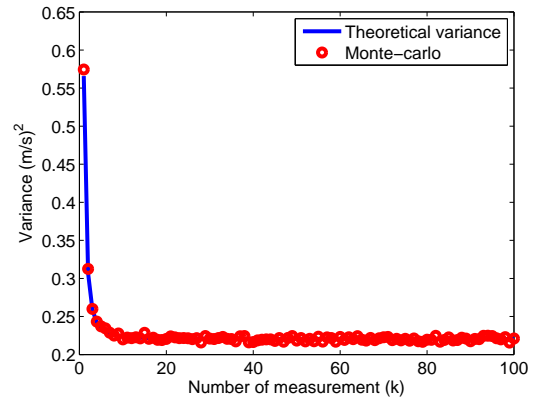


Figure III.5 – The estimated speed second order moment for $\delta_j \in [-0.01, 0.01]^2$.

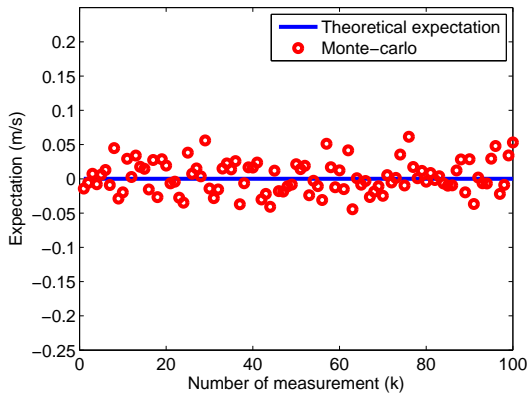


Figure III.6 – The estimated speed mean error for $\delta_j \in [-0.05, 0.05]^2$.

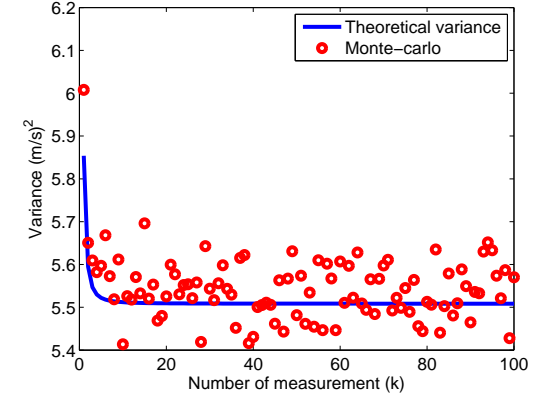


Figure III.7 – The estimated speed second order moment for $\delta_j \in [-0.05, 0.05]^2$.

III.4 Distance and Speed Estimation for a Variable Speed Case

The goal of this section is to estimate the travelled distance and speed of the train when its acceleration is not neglected. Hence, it is assumed that the train runs along the "non-ideal" railway centerline with a variable speed. The train dynamical model is described by an equation formulated in terms of the travelled distance, speed and acceleration (see Fig. III.8).

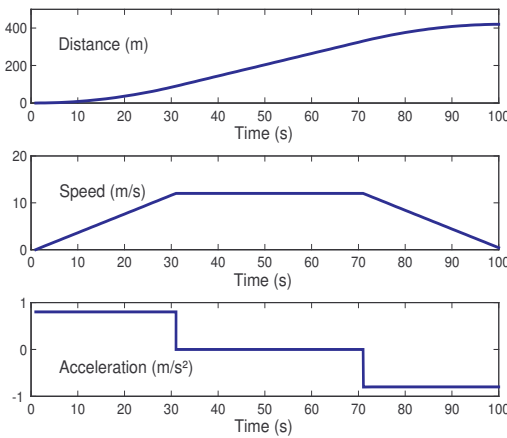


Figure III.8 – Typical train motion diagram.

Let $\Delta t = t_k - t_{k-1}$ be the GNSS sampling interval and t_k denotes the instant of the k -th measurement. Let us consider a short time period of length $T = (q+1) \cdot \Delta t$ where q is a positive integer. Over this time period, the distance ℓ_k covered by the train, its speed v_k and its acceleration a_k at instant t_k ($1 \leq k \leq q$) are given as follows

$$\begin{cases} \ell_k = \ell_{k-1} + v_{k-1} \cdot \Delta t + \frac{1}{2} a_{k-1} \cdot \Delta t^2 \\ v_k = v_{k-1} + a_{k-1} \cdot \Delta t \\ a_k = a_{k-1}. \end{cases} \quad (\text{III.12})$$

Let us consider the block of $q+1$ last GNSS measurements at time instant t_k . Assuming that the acceleration a_k is constant during T (s), the train position is given by

$$X(\ell_{k-q+p}) = Z_{j-1} + A_j \cdot [\ell_{k-q+p} - \lambda \cdot (j-1)], \quad (\text{III.13})$$

where $p = 0, 1, \dots, q$ and $A_j = (a_x^j, a_y^j, a_z^j)^T = \frac{1}{\lambda}(Z_{j+1} - Z_j)$ is the directional vector corresponding to the segment number j , $\|A_j\|_2 = 1$. The current segment number

$j = j(k - q + p)$, viewed as a function of $k - q + p$, is calculated as :

$$j(k - q + p) = \min \{j \in \mathbb{N} | j \geq \ell_{k-q+p}/\lambda\},$$

where \mathbb{N} is the set of natural numbers. The distance ℓ_{k-q+p} is given as

$$\ell_{k-q+p} = \begin{pmatrix} 1 & (p-q) \cdot \Delta t & \frac{1}{2}(p-q)^2 \cdot \Delta t^2 \end{pmatrix} \begin{pmatrix} \ell_k \\ v_k \\ a_k \end{pmatrix} = \omega_p \cdot \theta_k, \quad (\text{III.14})$$

where the vector θ_k is unknown and must be estimated.

III.4.1 Imprecise Pseudo-range Measurement Model and Estimation

Suppose that there are n satellites located at the known positions $X_i^s = (x_i, y_i, z_i)^T$, $i = 1, \dots, n$. The pseudo-range r_{k-q+p}^i from the i -th satellite to the train position $X(\ell_{k-q+p})$ at time $k - q + p$ can be written as :

$$\begin{cases} r_{k-q+p}^1 = d_{k-q+p}^1(\ell_{k-q+p}) + cb_r^{k-q+p} + \varepsilon_{k-q+p}^1 \\ r_{k-q+p}^2 = d_{k-q+p}^2(\ell_{k-q+p}) + cb_r^{k-q+p} + \varepsilon_{k-q+p}^2 \\ \vdots \\ r_{k-q+p}^n = d_{k-q+p}^n(\ell_{k-q+p}) + cb_r^{k-q+p} + \varepsilon_{k-q+p}^n \end{cases} \quad (\text{III.15})$$

where $p = 0, 1, \dots, q$, $d_{k-q+p}^i(\ell_{k-q+p}) = \|X(\ell_{k-q+p}) - X_i^s\|_2$ is the true distance from the i -th satellite to the train. b_r^{k-q+p} is a user clock bias, $c \simeq 2.9979 \cdot 10^8 m/s$ is the speed of light and $\varepsilon_{k-q+p}^i \sim \mathcal{N}(0, \sigma^2)$ is the pseudo-range noise at time $k - q + p$. $\Xi_{k-q+p} = (\varepsilon_{k-q+p}^1, \dots, \varepsilon_{k-q+p}^n)^T$ is the vector of pseudo-range noises. Let us introduce the following vector : $R_{k-q+p} = (r_{k-q+p}^1, \dots, r_{k-q+p}^n)^T$. By linearizing the pseudo-range equation with respect to the state variable ℓ_{k-q+p} around the working point $\ell_{k-q+p,0}$, we get the measurement equation

$$\begin{aligned} \begin{pmatrix} r_{k-q+p}^1 \\ r_{k-q+p}^2 \\ \vdots \\ r_{k-q+p}^n \end{pmatrix} - \begin{pmatrix} d_{k-q+p,0}^1 \\ d_{k-q+p,0}^2 \\ \vdots \\ d_{k-q+p,0}^n \end{pmatrix} &\simeq \begin{pmatrix} h_{k-q+p,0}^1 \\ h_{k-q+p,0}^2 \\ \vdots \\ h_{k-q+p,0}^n \end{pmatrix} \cdot (\ell_{k-q+p} - \ell_{k-q+p,0}) + \begin{pmatrix} cb_r^{k-q+p} \\ cb_r^{k-q+p} \\ \vdots \\ cb_r^{k-q+p} \end{pmatrix} \\ &+ \begin{pmatrix} \varepsilon_{k-q+p}^1 \\ \varepsilon_{k-q+p}^2 \\ \vdots \\ \varepsilon_{k-q+p}^n \end{pmatrix}, \end{aligned} \quad (\text{III.16})$$

where $d_{k-q+p,0}^i = d_{k-q+p}^i(\ell_{k-q+p,0}) = \|X(\ell_{k-q+p,0}) - X_i^s\|_2$ is the distance from the i -th satellite to the working point and the coefficients of the Jacobian matrix $H_{k-q+p,0}$ of size $(n \times 1)$ are given by

$$h_{k-q+p,0}^i = \frac{[X(\ell_{k-q+p,0}) - X_i^s]^T \cdot \left. \frac{\partial X(\ell_{k-q+p,0})}{\partial \ell_{k-q+p}} \right|_{\ell_{k-q+p,0}}}{\|X(\ell_{k-q+p,0}) - X_i^s\|_2}.$$

The above mentioned linearized measurement equations (III.16) can be rewritten in the following matrix form

$$R_{k-q+p} - D_{k-q+p,0} \simeq H_{k-q+p,0} \cdot (\ell_{k-q+p} - \ell_{k-q+p,0}) + \mathbf{1}_n \cdot cb_r^{k-q+p} + \Xi_{k-q+p}, \quad (\text{III.17})$$

where $\mathbf{1}_n$ is a vector of dimension n whose each element is one. It follows that

$$\begin{aligned} \begin{pmatrix} R_k \\ \vdots \\ R_{k-q} \end{pmatrix} - \begin{pmatrix} D_{k,0} \\ \vdots \\ D_{k-q,0} \end{pmatrix} &\simeq \begin{pmatrix} H_{k,0} \cdot \ell_k + \mathbf{1}_n \cdot cb_r^k \\ \vdots \\ H_{k-q,0} \cdot \ell_{k-q} + \mathbf{1}_n \cdot cb_r^{k-q} \end{pmatrix} - \begin{pmatrix} H_{k,0} \cdot \ell_{k,0} \\ \vdots \\ H_{k-q,0} \cdot \ell_{k-q,0} \end{pmatrix} \\ &+ \begin{pmatrix} \Xi_k \\ \vdots \\ \Xi_{k-q} \end{pmatrix}. \end{aligned} \quad (\text{III.18})$$

To estimate the travelled distance, speed and acceleration simultaneously, substituting equation (III.14) into equation (III.18) yields to

$$\begin{aligned} \begin{pmatrix} R_k \\ \vdots \\ R_{k-q} \end{pmatrix} - \begin{pmatrix} D_{k,0} \\ \vdots \\ D_{k-q,0} \end{pmatrix} &+ \begin{pmatrix} H_{k,0} & & & \\ & \ddots & & \\ & & H_{k-q,0} & \end{pmatrix} \begin{pmatrix} \ell_{k,0} \\ \vdots \\ \ell_{k-q,0} \end{pmatrix} \simeq \\ &\begin{pmatrix} H_{k,0} \cdot \omega_q & \mathbf{1}_n & & \\ \vdots & & \ddots & \\ H_{k-q,0} \cdot \omega_0 & & \mathbf{1}_n & \end{pmatrix} \begin{pmatrix} \theta_k \\ cb_r^k \\ \vdots \\ cb_r^{k-q} \end{pmatrix} + \begin{pmatrix} \Xi_k \\ \vdots \\ \Xi_{k-q} \end{pmatrix}. \end{aligned}$$

Finally, the pseudo-range measurement model is rewritten in the matrix form as

$$Y^k = R^k - D_0^k + Y_0^k \simeq H_0^k \cdot \beta_k + \Xi^k, \quad (\text{III.19})$$

where the vector $\beta_k = (\theta_k^T, cb_r^k, \dots, cb_r^{k-q})^T$ is unknown and must be estimated. The working point is equal to the product of factor ω_p and previously calculated estimation $\hat{\theta}_{k-1}$, i.e., $\ell_{k-q+p,0} = \omega_p \cdot \theta_{k,0} = \omega_p \cdot \hat{\theta}_{k-1}$.

Let us discuss now an unprecise measurement model. Since the true vertex position Z_j is unknown and only its imprecise estimation \tilde{Z}_j is available, the linearized measurement equation (III.19) cannot be used to compute the travelled distance, speed and

acceleration. To estimate the impact of this uncertainty, let us assume that the random vector $\xi_j = Z_j - \tilde{Z}_j$, where $\xi_j = (\xi_x^j, \xi_y^j, \xi_z^j)^T$ is assumed to be uniformly distributed in the cube $[-b, b]^3$ with $b > 0$. To measure the imprecise vertex position \tilde{Z}_j , some estimated methods have been used. Due to the instrument errors, this value b depends on which methods have been adopted. For example, if a GNSS receiver is used to collect these vertex positions, b depends on the receiver accuracy.

Finally, the imprecise pseudo-range measurement model (III.20) is defined for the imprecise vertex position \tilde{Z}_j in the following manner

$$R^k - \tilde{D}_0^k + \tilde{Y}_0^k \simeq \tilde{H}_0^k \cdot \beta_k + \Xi^k, \quad (\text{III.20})$$

where \tilde{D}_0^k , \tilde{Y}_0^k , and \tilde{H}_0^k are calculated exactly as in equation (III.19) but with the vector \tilde{Z}_j , $\tilde{A}_j = \frac{\tilde{Z}_{j+1} - \tilde{Z}_j}{\|\tilde{Z}_{j+1} - \tilde{Z}_j\|_2}$ instead of Z_j , A_j .

III.4.2 Impact of The Track Geometry Imprecision on The Estimation Error

The goal of this section is to study the impact of the train track uncertainty ξ_j on the first and second moments of the LS estimator $\hat{\beta}_k$. To seek simplicity, let us assume that the track entirely belongs to the local tangent plane. We also follow here the analysis of the regression model uncertainties and their impact on the LS estimators. First, the measurement equation (III.20) can be written as follows :

$$Y^k + \Delta Y^k \simeq (H_0^k + \Delta H^k) \cdot \beta_k + \Xi^k,$$

where the responses Y^k are given by

$$Y^k = R^k - D_0^k + Y_0^k = \begin{pmatrix} R_k \\ R_{k-1} \\ \vdots \\ R_{k-q} \end{pmatrix} - \begin{pmatrix} D_{k,0} \\ D_{k-1,0} \\ \vdots \\ D_{k-q,0} \end{pmatrix} + \begin{pmatrix} H_{k,0}\ell_{k,0} \\ H_{k-1,0}\ell_{k-1,0} \\ \vdots \\ H_{k-q,0}\ell_{k-q,0} \end{pmatrix},$$

the matrix of regressors H_0^k are

$$H_0^k = \begin{pmatrix} H_{k,0} \cdot \omega_q & \mathbf{1}_n & & \\ H_{k-1,0} \cdot \omega_{q-1} & & \mathbf{1}_n & \\ \vdots & & & \ddots \\ H_{k-q,0} \cdot \omega_0 & & & \mathbf{1}_n \end{pmatrix},$$

the data uncertainties ΔY^k in the dependent variable are

$$\Delta Y^k = D_0^k - \widetilde{D}_0^k - Y_0^k + \widetilde{Y}_0^k = \begin{pmatrix} \Delta H_k \ell_{k,0} \\ \Delta H_{k-1} \ell_{k-1,0} \\ \vdots \\ \Delta H_{k-q} \ell_{k-q,0} \end{pmatrix} - \begin{pmatrix} \Delta D_k \\ \Delta D_{k-1} \\ \vdots \\ \Delta D_{k-q} \end{pmatrix},$$

the elements of the two n -dimensional column vectors ΔH_{k-q+p} and ΔD_{k-q+p} are

$$\Delta h_{k-q+p,0}^i = \frac{\partial \tilde{h}_{k-q+p,0}^i}{\xi_j} \Big|_{\xi_j=0} \cdot \xi_j = \frac{\partial \tilde{h}_{k-q+p,0}^i}{\partial \xi_x^j} \xi_x^j + \frac{\partial \tilde{h}_{k-q+p,0}^i}{\partial \xi_y^j} \xi_y^j,$$

and

$$\Delta d_{k-q+p,0}^i = \frac{\partial \tilde{d}_{k-q+p,0}^i}{\xi_j} \Big|_{\xi_j=0} \cdot \xi_j = \frac{\partial \tilde{d}_{k-q+p,0}^i}{\partial \xi_x^j} \xi_x^j + \frac{\partial \tilde{d}_{k-q+p,0}^i}{\partial \xi_y^j} \xi_y^j,$$

respectively. The data uncertainties ΔH^k in the independent variable are

$$\Delta H^k = \widetilde{H}_0^k - H_0^k = \begin{pmatrix} \Delta H_k \cdot \omega_q & \mathbf{0}_n & & \\ \Delta H_{k-1} \cdot \omega_{q-1} & \mathbf{0}_n & & \\ \vdots & & \ddots & \\ \Delta H_{k-q} \cdot \omega_0 & & & \mathbf{0}_n \end{pmatrix}.$$

$\mathbf{0}_n$ is a vector of dimension n whose element is zero.

The LS estimator is given by

$$\hat{\beta}_k = \left[(H_0^k + \Delta H^k)^T (H_0^k + \Delta H^k) \right]^{-1} (H_0^k + \Delta H^k)^T \cdot (Y^k + \Delta Y^k). \quad (\text{III.21})$$

Since the random vector ΔY^k acts in the same way as the pseudo-range noise Ξ^k , the two errors can be considered together. After expanding $\left[(H_0^k + \Delta H^k)^T (H_0^k + \Delta H^k) \right]^{-1}$ around H_0^k and computing the expectation of (III.21), it has been shown in Section A2 of the Appendix B that the mean error is calculated as

$$\mathbb{E}(\hat{\beta}_k - \beta_k) = (\overline{B}^k)^{-1} \left[(\overline{H}_0^k)^T C - F + G \right] \beta_k, \quad (\text{III.22})$$

where $\overline{B}^k = (\overline{H}_0^k)^T \overline{H}_0^k$. The matrices \overline{H}_0^k are calculated exactly as in equation (III.19) but with the working point $\ell_{k-q+p,0} = \omega_p \cdot \theta_{k-1}$. The matrix functions of second moments

$$G = \mathbb{E} \left[(\Delta H^k)^T \overline{H}_0^k (\overline{B}^k)^{-1} (\overline{H}_0^k)^T \Delta H^k \right], \quad C = \mathbb{E} \left[\Delta H^k (\overline{B}^k)^{-1} (\overline{H}_0^k)^T \Delta H^k \right]$$

and $F = \mathbb{E} \left[(\Delta H^k)^T \Delta H^k \right]$ underline only the impact of data uncertainties in the matrix of regressors on the mean error of the LS estimator.

Let us now define the following matrix

$$\gamma_{\ell,m} = \mathbb{E}(\Delta H_\ell \Delta H_m^T) = \frac{b^2}{3} \cdot \begin{pmatrix} \frac{\partial \tilde{h}_{\ell,0}^1}{\partial \xi_x^j} \frac{\partial \tilde{h}_{m,0}^1}{\partial \xi_x^j} + \frac{\partial \tilde{h}_{\ell,0}^1}{\partial \xi_y^j} \frac{\partial \tilde{h}_{m,0}^1}{\partial \xi_y^j} & \dots & \frac{\partial \tilde{h}_{\ell,0}^1}{\partial \xi_x^j} \frac{\partial \tilde{h}_{m,0}^n}{\partial \xi_x^j} + \frac{\partial \tilde{h}_{\ell,0}^1}{\partial \xi_y^j} \frac{\partial \tilde{h}_{m,0}^n}{\partial \xi_y^j} \\ \vdots & \ddots & \vdots \\ \frac{\partial \tilde{h}_{\ell,0}^n}{\partial \xi_x^j} \frac{\partial \tilde{h}_{m,0}^1}{\partial \xi_x^j} + \frac{\partial \tilde{h}_{\ell,0}^n}{\partial \xi_y^j} \frac{\partial \tilde{h}_{m,0}^1}{\partial \xi_y^j} & \dots & \frac{\partial \tilde{h}_{\ell,0}^n}{\partial \xi_x^j} \frac{\partial \tilde{h}_{m,0}^n}{\partial \xi_x^j} + \frac{\partial \tilde{h}_{\ell,0}^n}{\partial \xi_y^j} \frac{\partial \tilde{h}_{m,0}^n}{\partial \xi_y^j} \end{pmatrix}.$$

The matrix C is given by

$$C = \begin{pmatrix} \sum_{u=0}^q \gamma_{k,k-u} \chi_{1,u+1}^T \omega_q^T \omega_{q-u} & \mathbf{0}_{n,(q+1)} \\ \sum_{u=0}^q \gamma_{k-1,k-u} \chi_{1,u+1}^T \omega_{q-1}^T \omega_{q-u} & \mathbf{0}_{n,(q+1)} \\ \vdots & \vdots \\ \sum_{u=0}^q \gamma_{k-q,k-u} \chi_{1,u+1}^T \omega_0^T \omega_{q-u} & \mathbf{0}_{n,(q+1)} \end{pmatrix},$$

where $\chi_{1,u+1}^T$ and $\varpi_{2,u+1}^T$ are two matrices of size $n \times 3$ and $n \times (q+1)$, respectively, extracted from the following matrix :

$$(\overline{B}^k)^{-1} (\overline{H}_0^k)^T = \begin{pmatrix} \chi_{1,1} & \chi_{1,2} & \dots & \chi_{1,(q+1)} \\ \varpi_{2,1} & \varpi_{2,2} & \dots & \varpi_{2,(q+1)} \end{pmatrix}.$$

Finally, let us define the following matrices

$$F = \begin{pmatrix} \sum_{u=0}^q \text{tr} \gamma_{k-u,k-u} \omega_{q-u}^T \omega_{q-u} & \mathbf{0}_{3,(q+1)} \\ \mathbf{0}_{(q+1),3} & \mathbf{0}_{(q+1),(q+1)} \end{pmatrix}$$

and

$$G = \begin{pmatrix} \sum_{u=0}^q \sum_{v=0}^q \text{tr} Q_{u+1,v+1} \gamma_{k-v,k-u} \omega_{q-u}^T \omega_{q-v} & \mathbf{0}_{3,(q+1)} \\ \mathbf{0}_{(q+1),3} & \mathbf{0}_{(q+1),(q+1)} \end{pmatrix},$$

where $Q_{u+1,v+1}$ is a block of size $n \times n$ of the following $(q+1)n \times (q+1)n$ matrix $Q = \overline{H}_0^k (\overline{B}^k)^{-1} (\overline{H}_0^k)^T$:

$$Q = \begin{pmatrix} Q_{1,1} & Q_{1,2} & \dots & Q_{1,(q+1)} \\ Q_{2,1} & Q_{2,2} & \dots & Q_{2,(q+1)} \\ \vdots & \vdots & \ddots & \vdots \\ Q_{(q+1),1} & Q_{(q+1),2} & \dots & Q_{(q+1),(q+1)} \end{pmatrix}.$$

After expanding and ignoring the terms of order $(\Delta H^k)^2$ and under the assumption that the uncertainties ΔH^k are reasonably small, it has also been shown in Section A2 of the Appendix B that the second moment of $\hat{\beta}_k$ is given by

$$\mathbb{E}(\hat{\beta}_k - \beta_k)(\hat{\beta}_k - \beta_k)^T = (\overline{B}^k)^{-1} (\overline{H}_0^k)^T (\sigma^2 I + \Sigma_Y - N - N^T + M) \overline{H}_0^k (\overline{B}^k)^{-1}, \quad (\text{III.23})$$

where the matrix functions $\Sigma_Y = \mathbb{E} \left[\Delta Y^k \left(\Delta Y^k \right)^T \right]$, $M = \mathbb{E} \left[\Delta H^k \beta_k \beta_k^T \left(\Delta H^k \right)^T \right]$ and $N = \mathbb{E} \left[\Delta Y^k \beta_k^T \left(\Delta H^k \right)^T \right]$ underline the impact of the data uncertainties in both the matrix of regressors and the responses on the second order moment of the LS estimator. After calculating the covariance of ΔY^k , we get

$$\Sigma_Y = S = \begin{pmatrix} S_{1,1} & S_{1,2} & \cdots & S_{1,q+1} \\ S_{2,1} & S_{2,2} & \cdots & S_{2,q+1} \\ \vdots & \vdots & \ddots & \vdots \\ S_{(q+1),1} & S_{(q+1),2} & \cdots & S_{(q+1),q+1} \end{pmatrix},$$

where

$$S_{u+1,v+1} = \ell_{k-u,0} \ell_{k-v,0} \gamma_{k-u,k-v} - \ell_{k-u,0} \mathbb{E}(\Delta H_{k-u} \Delta D_{k-u}^T) - \ell_{k-v,0} \mathbb{E}(\Delta D_{k-u} \Delta H_{k-u}^T) + \mathbb{E}(\Delta D_{k-u} \Delta D_{k-v}^T),$$

is a block of size $n \times n$ of matrix S , the covariance matrices $\mathbb{E}(\Delta H_{k-u} \Delta D_{k-u}^T)$, $\mathbb{E}(\Delta D_{k-u} \Delta H_{k-u}^T)$ and $\mathbb{E}(\Delta D_{k-u} \Delta D_{k-v}^T)$ are given by

$$\begin{aligned} \mathbb{E}(\Delta H_{k-u} \Delta D_{k-u}^T) &= \mathbb{E}[(\Delta H_{k-u} \Delta D_{k-u}^T)]^T \\ &= \frac{b^2}{3} \cdot \begin{pmatrix} \frac{\partial \tilde{h}_{k-u,0}^1}{\partial \xi_x^j} \frac{\partial \tilde{d}_{k-u,0}^1}{\partial \xi_x^j} + \frac{\partial \tilde{h}_{k-u,0}^1}{\partial \xi_y^j} \frac{\partial \tilde{d}_{k-u,0}^1}{\partial \xi_y^j} & \cdots & \frac{\partial \tilde{h}_{k-u,0}^1}{\partial \xi_x^j} \frac{\partial \tilde{d}_{k-u,0}^n}{\partial \xi_x^j} + \frac{\partial \tilde{h}_{k-u,0}^1}{\partial \xi_y^j} \frac{\partial \tilde{d}_{k-u,0}^n}{\partial \xi_y^j} \\ \vdots & \ddots & \vdots \\ \frac{\partial \tilde{h}_{k-u,0}^n}{\partial \xi_x^j} \frac{\partial \tilde{d}_{k-u,0}^1}{\partial \xi_x^j} + \frac{\partial \tilde{h}_{k-u,0}^n}{\partial \xi_y^j} \frac{\partial \tilde{d}_{k-u,0}^1}{\partial \xi_y^j} & \cdots & \frac{\partial \tilde{h}_{k-u,0}^n}{\partial \xi_x^j} \frac{\partial \tilde{d}_{k-u,0}^n}{\partial \xi_x^j} + \frac{\partial \tilde{h}_{k-u,0}^n}{\partial \xi_y^j} \frac{\partial \tilde{d}_{k-u,0}^n}{\partial \xi_y^j} \end{pmatrix} \end{aligned}$$

and

$$\mathbb{E}(\Delta D_{k-u} \Delta D_{k-v}^T) = \frac{b^2}{3} \cdot \begin{pmatrix} \frac{\partial \tilde{d}_{k-u,0}^1}{\partial \xi_x^j} \frac{\partial \tilde{d}_{k-v,0}^1}{\partial \xi_x^j} + \frac{\partial \tilde{d}_{k-u,0}^1}{\partial \xi_y^j} \frac{\partial \tilde{d}_{k-v,0}^1}{\partial \xi_y^j} & \cdots & \frac{\partial \tilde{d}_{k-u,0}^1}{\partial \xi_x^j} \frac{\partial \tilde{d}_{k-v,0}^n}{\partial \xi_x^j} + \frac{\partial \tilde{d}_{k-u,0}^1}{\partial \xi_y^j} \frac{\partial \tilde{d}_{k-v,0}^n}{\partial \xi_y^j} \\ \vdots & \ddots & \vdots \\ \frac{\partial \tilde{d}_{k-u,0}^n}{\partial \xi_x^j} \frac{\partial \tilde{d}_{k-v,0}^1}{\partial \xi_x^j} + \frac{\partial \tilde{d}_{k-u,0}^n}{\partial \xi_y^j} \frac{\partial \tilde{d}_{k-v,0}^1}{\partial \xi_y^j} & \cdots & \frac{\partial \tilde{d}_{k-u,0}^n}{\partial \xi_x^j} \frac{\partial \tilde{d}_{k-v,0}^n}{\partial \xi_x^j} + \frac{\partial \tilde{d}_{k-u,0}^n}{\partial \xi_y^j} \frac{\partial \tilde{d}_{k-v,0}^n}{\partial \xi_y^j} \end{pmatrix}.$$

The matrix functions M and N are calculated as

$$M = \begin{pmatrix} M_{1,1} & M_{1,2} & \cdots & M_{1,(q+1)} \\ M_{2,1} & M_{2,2} & \cdots & M_{2,(q+1)} \\ \vdots & \vdots & \ddots & \vdots \\ M_{(q+1),1} & M_{(q+1),2} & \cdots & M_{(q+1),(q+1)} \end{pmatrix}$$

and

$$N = \begin{pmatrix} N_{1,1} & N_{1,2} & \cdots & N_{1,(q+1)} \\ N_{2,1} & N_{2,2} & \cdots & N_{2,(q+1)} \\ \vdots & \vdots & \ddots & \vdots \\ N_{(q+1),1} & N_{(q+1),2} & \cdots & N_{(q+1),(q+1)} \end{pmatrix},$$

where

$$M_{u+1,v+1} = \ell_{k-u} \ell_{k-v} \gamma_{k-u,k-v}$$

and

$$N_{u+1,v+1} = \ell_{k-u}\ell_{k-v,0}\gamma_{k-u,k-v} - \ell_{k-u}\mathbb{E}(\Delta H_{k-u}\Delta D_{k-v}^T)$$

are two blocks of size $n \times n$ of matrices, M and N , respectively, ℓ_{k-u}, ℓ_{k-v} are calculated exactly as in equation (III.14) and $u, v = 0, \dots, q$.

III.4.3 Numerical Simulations

The following scenario will be used in the sequel. The standard GNSS constellation with $n = 6$ visible satellites is used. The GNSS sampling interval is $\Delta t = 0.5$ s. The pseudo-range SD is assumed to be of $\sigma = 2$ m. The true acceleration during the acceleration, free-running and braking period is assumed to be of 0.8 m/s^2 , 0 m/s^2 and -0.8 m/s^2 , respectively.

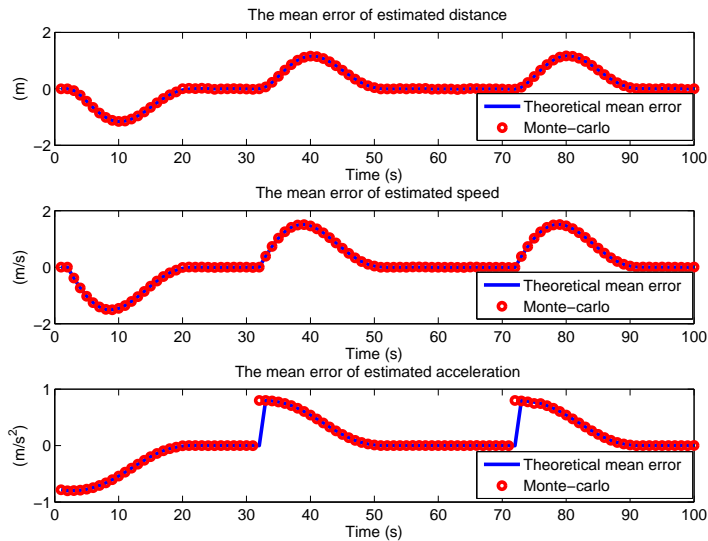


Figure III.9 – The mean error of the estimated distance, speed and acceleration for the centerline uncertainty of $\xi_j = 0$ and $q = 20$.

The train motion diagram is shown in Fig. III.8. The distance between two adjacent vertices has been chosen $\lambda = 50$ m. Different values of railway centerline uncertainty have been tested : $b = 0$ (no uncertainty) ; $b = 2$ (uncertainty $\simeq \pm 2$ m). The comparison of the theoretical moments for the estimated distance, speed and acceleration given by equation (III.22) and equation (III.23), respectively, with the results of a 10^4 -repetition Monte-Carlo simulation, is shown in Fig. III.9-III.12 for the length of sliding window $q = 20$.

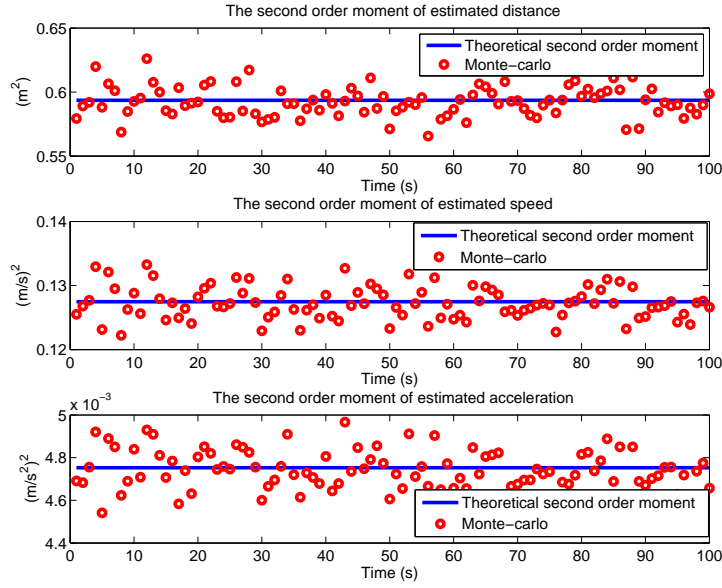


Figure III.10 – The second order moment of the estimated distance, speed and acceleration for the centerline uncertainty of $\xi_j = 0$ and $q = 20$.

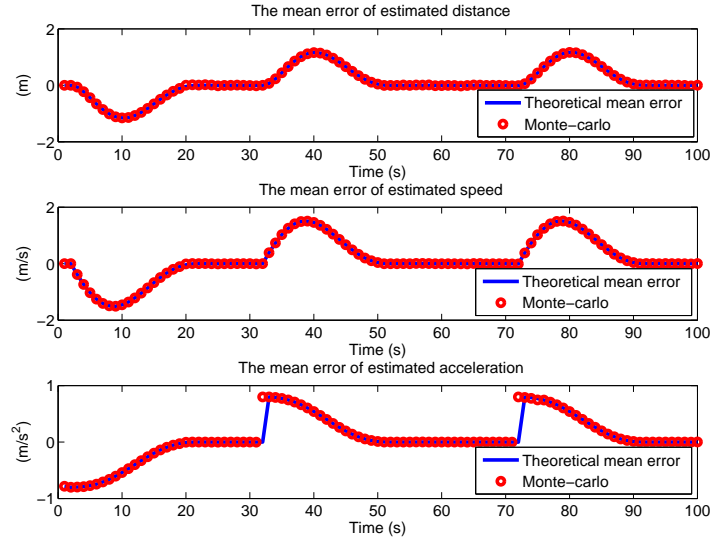


Figure III.11 – The mean error of the estimated distance, speed and acceleration for the centerline uncertainty of $\xi_j \in [-2, 2]^2$ and $q = 20$.

From Fig. III.9 and III.11, we can see that the change of acceleration causes an imprecise estimation of the train travelled distance, speed and acceleration for a short time period. It can also be seen that the second order moment of these estimations is augmented slightly due to the existence of the centerline uncertainties (see Fig. III.10)

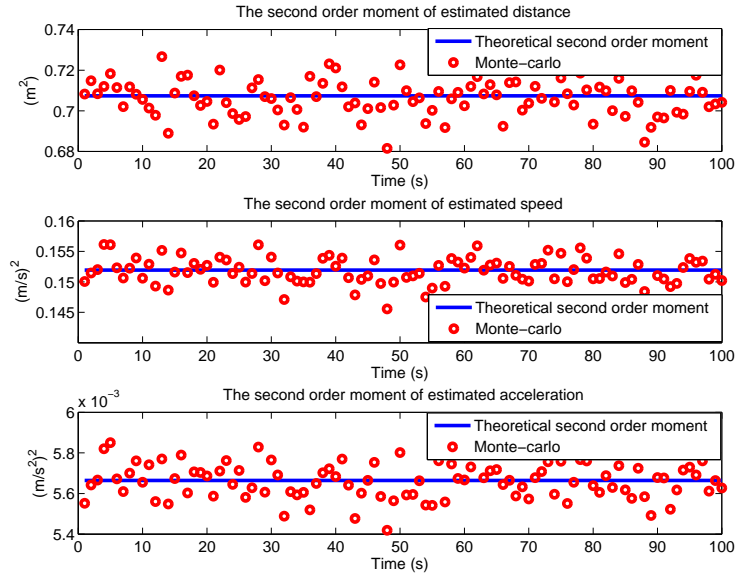


Figure III.12 – The second order moment of the estimated distance, speed and acceleration for the centerline uncertainty of $\xi_j \in [-2, 2]^2$ and $q = 20$.

and III.12).

III.5 Conclusions

In the constant speed case, the train speed estimation by GNSS is practically unbiased, even with an imprecise geometric model of the railway centerline. The centerline uncertainties considerably augment the estimated speed second order moment by comparison with the "ideal" case. The negative impact of centerline uncertainty on the train speed estimation by GNSS is nearly negligible.

In the variable speed case, analytic expressions for the first two moments of the estimated travelled distance, speed and acceleration have been obtained to estimate the negative impacts of the railway centerline uncertainty on the above parameters. It has been shown that the change of acceleration causes an imprecise estimation of the travelled distance, speed and acceleration for a short time period. The mean error is always practically unbiased except for a short time period after the acceleration changes, but the second order moment remains almost unchanged during this period. Railway centerline uncertainty also leads to a slight augmentation of the second order

moment of the train distance, velocity and acceleration estimation by comparison with the "ideal" case.

Chapitre IV

Distance and Speed Estimation Based on Integrating GNSS with The Track Database

IV.1 Introduction

In this chapter, the railway centerline geometry provides the users with some very reliable *a priori* information on the smooth character of the train trajectory. But this information is available within a track database with measurement errors. The goal of this chapter is to estimate the travelled distance and speed of the train by integrating the GNSS measurements with this database information. Two cases are studied : a constant and variable speed. For both cases, a rigorous mathematical model for the GNSS/track database integrated system is designed. Then the impact of errors in this integrated system on these estimations is studied.

IV.2 Description of Track Database Models

The railway track database is necessary for the GNSS-based train positioning system. It can be generated by using surveying methods, which can install a GNSS low-cost receiver previous on a train or use geodesic measuring to collect the data. Hence, the accuracy of the track database depends on which method has been adopted. Due to the instrument errors during the collection of the track data points, it's necessary to note that these collected track data points do not exactly coincide with the railway centerline in the real world. In this section, two track database models are studied : a continuous and a discrete model.

IV.2.1 Continuous Track Database Models

Let us first recall the parametric equations for an "ideal" railway centerline in the form of traditional design elements that have been discussed in Section II.3. Let us also assume that the track completely belongs to the local tangent plane. Fig. IV.1 shows three connected typical segments $[\ell_m; \ell_{m+1}]$, $[\ell_{m+1}; \ell_{m+2}]$ and $[\ell_{m+2}; \ell_{m+3}]$ indexed by ℓ_m which is the travelled distance corresponding to the m -th segment ($m = 1, 2, \dots$).

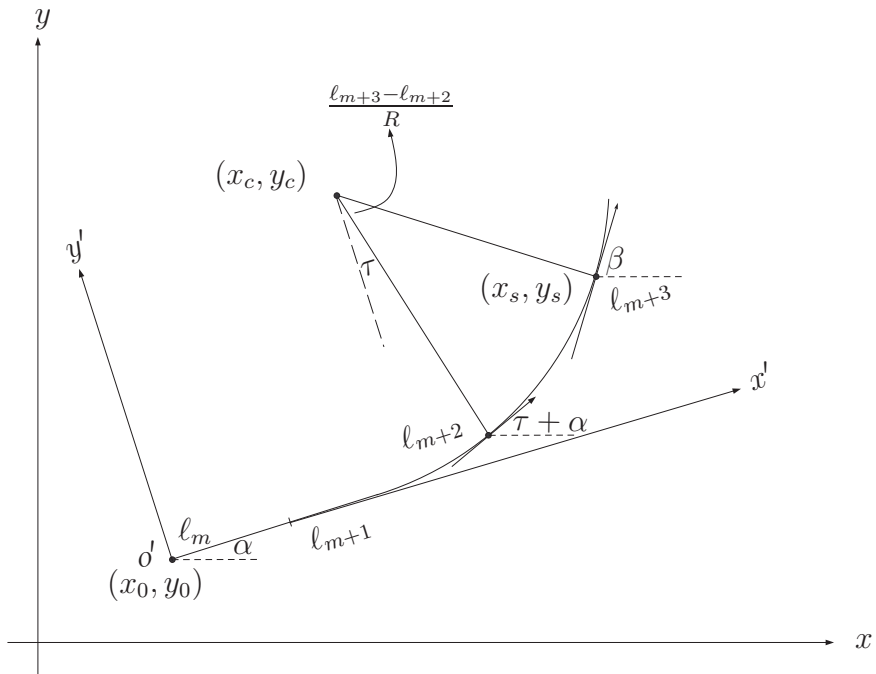


Figure IV.1 – Train track composed of three segments on the local tangent plane.

Straight Line Segment

As shown in Fig. IV.1, the equation for the straight line segment ($\ell_m < \ell \leq \ell_{m+1}$) is

$$\begin{cases} x(\varphi_{sl}, \ell) = x_0 + (\ell - \ell_m) \cdot \cos \alpha \\ y(\varphi_{sl}, \ell) = y_0 + (\ell - \ell_m) \cdot \sin \alpha, \end{cases} \quad (\text{IV.1})$$

where the vector $\varphi_{sl} = (x_0, y_0, \alpha)^T$ is the geometric parameters of a straight line segment, the subscript "sl" denotes the straight line. (x_0, y_0) is the starting point of the m -th segment, ℓ denotes the curvilinear abscissa and α is the initial azimuth of the m -th segment.

Transition Curve

The equation for the transition curve ($\ell_{m+1} < \ell \leq \ell_{m+2}$) in Fig. IV.1 is well approximated by

$$\begin{cases} x(\varphi_{tc}, \ell) = x_0 + (\ell - \ell_m) \cos \alpha - k_c (\ell - \ell_{m+1})^3 \sin \alpha \\ y(\varphi_{tc}, \ell) = y_0 + (\ell - \ell_m) \sin \alpha + k_c (\ell - \ell_{m+1})^3 \cos \alpha, \end{cases} \quad (\text{IV.2})$$

where the vector $\varphi_{tc} = (x_0, y_0, \alpha, k_c)^T$ is the geometric parameters of a transition curve, the subscript "tc" denotes the transition curve. $k_c = \frac{1}{6RL}$ is the coefficient of the transition curve, L and R are the transition curve length and the radius at the end of transition curve, respectively.

Circular Arc

The equation for the circular arc ($\ell_{m+2} < \ell \leq \ell_{m+3}$) illustrated in Fig. IV.1 is

$$\begin{cases} x(\varphi_{ca}, \ell) = x_0 + x' \cdot \cos \alpha - y' \cdot \sin \alpha \\ y(\varphi_{ca}, \ell) = y_0 + x' \cdot \sin \alpha + y' \cdot \cos \alpha, \end{cases} \quad (\text{IV.3})$$

where the vector $\varphi_{ca} = (x_0, y_0, \alpha, x_c, y_c, R)^T$ is the geometric parameters of a circular arc, the subscript "ca" denotes the circular arc.

$$\begin{cases} x' = x_c + R \sin \left(\tau + \frac{\ell - \ell_{m+2}}{R} \right) \\ y' = y_c - R \cos \left(\tau + \frac{\ell - \ell_{m+2}}{R} \right) \end{cases} \quad (\text{IV.4})$$

is the representation of circular arc on the $x'y'$ -plane, $\tau = \arctan(3k_c L^2)$ is the angle of the tangent at the end of transition curve and

$$\begin{cases} x_c = L \cdot (1 - 9k_c^2 L^4)/2 + \ell_{m+1} - \ell_m \\ y_c = (1 + 15k_c^2 L^4)/6k_c L \end{cases} \quad (\text{IV.5})$$

is the center of the circular arc.

IV.2.2 Discrete Track Database Models

Let us now consider that the train has already installed a GNSS receiver for collecting the discrete track database points, runs on an "ideal" railway centerline. Fig. IV.2 shows three connected typical segments $[\ell_m; \ell_{m+1}]$, $[\ell_{m+1}; \ell_{m+2}]$ and $[\ell_{m+2}; \ell_{m+3}]$ indexed

by ℓ_m which is the travelled distance corresponding to the m -th segment ($m = 1, 2, \dots$). The vector Z_{DB,j_m} denotes the measured first track database point of the m -th segment, i.e., the straight line segment, which corresponds to the j_m -th measured track database point of the whole train trajectory. According, $Z_{DB,j_{m+1}}$ and $Z_{DB,j_{m+2}}$ are the measured first track database point of the $(m+1)$ -th and $(m+2)$ -th segment, i.e., the transition curve and circular arc, respectively.

The accuracy of a GNSS receiver depends on many factors, such as the quality of the receiver, the position of the satellites at the time the data was recorded, the characteristics of the surroundings (buildings, tree cover, valleys, etc) and even the weather. Hence, it causes the collected track database points to be different from the true track database points. The relationship between them can be represented as (see Fig. IV.2) :

$$Z_{DB,j} = X_j(\varphi) + \xi_{DB,j} \quad \text{and} \quad j = j_m, \dots, j_{m+3}, \quad (\text{IV.6})$$

where $X_j(\varphi) = (x_j(\varphi), y_j(\varphi))^T$ is the j -th true track database point and j is calculated as a function of the travelled distance $\ell : j = \lceil \ell / \lambda \rceil$. φ denotes the track geometric parameters of the straight line, transition curve and circular arc , i.e., φ_{sl} , φ_{tc} and φ_{ca} . $\lambda = \|X_j(\varphi) - X_{j-1}(\varphi)\|_2 = \text{const}$ is the distance between two adjacent true track database points, $Z_{DB,j} = (x_{DB,j}, y_{DB,j})^T$ denotes the measured track database point, $\xi_{DB,j} = (\xi_{DB,j,x}, \xi_{DB,j,y})^T \sim \mathcal{N}(0, \sigma_{DB}^2 I_2)$ is the measurement error and the SD σ_{DB} depends on the accuracy of the GNSS receiver.

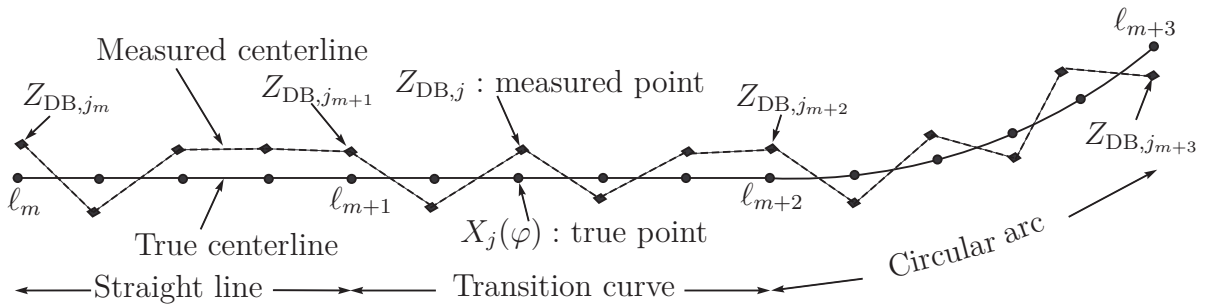


Figure IV.2 – The measurement errors in the track database.

Straight Line Segment

When the train runs into the straight line segment ($\ell_m < \ell \leq \ell_{m+1}$) of the railway

centerline, the equations for the true track database points are represented as

$$\begin{cases} x_j(\varphi_{sl}) = x_0 + (j\lambda - \ell_m) \cdot \cos \alpha \\ y_j(\varphi_{sl}) = y_0 + (j\lambda - \ell_m) \cdot \sin \alpha, \end{cases} \quad (\text{IV.7})$$

where $\varphi_{sl} = (x_0, y_0, \alpha)^T$ denotes the geometric parameters of a straight line, $j = j_m, \dots, j_{m+1}$ and the equations for the collected track database points are given by

$$\begin{cases} x_{DB,j} = x_j(\varphi_{sl}) + \xi_{DB,j,x} \\ y_{DB,j} = y_j(\varphi_{sl}) + \xi_{DB,j,y}. \end{cases} \quad (\text{IV.8})$$

Transition Curve

When the train runs into the transition curve ($\ell_{m+1} < \ell \leq \ell_{m+2}$) of the railway centerline, the equations for the true track database points are represented as

$$\begin{cases} x_j(\varphi_{tc}) = x_0 + (j\lambda - \ell_m) \cdot \cos \alpha - k_c(j\lambda - \ell_{m+1})^3 \sin \alpha \\ y_j(\varphi_{tc}) = y_0 + (j\lambda - \ell_m) \cdot \sin \alpha + k_c(j\lambda - \ell_{m+1})^3 \cos \alpha, \end{cases} \quad (\text{IV.9})$$

where $\varphi_{tc} = (x_0, y_0, \alpha, k_c)^T$ denotes the geometric parameters of a transition curve, $j = j_{m+1}, \dots, j_{m+2}$ and the equations for the collected track database points are given by

$$\begin{cases} x_{DB,j} = x_j(\varphi_{tc}) + \xi_{DB,j,x} \\ y_{DB,j} = y_j(\varphi_{tc}) + \xi_{DB,j,y}. \end{cases} \quad (\text{IV.10})$$

Circular Arc

When the train runs into the circular arc ($\ell_{m+2} < \ell \leq \ell_{m+3}$) of the railway centerline, the equations for the true track database points are represented as

$$\begin{cases} x_j(\varphi_{ca}) = x_0 + x'_j \cdot \cos \alpha - y'_j \cdot \sin \alpha \\ y_j(\varphi_{ca}) = y_0 + x'_j \cdot \sin \alpha + y'_j \cdot \cos \alpha, \end{cases} \quad (\text{IV.11})$$

where $\varphi_{ca} = (x_0, y_0, \alpha, x_c, y_c, R)^T$ denotes the geometric parameters of a circular arc, $j = j_{m+2}, \dots, j_{m+3}$ and

$$\begin{cases} x'_j = x_c + R \sin \left(\tau + \frac{j\lambda - \ell_{m+2}}{R} \right) \\ y'_j = y_c - R \cos \left(\tau + \frac{j\lambda - \ell_{m+2}}{R} \right) \end{cases} \quad (\text{IV.12})$$

is the representation of the true track database point $(x_j(\varphi_{ca}), y_j(\varphi_{ca}))$ on the $x'y'$ -plane. The equations for the collected track database points are given by

$$\begin{cases} x_{DB,j} = x_j(\varphi_{ca}) + \xi_{DB,j,x} \\ y_{DB,j} = y_j(\varphi_{ca}) + \xi_{DB,j,y}. \end{cases} \quad (\text{IV.13})$$

IV.3 Speed Estimation Based on a Model of Integrated System for a Constant Speed Case

This section assumes that the acceleration is negligible for some short periods. Hence, it is supposed that the train runs along the "ideal" railway track with an unknown constant speed v . The travelled distance ℓ_t at time t is equal to the product of speed v and duration t , i.e., $\ell_t = v \cdot t$ and $t = 1, 2, \dots$. Hence, the true train position is defined as : $X_t(\varphi, \ell_t) = (x(\varphi, \ell_t), y(\varphi, \ell_t), 0)^T$, where $(x(\varphi, \ell_t), y(\varphi, \ell_t))$ is the corresponding position, described by equations (IV.1), (IV.2), (IV.3) on the local tangent plane. Since the distance $\ell_t = v \cdot t$ and the speed v is unknown, the corresponding position $(x(\varphi, \ell_t), y(\varphi, \ell_t))$ can be regarded as a function of v , i.e., $(x(\varphi, v), y(\varphi, v))$.

IV.3.1 Model of GNSS/Track Database Integrated System

In this section, a rigorous mathematical model for the GNSS/track database integrated system is designed to estimate the train speed.

Nonlinear GNSS/Track Database Integrated System

Let us first combine the equations (IV.6) - (IV.8) for the discrete track database points collected from the straight segment and the pseudo-range equation r_i^t from the i -th satellite which located at known position $X_i^s = (x_i, y_i, z_i)^T$ to the train position $X_t(\varphi_{sl}, v)$ at time t , a nonlinear GNSS/track database integrated system can be written as

$$\begin{cases} Z_{DB,j} = X_j(\varphi_{sl}) + \xi_{DB,j} & j = j_m, \dots, j_{m+1} \\ r_i^t = d_i^t(\varphi_{sl}, v) + c b_r^t + \varepsilon_i^t & i = 1, \dots, n \end{cases}$$

where φ_{sl} and v are unknown parameters and must be estimated. $d_i^t(\varphi_{sl}, v) = \|X_t(\varphi_{sl}, v) - X_i^s\|_2$, is the true distance from the i -th satellite to the train position. b_r^t is a user clock bias, $c \simeq 2.9979 \cdot 10^8$ m/s is the speed of light and $\varepsilon_i^t \sim \mathcal{N}(0, \sigma_{PD}^2)$ is a pseudo-range noise.

The unknown parameters φ_{sl} and v appear nonlinearly in the nonlinear integrated system. It's difficult to directly estimate the unknown parameters from such a nonlinear model. To reduce the difficulties, the nonlinear model needs to be transformed to a linear model by means of some transformations. Hence, we follow here the linearization

of a nonlinear model which has been discussed in Section I.3. The nonlinear discrete track database model and the pseudo-range measurement model will be linearized around the working point, respectively. Then a final linear integrated system will be obtained by combining the two linearized models. Finally, the unknown parameters are estimated from the final linear integrated system.

Linearization of Discrete Track Database Model

Let us now introduce the following vectors $Z_{\text{DB}}^{sl} = (Z_{\text{DB},j_m}^T, \dots, Z_{\text{DB},j_{m+1}}^T)^T$ and $X_{sl}(\varphi_{sl}) = (X_{j_m}^T(\varphi_{sl}), \dots, X_{j_{m+1}}^T(\varphi_{sl}))^T$. By linearizing the function $\varphi_{sl} \mapsto Z_{\text{DB}}^{sl}(\varphi_{sl})$ with respect to the state vector φ_{sl} around the working point $\varphi_{sl,0} = (x_{00}, y_{00}, \alpha_0)^T$, and we get the system of linear equations

$$Z_{\text{DB}}^{sl,0} = Z_{\text{DB}}^{sl} - X_{sl}(\varphi_{sl,0}) \simeq H_0^{sl} \cdot (\varphi_{sl} - \varphi_{sl,0}) + \xi_{\text{DB}}^{sl}, \quad (\text{IV.14})$$

where $H_0^{sl} = \left. \frac{\partial Z_{\text{DB}}^{sl}(\varphi_{sl})}{\partial \varphi_{sl}} \right|_{\varphi_{sl}=\varphi_{sl,0}}$ is the Jacobian matrix of size $(2(j_{m+1} - j_m + 1) \times 3)$, which has been discussed in Appendix C and $\xi_{\text{DB}}^{sl} = (\xi_{\text{DB},j_m}^T, \dots, \xi_{\text{DB},j_{m+1}}^T)^T$.

Linearization of Pseudo-range Measurement Model

Let us introduce the pseudo-range vector $R^t = (r_1^t, \dots, r_n^t)^T$, the state vector $\beta_t^{sl} = (\varphi_{sl}^T, v, cb_r^t)^T$, the working point $\beta_{t,0}^{sl} = (\varphi_{sl,0}^T, v_0, cb_0)^T$ and $\varphi_{sl,0} = (x_{00}, y_{00}, \alpha_0)^T$. By linearizing the function $\beta_t^{sl} \mapsto R^t(\beta_t^{sl})$ with respect to the state vector β_t^{sl} around the working point $\beta_{t,0}^{sl}$, we get the measurement equation

$$Y^t = R^t - R_0^t \simeq H_0^t \cdot (\beta_t^{sl} - \beta_{t,0}^{sl}) + \Xi^t, \quad (\text{IV.15})$$

where $R_0^t = (r_{1,0}^t, \dots, r_{n,0}^t)^T$, $r_{i,0}^t = d_i^t(\varphi_{sl,0}, v_0) + cb_0$, $\Xi^t = (\varepsilon_1^t, \dots, \varepsilon_n^t)^T$ and $H_0^t = \left. \frac{\partial R^t}{\partial \beta_t^{sl}} \right|_{\beta_t^{sl}=\beta_{t,0}^{sl}}$ is the Jacobian matrix of size $(n \times 5)$, which has also been discussed in Appendix C.

Linear GNSS/Track Database Integrated System

Finally, by combining the system of linear equations (IV.14) for the straight line and the final linearized measurement equation (IV.15), we can get a linear integrated system

$$\begin{pmatrix} Z_{\text{DB}}^{sl,0} \\ Y^t \end{pmatrix} \simeq \begin{pmatrix} H_0^{sl} & | & \mathbf{0} \\ \hline H_0^t & & \end{pmatrix} \begin{pmatrix} \varphi_{sl} - \varphi_{sl,0} \\ v - v_0 \\ cb_r^t - cb_0 \end{pmatrix} + \begin{pmatrix} \xi_{\text{DB}}^{sl} \\ \Xi^t \end{pmatrix}. \quad (\text{IV.16})$$

The above linear integrated system (IV.16) can be rewritten in the following manner :

$$Y_t^{sl} \simeq H_t^{sl} \cdot (\beta_t^{sl} - \beta_{t,0}^{sl}) + \Upsilon_t^{sl}, \quad (\text{IV.17})$$

where the vector $\beta_t^{sl} = (\varphi_{sl}^T, v, cb_r^t)^T$ is unknown and must be estimated. The working point at instant t is equal to the previously calculated estimation : $\beta_{t,0}^{sl} = \hat{\beta}_{t-1}^{sl}$. To seek simplicity, let us assume that $\sigma_{PD}^2 = \sigma_{DB}^2 = \sigma^2$, the LS estimator is given by

$$\hat{\beta}_t^{sl} = \hat{\beta}_{t-1}^{sl} + \left[(H_t^{sl})^T H_t^{sl} \right]^{-1} (H_t^{sl})^T Y_t^{sl}. \quad (\text{IV.18})$$

The current estimation error is $\hat{\beta}_t^{sl} - \beta_t^{sl}$. After substituting the right side of equation (IV.17) into the LS estimator (IV.18), the mean of this error is calculated as

$$\mathbb{E}(\hat{\beta}_t^{sl} - \beta_t^{sl}) = \mathbb{E} \left\{ \left[(H_t^{sl})^T H_t^{sl} \right]^{-1} (H_t^{sl})^T \Upsilon_t^{sl} \right\}, \quad (\text{IV.19})$$

and using the delta method which has been described in Section II.4.2, we get

$$\mathbb{E}(\hat{\beta}_t^{sl} - \beta_t^{sl}) \simeq 0. \quad (\text{IV.20})$$

For the second order moment of this error, the delta method yields to

$$\mathbb{E}(\hat{\beta}_t^{sl} - \beta_t^{sl})(\hat{\beta}_t^{sl} - \beta_t^{sl})^T \simeq \sigma^2 \left[(\bar{H}_t^{sl})^T \bar{H}_t^{sl} \right]^{-1}, \quad (\text{IV.21})$$

where \bar{H}_t^{sl} is calculated exactly as in equation (IV.17) but with the working point $\beta_{t,0}^{sl} = \beta_{t-1}^{sl}$.

Exactly as in the case of straight line, two linear GNSS/track database integrated systems for the cases of transition curve and circular arc can be obtained by using the same procedure by analogy with (IV.14) - (IV.17), see Appendix D.

IV.3.2 Numerical Simulations

The following scenario will be used in the sequel. The segments of the simulated train trajectory stored in the onboard train database are summarized in Tab. IV.1. The centerline curvature and the simulated train trajectory are shown by Fig. IV.3 and IV.4, respectively. Fig. IV.4 also shows a complete train trajectory, composed of straight line segments, transition curves and circular arcs of radius R . But the measured track database points don't coincide with the true railway track, due to the existence of the measurement error.

m	Curves	Curvilinear abscissa	Curvature	j
1	Straight	$[\ell_1, \ell_2]$	0	$[j_1, j_2]$
2	Transition	$(\ell_2, \ell_3]$	$0 \rightarrow \frac{1}{R}$	$(j_2, j_3]$
3	Circular	$(\ell_3, \ell_4]$	$\frac{1}{R}$	$(j_3, j_4]$
4	Transition	$(\ell_4, \ell_5]$	$\frac{1}{R} \rightarrow 0$	$(j_4, j_5]$
5	Straight	$(\ell_5, \ell_6]$	0	$(j_5, j_6]$
6	Transition	$(\ell_6, \ell_7]$	$0 \rightarrow -\frac{1}{R}$	$(j_6, j_7]$
7	Circular	$(\ell_7, \ell_8]$	$-\frac{1}{R}$	$(j_7, j_8]$
8	Transition	$(\ell_8, \ell_9]$	$-\frac{1}{R} \rightarrow 0$	$(j_8, j_9]$
9	Straight	$(\ell_9, \ell_{10}]$	0	$(j_9, j_{10}]$

Tableau IV.1 – Segments of the tested simulation scenario.

The standard GNSS constellation with $n = 6$ visible satellites is used. The GNSS sampling interval is $\Delta t = 0.5$ s. The pseudo-range SD is assumed to be of $\sigma_{PD} = 2$ m. The true train speed is 20 m/s and the initial working point v_0 has been chosen as 10 m/s. The distance between two adjacent track database point has been chosen $\lambda = 10$ m. The accuracy of track database is assumed to be of $\sigma_{DB} = 2$ m. Different values of railway curve radius have been tested : $R = 100$ m and $R = 1000$ m. The comparison of the theoretical moments for the estimated speed given by equation (IV.20) and equation (IV.21), with the results of a 10^4 -repetition Monte-Carlo simulation, is shown in Fig. IV.5-IV.8.

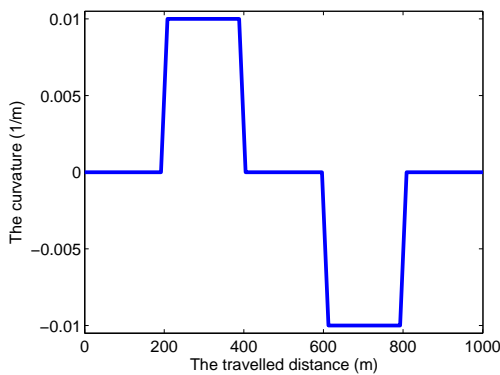


Figure IV.3 – The centerline curvature of the tested simulation scenario.

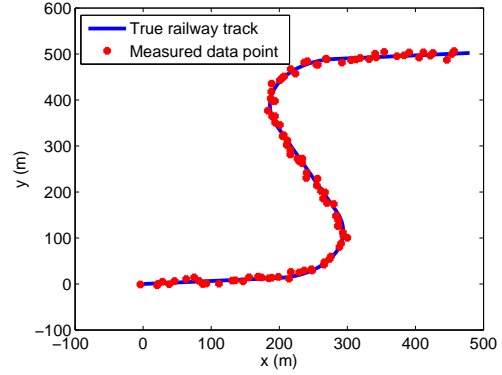


Figure IV.4 – The simulated train trajectory on the local horizontal plane.

As shown in Fig. IV.5 and IV.7, it can be seen that the estimated speed mean error is approaching zero after a short time period due to the nonlinearity of the model. Fig. IV.6 and IV.8 show that the estimated speed second order moment quickly becomes very weak, as in the "ideal" case.

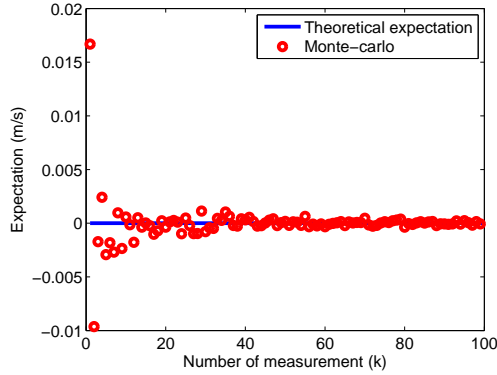


Figure IV.5 – The mean error of the estimated speed for $R = 1000$ m and $\sigma_{PD} = \sigma_{DB} = 2$ m.

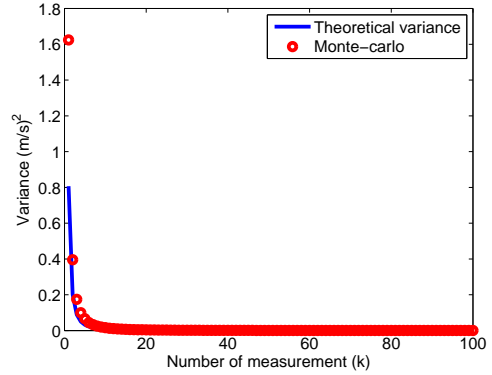


Figure IV.6 – The second order moment of the estimated speed for $R = 1000$ m and $\sigma_{PD} = \sigma_{DB} = 2$ m.

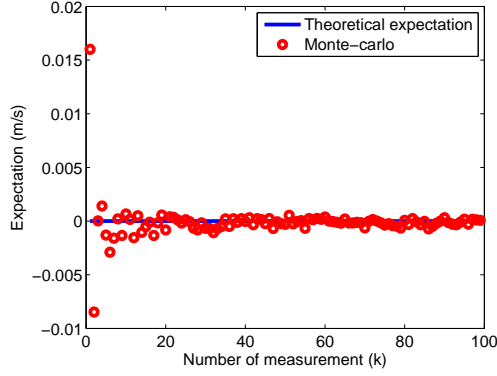


Figure IV.7 – The mean error of the estimated speed for $R = 100$ m and $\sigma_{PD} = \sigma_{DB} = 2$ m.

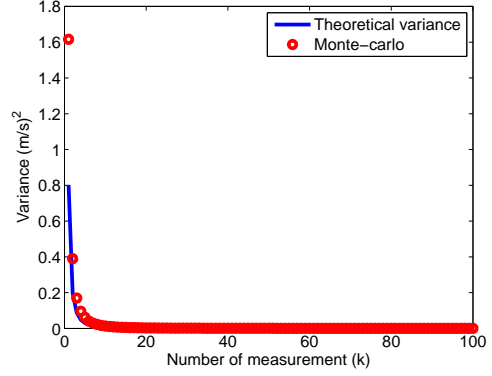


Figure IV.8 – The second order moment of the estimated speed for $R = 100$ m and $\sigma_{PD} = \sigma_{DB} = 2$ m.

IV.4 Speed and Distance Estimation Based on a Model of Integrated System for a Variable Speed Case

The goal of this section is to estimate the travelled distance and speed of the train when its acceleration is not neglected. Hence, it is assumed that the train runs along the "ideal" railway centerline with a variable speed. The train dynamical model is described by an equation formulated in terms of the travelled distance, speed and acceleration (see Fig. IV.9).

Let $\Delta t = t_k - t_{k-1}$ be the GNSS sampling interval and t_k denotes the instant of the k -th measurement. Let us consider a short time period of length $T = (q+1) \cdot \Delta t$ where

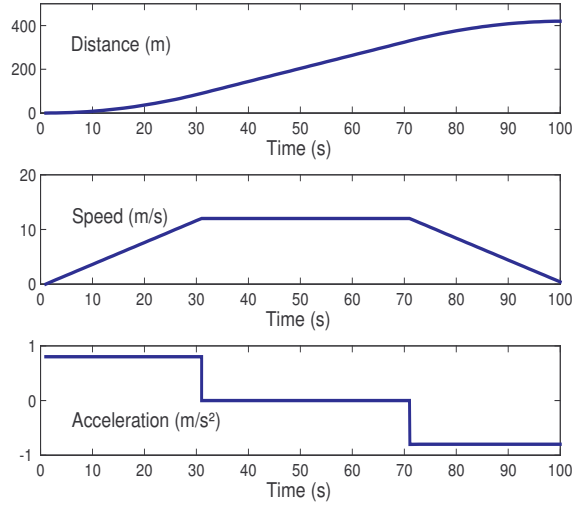


Figure IV.9 – Typical train motion diagram.

q is a positive integer. Over this time period, the distance ℓ_k covered by the train, its speed v_k and its acceleration a_k at instant t_k ($1 \leq k \leq q$) are given as follows

$$\begin{cases} \ell_k = \ell_{k-1} + v_{k-1} \cdot \Delta t + \frac{1}{2} a_{k-1} \cdot \Delta t^2 \\ v_k = v_{k-1} + a_{k-1} \cdot \Delta t \\ a_k = a_{k-1}. \end{cases} \quad (\text{IV.22})$$

Let us consider the block of $q+1$ last GNSS measurements at time instant t_k . Assuming that the acceleration a_k is constant during T (s), the train position is given by

$$X(\varphi, \ell_{k-q+p}) = [x(\varphi, \ell_{k-q+p}), y(\varphi, \ell_{k-q+p}), 0]^T,$$

where $(x(\varphi, \ell_{k-q+p}), y(\varphi, \ell_{k-q+p}))$ is the corresponding position, described by equations (IV.1), (IV.2), (IV.3) on the local tangent plane. $p = 0, 1, \dots, q$ and the distance is calculated as

$$\ell_{k-q+p} = \begin{pmatrix} 1 & (p-q) \cdot \Delta t & \frac{1}{2}(p-q)^2 \cdot \Delta t^2 \end{pmatrix} \begin{pmatrix} \ell_k \\ v_k \\ a_k \end{pmatrix} = \omega_p \cdot \theta_k \quad (\text{IV.23})$$

where the vector θ_k is unknown and must be estimated.

IV.4.1 Model of GNSS/Track Database Integrated System

In this section, a rigorous mathematical model for the GNSS/track database integrated system is designed to estimate the train travelled distance and speed.

Nonlinear GNSS/Track Database Integrated System

As discussed in the constant speed case, let us also combine the equations (IV.6) - (IV.8) for the track database points collected from the straight segment and the pseudo-range equation r_{k-q+p}^i from the i -th satellite which located at known position $X_i^s = (x_i, y_i, z_i)^T$ to the train position $X(\varphi_{sl}, \ell_{k-q+p})$ at time $k - q + p$, a nonlinear integrated system can be written as

$$\left\{ \begin{array}{ll} Z_{DB,j} = X_j(\varphi_{sl}) + \xi_{DB,j} & j = j_m, \dots, j_{m+1} \\ r_{k-q+p}^i = d_{k-q+p}^i(\varphi_{sl}, \ell_{k-q+p}) + cb_r^{k-q+p} + \varepsilon_{k-q+p}^i & i = 1, \dots, n \end{array} \right.$$

where $\varphi_{sl} = (x_0, y_0, \alpha)^T$ and ℓ_{k-q+p} are unknown parameters and must be estimated. $d_{k-q+p}^i(\varphi_{sl}, \ell_{k-q+p}) = \|X(\varphi_{sl}, \ell_{k-q+p}) - X_i^s\|_2$ is the true distance from the i -th satellite to the train position. b_r^{k-q+p} is a user clock bias, $c \simeq 2.9979 \cdot 10^8 m/s$ is the speed of light and $\varepsilon_{k-q+p}^i \sim \mathcal{N}(0, \sigma_{PD}^2)$ is the pseudo-range noise at time $k - q + p$.

To estimate the unknown parameters, the nonlinear integrated system also needs to be transformed to a linear integrated system. Since we have linearized the discrete track database model in equation (IV.14), we need merely to linearize the exact pseudo-range measurement model. Then a final linear integrated system will be obtained by combining the two linearized models. Finally, the unknown parameters are estimated from the final linear integrated system.

Linearization of Pseudo-range Measurement Model

Let us now introduce the pseudo-range vector $R_{k-q+p} = (r_{k-q+p}^1, \dots, r_{k-q+p}^n)^T$ and the vector $D_{k-q+p} = (d_{k-q+p}^1(\varphi_{sl}, \ell_{k-q+p}), \dots, d_{k-q+p}^n(\varphi_{sl}, \ell_{k-q+p}))^T$, the working point $\varphi_{sl,0} = (x_0, y_0, \alpha_0)^T$. By linearizing the pseudo-range vector R_{k-q+p} with respect to the state vector $(\varphi_{sl}^T, \ell_{k-q+p})^T$ around the working point $(\varphi_{sl,0}^T, \ell_{k-q+p,0})^T$, and we can get the measurement equation

$$R_{k-q+p} \simeq D_{k-q+p,0} + H_{\varphi_{sl}, k-q+p,0}(\varphi_{sl} - \varphi_{sl,0}) + H_{\ell, k-q+p,0}(\ell_{k-q+p} - \ell_{k-q+p,0}) + \mathbf{1}_n \cdot cb_r^{k-q+p} + \Xi_{k-q+p}, \quad (\text{IV.24})$$

where $D_{k-q+p,0} = (d_{k-q+p}^1(\varphi_{sl,0}, \ell_{k-q+p,0}), \dots, d_{k-q+p}^n(\varphi_{sl,0}, \ell_{k-q+p,0}))^T$ is the vector for the distances from the satellite to the working point and $H_{\varphi_{sl}, k-q+p,0} = \frac{\partial D_{k-q+p}}{\partial \varphi_{sl}} \Big|_{\varphi_{sl}=\varphi_{sl,0}}$, $H_{\ell, k-q+p,0} = \frac{\partial D_{k-q+p}}{\partial \ell_{k-q+p}} \Big|_{\ell_{k-q+p}=\ell_{k-q+p,0}}$ are two Jacobian matrices of size $(n \times 3)$ and $(n \times 1)$,

respectively. These two Jacobian matrices have also been discussed in Appendix C. $\mathbf{1}_n$ is a vector of dimension n whose each element is one.

The above mentioned linearized measurement equations (IV.24) can be rewritten in the following matrix form

$$Y_{k-q+p} \simeq H_{\varphi_{sl}, k-q+p, 0} \cdot \varphi_{sl} + H_{\ell, k-q+p, 0} \cdot \ell_{k-q+p} + \mathbf{1}_n \cdot cb_r^{k-q+p} + \Xi_{k-q+p}, \quad (\text{IV.25})$$

where $Y_{k-q+p} = R_{k-q+p} - D_{k-q+p, 0} + H_{\varphi_{sl}, k-q+p, 0} \cdot \varphi_{sl, 0} + H_{\ell, k-q+p, 0} \cdot \ell_{k-q+p, 0}$. It follows that

$$\begin{pmatrix} Y_k \\ \vdots \\ Y_{k-q} \end{pmatrix} \simeq \begin{pmatrix} H_{\varphi_{sl}, k, 0} \cdot \varphi_{sl} \\ \vdots \\ H_{\varphi_{sl}, k-q, 0} \cdot \varphi_{sl} \end{pmatrix} + \begin{pmatrix} H_{\ell, k, 0} \cdot \ell_k + \mathbf{1}_n \cdot cb_r^k \\ \vdots \\ H_{\ell, k-q, 0} \cdot \ell_{k-q} + \mathbf{1}_n \cdot cb_r^{k-q} \end{pmatrix} + \begin{pmatrix} \Xi_k \\ \vdots \\ \Xi_{k-q} \end{pmatrix}. \quad (\text{IV.26})$$

To estimate the distance, speed and acceleration simultaneously, substituting equation (IV.23) into equation (IV.26) yields to

$$\begin{pmatrix} Y_k \\ \vdots \\ Y_{k-q} \end{pmatrix} \simeq \begin{pmatrix} H_{\varphi_{sl}, k, 0} & H_{\ell, k, 0} \cdot \omega_q & \mathbf{1}_n & \\ & \vdots & & \ddots \\ H_{\varphi_{sl}, k-q, 0} & H_{\ell, k-q, 0} \cdot \omega_0 & & \mathbf{1}_n \end{pmatrix} \begin{pmatrix} \varphi_{sl} \\ \theta_k \\ cb_r^k \\ \vdots \\ cb_r^{k-q} \end{pmatrix} + \begin{pmatrix} \Xi_k \\ \vdots \\ \Xi_{k-q} \end{pmatrix}. \quad (\text{IV.27})$$

Linear GNSS/Track Database Integrated System

Finally, by combining the system of linear equations (IV.14) for the straight line and the final linearized measurement equation (IV.27), a final linear integrated system can be written as

$$\begin{pmatrix} \bar{Z}_{\text{DB}}^{sl, 0} \\ Y_k \\ \vdots \\ Y_{k-q} \end{pmatrix} \simeq \left(\begin{array}{c|cc} H_0^{sl} & \mathbf{0} & \\ \hline H_{\varphi_{sl}, k, 0} & H_{\ell, k, 0} \cdot \omega_q & \mathbf{1}_n \\ \vdots & \vdots & \ddots \\ H_{\varphi_{sl}, k-q, 0} & H_{\ell, k-q, 0} \cdot \omega_0 & \mathbf{1}_n \end{array} \right) \begin{pmatrix} \varphi_{sl} \\ \theta_k \\ cb_r^k \\ \vdots \\ cb_r^{k-q} \end{pmatrix} + \begin{pmatrix} \xi_{\text{DB}}^{sl} \\ \Xi_k \\ \vdots \\ \Xi_{k-q} \end{pmatrix}, \quad (\text{IV.28})$$

where $\bar{Z}_{\text{DB}}^{sl, 0} \simeq Z_{\text{DB}}^{sl, 0} + H_0^{sl} \varphi_{sl, 0}$ and the final linear integrated system (IV.28) can be rewritten in the following matrix :

$$Y_k^{sl} \simeq H_k^{sl} \beta_k^{sl} + \Upsilon_k^{sl}, \quad (\text{IV.29})$$

where the vector $\beta_k^{sl} = (\varphi_{sl}^T, \theta_k^T, cb_r^k, \dots, cb_r^{k-q})^T$ is unknown and must be estimated. The working point $\varphi_{sl, 0}$ at instant t_k is equal to the previously calculated estimation $\hat{\varphi}_{sl}$ and

$\ell_{k-q+p,0}$ is equal to the product of factor ω_p and previously calculated estimation $\hat{\theta}_{k-1}$, i.e., $\ell_{k-q+p,0} = \omega_p \cdot \theta_{k,0} = \omega_p \cdot \hat{\theta}_{k-1}$. To seek simplicity, let us assume that $\sigma_{\text{PD}}^2 = \sigma_{\text{DB}}^2 = \sigma^2$, the LS estimator is given by

$$\hat{\beta}_k^{sl} = \left[\left(H_k^{sl} \right)^T H_k^{sl} \right]^{-1} \left(H_k^{sl} \right)^T Y_k^{sl}. \quad (\text{IV.30})$$

The current estimation error is $\hat{\beta}_k^{sl} - \beta_k^{sl}$. After substituting the right side of equation (IV.29) into the LS estimator (IV.30), the mean of this error is computed as

$$\mathbb{E}(\hat{\beta}_k^{sl} - \beta_k^{sl}) = \mathbb{E} \left\{ \left[\left(H_k^{sl} \right)^T H_k^{sl} \right]^{-1} \left(H_k^{sl} \right)^T \Upsilon_k^{sl} \right\}, \quad (\text{IV.31})$$

and using the delta method, we get

$$\mathbb{E}(\hat{\beta}_k^{sl} - \beta_k^{sl}) = \mathbb{E} \left\{ \left[\left(H_k^{sl} \right)^T H_k^{sl} \right]^{-1} \left(H_k^{sl} \right)^T \Upsilon_k^{sl} \right\} \simeq 0. \quad (\text{IV.32})$$

For the second order moment of this error, the delta method yields to

$$\mathbb{E}(\hat{\beta}_k^{sl} - \beta_k^{sl})(\hat{\beta}_k^{sl} - \beta_k^{sl})^T \simeq \sigma^2 \left[\left(\bar{H}_k^{sl} \right)^T \bar{H}_k^{sl} \right]^{-1}, \quad (\text{IV.33})$$

where \bar{H}_k^{sl} is calculated exactly as in equation (IV.29) but with the working point $\varphi_{sl,0} = \varphi_{sl}$ and $\ell_{k-q+p,0} = \omega_p \cdot \theta_{k-1}$.

Exactly as in the case of straight line, two linear GNSS/track database integrated systems for the cases of transition curve and circular arc can be obtained by using the same procedure by analogy with (IV.24) - (IV.29), also see Appendix D.

IV.4.2 Numerical Simulations

The following scenario will be used in the sequel. The segments of the simulated train trajectory stored in the onboard train database are summarized in Tab. IV.1. The centerline curvature and the simulated train trajectory are shown by Fig. IV.10 and IV.11, respectively.

The standard GNSS constellation with $n = 6$ visible satellites is used. The GNSS sampling interval is $\Delta t = 0.5$ s. The pseudo-range SD is assumed to be of $\sigma_{\text{PD}} = 2$ m. The true acceleration during the acceleration, free-running and braking period is assumed to be of 0.8 m/s^2 , 0 m/s^2 and -0.8 m/s^2 , respectively.

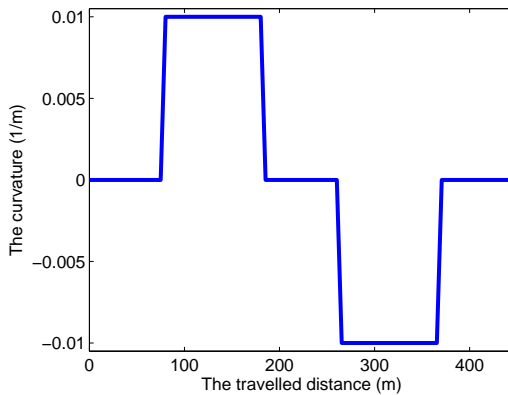


Figure IV.10 – The centerline curvature of the tested simulation scenario.

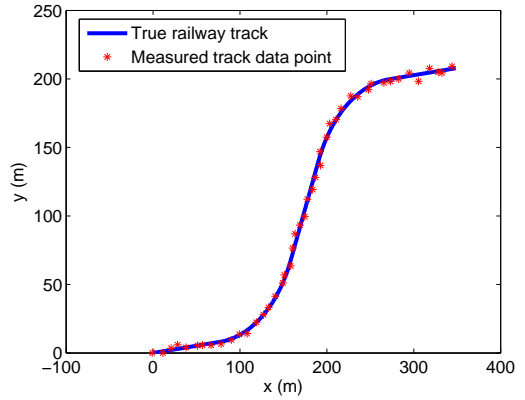


Figure IV.11 – The simulated train trajectory on the local horizontal plane.

The train motion diagram is shown in Fig. IV.9. The distance between two adjacent track database point has been chosen $\lambda = 10$ m. Different values of railway curve radius have been tested : $R = 100$ m and $R = 1000$ m. The accuracy of track database is assumed to be of $\sigma_{DB} = 2$ m. The comparison of the theoretical moments for the estimated distance, speed and acceleration given by equation (IV.32) and equation (IV.33), with the results of a 10^4 -repetition Monte-Carlo simulation, is shown in Fig. IV.12-IV.15 for the length of sliding window $q = 20$.

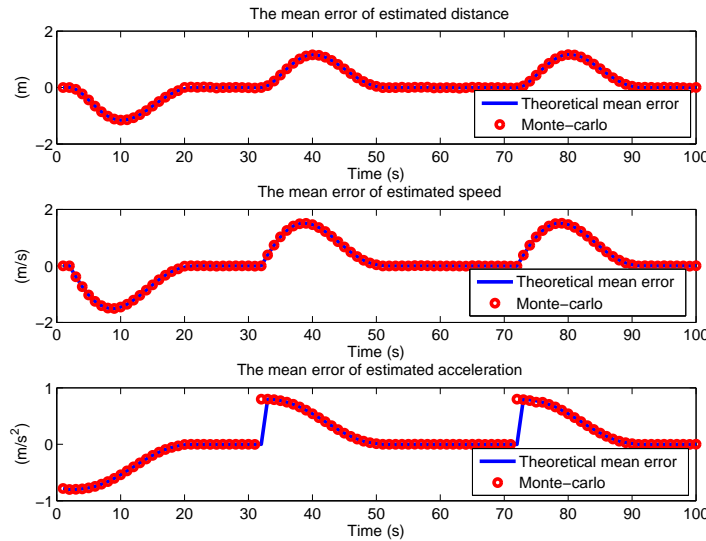


Figure IV.12 – The mean error of the estimated distance, speed and acceleration for $R = 1000$ m, $\sigma_{PD} = \sigma_{DB} = 2$ m and $q = 20$.

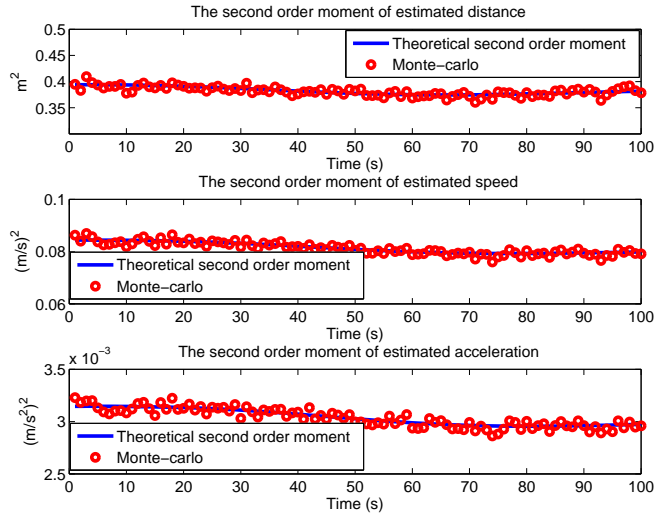


Figure IV.13 – The second order moment of the estimated distance, speed and acceleration for $R = 1000$ m, $\sigma_{\text{PD}} = \sigma_{\text{DB}} = 2$ m and $q = 20$.

From Fig. IV.12 and IV.14, we can see that the change of acceleration causes an imprecise estimation of the train travelled distance, speed and acceleration for a short time period, as in the precedent cases. The negative impact of both the centerline uncertainty and the railroad curvature on the second order moment of these estimations is nearly negligible. (see Fig. IV.13 and IV.15).

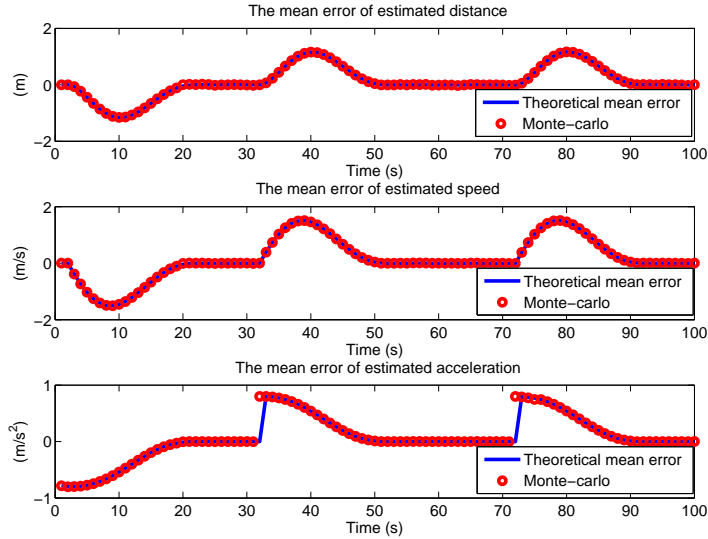


Figure IV.14 – The mean error of the estimated distance, speed and acceleration for $R = 100$ m, $\sigma_{\text{PD}} = \sigma_{\text{DB}} = 2$ m and $q = 20$.

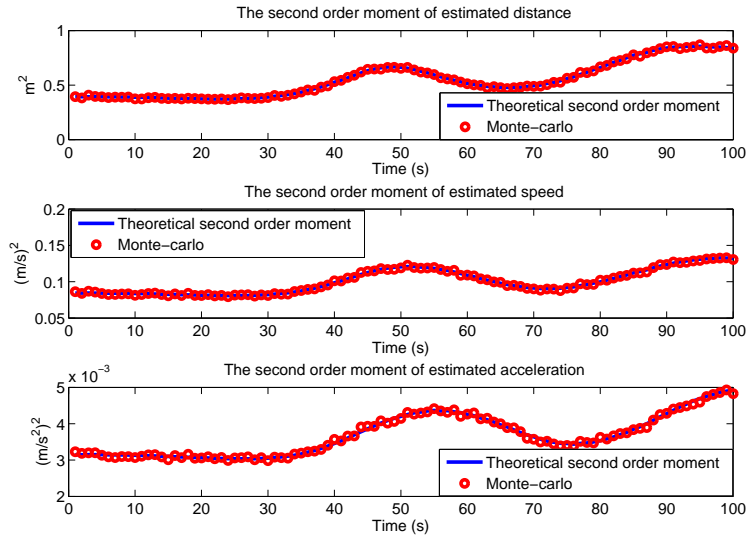


Figure IV.15 – The second order moment of the estimated distance, speed and acceleration for $R = 100$ m, $\sigma_{PD} = \sigma_{DB} = 2$ m and $q = 20$.

IV.5 Conclusions

In absence of acceleration, a linear GNSS/track database integrated system is designed to estimate the train speed. The train speed estimation by GNSS is practically unbiased. The estimated speed second order moment quickly becomes very weak, as in the "ideal" case. The negative impact of both the centerline uncertainty and the minimum railway curve radius on the estimated speed is nearly negligible.

In the variable speed case, a linear GNSS/track database integrated system is designed to estimate the travelled distance and speed of the train. The first two moments of the estimated travelled distance, speed and acceleration have been obtained to estimate the negative impacts of the errors from both the GNSS signals and track database on the above parameters. It has been shown that the change of acceleration causes an imprecise estimation of the travelled distance, speed and acceleration for a short time period, as in the precedent cases. The negative impact of both the centerline uncertainty and the minimum railway curve radius on these estimations is nearly negligible.

Chapitre V

Conclusions and Future Researches

V.1 Conclusions

As mentioned before, some advanced railway operating systems have been widely used to guarantee the safety and efficiency of the railway network. The efficiency of these systems is based on the availability of reliable train positioning. On the other hand, GNSS technology has attracted many attention around world and it has been widely applied in aviation, vehicle and marine application. Hence, applying GNSS technology in the train positioning is a very promising research area.

The algorithms described in this thesis are devoted to the train positioning by using GNSS signals. We have proposed the method of train positioning by using GNSS signals and a railway track. Then the impact of the track geometric model imprecision is studied for train positioning performance. The impact of the geometric characteristic of the railway centerline such as minimum railway curve radius on the train positioning performance is also discussed.

In Chapter II, the "ideal" railway centerline, composed of straight line segments, transition curves and arcs of circles, is defined by parametric equation. The train travelled distance and speed are estimated by using GNSS measurements and the "ideal" railway centerline. Two cases have been considered : a constant and variable speed. For both cases, a LS estimator is designed. For the constant speed case, the train speed estimation is practically unbiased, even with minimum railway curve radius. The estimated speed second order moment quickly becomes very weak. The impact of the railroad curvature on the mean error and on the second order moment of the estimated speed is nearly negligible. For the variable speed case, it has been shown that the change of acceleration causes an imprecise estimation of the travelled distance, speed

and acceleration for a short time period. The mean error is always practically unbiased except for a short time period after the acceleration changes, but the second order moment remains almost unchanged during this period. Small railway centerline curve radius can augment slightly the second order moment of the train distance, velocity and acceleration estimation.

In Chapter III, the "non-ideal" model of railway centerline is defined by a polygonal line with some level of uncertainty in the train onboard database. It represents a piecewise linear approximation of the "ideal" model. The train travelled distance and speed are estimated by using GNSS measurements and the "non-ideal" railway centerline. Two cases have been considered : a constant and variable speed. For both cases, a LS estimator is designed. For the constant speed case, the train speed estimation is practically unbiased, even with an imprecise geometric model of the railway centerline. The centerline uncertainties considerably augment the estimated speed second order moment by comparison with the "ideal" case. For the variable speed case, the results show that the change of acceleration causes an imprecise estimation of the travelled distance, speed and acceleration for a short time period. The mean error is always practically unbiased except for a short time period after the acceleration changes, but the second order moment remains almost unchanged during this period. Railway centerline uncertainty also leads to a slight augmentation of the second order moment of these estimations by comparison with the "ideal" case.

In Chapter IV, the travelled distance and speed of the train are estimated by integrating GNSS with a track database with measurement errors. Two cases have been considered : a constant and variable speed. For both cases, a rigorous mathematical model for the GNSS/track database integrated system is designed. For the constant speed case, the train speed estimation is practically unbiased. The estimated speed second order moment quickly becomes very weak, as in the "ideal" case. The impact of both the centerline uncertainty and the railroad curvature on the mean error and on the second order moment of the estimated speed is nearly negligible. For the variable speed case, it has been shown that the change of acceleration causes an imprecise estimation of the travelled distance, speed and acceleration for a short time period, as in the precedent cases. The negative impact of both the centerline uncertainty and the railroad curvature on these estimations is nearly negligible.

V.2 Future Researches

In this section, we briefly discuss a number of promising directions for future researches.

Using Real Data to Test the Proposed Algorithms

When testing the performance of these proposed algorithms, we used simulated track database and a few assumptions. Currently, the real track database available is limited, we look forward to a more solid analysis of performance of train positioning information in a real world.

Extending 2D Train Trajectory to 3D Train Trajectory

It's interesting to extend the 2D train trajectory (on the local tangent plane) to approximate a 3D train trajectory in a real world.

Applying Kalman Filter in Train GNSS Positioning

Throughout this dissertation, the train positioning information is obtained by using the LS algorithm. It's interesting to apply the Kalman filter in train positioning, because it's very useful for a dynamical model.

Comparing the Obtained Results with that from Other Positioning Methods

We would like to compare the results obtained from our algorithms with that from other positioning methods, for example, using the odometric measurements (see details in Malvezzi et al. (2008, 2011)).

Using Doppler Measurements to Estimate the Speed

It's very common and useful to estimate the speed of the receiver by using Doppler measurements.

Integrating GNSS-based Navigation with Other Positioning Solutions

To reach the required safety level, we would like to perform the GNSS-based navigation with other positioning solutions, such as odometer, eddy current sensor, radar

sensors and inertial systems. The integration of additional independent sensors can improve the accuracy of the train positioning.

Designing Integrity Monitoring Algorithms for Train Positioning Using GNSS

Finally, we would like to develop the integrity monitoring algorithms for train positioning using GNSS. When the train always travels through deep cuttings, urban areas, forests and tunnels, the problem of integrity monitoring becomes very important.

Annexe A

Basic Notions in Estimation Theory

The Appendix A introduces some basic notions in estimation theory.

Convergence of Random Variables

Definition 6 (Convergence in law). *Let $(\xi_n)_{n \geq 1} = \xi_1, \xi_2, \dots$ be a sequence of random variables and let $\{F_n(x)\}_{n \geq 1} = F_1(x), F_2(x), \dots$ be a sequence of their distribution functions. A sequence $(\xi_n)_{n \geq 1}$ of random variables is said to converge in distribution, or converge weakly, or converge in law to a random variable ξ if*

$$\lim_{n \rightarrow \infty} F_n(x) = F(x),$$

where $F(x)$ is the distribution function of ξ , for every number $x \in \mathbb{R}$ at which F is continuous. This fact is denoted as $\xi_n \xrightarrow{\mathcal{L}} \xi$ or $\mathcal{L}(\xi_n) \xrightarrow{\mathcal{L}} \mathcal{L}(\xi)$.

Definition 7 (Convergence in probability). *Let $(\xi_n)_{n \geq 1} = \xi_1, \xi_2, \dots$ be a sequence of random variables. A sequence $(\xi_n)_{n \geq 1} = \xi_1, \xi_2, \dots$ of random variables converges in probability to a random variable ξ if*

$$\forall \varepsilon > 0 : \lim_{n \rightarrow \infty} \mathbb{P}(|\xi_n - \xi| > \varepsilon) = 0.$$

This fact is denoted as $\xi_n \xrightarrow{\mathbb{P}} \xi$.

Properties A.0.1 (Convergence in probability). *Let $\xi_n \xrightarrow{\mathbb{P}} \xi$ and $\eta_n \xrightarrow{\mathbb{P}} \eta$. It implies that*

$$\xi_n + \eta_n \xrightarrow{\mathbb{P}} \xi + \eta, \quad \xi_n \cdot \eta_n \xrightarrow{\mathbb{P}} \xi \cdot \eta.$$

Definition 8 (Converges almost surely (a.s.)). *A sequence $(\xi_n)_{n \geq 1} = \xi_1, \xi_2, \dots$ of random variables converges almost surely or almost everywhere or with probability 1 or strongly to a random variable ξ if*

$$\forall \varepsilon > 0 : \lim_{n \rightarrow \infty} \mathbb{P} \left[\sup_{k \geq n} |\xi_k - \xi| > \varepsilon \right] = 0.$$

This fact is denoted as $\xi_n \xrightarrow{a.s.} \xi$.

Properties A.0.2. *The almost sure convergence implies the convergence in probability. The convergence in probability implies the convergence in distribution.*

If $\xi_n \xrightarrow{a.s.} \xi$, then $\xi_n \xrightarrow{\mathbb{P}} \xi$. If $\xi_n \xrightarrow{\mathbb{P}} \xi$, then $\xi_n \xrightarrow{\mathcal{L}} \xi$

Theorem 2 (Continuity theorem). Let $(\xi_n)_{n \geq 1}$ be a sequence of (scalar \mathbb{R}^1 or vector \mathbb{R}^m) statistics such that $\xi_n \xrightarrow{a.s.} \xi$ or $\xi_n \xrightarrow{\mathbb{P}} \xi$ and g be a function of $m \geq 1$ variables which is continuous almost everywhere with respect to the distribution of the random variable ξ (that is, $g(\xi)$ is continuous at every point of a set D such that $\mathbb{P}(\xi \in D) = 1$). Then $g(\xi_n) \xrightarrow{a.s.} g(\xi)$, $g(\xi_n) \xrightarrow{\mathbb{P}} g(\xi)$, respectively.

Limit Theorems

Theorem 3 (Law of large numbers). Let ξ_1, \dots, ξ_n be a sequence of i.i.d. random variables. It is assumed that the random variables are integrable : $\mathbb{E}(|\xi|) < \infty$. Then

$$\text{weak law : } \frac{\xi_1 + \dots + \xi_n}{n} \xrightarrow{\mathbb{P}} \mathbb{E}(\xi), \quad \text{strong law : } \frac{\xi_1 + \dots + \xi_n}{n} \xrightarrow{a.s.} \mathbb{E}(\xi)$$

Theorem 4 (Central limit theorem). Let ξ_1, \dots, ξ_n be a sequence of i.i.d. random variables with means $\mathbb{E}(\xi)$ and variances $\text{var}(\xi)$ positive and finite $0 < \text{var}(\xi) < \infty$. Consider the sum $S_n = \xi_1 + \dots + \xi_n$. Then, $\forall x < y$

$$\mathbb{P}\left(x < \frac{S_n - n\mathbb{E}(\xi)}{\sqrt{n\text{var}(\xi)}} < y\right) \rightarrow \Phi(y) - \Phi(x) = \int_x^y \frac{1}{\sqrt{2\pi}} e^{-\frac{u^2}{2}} du \quad \text{when } n \rightarrow \infty.$$

Substitution Principle

Almost all estimation methods are based on the following substitution principle. The i.i.d. observations (ξ_1, \dots, ξ_n) are assumed to come from a law P_θ with Cumulative Distribution Function (CDF) $F_\theta(x)$. Let us assume that the unknown parameter θ can be represented by the following functional relation :

$$\theta = G(P)$$

Theorem 5 (Principle of substitution). Let $\theta = G(P)$. It is assumed that the functional G belongs to one of two classes :

1. Let $G(P) = h(\int g(x)dF(x))$, where the function $h : u \mapsto h(u)$ is continuous at the point $u_0 = \int g(x)dF_0(x)$.

2. Let $G(P) = \mathcal{G}(F)$, where the functional \mathcal{G} is continuous at the «point» F_0 in a uniform metric : for $n \rightarrow \infty$ $\mathcal{G}(F_n) \rightarrow \mathcal{G}(F_0)$ if $\sup_x |F_n(x) - F_0(x)| \rightarrow 0$ and the sample spaces of the distributions $F_n(x)$ belong to the sample space of F_0 .

Let \hat{P}_n be an empirical distribution. If $\xi \sim F_0$, then $\hat{\theta}_n = G(\hat{P}_n)$ is a strongly consistent estimator :

$$\hat{\theta}_n \xrightarrow{a.s.} \theta.$$

Asymptotic Normality

Definition 9. An estimator $\hat{\theta}$ is said to be asymptotically normal if

$$(\hat{\theta}_n - \theta)\sqrt{n} \xrightarrow{\mathcal{L}} \zeta \text{ with } \mathcal{L}(\zeta) = \mathcal{N}(0, \sigma^2).$$

Let $\hat{\theta}_n = G(\hat{P}_n)$ be a substitution estimator belonging to the first class, i.e.

$$G(P) = h \left(\int g(x)dF(x) \right) \text{ and } \hat{\theta}_n = G(\hat{P}_n) = h \left(\frac{1}{n} \sum_{i=1}^n g(y_i) \right).$$

Let $\xi \sim F_0$. If the function $h : u \mapsto h(u)$ is differentiable at the point $u_0 = \int g(x)dF_0(x)$ where

$$0 < \left| \frac{dh}{du}(u_0) \right| < \infty \text{ and } \int g^2(x)dF_0(x) < \infty,$$

then $\hat{\theta}_n$ is an asymptotically normal estimator : $(\hat{\theta}_n - \theta)\sqrt{n} \xrightarrow{\mathcal{L}} \zeta$ where $\mathcal{L}(\zeta) = \mathcal{N}(0, \sigma^2)$ and

$$\sigma^2 = \left[\frac{dh}{du}(u_0) \right]^2 \int (g(x) - u_0)^2 dF_0(x).$$

Cramér-Rao Inequality

Scalar case : regularity conditions

Let us consider a parametric family $\mathcal{P} = \{P_\theta\}_{\theta \in \Theta}$. The observations ξ_1, \dots, ξ_n are assumed to come from P_θ , where $P_\theta \in \mathcal{P}$. The likelihood function for these observations is given by

$$L(\xi_1, \dots, \xi_n; \theta) = \sum_{i=1}^n l(\xi_i, \theta), \quad l(\xi, \theta) = \log f_\theta(\xi),$$

where $f_\theta(x)$ is the PDF of P_θ . Let us also define the function $a(\theta) = \mathbb{E}_\theta(\hat{\theta}) = \theta + b(\theta)$.

Suppose that the following condition is satisfied :

r 1 : the function $\theta \mapsto \sqrt{f_\theta(x)}$, for almost all values of x , is continuously differentiable in θ (i.e. $\sqrt{f_\theta(x)} \in C^1$)¹

r 2 : the integral

$$\mathcal{F}(\theta) = \mathbb{E}_\theta[(l'(\xi, \theta))^2] = \mathbb{E}_\theta\left[\left(\frac{\partial l(\xi, \theta)}{\partial \theta}\right)^2\right] = \mathbb{E}_\theta\left[\left(\frac{f'_\theta(\xi)}{f_\theta(\xi)}\right)^2\right] = \int \frac{(f'_\theta(x))^2}{f_\theta(x)} dx,$$

where $f'_\theta(x) = \frac{\partial f_\theta}{\partial \theta}(x)$, exists and $\theta \mapsto \mathcal{F}(\theta)$ is positive and continuous in θ ².

Theorem 6 (Cramér-Rao inequality). *Let $\hat{\theta} \in \mathcal{K}_b$ be an estimator. If the conditions of regularity r 1 and r 2 are satisfied, then*

$$\text{var}_\theta(\hat{\theta}) \geq \frac{[1 + b'(\theta)]^2}{n\mathcal{F}(\theta)},$$

where $b(\theta) = \mathbb{E}_\theta(\hat{\theta}) - \theta$ and $b'(\theta) = \frac{db}{d\theta}(\theta)$.

It follows that

$$\mathbb{E}_\theta[(\hat{\theta} - \theta)^2] \geq \frac{[1 + b'(\theta)]^2}{n\mathcal{F}(\theta)} + b^2(\theta).$$

For the class \mathcal{K}_0 of unbiased estimators, the so-called *Cramar-Rao lower bound* is

$$\mathbb{E}_\theta[(\hat{\theta} - \theta)^2] \geq \frac{1}{n\mathcal{F}(\theta)}.$$

1. A condition, say \mathcal{A} , is satisfied for almost all values of x if there exists a set $\mathcal{M} : \mathbb{P}(\xi \in \mathcal{M}) = 0$ such that the condition \mathcal{A} is satisfied for all $x \notin \mathcal{M}$.

2. It is considered that the integrals $\mathbb{E}_\theta[\varphi(\xi, \theta)]$ are defined over the set $D_{P_\theta} = \{x : f_\theta(x) > 0\}$.

Annexe B

Mathematical Derivations

The Appendix B provides the derivation of equations (III.9), (III.10), (III.22) and (III.23) in Chapter III.

A1. Derivation of Equations (III.9) And (III.10) :

As described in Section III.3.2, the imprecise pseudo-range measurement equation (III.6) can be written as follows :

$$Y^k + \Delta Y^k \simeq (H_0^k + \Delta H^k) \cdot \beta_k + \Xi^k,$$

where the unknown vector is $\beta_k = (\beta_1, \beta_2)^T$, the responses are

$$Y^k = \begin{pmatrix} y_1^k \\ y_2^k \\ \vdots \\ y_n^k \end{pmatrix},$$

the matrix of regressors are

$$H_0^k = \begin{pmatrix} h_{1,0}^k & 0 \\ h_{2,0}^k & 0 \\ \vdots & \vdots \\ h_{n,0}^k & 0 \end{pmatrix},$$

the data uncertainties in the dependent variable are

$$\Delta Y^k = \begin{pmatrix} \Delta y_1^k \\ \Delta y_2^k \\ \vdots \\ \Delta y_n^k \end{pmatrix},$$

whose elements are

$$\Delta y_i^k = -\frac{\partial \tilde{r}_{i,0}}{\partial \delta_j} \Big|_{\delta_j=0} \cdot \delta_j = -\frac{\partial \tilde{r}_{i,0}}{\partial \delta_x^j} \delta_x^j - \frac{\partial \tilde{r}_{i,0}}{\partial \delta_y^j} \delta_y^j$$

and the data uncertainties in the independent variable are

$$\Delta H^k = \begin{pmatrix} \Delta h_1^k & 0 \\ \Delta h_2^k & 0 \\ \vdots & \vdots \\ \Delta h_n^k & 0 \end{pmatrix},$$

whose elements are

$$\Delta h_i^k = \left. \frac{\partial \tilde{h}_{i,0}}{\partial \delta_j} \right|_{\delta_j=0} \cdot \delta_j = \frac{\partial \tilde{h}_{i,0}}{\partial \delta_x^j} \delta_x^j + \frac{\partial \tilde{h}_{i,0}}{\partial \delta_y^j} \delta_y^j.$$

Derivation of Equation (III.9) :

We compute the expectation of the LS estimator :

$$\begin{aligned} \mathbb{E}(\widehat{\beta}_k - \beta_k) &= B_0^{-1} \left\{ \left(H_0^k \right)^T \mathbb{E} \left[\Delta H^k B_0^{-1} \left(H_0^k \right)^T \Delta H^k \right] - \mathbb{E} \left[\left(\Delta H^k \right)^T \Delta H^k \right] \right. \\ &\quad \left. - \mathbb{E} \left[\left(\Delta H^k \right)^T H_0^k B_0^{-1} \left(H_0^k \right)^T \Delta H^k \right] \right\} \beta_k. \end{aligned} \quad (\text{B.1})$$

In the above equation (B.1), firstly three matrix functions are calculated as follows

(1) Calculation of $\mathbb{E} \left[\Delta H^k B_0^{-1} \left(H_0^k \right)^T \Delta H^k \right]$

Let $B_0^{-1}(H_0^k)^T = \tilde{C}_{2 \times n} = [\tilde{c}_{ij}]_{2 \times n}$ and we have

$$\begin{aligned} \Delta H^k B_0^{-1} (H_0^k)^T \Delta H^k &= \begin{pmatrix} \Delta h_1^k & 0 \\ \Delta h_2^k & 0 \\ \vdots & \vdots \\ \Delta h_n^k & 0 \end{pmatrix} \begin{pmatrix} \tilde{c}_{11} & \tilde{c}_{12} & \cdots & \tilde{c}_{1n} \\ \tilde{c}_{21} & \tilde{c}_{22} & \cdots & \tilde{c}_{2n} \end{pmatrix} \begin{pmatrix} \Delta h_1^k & 0 \\ \Delta h_2^k & 0 \\ \vdots & \vdots \\ \Delta h_n^k & 0 \end{pmatrix} \\ &= \begin{pmatrix} \Delta(h_1^k)^2 & \Delta h_1^k \Delta h_2^k & \cdots & \Delta h_1^k \Delta h_n^k \\ \Delta h_2^k \Delta h_1^k & (\Delta h_2^k)^2 & \cdots & \Delta h_2^k \Delta h_n^k \\ \vdots & \vdots & \ddots & \vdots \\ \Delta h_n^k \Delta h_1^k & \Delta h_n^k \Delta h_2^k & \cdots & (\Delta h_n^k)^2 \end{pmatrix} \begin{pmatrix} \tilde{c}_{11} & 0 \\ \tilde{c}_{12} & 0 \\ \vdots & \vdots \\ \tilde{c}_{1n} & 0 \end{pmatrix} \\ &= \Delta H^k (\Delta H^k)^T C. \end{aligned}$$

Taking expected values of $\Delta H^k (\Delta H^k)^T C$ gives

$$\mathbb{E} \left[\Delta H^k B_0^{-1} \left(H_0^k \right)^T \Delta H^k \right] = \mathbb{E} \left[\Delta H^k \left(\Delta H^k \right)^T C \right] = \Sigma_H C, \quad (\text{B.2})$$

where the covariance Σ_H is equal to

$$\Sigma_H = \frac{b^2}{3} \cdot \begin{pmatrix} \left(\frac{\partial \tilde{h}_{1,0}}{\partial \delta_x^j} \right)^2 + \left(\frac{\partial \tilde{h}_{1,0}}{\partial \delta_y^j} \right)^2 & \dots & \frac{\partial \tilde{h}_{1,0}}{\partial \delta_x^j} \frac{\partial \tilde{h}_{n,0}}{\partial \delta_x^j} + \frac{\partial \tilde{h}_{1,0}}{\partial \delta_y^j} \frac{\partial \tilde{h}_{n,0}}{\partial \delta_y^j} \\ \vdots & \ddots & \vdots \\ \frac{\partial \tilde{h}_{1,0}}{\partial \delta_x^j} \frac{\partial \tilde{h}_{n,0}}{\partial \delta_x^j} + \frac{\partial \tilde{h}_{1,0}}{\partial \delta_y^j} \frac{\partial \tilde{h}_{n,0}}{\partial \delta_y^j} & \dots & \left(\frac{\partial \tilde{h}_{n,0}}{\partial \delta_x^j} \right)^2 + \left(\frac{\partial \tilde{h}_{n,0}}{\partial \delta_y^j} \right)^2 \end{pmatrix}.$$

(2) Calculation of $\mathbb{E} \left[(\Delta H^k)^T \Delta H^k \right]$

The matrix product $(\Delta H^k)^T \Delta H^k$ is calculated as

$$(\Delta H^k)^T \Delta H^k = \begin{pmatrix} \Delta h_1^k & \Delta h_2^k & \cdots & \Delta h_n^k \\ 0 & 0 & \cdots & 0 \end{pmatrix} \begin{pmatrix} \Delta h_1^k & 0 \\ \Delta h_2^k & 0 \\ \vdots & \vdots \\ \Delta h_n^k & 0 \end{pmatrix} = \begin{pmatrix} \sum_{i=1}^n (\Delta h_i^k)^2 & 0 \\ 0 & 0 \end{pmatrix},$$

so computing the expectation yields to

$$\mathbb{E} \left[(\Delta H^k)^T H^k \right] = \begin{pmatrix} \mathbb{E} \left(\sum_{i=1}^n \Delta h_i^2 \right) & 0 \\ 0 & 0 \end{pmatrix} = \begin{pmatrix} \text{tr}(\Sigma_H) & 0 \\ 0 & 0 \end{pmatrix} = F. \quad (\text{B.3})$$

(3) Calculation of $\mathbb{E} \left[(\Delta H^k)^T H_0^k B_0^{-1} (H_0^k)^T \Delta H^k \right]$

Now let $\widetilde{H}^k = (\Delta h_1^k, \Delta h_2^k, \dots, \Delta h_n^k)^T$, which is equal to the first column of ΔH^k . It's clear that $H_0^k B_0^{-1} (H_0^k)^T = D = [d_{ij}]_{n \times n}$ is a symmetric matrix, and then we have

$$\begin{aligned} & (\Delta H^k)^T H_0^k B_0^{-1} (H_0^k)^T \Delta H^k \\ &= \begin{pmatrix} \Delta h_1^k & \Delta h_2^k & \cdots & \Delta h_n^k \\ 0 & 0 & \cdots & 0 \end{pmatrix} \begin{pmatrix} d_{11} & d_{12} & \cdots & d_{1n} \\ d_{21} & d_{22} & \cdots & d_{2n} \\ \vdots & \vdots & \ddots & \vdots \\ d_{n1} & d_{n2} & \cdots & d_{nn} \end{pmatrix} \begin{pmatrix} \Delta h_1^k & 0 \\ \Delta h_2^k & 0 \\ \vdots & \vdots \\ \Delta h_n^k & 0 \end{pmatrix} \\ &= \begin{pmatrix} \sum_{i,j=1}^n d_{ij} \Delta h_i^k \Delta h_j^k & 0 \\ 0 & 0 \end{pmatrix} = \begin{pmatrix} (\Delta \widetilde{H}^k)^T H_0^k B_0^{-1} (H_0^k)^T \Delta \widetilde{H}^k & 0 \\ 0 & 0 \end{pmatrix}. \end{aligned}$$

It's evident that $(\Delta \widetilde{H}^k)^T H_0^k B_0^{-1} (H_0^k)^T \Delta \widetilde{H}^k$ is a quadratic form, the expectation $\mathbb{E} \left[(\Delta H^k)^T H_0^k B_0^{-1} (H_0^k)^T \Delta H^k \right]$ is calculated as

$$\mathbb{E} \left[(\Delta H^k)^T H_0^k B_0^{-1} (H_0^k)^T \Delta H^k \right] = \begin{pmatrix} \text{tr} \left(H_0^k B_0^{-1} (H_0^k)^T \Sigma_H \right) & 0 \\ 0 & 0 \end{pmatrix} = G. \quad (\text{B.4})$$

Finally, substituting the equations (B.2), (B.3), (B.4) into the right side of equation (B.1) yields to equation (III.9).

Derivation of Equation (III.10) :

Now the LS estimator is written as

$$\widehat{\beta}_k - \beta_k = B_0^{-1} (H_0^k)^T (\Xi^k + \Delta Y^k - \Delta H^k \beta_k),$$

so the second order moment of $\widehat{\beta}_k$ can be calculated as

$$\begin{aligned} & \mathbb{E} \left[(\widehat{\beta}_k - \beta_k) (\widehat{\beta}_k - \beta_k)^T \right] \\ &= B_0^{-1} (H_0^k)^T \mathbb{E} \left[(\Xi^k + \Delta Y^k - \Delta H^k \beta_k) (\Xi^k + \Delta Y^k - \Delta H^k \beta_k)^T \right] H_0^k B_0^{-1} \\ &= B_0^{-1} (H_0^k)^T \left\{ \sigma^2 I_n + \Sigma_Y - \mathbb{E} \left[\Delta Y^k \beta_k^T (\Delta H^k)^T \right] - \mathbb{E} \left[\Delta H^k \beta_k (\Delta Y^k)^T \right] \right. \\ &\quad \left. + \mathbb{E} \left[\Delta H^k \beta_k \beta_k^T (\Delta H^k)^T \right] \right\} H_0^k B_0^{-1}. \end{aligned} \quad (\text{B.5})$$

In the above equation (B.5), firstly four matrix functions are calculated as follows

(1) Calculation of the covariance Σ_Y

The covariance $\Sigma_Y = \mathbb{E} \left[\Delta Y^k (\Delta Y^k)^T \right]$ is equal to

$$\Sigma_Y = \frac{b^2}{3} \cdot \begin{pmatrix} \left(\frac{\partial \tilde{r}_{1,0}}{\partial \delta_x^j} \right)^2 + \left(\frac{\partial \tilde{r}_{1,0}}{\partial \delta_y^j} \right)^2 & \dots & \frac{\partial \tilde{r}_{1,0}}{\partial \delta_x^j} \frac{\partial \tilde{r}_{n,0}}{\partial \delta_x^j} + \frac{\partial \tilde{r}_{1,0}}{\partial \delta_y^j} \frac{\partial \tilde{r}_{n,0}}{\partial \delta_y^j} \\ \vdots & \ddots & \vdots \\ \frac{\partial \tilde{r}_{1,0}}{\partial \delta_x^j} \frac{\partial \tilde{r}_{n,0}}{\partial \delta_x^j} + \frac{\partial \tilde{r}_{1,0}}{\partial \delta_y^j} \frac{\partial \tilde{r}_{n,0}}{\partial \delta_y^j} & \dots & \left(\frac{\partial \tilde{r}_{n,0}}{\partial \delta_x^j} \right)^2 + \left(\frac{\partial \tilde{r}_{n,0}}{\partial \delta_y^j} \right)^2 \end{pmatrix}. \quad (\text{B.6})$$

(2) Calculation of $\mathbb{E} \left[\Delta Y^k \beta_k^T (\Delta H^k)^T \right]$ and $\mathbb{E} \left[\Delta H^k \beta_k (\Delta Y^k)^T \right]$

The matrix product $\Delta Y^k \beta_k^T (\Delta H^k)^T$ is calculated as

$$\begin{aligned} \Delta Y^k \beta_k^T (\Delta H^k)^T &= \begin{pmatrix} \Delta y_1^k \\ \Delta y_2^k \\ \vdots \\ \Delta y_n^k \end{pmatrix} \begin{pmatrix} \beta_1 & \beta_2 \end{pmatrix} \begin{pmatrix} \Delta h_1^k & \Delta h_2^k & \dots & \Delta h_n^k \\ 0 & 0 & \dots & 0 \end{pmatrix} \\ &= \beta_1 \begin{pmatrix} \Delta y_1^k \\ \Delta y_2^k \\ \vdots \\ \Delta y_n^k \end{pmatrix} \begin{pmatrix} \Delta h_1^k & \Delta h_2^k & \dots & \Delta h_n^k \end{pmatrix} = \beta_1 \Delta Y^k (\Delta \tilde{H}^k)^T, \end{aligned} \quad (\text{B.7})$$

so taking the expected value of $\Delta Y^k \beta_k^T (\Delta H^k)^T$ gives

$$\mathbb{E} \left[\Delta Y^k \beta_k^T (\Delta H^k)^T \right] = \mathbb{E} \left[\beta_1 \Delta Y^k (\Delta \tilde{H}^k)^T \right] = \beta_1 \Sigma_{Y \tilde{H}}, \quad (\text{B.8})$$

where the covariance $\Sigma_{Y \tilde{H}}$ is

$$\Sigma_{Y \tilde{H}} = -\frac{b^2}{3} \cdot \begin{pmatrix} \frac{\partial \tilde{r}_{1,0}}{\partial \delta_x^j} \frac{\partial \tilde{h}_{1,0}}{\partial \delta_x^j} + \frac{\partial \tilde{r}_{1,0}}{\partial \delta_y^j} \frac{\partial \tilde{h}_{1,0}}{\partial \delta_y^j} & \dots & \frac{\partial \tilde{r}_{1,0}}{\partial \delta_x^j} \frac{\partial \tilde{h}_{n,0}}{\partial \delta_x^j} + \frac{\partial \tilde{r}_{1,0}}{\partial \delta_y^j} \frac{\partial \tilde{h}_{n,0}}{\partial \delta_y^j} \\ \vdots & \ddots & \vdots \\ \frac{\partial \tilde{r}_{n,0}}{\partial \delta_x^j} \frac{\partial \tilde{h}_{1,0}}{\partial \delta_x^j} + \frac{\partial \tilde{r}_{n,0}}{\partial \delta_y^j} \frac{\partial \tilde{h}_{1,0}}{\partial \delta_y^j} & \dots & \frac{\partial \tilde{r}_{n,0}}{\partial \delta_x^j} \frac{\partial \tilde{h}_{n,0}}{\partial \delta_x^j} + \frac{\partial \tilde{r}_{n,0}}{\partial \delta_y^j} \frac{\partial \tilde{h}_{n,0}}{\partial \delta_y^j} \end{pmatrix}.$$

Because $\Delta H^k \beta_k (\Delta Y^k)^T = [\Delta Y^k \beta_k^T (\Delta H^k)^T]^T$, we get

$$\mathbb{E} [\Delta H^k \beta_k (\Delta Y^k)^T] = (\beta_1 \Sigma_{Y \tilde{H}})^T = \beta_1 \Sigma_{\tilde{H} Y}. \quad (\text{B.9})$$

(3) Calculation of $\mathbb{E} [\Delta H^k \beta_k \beta_k^T (\Delta H^k)^T]$

The matrix product $\Delta H^k \beta_k \beta_k^T (\Delta H^k)^T$ is calculated as

$$\begin{aligned} \Delta H^k \beta_k \beta_k^T (\Delta H^k)^T &= \begin{pmatrix} \Delta h_1^k & 0 \\ \Delta h_2^k & 0 \\ \vdots & \vdots \\ \Delta h_n^k & 0 \end{pmatrix} \begin{pmatrix} \beta_1 \\ \beta_2 \end{pmatrix} \begin{pmatrix} \beta_1 & \beta_2 \end{pmatrix} \begin{pmatrix} \Delta h_1^k & \Delta h_2^k & \cdots & \Delta h_n^k \\ 0 & 0 & \cdots & 0 \end{pmatrix} \\ &= \beta_1^2 \begin{pmatrix} \Delta(h_1^k)^2 & \Delta h_1^k \Delta h_2^k & \cdots & \Delta h_1^k \Delta h_n^k \\ \Delta h_2^k \Delta h_1^k & (\Delta h_2^k)^2 & \cdots & \Delta h_2^k \Delta h_n^k \\ \vdots & \vdots & \ddots & \vdots \\ \Delta h_n^k \Delta h_1^k & \Delta h_n^k \Delta h_2^k & \cdots & (\Delta h_n^k)^2 \end{pmatrix} \\ &= \beta_1^2 \Delta H^k (\Delta H^k)^T, \end{aligned}$$

so computing the expectation of $\Delta H^k \beta_k \beta_k^T (\Delta H^k)^T$ gives

$$\mathbb{E} [\Delta H^k \beta_k \beta_k^T (\Delta H^k)^T] = \mathbb{E} [\beta_1^2 \Delta H^k (\Delta H^k)^T] = \beta_1^2 \Sigma_H. \quad (\text{B.10})$$

Finally, substituting the equations (B.6), (B.8), (B.9), (B.10) into the right side of equation (B.5) yields to equation (III.10).

A2. Derivation of Equations (III.22) And (III.23) :

As described in Section III.4.2, the imprecise pseudo-range measurement (III.20) can also be written in the following form :

$$Y^k + \Delta Y^k \simeq (H_0^k + \Delta H^k) \cdot \beta_k + \Xi^k,$$

where the responses are

$$Y^k = R^k - D_0^k + Y_0^k = \begin{pmatrix} R_k \\ R_{k-1} \\ \vdots \\ R_{k-q} \end{pmatrix} - \begin{pmatrix} D_{k,0} \\ D_{k-1,0} \\ \vdots \\ D_{k-q,0} \end{pmatrix} + \begin{pmatrix} H_{k,0} \ell_{k,0} \\ H_{k-1,0} \ell_{k-1,0} \\ \vdots \\ H_{k-q,0} \ell_{k-q,0} \end{pmatrix},$$

the matrix of regressors are

$$H_0^k = \begin{pmatrix} H_{k,0} \cdot \omega_q & \mathbf{1}_n & & \\ H_{k-1,0} \cdot \omega_{q-1} & & \mathbf{1}_n & \\ \vdots & & & \ddots \\ H_{k-q,0} \cdot \omega_0 & & & \mathbf{1}_n \end{pmatrix},$$

the data uncertainties in the dependent variable are

$$\Delta Y^k = D_0^k - \widetilde{D}_0^k - Y_0^k + \widetilde{Y}_0^k = \begin{pmatrix} \Delta H_k \ell_{k,0} \\ \Delta H_{k-1} \ell_{k-1,0} \\ \vdots \\ \Delta H_{k-q} \ell_{k-q,0} \end{pmatrix} - \begin{pmatrix} \Delta D_k \\ \Delta D_{k-1} \\ \vdots \\ \Delta D_{k-q} \end{pmatrix},$$

the elements of the two n -dimensional column vectors ΔH_{k-q+p} and ΔD_{k-q+p} are

$$\Delta h_{k-q+p,0}^i = \frac{\partial \tilde{h}_{k-q+p,0}^i}{\xi_j} \Big|_{\xi_j=0} \cdot \xi_j = \frac{\partial \tilde{h}_{k-q+p,0}^i}{\partial \xi_x^j} \xi_x^j + \frac{\partial \tilde{h}_{k-q+p,0}^i}{\partial \xi_y^j} \xi_y^j$$

and

$$\Delta d_{k-q+p,0}^i = \frac{\partial \tilde{d}_{k-q+p,0}^i}{\xi_j} \Big|_{\xi_j=0} \cdot \xi_j = \frac{\partial \tilde{d}_{k-q+p,0}^i}{\partial \xi_x^j} \xi_x^j + \frac{\partial \tilde{d}_{k-q+p,0}^i}{\partial \xi_y^j} \xi_y^j,$$

respectively. The data uncertainties in the independent variable are

$$\Delta H^k = \widetilde{H}_0^k - H_0^k = \begin{pmatrix} \Delta H_k \cdot \omega_q & \mathbf{0}_n & & \\ \Delta H_{k-1} \cdot \omega_{q-1} & & \mathbf{0}_n & \\ \vdots & & & \ddots \\ \Delta H_{k-q} \cdot \omega_0 & & & \mathbf{0}_n \end{pmatrix}.$$

$\mathbf{0}_n$ is a vector of dimension n whose element is zero.

Derivation of Equation (III.22) :

We compute the expectation of the LS estimator :

$$\begin{aligned} \mathbb{E}(\hat{\beta}_k - \beta_k) &= (\overline{B}^k)^{-1} \left\{ (\overline{H}_0^k)^{-1} \mathbb{E} \left[\Delta H^k (\overline{B}^k)^{-1} (\overline{H}_0^k)^T \Delta H^k \right] - \mathbb{E} \left[(\Delta H^k)^T \Delta H^k \right] \right. \\ &\quad \left. + \mathbb{E} \left[\Delta H^k \overline{H}_0^k (\overline{B}^k)^{-1} (\overline{H}_0^k)^T \Delta H^k \right] \right\} \beta_k, \end{aligned} \quad (\text{B.11})$$

where $\overline{B}^k = (\overline{H}_0^k)^T \overline{H}_0^k$. The matrices \overline{H}_0^k are calculated exactly as in equation (III.19) but with the working point $\ell_{k-q+p,0} = \omega_p \cdot \theta_{k-1}$. At first, we calculate three matrix functions in the above equation (B.11) :

(1) Calculation of $\mathbb{E} \left[\Delta H^k (\overline{B}^k)^{-1} (\overline{H}_0^k)^T \Delta H^k \right]$

The matrix product $(\bar{B}^k)^{-1} (\bar{H}_0^k)^T$ is denoted to be the $2 \times (q+1)$ matrix :

$$(\bar{B}^k)^{-1} (\bar{H}_0^k)^T = \begin{pmatrix} \chi_{1,1} & \chi_{1,2} & \cdots & \chi_{1,q+1} \\ \varpi_{2,1} & \varpi_{2,2} & \cdots & \varpi_{2,q+1} \end{pmatrix},$$

where $\chi_{1,u+1}$ and $\varpi_{2,u+1}$ are two matrices of size $3 \times n$ and $(q+1) \times n$, respectively. The following matrix product is calculated as

$$\begin{aligned} & \Delta H^k (\bar{B}^k)^{-1} (\bar{H}_0^k)^T \Delta H^k \\ &= \begin{pmatrix} \Delta H_k \cdot \omega_q & \mathbf{0}_{n,q+1} \\ \Delta H_{k-1} \cdot \omega_{q-1} & \mathbf{0}_{n,q+1} \\ \vdots & \vdots \\ \Delta H_{k-q} \cdot \omega_0 & \mathbf{0}_{n,q+1} \end{pmatrix} \begin{pmatrix} \chi_{1,1} & \chi_{1,2} & \cdots & \chi_{1,q+1} \\ \varpi_{2,1} & \varpi_{2,2} & \cdots & \varpi_{2,q+1} \end{pmatrix} \begin{pmatrix} \Delta H_k \cdot \omega_q & \mathbf{0}_{n,q+1} \\ \Delta H_{k-1} \cdot \omega_{q-1} & \mathbf{0}_{n,q+1} \\ \vdots & \vdots \\ \Delta H_{k-q} \cdot \omega_0 & \mathbf{0}_{n,q+1} \end{pmatrix} \\ &= \begin{pmatrix} \Delta H_k \cdot \omega_q \chi_{1,1} & \Delta H_k \cdot \omega_q \chi_{1,2} & \cdots & \Delta H_k \cdot \omega_q \chi_{1,q+1} \\ \Delta H_{k-1} \cdot \omega_{q-1} \chi_{1,1} & \Delta H_{k-1} \cdot \omega_{q-1} \chi_{1,2} & \cdots & \Delta H_{k-1} \cdot \omega_{q-1} \chi_{1,q+1} \\ \vdots & \vdots & \ddots & \vdots \\ \Delta H_{k-q} \cdot \omega_0 \chi_{1,1} & \Delta H_{k-q} \cdot \omega_0 \chi_{1,2} & \cdots & \Delta H_{k-q} \cdot \omega_0 \chi_{1,q+1} \end{pmatrix} \\ & \begin{pmatrix} \Delta H_k \cdot \omega_q & \mathbf{0}_{n,q+1} \\ \Delta H_{k-1} \cdot \omega_{q-1} & \mathbf{0}_{n,q+1} \\ \vdots & \vdots \\ \Delta H_{k-q} \cdot \omega_0 & \mathbf{0}_{n,q+1} \end{pmatrix} = \begin{pmatrix} \sum_{u=0}^q \Delta H_k \omega_q \chi_{1,u+1} \Delta H_{k-u} \omega_{q-u} & \mathbf{0}_{n,(q+1)} \\ \sum_{u=0}^q \Delta H_{k-1} \omega_{q-1} \chi_{1,u+1} \Delta H_{k-u} \omega_{q-u} & \mathbf{0}_{n,(q+1)} \\ \vdots & \vdots \\ \sum_{u=0}^q \Delta H_{k-q} \omega_0 \chi_{1,u+1} \Delta H_{k-u} \omega_{q-u} & \mathbf{0}_{n,(q+1)} \end{pmatrix}. \end{aligned}$$

Let us now define the following matrix

$$\gamma_{\ell,m} = \mathbb{E}(\Delta H_\ell \Delta H_m^T) = \frac{b^2}{3} \cdot \begin{pmatrix} \frac{\partial \tilde{h}_{\ell,0}^1}{\partial \xi_x^j} \frac{\partial \tilde{h}_{m,0}^1}{\partial \xi_x^j} + \frac{\partial \tilde{h}_{\ell,0}^1}{\partial \xi_y^j} \frac{\partial \tilde{h}_{m,0}^1}{\partial \xi_y^j} & \cdots & \frac{\partial \tilde{h}_{\ell,0}^1}{\partial \xi_x^j} \frac{\partial \tilde{h}_{m,0}^n}{\partial \xi_x^j} + \frac{\partial \tilde{h}_{\ell,0}^1}{\partial \xi_y^j} \frac{\partial \tilde{h}_{m,0}^n}{\partial \xi_y^j} \\ \vdots & \ddots & \vdots \\ \frac{\partial \tilde{h}_{\ell,0}^n}{\partial \xi_x^j} \frac{\partial \tilde{h}_{m,0}^1}{\partial \xi_x^j} + \frac{\partial \tilde{h}_{\ell,0}^n}{\partial \xi_y^j} \frac{\partial \tilde{h}_{m,0}^1}{\partial \xi_y^j} & \cdots & \frac{\partial \tilde{h}_{\ell,0}^n}{\partial \xi_x^j} \frac{\partial \tilde{h}_{m,0}^1}{\partial \xi_x^j} + \frac{\partial \tilde{h}_{\ell,0}^n}{\partial \xi_y^j} \frac{\partial \tilde{h}_{m,0}^1}{\partial \xi_y^j} \end{pmatrix}.$$

The expectation of $\Delta H^k (\bar{B}^k)^{-1} (\bar{H}_0^k)^T \Delta H^k$ is given by

$$\mathbb{E} \left[\Delta H^k (\bar{B}^k)^{-1} (\bar{H}_0^k)^T \Delta H^k \right] = \begin{pmatrix} \sum_{u=0}^q \gamma_{k,k-u} \chi_{1,u+1}^T \omega_q^T \omega_{q-u} & \mathbf{0}_{n,(q+1)} \\ \sum_{u=0}^q \gamma_{k-1,k-u} \chi_{1,u+1}^T \omega_{q-1}^T \omega_{q-u} & \mathbf{0}_{n,(q+1)} \\ \vdots & \vdots \\ \sum_{u=0}^q \gamma_{k-q,k-u} \chi_{1,u+1}^T \omega_0^T \omega_{q-u} & \mathbf{0}_{n,(q+1)} \end{pmatrix}. \quad (\text{B.12})$$

(2) Calculation of $\mathbb{E} \left[(\Delta H^k)^T \Delta H^k \right]$

The matrix product $(\Delta H^k)^T \Delta H^k$ is computed as

$$\begin{aligned} (\Delta H^k)^T \Delta H^k &= \begin{pmatrix} \Delta H_k \cdot \omega_q & \mathbf{0}_{n,q+1} \\ \Delta H_{k-1} \cdot \omega_{q-1} & \mathbf{0}_{n,q+1} \\ \vdots & \vdots \\ \Delta H_{k-q} \cdot \omega_0 & \mathbf{0}_{n,q+1} \end{pmatrix}^T \begin{pmatrix} \Delta H_k \cdot \omega_q & \mathbf{0}_{n,q+1} \\ \Delta H_{k-1} \cdot \omega_{q-1} & \mathbf{0}_{n,q+1} \\ \vdots & \vdots \\ \Delta H_{k-q} \cdot \omega_0 & \mathbf{0}_{n,q+1} \end{pmatrix} \\ &= \begin{pmatrix} \sum_{u=0}^q \omega_{q-u}^T \Delta H_{k-u}^T \Delta H_{k-u} \omega_{q-u} & \mathbf{0}_{3,(q+1)} \\ \mathbf{0}_{(q+1),3} & \mathbf{0}_{(q+1),(q+1)} \end{pmatrix}, \end{aligned}$$

so the expectation of $(\Delta H^k)^T \Delta H^k$ is

$$\mathbb{E} \left[(\Delta H^k)^T \Delta H^k \right] = \begin{pmatrix} \sum_{u=0}^q \text{tr} \gamma_{k-u,k-u} \omega_{q-u}^T \omega_{q-u} & \mathbf{0}_{3,(q+1)} \\ \mathbf{0}_{(q+1),3} & \mathbf{0}_{(q+1),(q+1)} \end{pmatrix}. \quad (\text{B.13})$$

(3) Calculation of $\mathbb{E} \left[\Delta H^k \bar{H}_0^k (\bar{B}^k)^{-1} (\bar{H}_0^k)^T \Delta H^k \right]$

Let us define the following matrix :

$$Q = \begin{pmatrix} Q_{1,1} & Q_{1,2} & \cdots & Q_{1,q+1} \\ Q_{2,1} & Q_{2,2} & \cdots & Q_{2,q+1} \\ \vdots & \vdots & \ddots & \vdots \\ Q_{(q+1),1} & Q_{(q+1),2} & \cdots & Q_{(q+1),q+1} \end{pmatrix},$$

where $Q_{u+1,v+1}$ is a block of size $n \times n$ of matrix $Q = \bar{H}_0^k (\bar{B}^k)^{-1} (\bar{H}_0^k)^T$. The following matrix product is calculated as

$$\begin{aligned} &\Delta H^k \bar{H}_0^k (\bar{B}^k)^{-1} (\bar{H}_0^k)^T \Delta H^k \\ &= \begin{pmatrix} \Delta H_k \cdot \omega_q & \mathbf{0}_{n,q+1} \\ \Delta H_{k-1} \cdot \omega_{q-1} & \mathbf{0}_{n,q+1} \\ \vdots & \vdots \\ \Delta H_{k-q} \cdot \omega_0 & \mathbf{0}_{n,q+1} \end{pmatrix}^T \begin{pmatrix} Q_{1,1} & Q_{1,2} & \cdots & Q_{1,q+1} \\ Q_{2,1} & Q_{2,2} & \cdots & Q_{2,q+1} \\ \vdots & \vdots & \ddots & \vdots \\ Q_{(q+1),1} & Q_{(q+1),2} & \cdots & Q_{(q+1),q+1} \end{pmatrix} \\ &\begin{pmatrix} \Delta H_k \cdot \omega_q & \mathbf{0}_{n,q+1} \\ \Delta H_{k-1} \cdot \omega_{q-1} & \mathbf{0}_{n,q+1} \\ \vdots & \vdots \\ \Delta H_{k-q} \cdot \omega_0 & \mathbf{0}_{n,q+1} \end{pmatrix} = \begin{pmatrix} \sum_{u=0}^q \sum_{v=0}^q \omega_{q-u}^T \Delta H_{k-v}^T Q_{u+1,v+1} \Delta H_{k-u} \omega_{q-v} & \mathbf{0}_{3,(q+1)} \\ \mathbf{0}_{(q+1),3} & \mathbf{0}_{(q+1),(q+1)} \end{pmatrix}, \end{aligned}$$

so the expectation of $\Delta H^k \bar{H}_0^k (\bar{B}^k)^{-1} (\bar{H}_0^k)^T \Delta H^k$ is

$$\mathbb{E} \left[\Delta H^k \bar{H}_0^k (\bar{B}^k)^{-1} (\bar{H}_0^k)^T \Delta H^k \right] = \begin{pmatrix} \sum_{u=0}^q \sum_{v=0}^q \text{tr} Q_{u+1,v+1} \gamma_{k-v,k-u} \omega_{q-u}^T \omega_{q-v} & \mathbf{0}_{3,(q+1)} \\ \mathbf{0}_{(q+1),3} & \mathbf{0}_{(q+1),(q+1)} \end{pmatrix}. \quad (\text{B.14})$$

Finally, substituting the equations (B.12), (B.13), (B.14) in the right side of equation (B.11) gives equation (III.22).

Derivation of Equation (III.23) :

The second order moment of $\hat{\beta}_k$ can be calculated as

$$\begin{aligned} & \mathbb{E}(\hat{\beta}_k - \beta_k)(\hat{\beta}_k - \beta_k)^T \\ &= (\bar{B}^k)^{-1} (\bar{H}_0^k)^T \left\{ \mathbb{E}\left[\Xi^k (\Xi^k)^T\right] + \mathbb{E}\left[\Delta Y^k (\Delta Y^k)^T\right] - \mathbb{E}\left[\Delta Y^k \beta_k^T (\Delta H^k)^T\right] \right. \\ &\quad \left. - \mathbb{E}\left[\Delta H^k \beta_k (\Delta Y^k)^T\right] + \mathbb{E}\left[\Delta H^k \beta_k \beta_k^T (\Delta H^k)^T\right] \right\} (\bar{H}_0^k) (\bar{B}^k)^{-1}. \end{aligned} \quad (\text{B.15})$$

We also firstly calculate four covariance functions in the above equation (B.15) :

$$(1) \text{ Calculation of } \mathbb{E}\left[\Delta Y^k (\Delta Y^k)^T\right]$$

The matrix product $\Delta Y^k (\Delta Y^k)^T$ is calculated as

$$\begin{aligned} \Delta Y^k (\Delta Y^k)^T &= \begin{pmatrix} \Delta H_k \ell_{k,0} - \Delta D_k \\ \Delta H_{k-1} \ell_{k-1,0} - \Delta D_{k-1} \\ \vdots \\ \Delta H_{k-q} \ell_{k-q,0} - \Delta D_{k-q} \end{pmatrix} \begin{pmatrix} \Delta H_k \ell_{k,0} - \Delta D_k \\ \Delta H_{k-1} \ell_{k-1,0} - \Delta D_{k-1} \\ \vdots \\ \Delta H_{k-q} \ell_{k-q,0} - \Delta D_{k-q} \end{pmatrix}^T \\ &= \begin{pmatrix} \ell_{k,0}^2 \Delta H_k \Delta H_k^T & \ell_{k,0} \ell_{k-1,0} \Delta H_k \Delta H_{k-1}^T & \cdots & \ell_{k,0} \ell_{k-q,0} \Delta H_k \Delta H_{k-q}^T \\ \ell_{k-1,0} \ell_{k,0} \Delta H_{k-1} \Delta H_k^T & \ell_{k-1,0}^2 \Delta H_{k-1} \Delta H_{k-1}^T & \cdots & \ell_{k-1,0} \ell_{k-q,0} \Delta H_{k-1} \Delta H_{k-q}^T \\ \vdots & \vdots & \ddots & \vdots \\ \ell_{k-q,0} \ell_{k,0} \Delta H_{k-q} \Delta H_k^T & \ell_{k-q,0} \ell_{k-1,0} \Delta H_{k-1} \Delta H_{k-1}^T & \cdots & \ell_{k-q,0}^2 \Delta H_{k-q} \Delta H_{k-q}^T \end{pmatrix} \\ &- \begin{pmatrix} \ell_{k,0} \Delta H_k \Delta D_k^T & \ell_{k,0} \Delta H_k \Delta D_{k-1}^T & \cdots & \ell_{k,0} \Delta H_k \Delta D_{k-q}^T \\ \ell_{k-1,0} \Delta H_{k-1} \Delta D_k^T & \ell_{k-1,0} \Delta H_{k-1} \Delta D_{k-1}^T & \cdots & \ell_{k-1,0} \Delta H_{k-1} \Delta D_{k-q}^T \\ \vdots & \vdots & \ddots & \vdots \\ \ell_{k-q,0} \Delta H_{k-q} \Delta D_k^T & \ell_{k-q,0} \Delta H_{k-q} \Delta D_{k-1}^T & \cdots & \ell_{k-q,0} \Delta H_{k-q} \Delta D_{k-q}^T \end{pmatrix} \\ &- \begin{pmatrix} \ell_{k,0} \Delta D_k \Delta H_k^T & \ell_{k-1,0} \Delta D_k \Delta H_{k-1}^T & \cdots & \ell_{k-q,0} \Delta D_k \Delta H_{k-q}^T \\ \ell_{k,0} \Delta D_{k-1} \Delta H_k^T & \ell_{k-1,0} \Delta D_{k-1} \Delta H_{k-1}^T & \cdots & \ell_{k-q,0} \Delta D_{k-1} \Delta H_{k-q}^T \\ \vdots & \vdots & \ddots & \vdots \\ \ell_{k,0} \Delta D_{k-q} \Delta H_k^T & \ell_{k-1,0} \Delta D_{k-q} \Delta H_{k-1}^T & \cdots & \ell_{k-q,0} \Delta D_{k-q} \Delta H_{k-q}^T \end{pmatrix} \\ &+ \begin{pmatrix} \Delta D_k \Delta D_k^T & \Delta D_k \Delta D_{k-1}^T & \cdots & \Delta D_k \Delta D_{k-q}^T \\ \Delta D_{k-1} \Delta D_k^T & \Delta D_{k-1} \Delta D_{k-1}^T & \cdots & \Delta D_{k-1} \Delta D_{k-q}^T \\ \vdots & \vdots & \ddots & \vdots \\ \Delta D_{k-q} \Delta D_k^T & \Delta D_{k-q} \Delta D_{k-1}^T & \cdots & \Delta D_{k-q} \Delta D_{k-q}^T \end{pmatrix}, \end{aligned}$$

so the expectation of $\mathbb{E} \left[\Delta Y^k \left(\Delta Y^k \right)^T \right]$ is given by

$$\mathbb{E} \left[\Delta Y^k \left(\Delta Y^k \right)^T \right] = S = \begin{pmatrix} S_{1,1} & S_{1,2} & \cdots & S_{1,q+1} \\ S_{2,1} & S_{2,2} & \cdots & S_{2,q+1} \\ \vdots & \vdots & \ddots & \vdots \\ S_{(q+1),1} & S_{(q+1),2} & \cdots & S_{(q+1),q+1} \end{pmatrix}, \quad (\text{B.16})$$

where

$$\begin{aligned} S_{u+1,v+1} = & \ell_{k-u,0} \ell_{k-v,0} \gamma_{k-u,k-v} - \ell_{k-u,0} \mathbb{E}(\Delta H_{k-u} \Delta D_{k-u}^T) - \ell_{k-v,0} \mathbb{E}(\Delta D_{k-u} \Delta H_{k-u}^T) \\ & + \mathbb{E}(\Delta D_{k-u} \Delta D_{k-v}^T), \end{aligned}$$

is a block of size $n \times n$ of matrix S , the covariance matrices $\mathbb{E}(\Delta H_{k-u} \Delta D_{k-u}^T)$, $\mathbb{E}(\Delta D_{k-u} \Delta H_{k-u}^T)$ and $\mathbb{E}(\Delta D_{k-u} \Delta D_{k-v}^T)$ are given by

$$\begin{aligned} \mathbb{E}(\Delta H_{k-u} \Delta D_{k-u}^T) = \mathbb{E}[(\Delta D_{k-u} \Delta H_{k-u}^T)]^T = \\ \frac{b^2}{3} \cdot \begin{pmatrix} \frac{\partial \tilde{h}_{k-u,0}^1}{\partial \xi_x^j} \frac{\partial \tilde{d}_{k-u,0}^1}{\partial \xi_x^j} + \frac{\partial \tilde{h}_{k-u,0}^1}{\partial \xi_y^j} \frac{\partial \tilde{d}_{k-u,0}^1}{\partial \xi_y^j} & \cdots & \frac{\partial \tilde{h}_{k-u,0}^1}{\partial \xi_x^j} \frac{\partial \tilde{d}_{k-u,0}^n}{\partial \xi_x^j} + \frac{\partial \tilde{h}_{k-u,0}^1}{\partial \xi_y^j} \frac{\partial \tilde{d}_{k-u,0}^n}{\partial \xi_y^j} \\ \vdots & \ddots & \vdots \\ \frac{\partial \tilde{h}_{k-u,0}^n}{\partial \xi_x^j} \frac{\partial \tilde{d}_{k-u,0}^1}{\partial \xi_x^j} + \frac{\partial \tilde{h}_{k-u,0}^n}{\partial \xi_y^j} \frac{\partial \tilde{d}_{k-u,0}^1}{\partial \xi_y^j} & \cdots & \frac{\partial \tilde{h}_{k-u,0}^n}{\partial \xi_x^j} \frac{\partial \tilde{d}_{k-u,0}^n}{\partial \xi_x^j} + \frac{\partial \tilde{h}_{k-u,0}^n}{\partial \xi_y^j} \frac{\partial \tilde{d}_{k-u,0}^n}{\partial \xi_y^j} \end{pmatrix} \end{aligned}$$

and

$$\mathbb{E}(\Delta D_{k-u} \Delta D_{k-v}^T) = \frac{b^2}{3} \cdot \begin{pmatrix} \frac{\partial \tilde{d}_{k-u,0}^1}{\partial \xi_x^j} \frac{\partial \tilde{d}_{k-v,0}^1}{\partial \xi_x^j} + \frac{\partial \tilde{d}_{k-u,0}^1}{\partial \xi_y^j} \frac{\partial \tilde{d}_{k-v,0}^1}{\partial \xi_y^j} & \cdots & \frac{\partial \tilde{d}_{k-u,0}^1}{\partial \xi_x^j} \frac{\partial \tilde{d}_{k-v,0}^n}{\partial \xi_x^j} + \frac{\partial \tilde{d}_{k-u,0}^1}{\partial \xi_y^j} \frac{\partial \tilde{d}_{k-v,0}^n}{\partial \xi_y^j} \\ \vdots & \ddots & \vdots \\ \frac{\partial \tilde{d}_{k-u,0}^n}{\partial \xi_x^j} \frac{\partial \tilde{d}_{k-v,0}^1}{\partial \xi_x^j} + \frac{\partial \tilde{d}_{k-u,0}^n}{\partial \xi_y^j} \frac{\partial \tilde{d}_{k-v,0}^1}{\partial \xi_y^j} & \cdots & \frac{\partial \tilde{d}_{k-u,0}^n}{\partial \xi_x^j} \frac{\partial \tilde{d}_{k-v,0}^n}{\partial \xi_x^j} + \frac{\partial \tilde{d}_{k-u,0}^n}{\partial \xi_y^j} \frac{\partial \tilde{d}_{k-v,0}^n}{\partial \xi_y^j} \end{pmatrix}.$$

(2) Calculation of $\mathbb{E} \left[\Delta Y^k \beta_k^T \left(\Delta H^k \right)^T \right]$ and $\mathbb{E} \left[\Delta H^k \beta_k \left(\Delta Y^k \right)^T \right]$

The matrix product $\Delta Y^k \beta_k^T (\Delta H^k)^T$ is calculated as

$$\begin{aligned}
& \Delta Y^k \beta_k^T (\Delta H^k)^T \\
&= \begin{pmatrix} \Delta H_k \cdot \omega_q & \mathbf{0}_{n,q+1} \\ \Delta H_{k-1} \cdot \omega_{q-1} & \mathbf{0}_{n,q+1} \\ \vdots & \vdots \\ \Delta H_{k-q} \cdot \omega_0 & \mathbf{0}_{n,q+1} \end{pmatrix} \begin{pmatrix} \theta_k \\ cb_r^k \\ \vdots \\ cb_r^{k-q} \end{pmatrix} \begin{pmatrix} \Delta H_k \ell_{k,0} - \Delta D_{k,0} \\ \Delta H_{k-1} \ell_{k-1,0} - \Delta D_{k-1} \\ \vdots \\ \Delta H_{k-q} \ell_{k-q,0} - \Delta D_{k-q} \end{pmatrix}^T \\
&= \begin{pmatrix} \Delta H_k \ell_k \\ \Delta H_{k-1} \ell_{k-1} \\ \vdots \\ \Delta H_{k-q} \ell_{k-q} \end{pmatrix} \begin{pmatrix} \Delta H_k \ell_{k,0} - \Delta D_k \\ \Delta H_{k-1} \ell_{k-1,0} - \Delta D_{k-1} \\ \vdots \\ \Delta H_{k-q} \ell_{k-q,0} - \Delta D_{k-q} \end{pmatrix}^T \\
&= \begin{pmatrix} \ell_k \ell_{k,0} \Delta H_k \Delta H_k^T & \ell_k \ell_{k-1,0} \Delta H_k \Delta H_{k-1}^T & \cdots & \ell_k \ell_{k-q,0} \Delta H_k \Delta H_{k-q}^T \\ \ell_{k-1} \ell_{k,0} \Delta H_{k-1} \Delta H_k^T & \ell_{k-1} \ell_{k-1,0} \Delta H_{k-1} \Delta H_{k-1}^T & \cdots & \ell_{k-1} \ell_{k-q,0} \Delta H_{k-1} \Delta H_{k-q}^T \\ \vdots & \vdots & \ddots & \vdots \\ \ell_{k-q} \ell_{k,0} \Delta H_{k-q} \Delta H_k^T & \ell_{k-q} \ell_{k-q,0} \Delta H_{k-1} \Delta H_{k-1}^T & \cdots & \ell_{k-q} \ell_{k-q,0} \Delta H_{k-q} \Delta H_{k-q}^T \end{pmatrix} \\
&\quad - \begin{pmatrix} \ell_k \Delta H_k \Delta D_k^T & \ell_k \Delta H_k \Delta D_{k-1}^T & \cdots & \ell_k \Delta H_k \Delta D_{k-q}^T \\ \ell_{k-1} \Delta H_{k-1} \Delta D_k^T & \ell_{k-1} \Delta H_{k-1} \Delta D_{k-1}^T & \cdots & \ell_{k-1} \Delta H_{k-1} \Delta D_{k-q}^T \\ \vdots & \vdots & \ddots & \vdots \\ \ell_{k-q} \Delta H_{k-q} \Delta D_k^T & \ell_{k-q} \Delta H_{k-1} \Delta D_{k-1}^T & \cdots & \ell_{k-q} \Delta H_{k-q} \Delta D_{k-q}^T \end{pmatrix},
\end{aligned}$$

so the expectation of $\Delta Y^k \beta_k^T (\Delta H^k)^T$ is given by

$$\mathbb{E} [\Delta Y^k \beta_k^T (\Delta H^k)^T] = N = \begin{pmatrix} N_{1,1} & N_{1,2} & \cdots & N_{1,(q+1)} \\ N_{2,1} & N_{2,2} & \cdots & N_{2,(q+1)} \\ \vdots & \vdots & \ddots & \vdots \\ N_{(q+1),1} & N_{(q+1),2} & \cdots & N_{(q+1),(q+1)} \end{pmatrix}, \quad (\text{B.17})$$

where $N_{u+1,v+1} = \ell_{k-u} \ell_{k-v,0} \gamma_{k-u,k-v} - \ell_{k-u} \mathbb{E}(\Delta H_{k-u} \Delta D_{k-v}^T)$ and ℓ_{k-u}, ℓ_{k-v} are calculated exactly as in equation (III.14) and $u, v = 0, \dots, q$.

Because $\Delta H^k \beta_k (\Delta Y^k)^T = [\Delta Y^k \beta_k^T (\Delta H^k)^T]^T$, we get

$$\mathbb{E} [\Delta H^k \beta_k (\Delta Y^k)^T] = \mathbb{E} [\Delta Y^k \beta_k^T (\Delta H^k)^T]^T = N^T. \quad (\text{B.18})$$

(3) Calculation of $\mathbb{E} [\Delta H^k \beta_k \beta_k^T (\Delta H^k)^T]$

The matrix product $\Delta H^k \beta_k \beta_k^T (\Delta H^k)^T$ is calculated as

$$\begin{aligned}
& \Delta H^k \beta_k \beta_k^T (\Delta H^k)^T \\
&= \begin{pmatrix} \Delta H_k \cdot \omega_q & \mathbf{0}_{n,q+1} \\ \Delta H_{k-1} \cdot \omega_{q-1} & \mathbf{0}_{n,q+1} \\ \vdots & \vdots \\ \Delta H_{k-q} \cdot \omega_0 & \mathbf{0}_{n,q+1} \end{pmatrix} \begin{pmatrix} \theta_k \\ cb_r^k \\ \vdots \\ cb_r^{k-q} \end{pmatrix} \begin{pmatrix} \theta_k \\ cb_r^k \\ \vdots \\ cb_r^{k-q} \end{pmatrix}^T \begin{pmatrix} \Delta H_k \cdot \omega_q & \mathbf{0}_{n,q+1} \\ \Delta H_{k-1} \cdot \omega_{q-1} & \mathbf{0}_{n,q+1} \\ \vdots & \vdots \\ \Delta H_{k-q} \cdot \omega_0 & \mathbf{0}_{n,q+1} \end{pmatrix}^T \\
&= \begin{pmatrix} \Delta H_k \ell_k \\ \Delta H_{k-1} \ell_{k-1} \\ \vdots \\ \Delta H_{k-q} \ell_{k-q} \end{pmatrix} \begin{pmatrix} \Delta H_k \ell_k \\ \Delta H_{k-1} \ell_{k-1} \\ \vdots \\ \Delta H_{k-q} \ell_{k-q} \end{pmatrix}^T \\
&= \begin{pmatrix} \ell_k^2 \Delta H_k \Delta H_k^T & \ell_k \ell_{k-1} \Delta H_k \Delta H_{k-1}^T & \cdots & \ell_k \ell_{k-q} \Delta H_k \Delta H_{k-q}^T \\ \ell_{k-1} \ell_k \Delta H_{k-1} \Delta H_k^T & \ell_{k-1}^2 \Delta H_{k-1} \Delta H_{k-1}^T & \cdots & \ell_{k-1} \ell_{k-q} \Delta H_{k-1} \Delta H_{k-q}^T \\ \vdots & \vdots & \ddots & \vdots \\ \ell_{k-q} \ell_k \Delta H_{k-q} \Delta H_k^T & \ell_{k-q} \ell_{k-1} \Delta H_{k-1} \Delta H_{k-1}^T & \cdots & \ell_{k-q}^2 \Delta H_{k-q} \Delta H_{k-q}^T \end{pmatrix},
\end{aligned}$$

so the expectation of $\Delta H^k \beta_k \beta_k^T (\Delta H^k)^T$ is given by

$$\mathbb{E} \left[\Delta H^k \beta_k \beta_k^T (\Delta H^k)^T \right] = M = \begin{pmatrix} M_{1,1} & M_{1,2} & \cdots & M_{1,q+1} \\ M_{2,1} & M_{2,2} & \cdots & M_{2,q+1} \\ \vdots & \vdots & \ddots & \vdots \\ M_{(q+1),1} & M_{(q+1),2} & \cdots & M_{(q+1),q+1} \end{pmatrix}, \quad (\text{B.19})$$

where $M_{u+1,v+1} = \ell_{k-u} \ell_{k-v} \gamma_{k-u,k-v}$.

Finally, substituting the equations (B.16), (B.17), (B.18), (B.19) in the right side of equation (B.11) gives equation (III.23).

Annexe C

Expressions of Jacobian Matrix

The Appendix C gives the detailed expressions of Jacobian matrix in Chapter IV.

Linear GNSS/Track Database Integrated System for a Constant Speed Case

In this section, we give the expressions of Jacobian matrix in both the linearized discrete track database model and the linearized GNSS pseudo-range measurement model, respectively.

Jacobian Matrix of the Linearized Discrete Track Database Model

The Jacobian matrix H_0^{sl} is given by

$$H_0^{sl} = \left. \frac{\partial Z_{DB}^{sl}(\varphi_{sl})}{\partial \varphi_{sl}} \right|_{\varphi_{sl}=\varphi_{sl,0}} = \begin{pmatrix} \frac{\partial Z_{DB,jm}(\varphi_{sl})}{\partial \varphi_{sl}} \\ \vdots \\ \frac{\partial Z_{DB,j_{m+1}}(\varphi_{sl})}{\partial \varphi_{sl}} \end{pmatrix},$$

whose element is

$$\frac{\partial Z_{DB,j}(\varphi_{sl})}{\partial \varphi_{sl}} = \left(\frac{\partial Z_{DB,j}(\varphi_{sl})}{\partial x_0}, \frac{\partial Z_{DB,j}(\varphi_{sl})}{\partial y_0}, \frac{\partial Z_{DB,j}(\varphi_{sl})}{\partial \alpha} \right)$$

and

$$\frac{\partial Z_{DB,j}(\varphi_{sl})}{\partial x_0} = \begin{pmatrix} 1 \\ 0 \end{pmatrix}, \quad \frac{\partial Z_{DB,j}(\varphi_{sl})}{\partial y_0} = \begin{pmatrix} 1 \\ 0 \end{pmatrix}, \quad \frac{\partial Z_{DB,j}(\varphi_{sl})}{\partial \alpha} = \begin{pmatrix} -(j\lambda - \ell_m) \sin \alpha_0 \\ (j\lambda - \ell_m) \cos \alpha_0 \end{pmatrix}.$$

Jacobian Matrix of the Linearized GNSS Pseudo-range Measurement Model

The Jacobian matrix H_0^t is given by

$$H_0^t = \left. \frac{\partial R^t}{\partial \beta_t^{sl}} \right|_{\beta_t^{sl}=\beta_{t,0}^{sl}} = \begin{pmatrix} \frac{\partial r_1^t(\varphi_{sl}, v)}{\partial \varphi_{sl}} & \frac{\partial r_1^t(\varphi_{sl}, v)}{\partial v} & 1 \\ \frac{\partial r_2^t(\varphi_{sl}, v)}{\partial \varphi_{sl}} & \frac{\partial r_2^t(\varphi_{sl}, v)}{\partial v} & 1 \\ \vdots & \vdots & \vdots \\ \frac{\partial r_n^t(\varphi_{sl}, v)}{\partial \varphi_{sl}} & \frac{\partial r_n^t(\varphi_{sl}, v)}{\partial v} & 1 \end{pmatrix},$$

whose element is

$$\frac{\partial r_i^t(\varphi_{sl}, v)}{\partial \varphi_{sl}} = \frac{(X_t(\varphi_{sl,0}, v_0) - X_i^s)^T \cdot \frac{\partial X_t(\varphi_{sl}, v)}{\partial \varphi_{sl}}|_{\varphi_{sl}=\varphi_{sl,0}}}{d_i^t(\varphi_{sl,0}, v_0)}$$

and

$$\frac{\partial r_i^t(\varphi_{sl}, v)}{\partial v} = \frac{(X_t(\varphi_{sl,0}, v_0) - X_i^s)^T \cdot \frac{\partial X_t(\varphi_{sl}, v)}{\partial v}|_{v=v_0}}{d_i^t(\varphi_{sl,0}, v_0)}.$$

Linear GNSS/Track Database Integrated System for a Variable Speed Case

In this section, the expressions of Jacobian matrix in the linearized GNSS pseudo-range measurement model are provided.

Jacobian Matrix of the Linearized GNSS Pseudo-range Measurement Model

The Jacobian matrix $H_{\varphi_{sl}, k-q+p, 0}$ is calculated by

$$H_{\varphi_{sl}, k-q+p, 0} = \left. \frac{\partial D_{k-q+p}}{\partial \varphi_{sl}} \right|_{\varphi_{sl}=\varphi_{sl,0}} = \begin{pmatrix} \frac{\partial d_{k-q+p}^1(\varphi_{sl}, \ell_{k-q+p})}{\partial \varphi_{sl}} \\ \vdots \\ \frac{\partial d_{k-q+p}^n(\varphi_{sl}, \ell_{k-q+p})}{\partial \varphi_{sl}} \end{pmatrix},$$

whose element is

$$\frac{\partial d_{k-q+p}^i(\varphi_{sl}, \ell_{k-q+p})}{\partial \varphi_{sl}} = \frac{[X(\varphi_{sl,0}, \ell_{k-q+p,0}) - X_i^s]^T \cdot \frac{\partial X(\varphi_{sl}, \ell_{k-q+p})}{\partial \varphi_{sl}}|_{\varphi_{sl}=\varphi_{sl,0}}}{\|X(\varphi_{sl,0}, \ell_{k-q+p,0}) - X_i^s\|_2}.$$

The Jacobian matrix $H_{\ell, k-q+p, 0}$ is calculated by

$$H_{\ell, k-q+p, 0} = \left. \frac{\partial D_{k-q+p}}{\partial \ell_{k-q+p}} \right|_{\ell_{k-q+p}=\ell_{k-q+p,0}} = \begin{pmatrix} \frac{\partial d_{k-q+p}^1(\varphi_{sl}, \ell_{k-q+p})}{\partial \ell_{k-q+p}} \\ \vdots \\ \frac{\partial d_{k-q+p}^n(\varphi_{sl}, \ell_{k-q+p})}{\partial \ell_{k-q+p}} \end{pmatrix},$$

whose element is

$$\frac{\partial d_{k-q+p}^i(\varphi_{sl}, \ell_{k-q+p})}{\partial \ell_{k-q+p}} = \frac{[X(\varphi_{sl,0}, \ell_{k-q+p,0}) - X_i^s]^T \cdot \frac{\partial X(\varphi_{sl}, \ell_{k-q+p})}{\partial \ell_{k-q+p}}|_{\ell_{k-q+p}=\ell_{k-q+p,0}}}{\|X(\varphi_{sl,0}, \ell_{k-q+p,0}) - X_i^s\|_2},$$

where the working point $\ell_{k-q+p,0} = \omega_p \cdot \theta_{k,0} = \omega_p \cdot \hat{\theta}_{k-1}$.

Annexe D

Integrated System Models

The Appendix D gives two linear GNSS/track database integrated systems for the cases of transition curve and circular arc.

Model of GNSS/Track Database Integrated System for a Constant Speed Case

This section presents two linear GNSS/track database integrated systems for the cases of transition curve and circular arc when the train travels along the "ideal" railway track with a constant speed v .

Transition Curve

Nonlinear GNSS/Track Database Integrated System

Let us first combine the equations (IV.6), (IV.9) and (IV.10) for the track database points collected from the transition curve and the pseudo-range equation r_i^t from the i -th satellite which located at known position $X_i^s = (x_i, y_i, z_i)^T$ to the train position $X_t(\varphi_{tc}, v)$ at time t , a nonlinear GNSS/track database integrated system can be written as

$$\begin{cases} Z_{DB,j} = X_j(\varphi_{tc}) + \xi_{DB,j} & j = j_{m+1}, \dots, j_{m+2} \\ r_i^t = d_i^t(\varphi_{tc}, v) + cb_r^t + \varepsilon_i^t & i = 1, \dots, n \end{cases}$$

where φ_{tc} and v are unknown parameters and must be estimated. $d_i^t(\varphi_{tc}, v) = \|X_t(\varphi_{tc}, v) - X_i^s\|_2$ is the true distance from the i -th satellite to the train. b_r^t is a user clock bias, $c \simeq 2.9979 \cdot 10^8 \text{ m/s}$ is the speed of light and $\varepsilon_i^t \sim \mathcal{N}(0, \sigma_{PD}^2)$ is a pseudo-range noise.

Linearization of Discrete Track Database Model

Let us now introduce the following vectors $Z_{DB}^{tc} = (Z_{DB,j_{m+1}}^T, \dots, Z_{DB,j_{m+2}}^T)^T$ and

$X_{tc}(\varphi_{tc}) = (X_{j_{m+1}}^T(\varphi_{tc}), \dots, X_{j_{m+2}}^T(\varphi_{tc}))^T$. By linearizing the function $\varphi_{tc} \mapsto Z_{DB}^{tc}(\varphi_{tc})$ with respect to the state vector φ_{tc} around the working point $\varphi_{tc,0} = (x_{00}, y_{00}, \alpha_0, k_{c0})^T$, and we get the system of linear equations

$$Z_{DB}^{tc,0} = Z_{DB}^{tc} - X_{tc}(\varphi_{tc,0}) \simeq H_0^{tc} \cdot (\varphi_{tc} - \varphi_{tc,0}) + \xi_{DB}^{tc}, \quad (D.1)$$

where $H_0^{tc} = \left. \frac{\partial Z_{DB}^{tc}(\varphi_{tc})}{\partial \varphi_{tc}} \right|_{\varphi_{tc}=\varphi_{tc,0}}$ is the Jacobian matrix of size $(2(j_{m+2} - j_{m+1} + 1) \times 4)$ and $\xi_{DB}^{tc} = (\xi_{DB,j_{m+1}}^T, \dots, \xi_{DB,j_{m+2}}^T)^T$.

Linearization of Pseudo-range Measurement Model

Let us introduce the pseudo-range vector $R^t = (r_1^t, \dots, r_n^t)^T$, the state vector $\beta_t^{tc} = (\varphi_{tc}^T, v, cb_r^t)^T$, the working point $\beta_{t,0}^{tc} = (\varphi_{tc,0}^T, v_0, cb_0)^T$ and $\varphi_{tc,0} = (x_{00}, y_{00}, \alpha_0, k_{c0})^T$. By linearizing the function $\beta_t^{tc} \mapsto R^t(\beta_t^{tc})$ with respect to the state vector β_t^{tc} around the working point $\beta_{t,0}^{tc}$, we get the measurement equation

$$Y^t = R^t - R_0^t \simeq H_0^t \cdot (\beta_t^{tc} - \beta_{t,0}^{tc}) + \Xi^t, \quad (D.2)$$

where $R_0^t = (r_{1,0}^t, \dots, r_{n,0}^t)^T$, $r_{i,0}^t = d_i^t(\varphi_{tc,0}, v_0) + cb_0$, $\Xi^t = (\varepsilon_1^t, \dots, \varepsilon_n^t)^T$ and $H_0^t = \left. \frac{\partial R^t}{\partial \beta_t^{tc}} \right|_{\beta_t^{tc}=\beta_{t,0}^{tc}}$ is the Jacobian matrix of size $(n \times 6)$.

Linear GNSS/Track Database Integrated System

Finally, by combining the system of linear equations (D.1) for transition curve and the final linearized measurement equation (D.2), we can get a linear integrated system

$$\begin{pmatrix} Z_{DB}^{tc,0} \\ Y^t \end{pmatrix} \simeq \begin{pmatrix} H_0^{tc} & | & \mathbf{0} \\ \hline H_0^t & & \end{pmatrix} \begin{pmatrix} \varphi_{tc} - \varphi_{tc,0} \\ v - v_0 \\ cb_r^t - cb_0 \end{pmatrix} + \begin{pmatrix} \xi_{DB}^{tc} \\ \Xi^t \end{pmatrix}. \quad (D.3)$$

The above linear integrated system (D.3) can be rewritten in the following manner :

$$Y_t^{tc} \simeq H_t^{tc} \cdot (\beta_t^{tc} - \beta_{t,0}^{tc}) + \Upsilon_t^{tc}, \quad (D.4)$$

where the vector $\beta_t^{tc} = (\varphi_{tc}^T, v, cb_r^t)^T$ is unknown and must be estimated. The working point at instant t is equal to the previously calculated estimation : $\beta_{t,0}^{tc} = \hat{\beta}_{t-1}^{tc}$. To seek simplicity, let us assume that $\sigma_{PD}^2 = \sigma_{DB}^2 = \sigma^2$, the LS estimator is given by

$$\hat{\beta}_t^{tc} = \hat{\beta}_{t-1}^{tc} + \left[\left(H_t^{tc} \right)^T H_t^{tc} \right]^{-1} \left(H_t^{tc} \right)^T Y_t^{tc}. \quad (D.5)$$

The current estimation error is $\hat{\beta}_t^{tc} - \beta_t^{tc}$. After substituting the right side of equation (D.4) into the LS estimator (D.5), the mean of this error is calculated as

$$\mathbb{E}(\hat{\beta}_t^{tc} - \beta_t^{tc}) = \mathbb{E} \left\{ \left[\left(H_t^{tc} \right)^T H_t^{tc} \right]^{-1} \left(H_t^{tc} \right)^T \Upsilon_t^{tc} \right\}, \quad (D.6)$$

and using the delta method, we get

$$\mathbb{E}(\hat{\beta}_t^{tc} - \beta_t^{tc}) \simeq 0. \quad (\text{D.7})$$

For the second order moment of this error, the delta method yields to

$$\mathbb{E}(\hat{\beta}_t^{tc} - \beta_t^{tc})(\hat{\beta}_t^{tc} - \beta_t^{tc})^T \simeq \sigma^2 \left[(\bar{H}_t^{tc})^T \bar{H}_t^{tc} \right]^{-1}, \quad (\text{D.8})$$

where \bar{H}_t^{tc} is calculated exactly as in equation (D.4) but with the working point $\beta_{t,0}^{tc} = \beta_{t-1}^{tc}$.

Circular Arc

Nonlinear GNSS/Track Database Integrated System

Let us first combine the equations (IV.6), (IV.11) and (IV.13) for the track database points collected from the circular arc and the pseudo-range equation r_i^t from the i -th satellite which located at known position $X_i^s = (x_i, y_i, z_i)^T$ to the train position $X_t(\varphi_{ca}, v)$ at time t , a nonlinear GNSS/track database integrated system can be written as

$$\begin{cases} Z_{DB,j} = X_j(\varphi_{ca}) + \xi_{DB,j} & j = j_{m+2}, \dots, j_{m+3} \\ r_i^t = d_i^t(\varphi_{ca}, v) + cb_r^t + \varepsilon_i^t & i = 1, \dots, n \end{cases}$$

where φ_{ca} and v are unknown parameters and must be estimated. $d_i^t(\varphi_{ca}, v) = \|X_t(\varphi_{ca}, v) - X_i^s\|_2$ is the true distance from the i -th satellite to the train position. b_r^t is a user clock bias, $c \simeq 2.9979 \cdot 10^8 \text{ m/s}$ is the speed of light and $\varepsilon_i^t \sim \mathcal{N}(0, \sigma_{PD}^2)$ is a pseudo-range noise.

Linearization of Discrete Track Database Model

Let us now introduce the following vectors $Z_{DB}^{ca} = (Z_{DB,j_{m+2}}^T, \dots, Z_{DB,j_{m+3}}^T)^T$ and $X_{ca}(\varphi_{ca}) = (X_{j_{m+2}}^T(\varphi_{ca}), \dots, X_{j_{m+3}}^T(\varphi_{ca}))^T$. By linearizing the function $\varphi_{ca} \mapsto Z_{DB}^{ca}(\varphi_{ca})$ with respect to the state vector φ_{ca} around the working point $\varphi_{ca,0} = (x_{00}, y_{00}, \alpha_{00}, x_{c0}, y_{c0}, R_0)^T$, and we get the system of linear equations :

$$Z_{DB}^{ca,0} = Z_{DB}^{ca} - X_{ca}(\varphi_{ca,0}) \simeq H_0^{ca} \cdot (\varphi_{ca} - \varphi_{ca,0}) + \xi_{DB}^{ca}, \quad (\text{D.9})$$

where $H_0^{ca} = \frac{\partial Z_{DB}^{ca}(\varphi_{ca})}{\partial \varphi_{ca}} \Big|_{\varphi_{ca}=\varphi_{ca,0}}$ is the Jacobian matrix of size $(2(j_{m+3} - j_{m+2} + 1) \times 6)$ and $\xi_{DB}^{ca} = (\xi_{DB,j_{m+2}}^T, \dots, \xi_{DB,j_{m+3}}^T)^T$.

Linearization of Pseudo-range Measurement Model

Let us introduce the pseudo-range vector $R^t = (r_1^t, \dots, r_n^t)^T$, the state vector $\beta_t^{ca} = (\varphi_{ca}^T, v, cb_r^t)^T$, the working point $\beta_{t,0}^{ca} = (\varphi_{ca,0}^T, v_0, cb_0)^T$ and $\varphi_{ca,0} = (x_{00}, y_{00}, \alpha_{00}, x_{c0}, y_{c0}, R_0)^T$. By linearizing the function $\beta_t^{ca} \mapsto R^t(\beta_t^{ca})$ with respect to the state vector β_t^{ca} around the working point $\beta_{t,0}^{ca}$, we get the measurement equation

$$Y^t = R^t - R_0^t \simeq H_0^t \cdot (\beta_t^{ca} - \beta_{t,0}^{ca}) + \Xi^t, \quad (\text{D.10})$$

where $R_0^t = (r_{1,0}^t, \dots, r_{n,0}^t)^T$, $r_{i,0}^t = d_i^t(\varphi_{ca,0}, v_0) + cb_0$, $\Xi^t = (\varepsilon_1^t, \dots, \varepsilon_n^t)^T$ and $H_0^t = \frac{\partial R^t}{\partial \beta_t^{ca}} \Big|_{\beta_t^{ca}=\beta_{t,0}^{ca}}$ is the Jacobian matrix of size $(n \times 8)$.

Linear GNSS/Track Database Integrated System

Finally, by combining the system of linear equations (D.9) for circular arc and the final linearized measurement equation (D.10), we can get a linear integrated system

$$\begin{pmatrix} Z_{DB}^{ca,0} \\ Y^t \end{pmatrix} \simeq \begin{pmatrix} H_0^{ca} & | & \mathbf{0} \\ H_0^t & & \end{pmatrix} \begin{pmatrix} \varphi_{ca} - \varphi_{ca,0} \\ v - v_0 \\ cb_r^t - cb_0 \end{pmatrix} + \begin{pmatrix} \xi_{DB}^{ca} \\ \Xi^t \end{pmatrix}. \quad (\text{D.11})$$

The above linear integrated system (D.11) can be rewritten in the following manner :

$$Y_t^{ca} \simeq H_t^{ca} \cdot (\beta_t^{ca} - \beta_{t,0}^{ca}) + \Upsilon_t^{ca}, \quad (\text{D.12})$$

where the vector $\beta_t^{ca} = (\varphi_{ca}^T, v, cb_r^t)^T$ is unknown and must be estimated. The working point at instant t is equal to the previously calculated estimation : $\beta_{t,0}^{ca} = \hat{\beta}_{t-1}^{ca}$. To seek simplicity, let us assume that $\sigma_{PD}^2 = \sigma_{DB}^2 = \sigma^2$, the LS estimator is given by

$$\hat{\beta}_t^{ca} = \hat{\beta}_{t-1}^{ca} + [(H_t^{ca})^T H_t^{ca}]^{-1} (H_t^{ca})^T Y_t^{ca}. \quad (\text{D.13})$$

The current estimation error is $\hat{\beta}_t^{ca} - \beta_t^{ca}$. After substituting the right side of equation (D.12) into the LS estimator (D.13), the mean of this error is calculated as

$$\mathbb{E}(\hat{\beta}_t^{ca} - \beta_t^{ca}) = \mathbb{E}\left\{[(H_t^{ca})^T H_t^{ca}]^{-1} (H_t^{ca})^T \Upsilon_t^{ca}\right\}, \quad (\text{D.14})$$

and using the delta method, we get

$$\mathbb{E}(\hat{\beta}_t^{ca} - \beta_t^{ca}) \simeq 0. \quad (\text{D.15})$$

For the second order moment of this error, the delta method yields to

$$\mathbb{E}(\hat{\beta}_t^{ca} - \beta_t^{ca})(\hat{\beta}_t^{ca} - \beta_t^{ca})^T \simeq \sigma^2 \left[(\bar{H}_t^{ca})^T \bar{H}_t^{ca} \right]^{-1}, \quad (\text{D.16})$$

where \bar{H}_t^{ca} is calculated exactly as in equation (D.12) but with the working point $\beta_{t,0}^{ca} = \beta_{t-1}^{tc}$.

Model of GNSS/Track Database Integrated System for a Variable Speed Case

This section presents two linear GNSS/track database integrated systems for the cases of transition curve and circular arc when the train travels along the "ideal" railway track with a variable speed.

Transition Curve

Since we have linearized the discrete track database model for a transition curve in the constant speed case, we need merely to linearize the exact pseudo-range measurement model.

Linearization of Pseudo-range Measurement Model

Let us suppose that there are n satellites located at the known positions $X_i^s = (x_i, y_i, z_i)^T, i = 1, \dots, n$. The pseudo-range equation r_i^t from the i -th satellite to the train position $X(\varphi_{tc}, \ell_{k-q+p})$ at time $k - q + p$ can be written as

$$r_{k-q+p}^i = d_{k-q+p}^i(\varphi_{tc}, \ell_{k-q+p}) + cb_r^{k-q+p} + \varepsilon_{k-q+p}^i \quad (\text{D.17})$$

where $\varphi_{tc} = (x_0, y_0, \alpha, k_c)^T$ and ℓ_{k-q+p} are unknown parameters and must be estimated. $d_{k-q+p}^i(\varphi_{tc}, \ell_{k-q+p}) = \|X(\varphi_{tc}, \ell_{k-q+p}) - X_i^s\|_2, i = 1, \dots, n$ is the true distance from the i -th satellite to the train. b_r^{k-q+p} is a user clock bias, $c \simeq 2.9979 \cdot 10^8 \text{ m/s}$ is the speed of light and $\varepsilon_{k-q+p}^i \sim \mathcal{N}(0, \sigma_{\text{PD}}^2)$ is the pseudo-range noise at time $k - q + p$. Let us now introduce the pseudo-range vector $R_{k-q+p} = (r_{k-q+p}^1, \dots, r_{k-q+p}^n)^T$ and the vector $D_{k-q+p} = (d_{k-q+p}^1(\varphi_{tc}, \ell_{k-q+p}), \dots, d_{k-q+p}^n(\varphi_{tc}, \ell_{k-q+p}))^T$, the working point $\varphi_{tc,0} = (x_{00}, y_{00}, \alpha_0, k_{c0})^T$. By linearizing the pseudo-range vector R_{k-q+p} with respect to the state vector $(\varphi_{tc}^T, \ell_{k-q+p})^T$ around the working point $(\varphi_{tc,0}^T, \ell_{k-q+p,0})^T$, and we can get the measurement equation

$$\begin{aligned} R_{k-q+p} &\simeq D_{k-q+p,0} + H_{\varphi_{tc}, k-q+p, 0}(\varphi_{tc} - \varphi_{tc,0}) + H_{\ell, k-q+p, 0}(\ell_{k-q+p} - \ell_{k-q+p,0}) \\ &\quad + \mathbf{1}_n \cdot cb_r^{k-q+p} + \Xi_{k-q+p}, \end{aligned} \quad (\text{D.18})$$

where $D_{k-q+p,0} = (d_{k-q+p}^1(\varphi_{tc,0}, \ell_{k-q+p,0}), \dots, d_{k-q+p}^n(\varphi_{tc,0}, \ell_{k-q+p,0}))^T$ is the vector for the distances from the satellite to the working point and $H_{\varphi_{tc}, k-q+p, 0} = \frac{\partial D_{k-q+p}}{\partial \varphi_{tc}} \Big|_{\varphi_{tc}=\varphi_{tc,0}}$,

$H_{\ell,k-q+p,0} = \frac{\partial D_{k-q+p}}{\partial \ell_{k-q+p}} \Big|_{\ell_{k-q+p}=\ell_{k-q+p,0}}$ are two Jacobian matrices of size $(n \times 4)$ and $(n \times 1)$, respectively. $\mathbf{1}_n$ is a vector of dimension n whose each element is one.

The above mentioned linearized measurement equations (D.18) can be rewritten in the following matrix form

$$Y_{k-q+p} \simeq H_{\varphi_{tc},k-q+p,0} \cdot \varphi_{tc} + H_{\ell,k-q+p,0} \cdot \ell_{k-q+p} + \mathbf{1}_n \cdot cb_r^{k-q+p} + \Xi_{k-q+p}, \quad (\text{D.19})$$

where $Y_{k-q+p} = R_{k-q+p} - D_{k-q+p,0} + H_{\varphi_{tc},k-q+p,0} \cdot \varphi_{tc,0} + H_{\ell,k-q+p,0} \cdot \ell_{k-q+p,0}$. It follows that

$$\begin{pmatrix} Y_k \\ \vdots \\ Y_{k-q} \end{pmatrix} \simeq \begin{pmatrix} H_{\varphi_{tc},k,0} \cdot \varphi_{tc} \\ \vdots \\ H_{\varphi_{tc},k-q,0} \cdot \varphi_{tc} \end{pmatrix} + \begin{pmatrix} H_{\ell,k,0} \cdot \ell_k + \mathbf{1}_n \cdot cb_r^k \\ \vdots \\ H_{\ell,k-q,0} \cdot \ell_{k-q} + \mathbf{1}_n \cdot cb_r^{k-q} \end{pmatrix} + \begin{pmatrix} \Xi_k \\ \vdots \\ \Xi_{k-q} \end{pmatrix}. \quad (\text{D.20})$$

To estimate the distance, speed and acceleration simultaneously, substituting equation (IV.23) into equation (D.20) yields to

$$\begin{pmatrix} Y_k \\ \vdots \\ Y_{k-q} \end{pmatrix} \simeq \begin{pmatrix} H_{\varphi_{tc},k,0} & H_{\ell,k,0} \cdot \omega_q & \mathbf{1}_n & \\ & \vdots & & \ddots \\ H_{\varphi_{tc},k-q,0} & H_{\ell,k-q,0} \cdot \omega_0 & & \mathbf{1}_n \end{pmatrix} \begin{pmatrix} \varphi_{tc} \\ \theta_k \\ cb_r^k \\ \vdots \\ cb_r^{k-q} \end{pmatrix} + \begin{pmatrix} \Xi_k \\ \vdots \\ \Xi_{k-q} \end{pmatrix}. \quad (\text{D.21})$$

Linear GNSS/Track Database Integrated System

Finally, by combining the system of linear equations (D.1) for the transition curve and the final linearized measurement equation (D.21), a final linear integrated system can be written as

$$\begin{pmatrix} \bar{Z}_{\text{DB}}^{tc,0} \\ Y_k \\ \vdots \\ Y_{k-q} \end{pmatrix} \simeq \left(\begin{array}{c|c} H_0^{tc} & \mathbf{0} \\ \hline H_{\varphi_{tc},k,0} & H_{\ell,k,0} \cdot \omega_q & \mathbf{1}_n \\ \vdots & \vdots & \ddots \\ H_{\varphi_{tc},k-q,0} & H_{\ell,k-q,0} \cdot \omega_0 & \mathbf{1}_n \end{array} \right) \begin{pmatrix} \varphi_{tc} \\ \theta_k \\ cb_r^k \\ \vdots \\ cb_r^{k-q} \end{pmatrix} + \begin{pmatrix} \xi_{\text{DB}}^{tc} \\ \Xi_k \\ \vdots \\ \Xi_{k-q} \end{pmatrix}, \quad (\text{D.22})$$

where $\bar{Z}_{\text{DB}}^{tc,0} \simeq Z_{\text{DB}}^{tc,0} + H_0^{tc} \varphi_{tc,0}$ and the final linear integrated system (D.22) can be rewritten in the following matrix :

$$Y_k^{tc} \simeq H_k^{tc} \beta_k^{tc} + \Upsilon_k^{tc}, \quad (\text{D.23})$$

where the vector $\beta_k^{tc} = (\varphi_{tc}^T, \theta_k^T, cb_r^k, \dots, cb_r^{k-q})^T$ is unknown and must be estimated. The working point $\varphi_{tc,0}$ at instant t_k is equal to the previously calculated estimation $\hat{\varphi}_{tc}$

and $\ell_{k-q+p,0}$ is equal to the product of factor ω_p and previously calculated estimation $\hat{\theta}_{k-1}$, i.e., $\ell_{k-q+p,0} = \omega_p \cdot \theta_{k,0} = \omega_p \cdot \hat{\theta}_{k-1}$. To seek simplicity, let us assume that $\sigma_{\text{PD}}^2 = \sigma_{\text{DB}}^2 = \sigma^2$, the LS estimator is given by

$$\hat{\beta}_k^{tc} = \left[\left(H_k^{tc} \right)^T H_k^{tc} \right]^{-1} \left(H_k^{tc} \right)^T Y_k^{tc}. \quad (\text{D.24})$$

The current estimation error is $\hat{\beta}_k^{tc} - \beta_k^{tc}$. After substituting the right side of equation (D.23) into the LS estimator (D.24), the mean of this error is computed as

$$\mathbb{E}(\hat{\beta}_k^{tc} - \beta_k^{tc}) = \mathbb{E} \left\{ \left[\left(H_k^{tc} \right)^T H_k^{tc} \right]^{-1} \left(H_k^{tc} \right)^T \Upsilon_k^{tc} \right\}, \quad (\text{D.25})$$

and using the delta method, we get

$$\mathbb{E}(\hat{\beta}_k^{tc} - \beta_k^{tc}) = \mathbb{E} \left\{ \left[\left(H_k^{tc} \right)^T H_k^{tc} \right]^{-1} \left(H_k^{tc} \right)^T \Upsilon_k^{tc} \right\} \simeq 0. \quad (\text{D.26})$$

For the second order moment of this error, the delta method yields to

$$\mathbb{E}(\hat{\beta}_k^{tc} - \beta_k^{tc})(\hat{\beta}_k^{tc} - \beta_k^{tc})^T \simeq \sigma^2 \left[\left(\bar{H}_k^{tc} \right)^T \bar{H}_k^{tc} \right]^{-1}, \quad (\text{D.27})$$

where \bar{H}_k^{tc} is calculated exactly as in equation (D.23) but with the working point $\varphi_{tc,0} = \varphi_{tc}$ and $\ell_{k-q+p,0} = \omega_p \cdot \theta_{k-1}$.

Circular Arc

Since we have linearized the discrete track database model for a circular arc in the constant speed case, we need merely to linearize the exact pseudo-range measurement model.

Linearization of Pseudo-range Measurement Model

Let us suppose that there are n satellites located at the known positions $X_i^s = (x_i, y_i, z_i)^T, i = 1, \dots, n$. The pseudo-range equation r_i^t from the i -th satellite to the train position $X(\varphi_{ca}, \ell_{k-q+p})$ at time $k - q + p$ can be written as

$$r_{k-q+p}^i = d_{k-q+p}^i(\varphi_{ca}, \ell_{k-q+p}) + cb_r^{k-q+p} + \varepsilon_{k-q+p}^i \quad (\text{D.28})$$

where $\varphi_{ca} = (x_0, y_0, \alpha, x_c, y_c, R)^T$ and ℓ_{k-q+p} are unknown parameters and must be estimated. $d_{k-q+p}^i(\varphi_{ca}, \ell_{k-q+p}) = \|X(\varphi_{ca}, \ell_{k-q+p}) - X_i^s\|_2, i = 1, \dots, n$ is the true distance from the i -th satellite to the train. b_r^{k-q+p} is a user clock bias, $c \simeq 2.9979 \cdot 10^8 \text{ m/s}$ is the speed of light and $\varepsilon_{k-q+p}^i \sim \mathcal{N}(0, \sigma_{\text{PD}}^2)$ is the pseudo-range noise at time $k - q + p$.

p . Let us now introduce the pseudo-range vector $R_{k-q+p} = (r_{k-q+p}^1, \dots, r_{k-q+p}^n)^T$ and the vector $D_{k-q+p} = (d_{k-q+p}^1(\varphi_{ca}, \ell_{k-q+p}), \dots, d_{k-q+p}^n(\varphi_{ca}, \ell_{k-q+p}))^T$, the working point $\varphi_{ca,0} = (x_{00}, y_{00}, \alpha_0, x_{c0}, y_{c0}, R_0)^T$. By linearizing the pseudo-range vector R_{k-q+p} with respect to the state vector $(\varphi_{ca}^T, \ell_{k-q+p})^T$ around the working point $(\varphi_{ca,0}^T, \ell_{k-q+p,0})^T$, and we can get the measurement equation

$$\begin{aligned} R_{k-q+p} &\simeq D_{k-q+p,0} + H_{\varphi_{ca},k-q+p,0}(\varphi_{ca} - \varphi_{ca,0}) + H_{\ell,k-q+p,0}(\ell_{k-q+p} - \ell_{k-q+p,0}) \\ &\quad + \mathbf{1}_n \cdot cb_r^{k-q+p} + \Xi_{k-q+p}, \end{aligned} \quad (\text{D.29})$$

where $D_{k-q+p,0} = (d_{k-q+p}^1(\varphi_{ca,0}, \ell_{k-q+p,0}), \dots, d_{k-q+p}^n(\varphi_{ca,0}, \ell_{k-q+p,0}))^T$ is the vector for the distances from the satellite to the working point and $H_{\varphi_{ca},k-q+p,0} = \frac{\partial D_{k-q+p}}{\partial \varphi_{ca}} \Big|_{\varphi_{ca}=\varphi_{ca,0}}$, $H_{\ell,k-q+p,0} = \frac{\partial D_{k-q+p}}{\partial \ell_{k-q+p}} \Big|_{\ell_{k-q+p}=\ell_{k-q+p,0}}$ are two Jacobian matrices of size $(n \times 6)$ and $(n \times 1)$, respectively. $\mathbf{1}_n$ is a vector of dimension n whose each element is one.

The above mentioned linearized measurement equations (D.29) can be rewritten in the following matrix form

$$Y_{k-q+p} \simeq H_{\varphi_{ca},k-q+p,0} \cdot \varphi_{ca} + H_{\ell,k-q+p,0} \cdot \ell_{k-q+p} + \mathbf{1}_n \cdot cb_r^{k-q+p} + \Xi_{k-q+p}, \quad (\text{D.30})$$

where $Y_{k-q+p} = R_{k-q+p} - D_{k-q+p,0} + H_{\varphi_{ca},k-q+p,0} \cdot \varphi_{ca,0} + H_{\ell,k-q+p,0} \cdot \ell_{k-q+p,0}$. It follows that

$$\begin{pmatrix} Y_k \\ \vdots \\ Y_{k-q} \end{pmatrix} \simeq \begin{pmatrix} H_{\varphi_{ca},k,0} \cdot \varphi_{ca} \\ \vdots \\ H_{\varphi_{ca},k-q,0} \cdot \varphi_{ca} \end{pmatrix} + \begin{pmatrix} H_{\ell,k,0} \cdot \ell_k + \mathbf{1}_n \cdot cb_r^k \\ \vdots \\ H_{\ell,k-q,0} \cdot \ell_{k-q} + \mathbf{1}_n \cdot cb_r^{k-q} \end{pmatrix} + \begin{pmatrix} \Xi_k \\ \vdots \\ \Xi_{k-q} \end{pmatrix}. \quad (\text{D.31})$$

To estimate the distance, speed and acceleration simultaneously, substituting equation (IV.23) into equation (D.31) yields to

$$\begin{pmatrix} Y_k \\ \vdots \\ Y_{k-q} \end{pmatrix} \simeq \begin{pmatrix} H_{\varphi_{ca},k,0} & H_{\ell,k,0} \cdot \omega_q & \mathbf{1}_n & & \\ & \vdots & & \ddots & \\ H_{\varphi_{ca},k-q,0} & H_{\ell,k-q,0} \cdot \omega_0 & & & \mathbf{1}_n \end{pmatrix} \begin{pmatrix} \varphi_{ca} \\ \theta_k \\ cb_r^k \\ \vdots \\ cb_r^{k-q} \end{pmatrix} + \begin{pmatrix} \Xi_k \\ \vdots \\ \Xi_{k-q} \end{pmatrix}. \quad (\text{D.32})$$

Linear GNSS/Track Database Integrated System

Finally, by combining the system of linear equations (D.9) for the circular arc and the final linearized measurement equation (D.32), a final linear integrated system can be written as

$$\begin{pmatrix} \bar{Z}_{\text{DB}}^{ca,0} \\ Y_k \\ \vdots \\ Y_{k-q} \end{pmatrix} \simeq \left(\begin{array}{c|cc} H_0^{ca} & \mathbf{0} & \\ \hline H_{\varphi_{ca},k,0} & H_{\ell,k,0} \cdot \omega_q & \mathbf{1}_n \\ \vdots & \vdots & \ddots \\ H_{\varphi_{ca},k-q,0} & H_{\ell,k-q,0} \cdot \omega_0 & \mathbf{1}_n \end{array} \right) \begin{pmatrix} \varphi_{ca} \\ \theta_k \\ cb_r^k \\ \vdots \\ cb_r^{k-q} \end{pmatrix} + \begin{pmatrix} \xi_{\text{DB}}^{ca} \\ \Xi_k \\ \vdots \\ \Xi_{k-q} \end{pmatrix}, \quad (\text{D.33})$$

where $\bar{Z}_{\text{DB}}^{ca,0} \simeq Z_{\text{DB}}^{ca,0} + H_0^{ca}\varphi_{ca,0}$ and the final linear integrated system (D.33) can be rewritten in the following matrix :

$$Y_k^{ca} \simeq H_k^{ca}\beta_k^{ca} + \Upsilon_k^{ca}, \quad (\text{D.34})$$

where the vector $\beta_k^{ca} = (\varphi_{ca}^T, \theta_k^T, cb_r^k, \dots, cb_r^{k-q})^T$ is unknown and must be estimated. The working point $\varphi_{ca,0}$ at instant t_k is equal to the previously calculated estimation $\hat{\varphi}_{ca}$ and $\ell_{k-q+p,0}$ is equal to the product of factor ω_p and previously calculated estimation $\hat{\theta}_{k-1}$, i.e., $\ell_{k-q+p,0} = \omega_p \cdot \theta_{k,0} = \omega_p \cdot \hat{\theta}_{k-1}$. To seek simplicity, let us assume that $\sigma_{\text{PD}}^2 = \sigma_{\text{DB}}^2 = \sigma^2$, the LS estimator is given by

$$\hat{\beta}_k^{ca} = \left[(H_k^{ca})^T H_k^{ca} \right]^{-1} (H_k^{ca})^T Y_k^{ca}. \quad (\text{D.35})$$

The current estimation error is $\hat{\beta}_k^{ca} - \beta_k^{ca}$. After substituting the right side of equation (D.34) into the LS estimator (D.35), the mean of this error is computed as

$$\mathbb{E}(\hat{\beta}_k^{ca} - \beta_k^{ca}) = \mathbb{E} \left\{ \left[(H_k^{ca})^T H_k^{ca} \right]^{-1} (H_k^{ca})^T \Upsilon_k^{ca} \right\}, \quad (\text{D.36})$$

and using the delta method, we get

$$\mathbb{E}(\hat{\beta}_k^{ca} - \beta_k^{ca}) = \mathbb{E} \left\{ \left[(H_k^{ca})^T H_k^{ca} \right]^{-1} (H_k^{ca})^T \Upsilon_k^{ca} \right\} \simeq 0. \quad (\text{D.37})$$

For the second order moment of this error, the delta method yields to

$$\mathbb{E}(\hat{\beta}_k^{ca} - \beta_k^{ca})(\hat{\beta}_k^{ca} - \beta_k^{ca})^T \simeq \sigma^2 \left[(\bar{H}_k^{ca})^T \bar{H}_k^{ca} \right]^{-1}, \quad (\text{D.38})$$

where \bar{H}_k^{ca} is calculated exactly as in equation (D.34) but with the working point $\varphi_{ca,0} = \varphi_{ca}$ and $\ell_{k-q+p,0} = \omega_p \cdot \theta_{k-1}$.

Annexe E

Résumé de Thèse en Français

Cet annexe [E](#) se conforme aux règles de l'école doctorale de l'UTT : un résumé substantiel en Français de 20 à 30 pages, pour les mémoires rédigés en Anglais.

E.1 Introduction

Cette thèse porte principalement sur la précision du positionnement du train obtenu à l'aide des satellites GNSS (Global Navigation Satellite System, en anglais). Ici, nous introduisons d'abord les notations, l'importance et les questions fondamentales sur le positionnement du train, puis nous présentons les problèmes étudiés, les contributions principales de cette thèse.

E.1.1 Importance du positionnement du train

Au cours des dernières années, grâce à sa grande capacité, sa grande vitesse, sa haute fiabilité et sa faible consommation d'énergie, le transport ferroviaire joue un rôle de plus en plus important dans les transports en commun. Pour assurer la sécurité, la sûreté et l'efficacité du réseau ferroviaire, les systèmes d'exploitation ferroviaires avancés (par exemple les systèmes de protection/contrôle automatique) sont largement utilisés dans la gestion ferroviaire moderne. L'efficacité de ces systèmes se fonde, en grand partie, sur la précision, la disponibilité et l'intégrité du positionnement du train. Une estimation précise et fiable de la position et de la vitesse du train est donc très importante. Une erreur sur la position du train peut conduire potentiellement, à une surestimation de la distance disponible pour le freinage. De plus, les mesures précises de la position, de la vitesse et de l'accélération peuvent augmenter la capacité de la ligne ferroviaire sans

nécessiter d'infrastructure supplémentaire. Ainsi, une amélioration dans l'estimation du positionnement d'un train pourrait nous fournir non seulement des avantages en termes de performances mais aussi en termes de coût.

La navigation par satellite GNSS est appelée à révolutionner le secteur ferroviaire qui a un besoin de connaître la position de chaque train, de chaque wagon. La navigation ferroviaire par satellite offre de nombreux avantages, notamment les suivants :

1. Réduction de la consommation énergétique des trains en optimisant leurs accélérations et freinages en fonction des changements de condition de circulation le long du trajet.
2. Amélioration du service aux utilisateurs, que cela concerne le suivi des marchandises, l'information des retards aux usagers ou l'information aux usagers pendant le transport.
3. Minimisation de la distance entre les trains tout en garantissant la sécurité maximale, ce qui permettra un gain de capacité et de densification du trafic.

E.1.2 Questions clés dans le positionnement du train

Pour les applications ferroviaires critiques au niveau de sécurité, une attention particulière doit être portée à l'exactitude, l'intégrité, la continuité et la disponibilité des informations de positionnement.

Précision se réfère à la proximité de la position et la vitesse estimée par rapport aux valeurs réelles.

L'intégrité est souvent définie comme la capacité du système de fournir avec un retard acceptable des avertissements aux utilisateurs lorsque le système ne doit pas être utilisé pour le positionnement.

La continuité est la capacité d'un système de navigation à fournir l'exactitude et l'intégrité requises pendant une période de fonctionnement prévue.

Disponibilité représente le pourcentage de temps durant lequel le système de navigation est disponible pour remplir pleinement sa fonction.

Parmi les conditions mentionnées ci-dessus, l'exactitude et l'intégrité sont les deux

aspects les plus essentiels pour une application ferroviaire parce que le train a besoin de la position de haute précision pour des raisons économiques et l'intégrité est directement liée à la sécurité.

E.1.3 Problèmes étudiés dans cette thèse

Les méthodes décrites dans cette thèse sont consacrées au positionnement du train à l'aide d'un récepteur GNSS à bas coût. Deux approches de l'estimation de la distance parcourue et de la vitesse du train peuvent être considérées. La première approche est basée sur le positionnement classique (la navigation 3D). La deuxième approche est basée sur la connaissance de la trajectoire ferroviaire (la navigation 1D). La navigation 1D est plus efficace que la navigation classique 3D mais il y a trois questions importantes à considérer :

1. Quel est l'impact des incertitudes du modèle géométrique de voie ferroviaire sur l'estimation de la distance et de la vitesse du train ?
2. Quel est l'impact du rayon de courbure de la voie ferroviaire sur l'estimation de la vitesse et de la distance du train ?
3. Est-ce qu'un changement en accélération provoque une estimation imprécise de la vitesse et de la distance du train ?

L'algorithme des moindres carrées est une approche couramment utilisée dans la navigation GNSS et son critère d'optimisation est basée sur la minimisation de la somme des carrés résiduels. Cet algorithme sera utilisé dans la thèse.

E.1.4 Contributions

L'analyse, décrite dans cette thèse, peut être divisée en trois parties.

Dans la première partie, un modèle "idéal" de voie ferroviaire, composé de lignes droites, de courbes de transition et d'arcs de cercle, est défini par un ensemble d'équations paramétriques. L'objectif de cette partie est d'estimer la distance parcourue, la vitesse et l'accélération du train et d'étudier l'impact du rayon de courbure de la voie ferroviaire sur ces estimations. Deux cas sont étudiés : la vitesse constante et variable. Un algorithme des moindres carrés est conçu pour estimer la vitesse du train à partir

des signaux GNSS et du modèle géométrique de voie ferroviaire. L'impact du rayon de courbure de la voie ferroviaire sur l'erreur moyenne et le moment d'ordre deux de la vitesse estimée est calculé. Ensuite, il est supposé que la vitesse du train est variable. En supposant que l'accélération du train est constante pendant une courte période de temps, l'algorithme des moindres carrés à fenêtre glissante est conçu à partir des signaux GNSS et du modèle dynamique du train. L'impact du rayon de courbure de la voie ferroviaire sur l'erreur moyenne et le moment d'ordre deux de ces trois estimations est estimé. Dans les deux cas, les équations pour les deux premiers moments de ces estimations sont calculées de façon théorique et comparées avec les résultats de simulations Monte-Carlo.

Dans la deuxième partie, un modèle "non-idéal" de voie ferroviaire est approché par une ligne polygonale avec un certain niveau d'incertitude. Nous considérons également deux cas : la vitesse constante et variable. Dans le cas de vitesse constante, la vitesse du train est calculée en utilisant des signaux GNSS et du modèle "non-idéal" de voie ferroviaire. L'impact négatif de l'incertitude de la voie ferroviaire sur l'erreur moyenne et le moment d'ordre deux de la vitesse estimée est calculé. Dans le cas de vitesse variable, on exploite aussi un algorithme à fenêtre glissante pour estimer la distance parcourue, la vitesse et l'accélération. L'impact négatif de l'incertitude de la voie ferroviaire sur l'erreur moyenne et le moment d'ordre deux de ces trois estimations est estimé. Dans les deux cas, les équations pour les deux premiers moments de ces estimations sont calculées de façon théorique et comparées avec les résultats de simulations Monte-Carlo.

Enfin, on considère que la géométrie de voie est disponible dans d'une base de données avec des mesures bruitées (sans l'approximation par une ligne brisée). La distance parcourue, la vitesse du train est estimées en intégrant les mesures GNSS avec celles de la base de données. Nous considérons également deux cas : la vitesse constante et variable. Dans les deux cas, un modèle de système intégré est conçu. Ensuite, l'impact des erreurs dans les mesures GNSS et la base de données sur ces estimations sont étudié.

E.2 Estimation de la distance, vitesse du train à base de GNSS et une voie ferroviaire "idéale"

Dans le chapitre II, le modèle "idéal" de voie ferroviaire, composé de lignes droites, de courbes de transition et d'arcs de cercle, est défini par un ensemble d'équations paramétriques. L'objectif est d'estimer la distance parcourue et la vitesse du train en utilisant un récepteur GNSS à bas coût et d'étudier l'impact de la courbure de la voie sur ces estimations. Deux cas sont étudiés : une vitesse constante et variable. Dans les deux cas, un estimateur des moindres carrés est conçu. L'erreur moyenne et le moment d'ordre deux de ces estimations sont calculés de façon théorique et comparées avec les résultats de simulations Monte-Carlo.

E.2.1 Description du modèle "idéal" de voie ferroviaire

Dans cette section, le modèle "idéal" de voie ferroviaire, composé de lignes droites, de courbes de transition et d'arcs de cercle, défini par un ensemble d'équations paramétriques. La ligne droite, la courbe de transition et l'arc de cercle sont décrites par les équations formulées en fonction de l'abscisse curviligne ℓ . Pour simplifier, nous supposons que la trajectoire du train appartient entièrement au plan tangent local. La figure E.1 suivante montre trois segments $[\ell_m; \ell_{m+1}]$, $[\ell_{m+1}; \ell_{m+2}]$ et $[\ell_{m+2}; \ell_{m+3}]$ indexés par ℓ_m ce qui est la distance parcourue correspond au m -ème segment ($m = 1, 2, \dots$). Tout d'abord, l'équation pour le segment de droite ($\ell_m \leq \ell \leq \ell_{m+1}$), représentée sur la figure E.1 est

$$\begin{cases} x(\ell) = x_0 + (\ell - \ell_m) \cdot \cos \alpha \\ y(\ell) = y_0 + (\ell - \ell_m) \cdot \sin \alpha, \end{cases} \quad (\text{E.1})$$

où (x_0, y_0) est le point de démarrage du m -ème segment, ℓ désigne l'abscisse curviligne et α est l'azimut initial du m -ème segment. Ensuite, l'équation de la parabole cubique ($\ell_{m+1} < \ell \leq \ell_{m+2}$) sur la figure E.1 est bien approchée par

$$\begin{cases} x(\ell) = x_0 + (\ell - \ell_m) \cos \alpha - k_c (\ell - \ell_{m+1})^3 \sin \alpha \\ y(\ell) = y_0 + (\ell - \ell_m) \sin \alpha + k_c (\ell - \ell_{m+1})^3 \cos \alpha, \end{cases} \quad (\text{E.2})$$

où le coefficient $k_c = \frac{1}{6RL}$, R est le rayon à la fin de la courbe de transition et L est la longueur de la courbe de transition. Enfin, l'équation de l'arc de cercle ($\ell_{m+2} < \ell \leq$

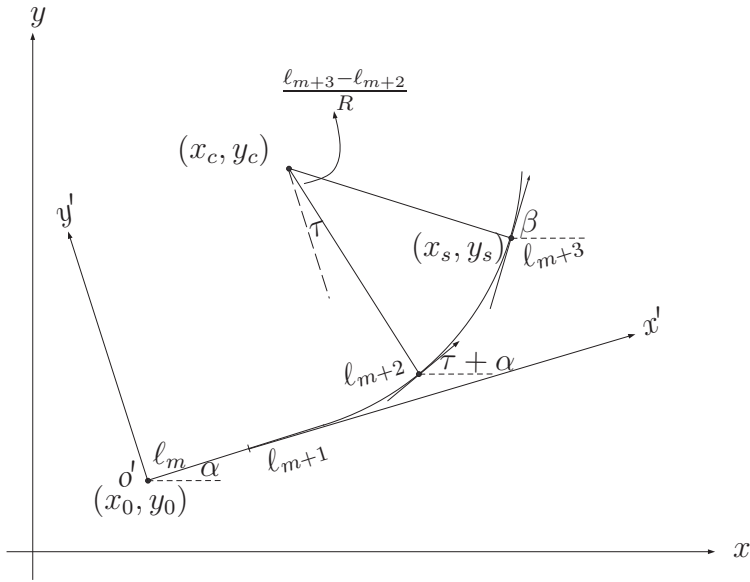


Figure E.1 – La voie ferroviaire composée de trois segments au plan tangent local.

ℓ_{m+3}) illustrée sur la figure E.1 est

$$\begin{cases} x(\ell) = x_0 + x'(\ell) \cdot \cos \alpha - y'(\ell) \cdot \sin \alpha \\ y(\ell) = y_0 + x'(\ell) \cdot \sin \alpha + y'(\ell) \cdot \cos \alpha, \end{cases} \quad (\text{E.3})$$

où

$$\begin{cases} x'(\ell) = x_c + R \sin \left(\tau + \frac{\ell - \ell_{m+2}}{R} \right) \\ y'(\ell) = y_c - R \cos \left(\tau + \frac{\ell - \ell_{m+2}}{R} \right) \end{cases} \quad (\text{E.4})$$

est la représentation de l'arc de cercle au $x'y'$ -plan, $\tau = \arctan(3k_c L^2)$ est l'angle de la tangente à la fin de la courbe de transition et

$$\begin{cases} x_c = L \cdot (1 - 9k_c^2 L^4)/2 + \ell_{m+1} - \ell_m \\ y_c = (1 + 15k_c^2 L^4)/6k_c L \end{cases} \quad (\text{E.5})$$

est le centre de l'arc de cercle.

E.2.2 Estimation de la vitesse pour le cas d'une vitesse constante

Dans cette section, on suppose que le train roule sur la voie ferroviaire E.1 au-dessus à une vitesse constante inconnue v . La distance parcourue ℓ_t au temps t est égale au

produit de la multiplication de la vitesse v par le temps t , soit $\ell_t = v \cdot t$. Par conséquent, la position du train est définie : $X_t = (x(\ell_t), y(\ell_t), 0)^T$, $t = 1, 2, \dots$, où $(x(\ell_t), y(\ell_t))$ est la position correspondante au plan tangent local.

E.2.2.1 Modèle exact de mesure de pseudo-distance et l'estimation

L'équation pour le vecteur de pseudo-distances R^t entre le train et les satellites est obtenue en linéarisant l'équation non-linéaire exacte par rapport au vecteur d'état $V_t = (v_t, cb_r^t)^T$ autour d'un point de travail $V_0 = (v_0, cb_0)^T$. L'équation de mesure linéaire est donnée sous la forme suivante :

$$R^t - R_0^t \simeq H_0^t \cdot (V_t - V_0) + \Xi^t, \quad (\text{E.6})$$

où R_0^t est le vecteur de distances entre les satellites et le point de travail. b_r^t est le biais d'horloge du récepteur, $c \simeq 2.9979 \cdot 10^8 \text{ m/s}$ est la vitesse de la lumière et $\Xi^t \sim \mathcal{N}(0, \sigma^2 I)$ est un bruit de mesure. Le point de travail au temps t est égal à l'estimation calculée précédemment : $V_0 = \hat{V}_{t-1}$.

E.2.2.2 Impact du rayon de courbure de la voie ferroviaire sur l'erreur d'estimation

Le but de cette section est d'étudier l'impact du rayon de courbure de la voie ferroviaire R sur les deux premiers moments de l'estimateur \hat{v}_t . Pour cela, l'équation de mesure peut être écrite sous la forme suivante :

$$R^t - R_0^t \simeq H_0^t \cdot (V_t - V_0) + \frac{1}{2} J_0^t \cdot (v_t - v_0)^2 + \Xi^t. \quad (\text{E.7})$$

En raison de la présence de J_0^t , cette équation souligne le rôle du rayon de courbure de la voie dans le modèle de mesure.

L'erreur d'estimation actuelle est $\hat{V}_t - V_t$. L'erreur moyenne et le moment d'ordre deux de cette erreur sont calculés comme suit :

$$\begin{aligned} \mathbb{E}(\hat{V}_t - V_t) &\simeq \frac{1}{2} \bar{B}_0^{-1} (\bar{H}_0^t)^T \bar{J}_0^t \cdot (v_t - v_0)^2, \\ \mathbb{E}(\hat{V}_t - V_t)(\hat{V}_t - V_t)^T &\simeq \frac{1}{4} \bar{B}_0^{-1} (\bar{H}_0^t)^T \bar{J}_0^t (\bar{J}_0^t)^T \bar{H}_0^t \bar{B}_0^{-1} (v_t - v_0)^4 + \sigma^2 \bar{B}_0^{-1}. \end{aligned} \quad (\text{E.8})$$

où $\bar{B}_0 = (\bar{H}_0^t)^T \bar{H}_0^t$. Les matrices \bar{H}_0^t et \bar{J}_0^t sont calculées exactement comme dans l'équation (E.7) mais avec le point de travail $v_0 = v_{t-1}$.

E.2.2.3 Simulations numériques

Le scénario suivant sera utilisé : la constellation GNSS avec $n = 6$ satellites visibles et l'écart-type des erreurs de pseudo-distance $\sigma = 2$ m. La période d'échantillonnage des mesures GNSS est $\Delta t = 0.5$ s. La vraie vitesse du train est 20 m/s et le point de travail initial v_0 est 10 m/s. Le rayon de courbure minimum de la voie est $R = 100$ m.

Les segments de la trajectoire du train stockés dans la base de données à bord du train sont résumés dans le tableau E.1. La courbure d'une voie ferroviaire et la trajectoire du train sont présentées sur la figure E.2 et E.3, respectivement.

Numéro	Courbes	Abscisse curviligne	Courbure
1	Droit	$[\ell_1, \ell_2]$	0
2	Transition	$(\ell_2, \ell_3]$	$0 \rightarrow \frac{1}{R}$
3	Cercle	$(\ell_3, \ell_4]$	$\frac{1}{R}$
4	Transition	$(\ell_4, \ell_5]$	$\frac{1}{R} \rightarrow 0$
5	Droit	$(\ell_5, \ell_6]$	0
6	Transition	$(\ell_6, \ell_7]$	$0 \rightarrow -\frac{1}{R}$
7	Cercle	$(\ell_7, \ell_8]$	$-\frac{1}{R}$
8	Transition	$(\ell_8, \ell_9]$	$-\frac{1}{R} \rightarrow 0$
9	Droit	$(\ell_9, \ell_{10}]$	0

Tableau E.1 – Segments de la trajectoire testée.

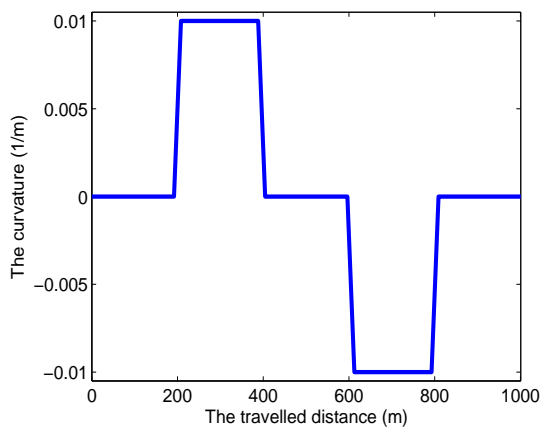


Figure E.2 – Courbure calculée pour la trajectoire.

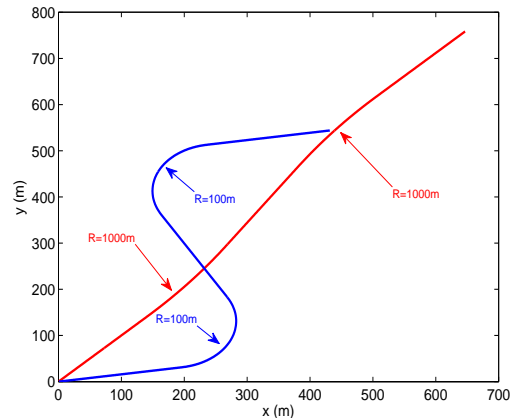


Figure E.3 – La trajectoire testée au plan tangent local.

La comparaison des deux premiers moments théoriques de ces estimations donnés

par (E.8), avec les résultats de simulation Monte-carlo utilisant 10^4 répétitions, est représentée sur la figure E.4-E.5.

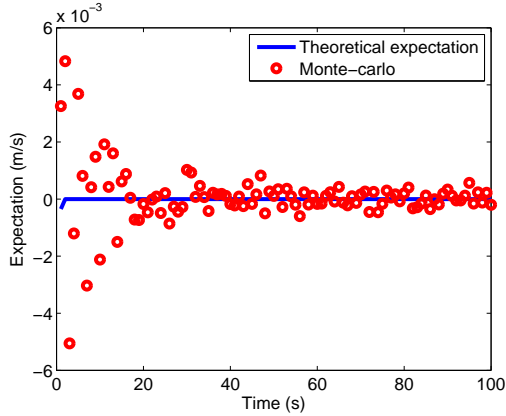


Figure E.4 – L'erreur moyenne de la vitesse estimée pour $R = 100$ m.

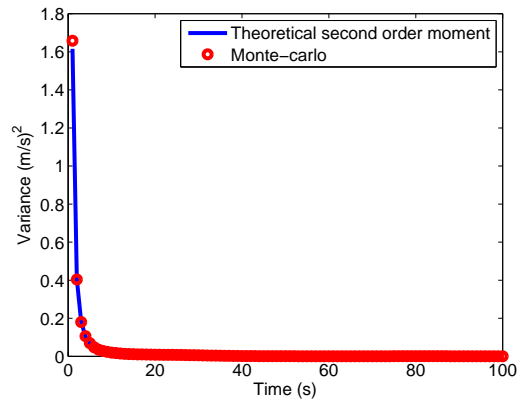


Figure E.5 – Le moment d'ordre deux de la vitesse estimée pour $R = 100$ m.

E.2.3 Estimation de la distance, vitesse pour le cas d'une vitesse variable

Le but de cette section est d'estimer la distance parcourue et la vitesse du train lorsque l'accélération n'est pas négligeable. Par conséquent, supposons que le train roule sur la voie ferroviaire E.1 au-dessus à une vitesse variable. Le modèle dynamique du train est décrit par une équation formulée en fonction de la distance parcourue, la vitesse et l'accélération (voir la figure E.6).

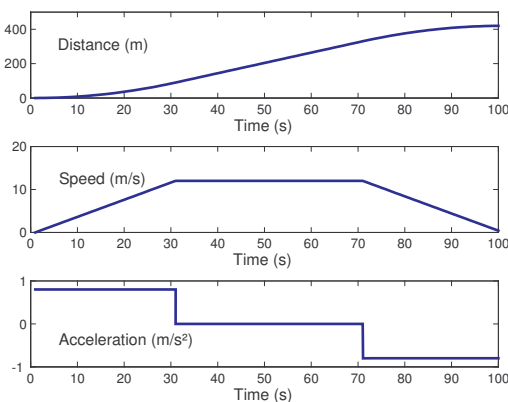


Figure E.6 – Schéma de mouvement de train.

Soit $\Delta t = t_k - t_{k-1}$ est la période d'échantillonnage des mesures GNSS et t_k désigne l'instant du k -ème mesure. Considérons une courte période de temps $T = (q + 1) \cdot \Delta t$ où q est un entier positif. Pendant cette période, la distance ℓ_k couverte par le train, la vitesse v_k et l'accélération a_k à l'instant t_k ($1 \leq k \leq q$) sont données par

$$\begin{cases} \ell_k = \ell_{k-1} + v_{k-1} \cdot \Delta t + \frac{1}{2} a_{k-1} \cdot \Delta t^2 \\ v_k = v_{k-1} + a_{k-1} \cdot \Delta t \\ a_k = a_{k-1}. \end{cases} \quad (\text{E.9})$$

Considérons un bloc de dernières $q + 1$ mesures GNSS à l'instant t_k . En supposant que l'accélération a_k est constante pendant la période T (s), la position du train est donnée par

$$X(\ell_{k-q+p}) = [x(\ell_{k-q+p}), y(\ell_{k-q+p}), 0]^T,$$

où $(x(\ell_{k-q+p}), y(\ell_{k-q+p}))$ est la position correspondante au plan tangent local, $p = 0, 1, \dots, q$ et

$$\ell_{k-q+p} = \begin{pmatrix} 1 & (p-q) \cdot \Delta t & \frac{1}{2}(p-q)^2 \cdot \Delta t^2 \end{pmatrix} \begin{pmatrix} \ell_k \\ v_k \\ a_k \end{pmatrix} = \omega_p \cdot \theta_k, \quad (\text{E.10})$$

où le vecteur θ_k est inconnue et doit être estimé.

E.2.3.1 Modèle exact de mesure de pseudo-distance et l'estimation

L'équation pour le vecteur de pseudo-distances R_{k-q+p} entre le train et les satellites est obtenue en linéarisant l'équation non-linéaire exacte autour d'un point de travail $\ell_{k-q+p,0}$. L'équation de mesure linéaire est donnée sous la forme suivante :

$$R_{k-q+p} - D_{k-q+p,0} \simeq H_{k-q+p,0} \cdot (\ell_{k-q+p} - \ell_{k-q+p,0}) + \mathbf{1}_n \cdot cb_r^{k-q+p} + \Xi_{k-q+p}, \quad (\text{E.11})$$

où $D_{k-q+p,0}$ est le vecteur de distances entre les satellites et le point de travail. b_r^{k-q+p} est le biais d'horloge du récepteur et $\Xi_{k-q+p} \sim \mathcal{N}(0, \sigma^2 I)$ est un bruit de mesure à l'instant $k - q + p$. Finalement, l'équation de mesure linéaire mentionnée (E.11) est réécrite comme :

$$R^k - D_0^k + Y_0^k \simeq H_0^k \cdot \beta_k + \Xi^k, \quad (\text{E.12})$$

où le vecteur $\beta_k = (\theta_k^T, cb_r^k, \dots, cb_r^{k-q})^T$ est inconnu et doit être estimé. Le point de travail est égal au produit de la multiplication du facteur ω_p par l'estimation calculée précédemment : $\ell_{k-q+p,0} = \omega_p \cdot \hat{\theta}_{k-1}$.

E.2.3.2 Impact du rayon de courbure de la voie ferroviaire sur l'erreur d'estimation

Le but de cette section est d'étudier l'impact du rayon de la courbe R sur les deux premiers moments de l'estimateur $\hat{\beta}_k$. Pour cela, l'équation de mesure peut être écrite sous la forme suivante :

$$R^k - D_0^k + Y_0^k \simeq H_0^k \cdot \beta_k + \frac{1}{2} J_0^k + \Xi^k. \quad (\text{E.13})$$

En raison de la présence de J_0^k , cette équation souligne le rôle du rayon de courbure de la voie dans le modèle de mesure.

L'erreur d'estimation actuelle est $\hat{\beta}_k - \beta_k$. L'erreur moyenne et le moment d'ordre deux de cette erreur sont calculés comme suit :

$$\begin{aligned} \mathbb{E}(\hat{\beta}_k - \beta_k) &\simeq \frac{1}{2} (\bar{B}^k)^{-1} (\bar{H}_0^k)^T \bar{J}_0^k, \\ \mathbb{E}(\hat{\beta}_k - \beta_k)(\hat{\beta}_k - \beta_k)^T &\simeq \frac{1}{4} (\bar{B}^k)^{-1} (\bar{H}_0^k)^T \bar{J}_0^k (\bar{J}_0^k)^T \bar{H}_0^k (\bar{B}^k)^{-1} + \sigma^2 (\bar{B}^k)^{-1}. \end{aligned} \quad (\text{E.14})$$

où $\bar{B}^k = (\bar{H}_0^k)^T \bar{H}_0^k$. Les matrices \bar{J}_0^k et \bar{H}_0^k sont calculées exactement comme dans l'équation (E.13) mais avec le point de travail $\ell_{k-q+p,0} = \omega_p \cdot \theta_{k-1}$.

E.2.3.3 Simulations numériques

Le scénario suivant sera utilisé : la constellation GNSS avec $n = 6$ satellites visibles et l'écart-type des erreurs de pseudo-distance $\sigma = 2$ m. La période d'échantillonnage des mesures GNSS est $\Delta t = 0.5$ s. La vraie valeur pour la période de l'accélération, du mouvement uniforme et du freinage est 0.8 m/s 2 , 0 m/s 2 et -0.8 m/s 2 , respectivement. Le rayon de courbure de voie minimal est $R = 100$ m. Le schéma de mouvement de train est représenté sur la figure E.6.

Les segments de la trajectoire du train stockés dans la base de données à bord du train sont résumés dans le tableau E.1. La courbure d'une voie ferroviaire et la trajectoire du train sont présentées sur la figure E.7 and E.8, respectivement.

La comparaison des deux premiers moments théoriques de ces estimations donnés par (E.14), avec les résultats de simulation Monte-carlo utilisant 10^4 répétitions, est représentée sur la figure E.9-E.10.

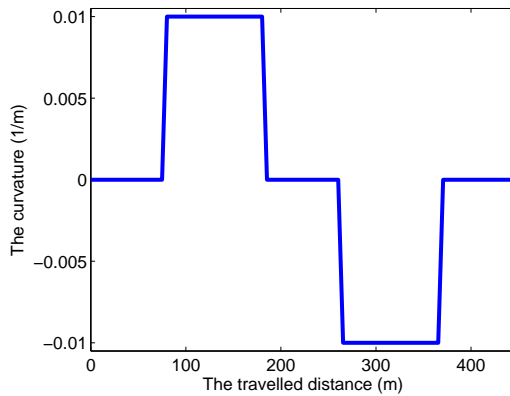


Figure E.7 – Courbure calculée pour la trajectoire.

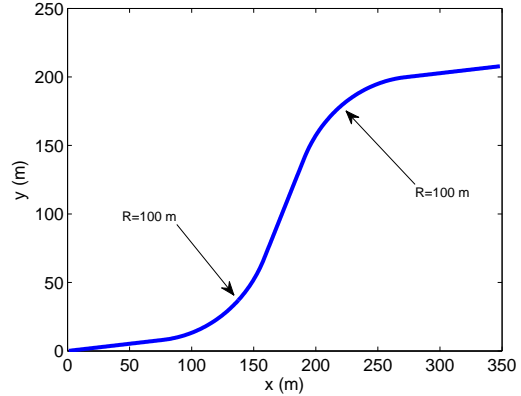


Figure E.8 – La trajectoire testée au plan tangent local.

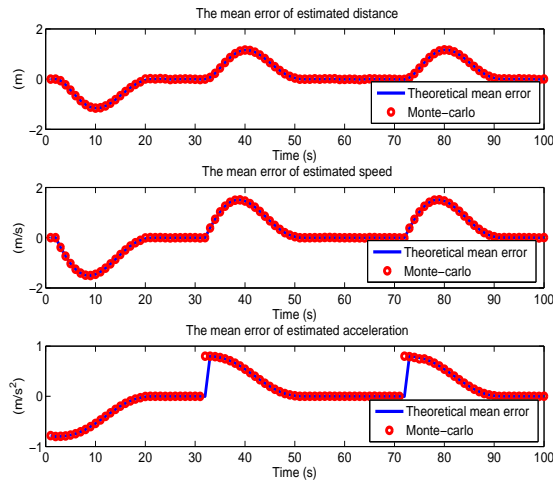


Figure E.9 – L'erreur moyenne de la dis-
tance, de la vitesse et de l'accélération pour
 $R = 100 \text{ m}$ et $q = 20$.

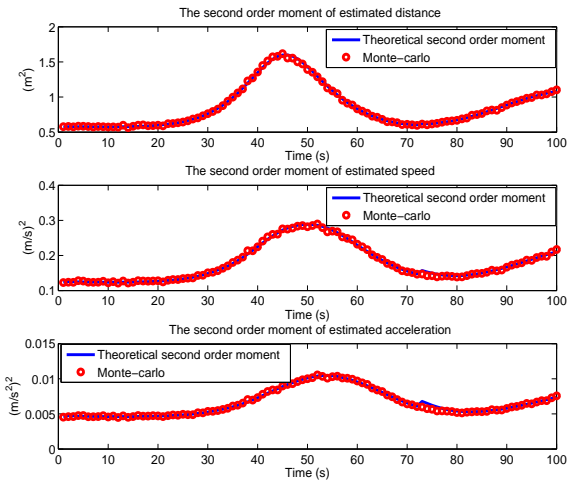


Figure E.10 – Le moment d'ordre deux de
la distance, de la vitesse et de l'accélération
pour $R = 100 \text{ m}$ et $q = 20$.

E.2.4 Conclusions

Dans le cas d'une vitesse constante, l'estimateur est pratiquement non biaisé, même avec le rayon de courbure de voie minimal. L'impact négatif du rayon de courbure sur la vitesse estimée du train est presque négligeable. La variance de l'estimation de vitesse devient rapidement très faible.

Dans le cas d'une vitesse variable, il a été démontré que le changement d'accélération

provoque l'apparition des biais dans les estimations de distance parcourue, de vitesse et d'accélération pour une courte période. Un faible rayon de courbure peut augmenter le moment d'ordre deux de ces estimations.

E.3 Estimation de la distance, vitesse du train à base de GNSS et une voie ferroviaire "non-idéale"

Dans le chapitre III, le modèle "non-idéal" de voie ferroviaire est défini dans la base de données à bord du train par une ligne polygonale avec un certain niveau d'incertitude. Il représente une approximation linéaire par morceaux du modèle "idéal". Le but de ce chapitre est d'estimer la distance parcourue et la vitesse du train en utilisant un récepteur GNSS à bas coût et d'étudier l'impact de l'incertitude sur ces estimations. Deux cas sont étudiés : une vitesse constante et variable. Dans les deux cas, un estimateur des moindres carrés est conçu. L'erreur moyenne et le moment d'ordre deux de ces estimations sont calculés de façon théorique et comparés avec les résultats de simulations Monte-Carlo.

E.3.1 Description du modèle "non-idéal" de voie ferroviaire

Dans cette section, le modèle "non-idéal" de voie ferroviaire est défini par une ligne polygonale (courbe linéaire par morceaux), ce qui représente une série connexe de segments linéaires dans le système de référence géodésique (ECEF, en anglais). Plus formellement, la voie est définie par une séquence de sommets $Z_0, Z_1, Z_2, \dots, Z_n$, $Z_i \in \mathbb{R}^3$, de sorte que la courbe est composée des segments linéaires reliant les sommets consécutifs. Supposons que les erreurs lient à une telle approximation de la fonction de vecteur $\ell \mapsto X(\ell)$, $\ell \in \mathbb{R}$, $X(\ell) \in \mathbb{R}^3$, en définissant la voie ferroviaire est négligeable pour notre étude. Ici et dans le reste de la discussion, ℓ désigne l'abscisse curviligne, ou la distance parcourue, et $\lambda = \|Z_{j+1} - Z_j\|_2 = \text{const}$ est la distance entre deux sommets adjacents, respectivement.

Malheureusement, la base de données à bord du train utilise une information imprécise sur les positions des sommets, à savoir : $\tilde{Z}_0, \tilde{Z}_1, \tilde{Z}_2, \dots, \tilde{Z}_n$. La quantité $\xi_i = Z_i - \tilde{Z}_i$

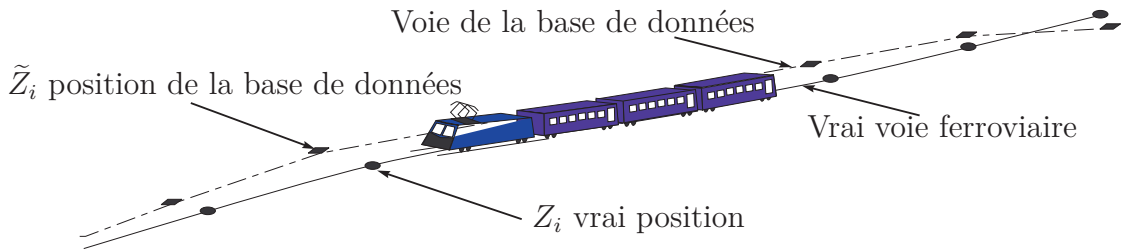


Figure E.11 – Le modèle ”non-idéal” de voie ferroviaire.

définit l’incertitude des connaissances concernant la voie ferroviaire. Cette situation est illustrée par la figure E.11. Pour simplifier la présentation, une trajectoire de train en deux dimensions est considérée.

E.3.2 Estimation de la vitesse pour le cas d'une vitesse constante

Dans cette section, on suppose que le train roule sur la voie ferroviaire E.11 au-dessus à une vitesse constante inconnue v . Par conséquent, la position du train est définie :

$$X_k = X_{k-1} + A_{j(k)} \cdot v \cdot \Delta t \quad k = 1, 2, \dots, \quad (\text{E.15})$$

où $X_k = (x_k, y_k, z_k)^T$ est la position du train au k -ème mesure GNSS, t_k désigne l’instant de la k -ème mesure GNSS, $\Delta t = t_k - t_{k-1}$ représente la période d’échantillonnage des mesures GNSS, $A_j = (a_x^j, a_y^j, a_z^j)^T = \frac{1}{\lambda}(Z_{j+1} - Z_j)$ est le vecteur directionnel correspondant au numéro de segment $j = j(k)$ est calculé en fonction de k par utiliser l’équation suivante :

$$j(k) = \min \{j \in \mathbb{N} | j \geq (v \cdot \Delta t \cdot k) / \lambda\}, \quad (\text{E.16})$$

où \mathbb{N} est l’ensemble des nombres naturels. La position du train X_k peut être réécrite comme

$$X_k = X_0 + v \Delta t \sum_{t=1}^k A_{j(t)}, \quad (\text{E.17})$$

où $X_0 = (x_0, y_0, z_0)^T$ est le point de démarrage.

E.3.2.1 Modèle imprécis de mesure de pseudo-distance et l'estimation.

L'équation pour le vecteur de pseudo-distances R^k entre le train et les satellites est obtenue en linéarisant l'équation non-linéaire exacte par rapport au vecteur d'état $V_k = (v, cb_r^k)^T$ autour d'un point de travail $V_0 = (v_0, cb_0)^T$. L'équation de mesure linéaire est donnée sous la forme suivante :

$$R^k - R_0^k \simeq H_0^k \cdot (V_k - V_0) + \Xi^k, \quad (\text{E.18})$$

où R_0^k est le vecteur de distances entre les satellites et le point de travail. b_r^k est le biais d'horloge du récepteur et $\Xi^k \sim \mathcal{N}(0, \sigma^2 I)$ est un bruit de mesure. Parce que la vraie vitesse du train v est inconnue, le numéro du segment actuel $\hat{j} = \hat{j}(t)$ est calculé en fonction du point de travail v_0 en utilisant (E.16) avec $v = v_0$ et le point de travail à l'étape k est égale à l'estimation calculée précédemment : $V_0 = \hat{V}_{k-1}$.

Maintenant on considère un modèle imprécis de mesure de pseudo-distance. Puisque la vraie position du sommet Z_j est inconnue et une seule estimation imprécise \tilde{Z}_j est disponible, l'équation de mesure linéarisée (E.18) ne peut être utilisée pour calculer la vitesse du train. Pour estimer l'impact de cette incertitude, nous définissons le vecteur directionnel $\tilde{A}_j = A_j + \delta_j$, où le vecteur aléatoire $\delta_j = (\delta_x^j, \delta_y^j, \delta_Z^j)$ est supposé être réparti uniformément dans le cube $[-b, b]^3$ avec $b > 0$. Enfin, un modèle imprécis de mesure de pseudo-distance (E.19) est défini pour le vecteur directionnel imprécis \tilde{A}_j de la manière suivante :

$$R^k - \tilde{R}_0^k \simeq \tilde{H}_0^k \cdot (V_k - V_0) + \Xi^k, \quad (\text{E.19})$$

où \tilde{R}_0^k et \tilde{H}_0^k sont calculés exactement comme dans l'équation (E.18) mais avec le vecteur \tilde{A}_j à la place de A_j .

E.3.2.2 Impact de l'incertitude des données sur l'erreur d'estimation

Le but de cette section est d'étudier l'impact de l'incertitude δ_j sur les deux premiers moments de l'estimateur \hat{v}_k . Pour cela, l'équation de mesure (E.19) peut être écrite sous la forme suivante :

$$Y^k + \Delta Y^k \simeq (H_0^k + \Delta H^k) \cdot \beta_k + \Xi^k, \quad (\text{E.20})$$

où $Y^k = R^k - R_0^k$, $\Delta Y^k = R_0^k - \tilde{R}_0^k$, $\Delta H^k = \tilde{H}_0^k - H_0^k$ et $\beta_k = V_k - V_0$. Nous suivons ici l'analyse de l'incertitude dans le modèle de régression et son impact sur l'estimateur des

moindres carrés développés dans les articles (Hodges et Moore - 1972; Davies et Hutton - 1975; Swindel et Bower - 1972). On peut montrer que les deux premiers moments de l'estimateur $\hat{\beta}_k$ sont calculés comme

$$\begin{aligned}\mathbb{E}(\hat{V}_k - V) &= B_0^{-1} \left[(H_0^k)^T \Sigma_H C - F + G \right] \beta_k, \quad B_0 = (H_0^k)^T H_0^k. \\ \mathbb{E}(\hat{V}_k - V)(\hat{V}_k - V)^T &= B_0^{-1} (H_0^k)^T \left[\sigma^2 I_n + \Sigma_Y - \beta_1 (\Sigma_{\tilde{H}Y} + \Sigma_{Y\tilde{H}}) + \beta_1^2 \Sigma_H \right] H_0^k B_0^{-1}. \quad (\text{E.21})\end{aligned}$$

où Σ_H désigne la matrice de covariance de ΔH^k , $F = \begin{pmatrix} \text{tr}(\Sigma_H) & 0 \\ 0 & 0 \end{pmatrix}$, $G = \begin{pmatrix} \text{tr}[H_0^k B_0^{-1} (H_0^k)^T \Sigma_H] & 0 \\ 0 & 0 \end{pmatrix}$, la première colonne de la matrice C de dimension $(n \times 2)$ est égale à celle de $H_0^k B_0^{-1}$ et la deuxième colonne est égale à zéro. $\beta_1 = v - v_0$, Σ_Y désigne la matrice de covariance de ΔY^k , $\Sigma_{\tilde{H}Y} = \mathbb{E}[\Delta \tilde{H}^k (\Delta Y^k)^T]$, le vecteur $\Delta \tilde{H}^k$ de dimension n est égal à la première colonne de ΔH^k , et $\Sigma_{Y\tilde{H}} = \Sigma_{\tilde{H}Y}^T$.

E.3.2.3 Simulations numériques

Le scénario suivant sera utilisé : la constellation GNSS avec $n = 6$ satellites visibles et l'écart-type des erreurs de pseudo-distance $\sigma = 2$ m. La période d'échantillonnage des mesures GNSS est $\Delta t = 0.5$ s. La distance entre deux sommets adjointifs est choisie $\lambda = 50$ m. La valeur d'incertitude est $b = 0.05$ (incertitude $\simeq \pm 2.5$ m).

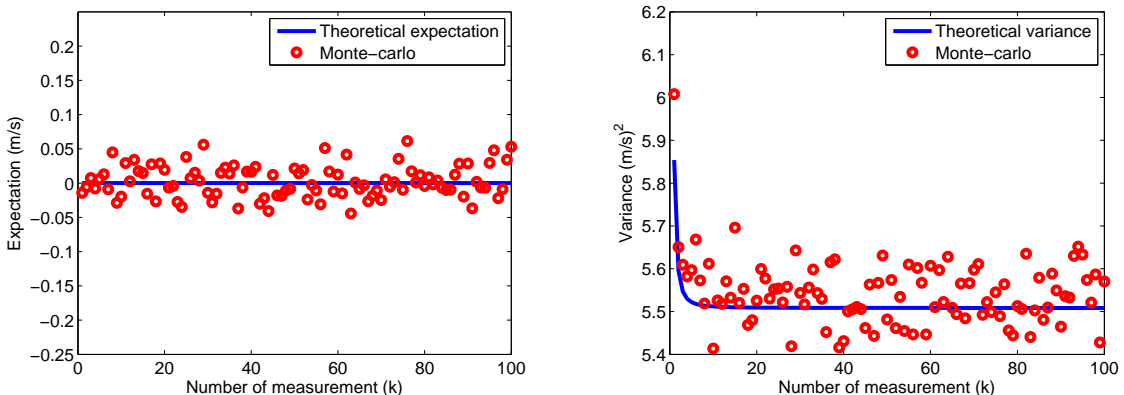


Figure E.12 – L'erreur moyenne de la vitesse estimée pour $\delta_j \in [-0.05, 0.05]^2$.
Figure E.13 – Le moment d'ordre deux de la vitesse estimée pour $\delta_j \in [-0.05, 0.05]^2$.

La comparaison des deux premiers moments théoriques de l'estimation donnés par (E.21), avec les résultats de simulation Monte-carlo utilisant 10^4 répétitions, est représentée sur la figure E.12-E.13.

E.3.3 Estimation de la distance, vitesse pour le cas d'une vitesse variable

Le but de cette section est d'estimer la distance parcourue et la vitesse du train lorsque l'accélération n'est pas négligeable. Par conséquent, supposons que le train roule sur la voie ferroviaire E.11 au-dessus à une vitesse variable. En utilisant l'équation pour le modèle dynamique du train (E.9), la position du train est donnée par

$$X(\ell_{k-q+p}) = Z_{j-1} + A_j \cdot [\ell_{k-q+p} - \lambda \cdot (j-1)], \quad (\text{E.22})$$

où $p = 0, 1, \dots, q$ et $A_j = (a_x^j, a_y^j, a_z^j)^T = \frac{1}{\lambda}(Z_{j+1} - Z_j)$ est le vecteur directionnel qui correspond au numéro de segment j , $\|A_j\|_2 = 1$. Le numéro de segment actuel $j = j(k - q + p)$, considéré comme une fonction de $k - q + p$, est calculé comme :

$$j(k - q + p) = \min \{j \in \mathbb{N} | j \geq \ell_{k-q+p}/\lambda\},$$

où \mathbb{N} est l'ensemble des nombres naturels.

E.3.3.1 Modèle imprécis de mesure de pseudo-distance et l'estimation.

Comme nous avons discuté dans la section E.2.3.1 ci-dessus, l'équation pour le vecteur de pseudo-distances R_{k-q+p} entre le train et les satellites est obtenue par linéariser l'équation non-linéaire exact autour d'un point de travail $\ell_{k-q+p,0}$. L'équation de mesure finale est calculée exactement comme dans l'équation (E.12), à savoir :

$$R^k - D_0^k + Y_0^k \simeq H_0^k \cdot \beta_k + \Xi^k. \quad (\text{E.23})$$

Puisque la vraie position du sommet Z_j est inconnue et une seule estimation imprécise \tilde{Z}_j est disponible, l'équation de mesure linéarisée (E.23) ne peut être utilisée pour le calcul. Supposons le vecteur aléatoire $\xi_j = Z_j - \tilde{Z}_j$ est supposé être réparti uniformément dans le cube $[-b, b]^3$ avec $b > 0$. Enfin, un modèle imprécis de mesure de pseudo-distance est calculé comme :

$$R^k - \tilde{D}_0^k + \tilde{Y}_0^k \simeq \tilde{H}_0^k \cdot \beta_k + \Xi^k, \quad (\text{E.24})$$

où \tilde{D}_0^k , \tilde{Y}_0^k , et \tilde{H}_0^k sont calculés exactement comme dans l'équation (E.23) mais avec les vecteurs \tilde{Z}_j , $\tilde{A}_j = \frac{\tilde{Z}_{j+1} - \tilde{Z}_j}{\|\tilde{Z}_{j+1} - \tilde{Z}_j\|_2}$ à la place de Z_j , A_j .

E.3.3.2 Impact de l'incertitude des données sur l'erreur d'estimation

Le but de cette section est d'étudier l'impact de l'incertitude ξ_j sur les deux premiers moments de l'estimateur $\hat{\beta}_k$. Nous suivons aussi ici l'analyse de l'incertitude dans le modèle de régression et son impact sur l'estimateur des moindres carrés. L'équation de mesure (E.24) peut être réécrite de la façon suivante :

$$Y^k + \Delta Y^k \simeq (H_0^k + \Delta H^k) \cdot \beta_k + \Xi^k,$$

où $Y^k = R^k - D_0^k + Y_0^k$ sont les réponses, $\Delta Y^k = D_0^k - \tilde{D}_0^k - Y_0^k + \tilde{Y}_0^k$ et $\Delta H^k = \tilde{H}_0^k - H_0^k$ désigne l'incertitude des données dans le modèle de régression. On peut montrer que les deux premiers moments de l'estimateur $\hat{\beta}_k$ sont calculés comme

$$\begin{aligned} \mathbb{E}(\hat{\beta}_k - \beta_k) &= (\bar{B}^k)^{-1} \left[(\bar{H}_0^k)^T C - F + G \right] \beta_k, \\ \mathbb{E}(\hat{\beta}_k - \beta_k)(\hat{\beta}_k - \beta_k)^T &= (\bar{B}^k)^{-1} (\bar{H}_0^k)^T (\sigma^2 I + \Sigma_Y - N - N^T + M) \bar{H}_0^k (\bar{B}^k)^{-1}. \end{aligned} \quad (\text{E.25})$$

où $\bar{B}^k = (\bar{H}_0^k)^T \bar{H}_0^k$. Les matrices \bar{H}_0^k sont calculées exactement comme dans l'équation (E.23) mais avec le point de travail $\ell_{k-q+p,0} = \omega_p \cdot \theta_{k-1}$. C, F et G désignent les fonctions matricielles de moment d'ordre deux de ΔH^k , Σ_Y désigne la matrice de covariance de ΔY^k , N et M sont les fonctions matricielles de moment d'ordre deux de ΔH^k et $\tilde{D}_0^k - D_0^k$.

E.3.3.3 Simulations numériques

Le scénario suivant sera utilisé : la constellation GNSS avec $n = 6$ satellites visibles et l'écart-type des erreurs de pseudo-distance $\sigma = 2$ m. La période d'échantillonnage des mesures GNSS est $\Delta t = 0.5$ s. La vraie valeur pour la période de l'accélération, du mouvement uniforme, du freinage est 0.8 m/s², 0 m/s² et -0.8 m/s², respectivement. La distance entre deux sommets adjectifs est $\lambda = 50$ m. La valeur d'incertitude est $b = 2$ m. Le schéma de mouvement typique de train est représenté sur la figure E.6. La comparaison des deux premiers moments théoriques de ces estimations donnés par (E.25), avec les résultats de simulation Monte-carlo utilisant 10^4 répétitions, est représentée sur la figure E.14-E.15.

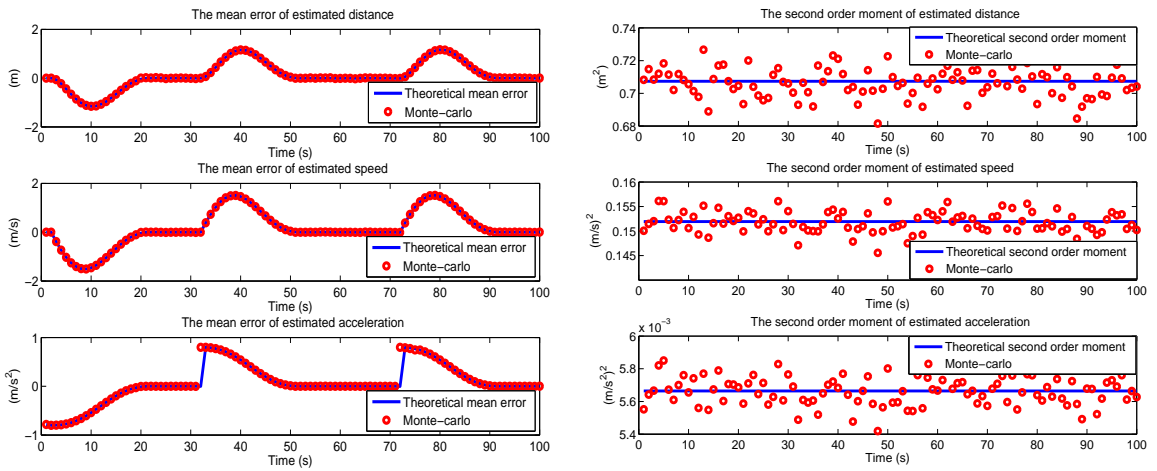


Figure E.14 – L'erreur moyenne de la distance, de la vitesse et de l'accélération pour l'incertitude de $\xi_j \in [-2, 2]^2$ et $q = 20$.

Figure E.15 – Le moment d'ordre deux de la distance, de la vitesse et de l'accélération pour l'incertitude de $\xi_j \in [-2, 2]^2$ et $q = 20$.

E.3.4 Conclusions

Dans le cas d'une vitesse constante, l'estimateur est pratiquement non biaisé, même avec un modèle géométrique imprécis de voie ferroviaire. L'impact négatif de l'incertitude sur l'estimation de la vitesse se manifeste à travers une augmentation très considérable de la variance de vitesse par rapport au cas "idéal".

Dans le cas d'une vitesse variable, les résultats montrent que le changement d'accélération provoque une estimation imprécise de la distance parcourue, la vitesse et l'accélération pour une courte période. L'estimateur est toujours presque non biaisé, à l'exception d'une courte période de temps après le changement d'accélération, mais la variance reste inchangée pendant cette période. L'incertitude des données conduit à une légère augmentation du moment d'ordre deux de ces estimations par rapport au cas "idéal".

E.4 Estimation de la distance, vitesse du train à base de l'intégration GNSS avec la base de données

Dans le chapitre IV, on considère que la géométrie de voie est disponible dans d'une base de données avec des mesures bruitées (sans l'approximation par une ligne brisée). Le but de ce chapitre est d'estimer la distance parcourue et la vitesse du train en intégrant les mesures GNSS avec celles de la base de données. Deux cas sont étudiés : une vitesse constante et variable. Dans les deux cas, un modèle de système intégré est conçu. Ensuite, l'impact des erreurs dans les mesures GNSS et la base de données sur ces estimations sont étudié.

E.4.1 Description de la base de données d'une voie ferroviaire

La base de données d'une voie ferroviaire est nécessaire pour le système de positionnement du train basé sur GNSS. Il peut être généré à l'aide des méthodes d'enquête, qui peut installer un récepteur GNSS dans un train ou utiliser des mesures géodésiques pour recueillir les données. En raison des erreurs instrumentales au cours de la collecte des données de la trajectoire, il est nécessaire de noter que les données recueillies ne coïncident pas exactement avec la vraie voie dans le monde réel. Par conséquent, nous considérons maintenant que un train, a installé un récepteur GNSS, roule sur une voie ferroviaire "idéale" décrite dans la section E.2.1, qui est généralement composée de lignes droites, de courbes de transition et d'arcs de cercle (voir la figure E.1). Ici, pour simplifier, nous supposons que la trajectoire appartient entièrement au plan tangent local. La relation entre les vrais points et les points recueillis de la base de données est donnée par (voir la figure E.16)

$$Z_{DB,j} = X_j(\varphi) + \xi_{DB,j}, \quad (E.26)$$

où φ désignent les paramètres géométriques de voie ferroviaire pour les lignes droites, les courbes de transition et les arcs de cercle, c'est-à-dire φ_{sl} , φ_{tc} et φ_{ca} , respectivement. $X_j(\varphi)$ est le vrai point qui correspond au numéro de point j , qui est calculé en fonction de la distance ℓ par utiliser l'équation suivante : $j = \lceil \ell / \lambda \rceil$. $\lambda = \|X_j(\varphi) - X_{j-1}(\varphi)\|_2 = \text{const}$ est la distance entre deux points adjointifs. $Z_{DB,j}$ désigne le point recueilli de la

base de données et $\xi_{DB,j} \sim \mathcal{N}(0, \sigma_{DB}^2 I_2)$ est l'erreur de mesure.

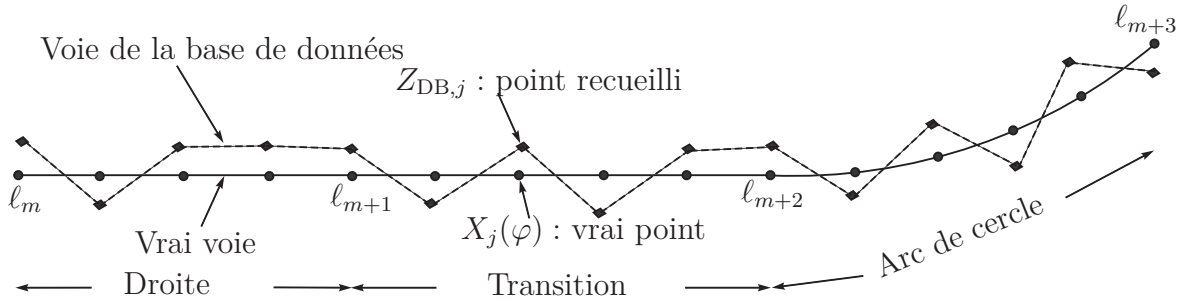


Figure E.16 – Les erreurs de mesure dans la base de données.

E.4.2 Estimation de la vitesse à base du système intégré pour le cas d'une vitesse constante

Dans cette section, un modèle mathématique rigoureux pour le système intégré est conçu pour estimer la vitesse du train. On suppose que le train roule sur la voie ferroviaire E.1 au-dessus à une vitesse constante inconnue v . La distance parcourue ℓ_t au temps t est égale au produit de la multiplication de la vitesse v par le temps t , soit $\ell_t = v \cdot t$ et $t = 1, 2, \dots$. Par conséquent, la position du train est définie : $X_t(\varphi, \ell_t) = (x(\varphi, \ell_t), y(\varphi, \ell_t), 0)^T$, où $(x(\varphi, \ell_t), y(\varphi, \ell_t))$ est la position correspondante au plan tangent local. Comme la distance $\ell_t = v \cdot t$ et la vitesse v est inconnue, la position correspondante $(x(\varphi, \ell_t), y(\varphi, \ell_t))$ peut être considérée comme une fonction de v , soit, $(x(\varphi, v), y(\varphi, v))$.

E.4.2.1 Modèle du système intégré

Premièrement, un système d'équations linéaires est obtenu en linéarisant l'équation non-linéaire (E.26) pour les points recueillis dans le segment de droite au vecteur d'état φ_{sl} autour d'un point de travail $\varphi_{sl,0}$. Le système d'équations linéaires est donné sous la forme suivante :

$$Z_{DB}^{sl,0} = Z_{DB}^{sl} - X_{sl}(\varphi_{sl,0}) \simeq H_0^{sl} \cdot (\varphi_{sl} - \varphi_{sl,0}) + \xi_{DB}^{sl}, \quad (E.27)$$

où le vecteur φ_{sl} est inconnu et doit être estimé.

Ensuite, l'équation pour le vecteur de pseudo-distances R^t entre les satellites et le train est obtenue en linéarisant l'équation non-linéaire exacte par rapport au vecteur d'état $\beta_t^{sl} = (\varphi_{sl}^T, v, cb_r^t)^T$ autour d'un point de travail $\beta_{t,0}^{sl} = (\varphi_{sl,0}^T, v_0, cb_0)^T$. L'équation de mesure linéaire est donnée sous la forme suivante :

$$Y^t = R^t - R_0^t \simeq H_0^t \cdot (\beta_t^{sl} - \beta_{t,0}^{sl}) + \Xi^t, \quad (\text{E.28})$$

où le vecteur $\beta_t^{sl} = (\varphi_{sl}^T, v, cb_r^t)^T = (x_0, y_0, \alpha, v, cb_r^t)^T$ est inconnu et doit être estimé. $\Xi^t \sim \mathcal{N}(0, \sigma_{\text{PD}}^2 I)$ est un bruit de mesure.

Finalement, avec ces deux équations linéaires (E.27) et (E.28), on peut obtenir un système intégré de la façon suivante :

$$\begin{pmatrix} Z_{\text{DB}}^{sl,0} \\ Y^t \end{pmatrix} \simeq \begin{pmatrix} H_0^{sl} & | & \mathbf{0} \\ H_0^t & \end{pmatrix} \begin{pmatrix} \varphi_{sl} - \varphi_{sl,0} \\ v - v_0 \\ cb_r^t - cb_0 \end{pmatrix} + \begin{pmatrix} \xi_{\text{DB}}^{sl} \\ \Xi^t \end{pmatrix}. \quad (\text{E.29})$$

Le système intégré final (E.29) peut être réécrit de la manière suivante :

$$Y_t^{sl} = H_t^{sl} \cdot (\beta_t^{sl} - \beta_{t,0}^{sl}) + \Upsilon_t^{sl}, \quad (\text{E.30})$$

où le point de travail $\beta_{t,0}^{sl}$ au temps t est égal à l'estimation calculée précédemment : $\beta_{t,0}^{sl} = \hat{\beta}_{t-1}^{sl}$. Supposons que $\sigma_{\text{PD}}^2 = \sigma_{\text{DB}}^2 = \sigma^2$, la méthode des moindres carrés est

$$\hat{\beta}_t^{sl} = \hat{\beta}_{t-1}^{sl} + \left[(H_t^{sl})^T H_t^{sl} \right]^{-1} (H_t^{sl})^T Y_t^{sl}. \quad (\text{E.31})$$

L'erreur moyenne et le moment d'ordre deux sont calculés comme

$$\begin{aligned} \mathbb{E}(\hat{\beta}_t^{sl} - \beta_t^{sl}) &= \mathbb{E} \left\{ \left[(H_t^{sl})^T H_t^{sl} \right]^{-1} (H_t^{sl})^T \Upsilon_t^{sl} \right\} \simeq 0, \\ \mathbb{E}(\hat{\beta}_t^{sl} - \beta_t^{sl})(\hat{\beta}_t^{sl} - \beta_t^{sl})^T &\simeq \sigma^2 \left[(\bar{H}_t^{sl})^T \bar{H}_t^{sl} \right]^{-1}, \end{aligned} \quad (\text{E.32})$$

où la matrice \bar{H}_t^{sl} est calculée exactement comme dans l'équation (E.30) mais avec le point de travail $\beta_{t,0}^{sl} = \beta_{t-1}^{sl}$.

Par ailleurs, deux systèmes intégrés pour la courbe de transition et l'arc de cercle sont obtenus par analogie avec la procédure (E.27) - (E.30) pour le segment de droite.

E.4.2.2 Simulations numériques

Le scénario suivant sera utilisé : la constellation GNSS avec $n = 6$ satellites visibles et l'écart-type des erreurs de pseudo-distance $\sigma_{\text{PD}} = 2$ m. La période d'échantillonnage

des mesures GNSS est $\Delta t = 0.5$ s. La vraie vitesse du train est 20 m/s et le point de travail initial v_0 est 10 m/s. La distance entre deux sommets adjointifs est $\lambda = 10$ m. La précision de base de données de la voie est $\sigma_{DB} = 2$ m. Le valeur de rayon de courbure est $R = 100$ m.

Les segments de la trajectoire du train stockés dans la base de données à bord du train sont résumés dans le tableau E.1. La courbure d'une voie ferroviaire et la trajectoire du train sont présentées sur la figure E.17 et E.18, respectivement.

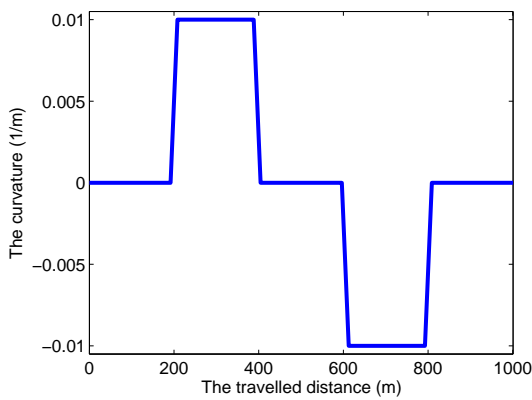


Figure E.17 – Courbure calculée pour la trajectoire.

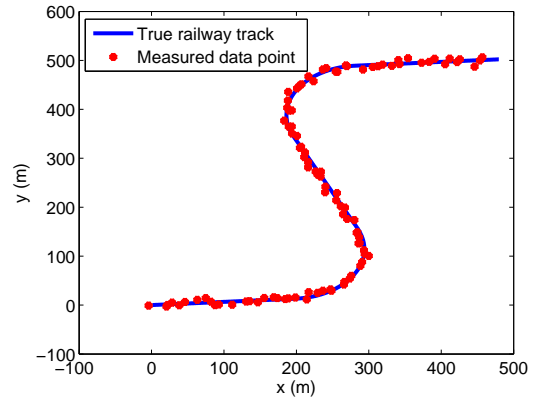


Figure E.18 – La trajectoire testée au plan tangent local.

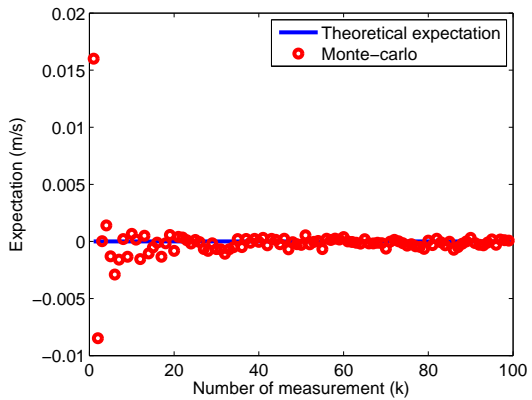


Figure E.19 – L'erreur moyenne de la vitesse estimée pour $R = 100$ m et $\sigma_{PD} = \sigma_{DB} = 2$ m.

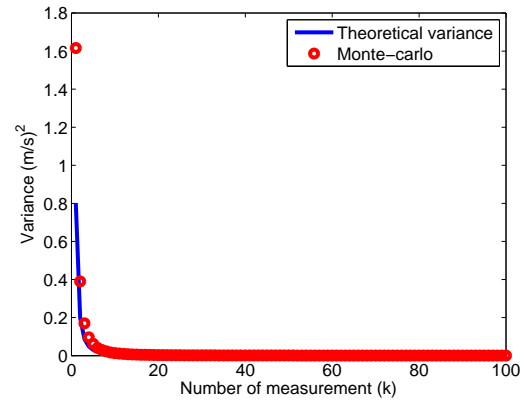


Figure E.20 – Le moment d'ordre deux de la vitesse estimée pour $R = 100$ m et $\sigma_{PD} = \sigma_{DB} = 2$ m.

La comparaison des deux premiers moments théoriques de la vitesse estimée donnés

par (E.32), avec les résultats de simulation Monte-carlo utilisant 10^4 répétitions, est représentée sur la figure E.19-E.20.

E.4.3 Estimation de la distance, vitesse à base du système intégré pour le cas d'une vitesse variable

Le but de cette section est d'estimer la distance parcourue et la vitesse du train lorsque l'accélération n'est pas négligeable. Par conséquent, on considère que le train roule la voie ferroviaire E.1 ci-dessus avec une vitesse variable. Avec les équations pour le modèle dynamique du train (E.9) et les éléments de conception traditionnelle concernant la voie ferroviaire (E.1), (E.2), (E.3), la position du train est donnée par

$$X(\varphi, \ell_{k-q+p}) = [x(\varphi, \ell_{k-q+p}), y(\varphi, \ell_{k-q+p}), 0]^T,$$

où $(x(\varphi, \ell_{k-q+p}), y(\varphi, \ell_{k-q+p}))$ est la position correspondante au plan tangent local.

E.4.3.1 Modèle du système intégré

L'équation pour le vecteur de pseudo-distances R_{k-q+p} entre les satellites et le train est obtenue en linéarisant l'équation non-linéaire exacte autour d'un point de travail $(\varphi_{sl,0}^T, \ell_{k-q+p,0})^T$. L'équation de mesure linéaire est donnée sous la forme suivante :

$$Y_{k-q+p} \simeq H_{\varphi_{sl}, k-q+p, 0} \varphi_{sl} + H_{\ell, k-q+p, 0} \ell_{k-q+p} + \mathbf{1}_n \cdot cb_r^{k-q+p} + \Xi_{k-q+p}. \quad (\text{E.33})$$

où $\Xi_{k-q+p} \sim \mathcal{N}(0, \sigma_{\text{PD}}^2 I)$ est un bruit de mesure.

En combinant le système d'équations linéaires (E.27) pour les points recueillis dans le segment de droite et l'équation de mesure linéaire (E.33), on peut obtenir un système intégré de la façon suivante :

$$\begin{pmatrix} \bar{Z}_{\text{DB}}^{sl,0} \\ Y_k \\ \vdots \\ Y_{k-q} \end{pmatrix} \simeq \left(\begin{array}{c|cc} H_0^{sl} & \mathbf{0} \\ \hline H_{\varphi_{sl}, k, 0} & H_{\ell, k, 0} \cdot \omega_q & \mathbf{1}_n \\ \vdots & \vdots & \ddots \\ H_{\varphi_{sl}, k-q, 0} & H_{\ell, k-q, 0} \cdot \omega_0 & \mathbf{1}_n \end{array} \right) \begin{pmatrix} \varphi_{sl} \\ \theta_k \\ cb_r^k \\ \vdots \\ cb_r^{k-q} \end{pmatrix} + \begin{pmatrix} \xi_{\text{DB}}^{sl} \\ \Xi_k \\ \vdots \\ \Xi_{k-q} \end{pmatrix}, \quad (\text{E.34})$$

où $\bar{Z}_{\text{DB}}^{sl,0} \simeq Z_{\text{DB}}^{sl,0} + H_0^{sl} \varphi_{sl,0}$, le système intégré final (E.34) peut être écrit dans la matrice suivante :

$$Y_k^{sl} \simeq H_k^{sl} \beta_k^{sl} + \Upsilon_k^{sl}, \quad (\text{E.35})$$

où le vecteur $\beta_k^{sl} = (\varphi_{sl}^T, \theta_k^T, cb_r^k, \dots, cb_r^{k-q})^T$ est inconnu et doit être estimé. Le point de travail $\varphi_{sl,0}$ au temps t_k est égal à l'estimation calculée précédemment $\hat{\varphi}_{sl}$ et $\ell_{k-q+p,0}$ est égal au produit de la multiplication du facteur ω_p par l'estimation calculée précédemment : $\ell_{k-q+p,0} = \omega_p \cdot \hat{\theta}_{k-1}$. Supposons que $\sigma_{PD}^2 = \sigma_{DB}^2 = \sigma^2$, la méthode des moindres carrés est

$$\hat{\beta}_k^{sl} = \left[(H_k^{sl})^T H_k^{sl} \right]^{-1} (H_k^{sl})^T Y_k^{sl}. \quad (\text{E.36})$$

L'erreur moyenne et le moment d'ordre deux sont calculés comme

$$\begin{aligned} \mathbb{E}(\hat{\beta}_k^{sl} - \beta_k^{sl}) &= \mathbb{E} \left\{ \left[(H_k^{sl})^T H_k^{sl} \right]^{-1} (H_k^{sl})^T \Upsilon_k^{sl} \right\} \simeq 0, \\ \mathbb{E}(\hat{\beta}_k^{sl} - \beta_k^{sl})(\hat{\beta}_k^{sl} - \beta_k^{sl})^T &\simeq \sigma^2 \left[(\bar{H}_k^{sl})^T \bar{H}_k^{sl} \right]^{-1}, \end{aligned} \quad (\text{E.37})$$

où la matrice \bar{H}_k^{sl} est calculée exactement comme dans l'équation (E.35) mais avec le point de travail $\varphi_{sl,0} = \varphi_{sl}$ et $\ell_{k-q+p,0} = \omega_p \cdot \theta_{k-1}$.

Par ailleurs, deux systèmes intégrés pour la courbe de transition et l'arc de cercle sont obtenus par analogie avec la procédure (E.33) - (E.35) pour le segment de droite.

E.4.3.2 Simulations numériques

Le scénario suivant sera utilisé : la constellation GNSS avec $n = 6$ satellites visibles et l'écart-type des erreurs de pseudo-distance $\sigma_{PD} = 2$ m. La période d'échantillonnage des mesures GNSS est $\Delta t = 0.5$ s. La vraie valeur pour la période de l'accélération, du mouvement uniforme, du freinage est 0.8 m/s 2 , 0 m/s 2 et -0.8 m/s 2 , respectivement. La distance entre deux sommets adjectifs est $\lambda = 10$ m. La précision de base de données de la voie est $\sigma_{DB} = 2$ m. Le valeur de rayon de courbure est $R = 100$ m. Le schéma de mouvement de train est représenté sur la figure E.6.

Les segments de la trajectoire du train stockés dans la base de données à bord du train sont résumés dans le tableau E.1. La courbure d'une voie ferroviaire et la trajectoire du train sont présentées sur la figure E.21 and E.22, respectivement.

La comparaison des deux premiers moments théoriques de ces estimations donnés par (E.37), avec les résultats de simulation Monte-carlo utilisant 10^4 répétitions, est représentée sur la figure E.23-E.24.

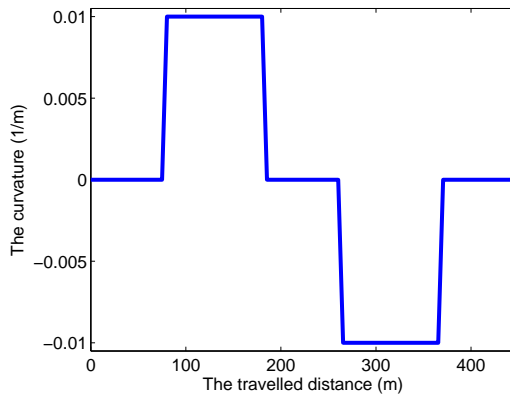


Figure E.21 – Courbure calculée pour la trajectoire.

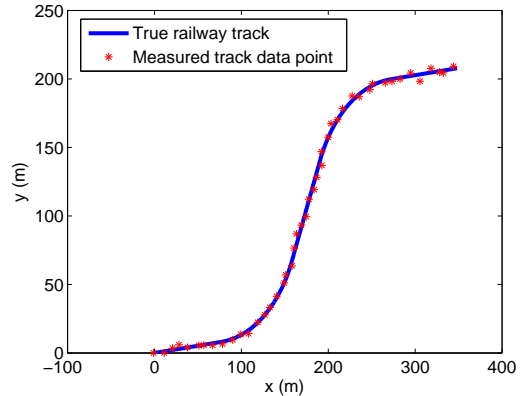


Figure E.22 – La trajectoire testée au plan tangent local.

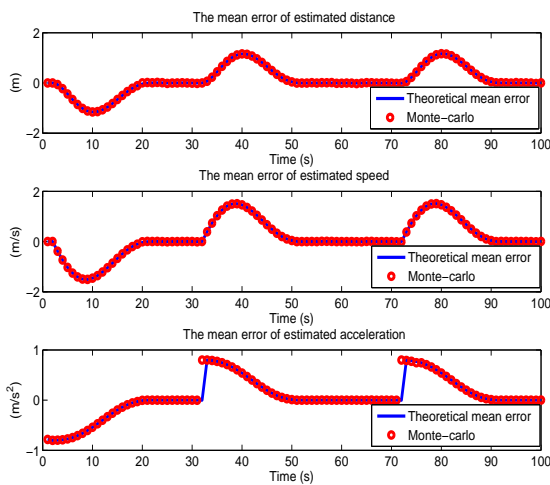


Figure E.23 – L'erreur moyenne de la distance, de la vitesse et de l'accélération pour $R = 100$ m, $\sigma_{PD} = \sigma_{DB} = 2$ m et $q = 20$.

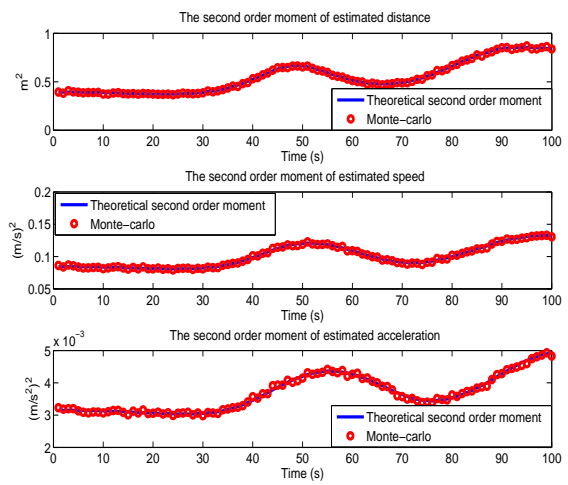


Figure E.24 – Le moment d'ordre deux de la distance, de la vitesse et de l'accélération pour $R = 100$ m, $\sigma_{PD} = \sigma_{DB} = 2$ m et $q = 20$.

E.4.4 Conclusions

Dans le cas d'une vitesse constante, l'estimateur est pratiquement non biaisé. L'impact négatif de l'incertitude et du rayon de courbure minimum de la voie sur la vitesse estimée est presque négligeable. La variance de l'estimation de la vitesse devient rapidement très faible, presque comme dans le cas "idéal".

Dans le cas d'une vitesse variable, le changement d'accélération provoque l'apparition de biais dans les estimations pour une courte période, comme dans les cas précédents. L'impact négatif du rayon de courbure de voie minimal sur ces estimations est presque négligeable.

E.5 Conclusions et recherches futures

E.5.1 Conclusions

Comme mentionné précédemment, certains systèmes d'exploitation ferroviaire ont été largement utilisés pour garantir la sécurité et l'efficacité du réseau ferroviaire. L'efficacité des systèmes est basée sur le positionnement fiable du train. D'autre part, la technologie GNSS a attiré beaucoup d'attention autour du monde et elle a été largement appliquée dans le domaine des transports, tels que l'aviation, le ferroviaire, et la marine. Par conséquent, application de la technologie GNSS au positionnement du train est un domaine de recherche très prometteur.

Les algorithmes décrits dans cette thèse sont consacrés à la précision du positionnement du train obtenu à l'aide des satellites GNSS et de l'information sur la trajectoire du train, stockée dans une base de données de l'ordinateur du bord.

Dans le chapitre II, un modèle "idéal" de voie ferroviaire, composé de lignes droites, de courbes de transition et d'arcs de cercle, est défini par un ensemble d'équations paramétriques. La distance parcourue et la vitesse du train sont estimées en utilisant les mesures GNSS et le modèle "idéal" de la trajectoire. Deux cas sont étudiés : la vitesse constante et variable. Dans les deux cas, un estimateur des moindres carrés est conçu. Dans le cas d'une vitesse constante, l'estimateur est pratiquement non biaisé, même avec le rayon de courbure de voie minimal. L'impact négatif du rayon de courbure sur la vitesse estimée du train est presque négligeable. La variance de l'estimation de vitesse devient rapidement très faible. Dans le cas d'une vitesse variable, il a été démontré que le changement d'accélération provoque l'apparition des biais dans les estimations de distance parcourue, de vitesse et d'accélération pour une courte période. Un faible rayon de courbure peut augmenter le moment d'ordre deux de ces estimations.

Dans le chapitre III, un modèle "non-idéal" de voie ferroviaire est défini par une ligne polygonale avec un certain niveau d'incertitude dans la base de données à bord du train. La distance parcourue et la vitesse du train sont estimées en utilisant des mesures GNSS et un modèle "non-idéal". Deux cas sont étudiés : une vitesse constante et variable. Dans les deux cas, un estimateur des moindres carrés est conçu. Dans le cas d'une vitesse constante, l'estimateur est pratiquement non biaisé, même avec un modèle géométrique imprécis de voie ferroviaire. L'impact négatif de l'incertitude sur l'estimation de la vitesse se manifeste à travers une augmentation très considérable de la variance de vitesse par rapport au cas "idéal". Dans le cas d'une vitesse variable, les résultats montrent que le changement d'accélération provoque une estimation imprécise de la distance parcourue, la vitesse et l'accélération pour une courte période. L'estimateur est toujours presque non biaisé, à l'exception d'une courte période de temps après le changement d'accélération, mais la variance reste inchangée pendant cette période. L'incertitude des données conduit à une légère augmentation du moment d'ordre deux de ces estimations par rapport au cas "idéal".

Enfin, dans le chapitre IV, on considère que la géométrie de voie est disponible dans d'une base de données avec des mesures bruitées (sans l'approximation par une ligne brisée). La distance parcourue et la vitesse du train sont estimées en intégrant les mesures GNSS avec celles de la base de données. Deux cas sont étudiés : une vitesse constante et variable. Dans les deux cas, un modèle de système intégré est conçu. Dans le cas d'une vitesse constante, l'estimateur est pratiquement non biaisé. L'impact négatif de l'incertitude et du rayon de courbure minimum de la voie sur la vitesse estimée est presque négligeable. La variance de l'estimation de la vitesse devient rapidement très faible, presque comme dans le cas "idéal". Dans le cas d'une vitesse variable, le changement d'accélération provoque l'apparition de biais dans les estimations pour une courte période, comme dans les cas précédents. L'impact négatif du rayon de courbure de voie minimal sur ces estimations est presque négligeable.

E.5.2 Recherches futures

Dans cette section, nous discutons brièvement plusieurs directions prometteuses pour la recherche future.

Utiliser des données réelles pour tester les algorithmes proposés

Lors du test de performances de ces algorithmes proposés, nous avons utilisé la base de données de la trajectoire simulée du train et quelques hypothèses. Actuellement, la base de données de la trajectoire réaliste disponible est très limitée. Il est intéressant d'approfondir l'analyse des algorithmes proposés à base de données réelles.

Améliorer la base de données d'une voie ferroviaire

Il est intéressant d'élargir le modèle géométrique de voie 2D (dans un plan tangent) pour se rapprocher d'une trajectoire du train en 3D dans un monde réel.

Appliquer un filtre de Kalman dans le positionnement du train

Dans cette thèse, le problème du positionnement du train est résolu à l'aide de la méthode des moindres carrés basée sur la minimisation de la somme des carrés résiduels. On peut imaginer ici l'application d'un filtre de Kalman, étant donné que le filtre de Kalman est utilisable pour un modèle dynamique.

Comparer les résultats obtenus avec d'autres méthodes de positionnement

On souhaite comparer les résultats obtenus à partir de nos algorithmes avec d'autre méthodes qui utilisent, par exemple, les mesures odométriques.

Intégrer les mesures GNSS avec d'autres capteurs de positionnement

Pour atteindre le niveau de sûreté requis, nous souhaitons également intégrer les mesures GNSS avec d'autres capteurs de positionnement. L'intégration des capteurs indépendants supplémentaires peut améliorer la précision de l'estimation de la position du train.

Concevoir des algorithmes de contrôle d'intégrité pour le positionnement du train utilisant GNSS

Enfin, nous souhaitons ici développer des algorithmes de contrôle d'intégrité pour le positionnement du train à base de GNSS. Lorsque le train se déplace dans les zones urbaines, dans les forêts et dans les tunnels le problème du contrôle d'intégrité devient très important.

Bibliographie

- Yong-Won Ahn. *Advanced surveying : principles of GNSS positioning and different methodology*. University of New Brunswick, 2013.
- Antonella Albanese, Giovanni Labblento, Livio Marradi, et Giovanni Venturi. The RUNE project : the integrity performances of GNSS-based railway user navigation equipment. In *Proceedings of 2005 Joint Rail Conference*, 16-18 Mar. 2005.
- B. Allotta, V. Colla, M. Malvezzi, P. Presciani, et G. Cocci. Train speed and position evaluation using wheel velocity measurements. *Proc. Inst. Mech. Eng. FJ. Rail Rapid Transit* 216, pages 207–225, 2002.
- Uwe Becker, Frank Hänsel, Jörg May, Jan Poliak, et Eckehard Schnieder. Vehicle autarkic positioning as a basis for a low cost train protection system on secondary lines. In *7th World Congress on Railway Research*, 2006a.
- Uwe Becker, Frank Hänsel, Jörg May, Jan Poliak, et Eckehard Schnieder. Vehicle autarkic positioning as a basis for a low cost train protection system on secondary lines. In *The 7th World Congress on Railway Research*, 2006b.
- Uwe Becker, Frank Hänsel, Jörg May, Jan Poliak, et Eckehard Schnieder. Vehicle autonomous positioning as a basis for a low cost train protection system. In *Proceedings of the 13th ITS world congress*, 2006c.
- S. Bedrich et X. Gu. GNSS-based sensor fusion for safety-critical applications in rail traffic. In *Galileo and EGNOS Information Catalogue*, 2004.
- B.Hofmann-Wellenhof, H.Lichtenegger, et J.Collins. *GPS : Theory and Practice*. Springer Wien NewYork, 1992.
- B. Caulfield. *Engineering surveying*. Trinity College Dublin, 2012.
- V. Colla, M. Vannucci, B. Allotta, et M. Malvezzi. Comparison of traditional and neural systems for train speed estimation. *ESANN*, 23-25 Apr. 2003.

- V. Colla, M. Vannucci, B. Allotta, et M. Malvezzi. Estimation of train speed via neuro-fuzzy techniques. *IWANN*, 3-6 Jun. 2003.
- R.B. Davies et B. Hutton. The effect of errors in the independent variables in linear regression. *Biometrika*, Volume : 62, No. 2 :383–391, 1975.
- Rod Deakin. *Lecture notes on horizontal curves, including the clothoid spiral, used in surveying*. RMIT University, 2013a.
- Rod Deakin. *Lecture notes on parabolic vertical curves in surveying applications*. RMIT University, 2013b.
- Patricia Dingwall. *Track standards manual - track geometry*. Richard Spoors, Controller, Railway Group Standards, 1998.
- Ahmed El-Rabbany. *Introduction to GPS : the Global Positioning System*. Artech House, 2002.
- Alan H. Feiveson. Explanation of the delta method. *NASA*, pages 1–19, 2008.
- A. Filip. Safety aspects of GNSS based train position determination for railway signalling. In *UIC Galileo for Rail Symposium*, pages 1–23, 2007.
- A. Filip, L. Bazant, H. Mocek, et J. Cach. GPS/GNSS based train position locator for railways signalling. In *Seventh International Conference on Computers in Railways. Computers in Railways VII*, pages 1227–1241. WIT Press, 2000.
- A. Filip, L. Bazant, H. Mocek, J. Taufer, et V. Maixner. Dynamic properties of GNSS/INS based train position locator for signalling applications. In *Eighth International Conference on Computers in Railways. Computers in Railways VIII*, pages 1021–1030. WIT Press, 2002.
- A. Filip, L. Bazant, H. Mocek, J. Taufer, et V. Maixner. The high integrity GNSS/INS based train position locator. In *Ninth International Conference on Computers in Railways. Computers in Railways IX*, pages 497–506. WIT Press, 2004.
- A. Filip, J. Beugin, J. Marais, et H. Mocek. Safety concept of railway signalling based on Galileo safety-of-life service. *11th International Conference on Computer System Design and Operation in the Railway and Other Transit Systems (COMPRAIL08)*, Volume : 49, No.5 :103–112, 2008.

- M. Foulardirad et I. Nikiforov. Détection statistique optimale dans un système linéaire en présence de paramètres de nuisance. In *GRETISI*, 2003.
- Grace Gao. *Towards navigation based on 120 satellites : analyzing the new signals.* PHD thesis, Standford University, 2008.
- V. Gikas et J. Stratakos. A novel geodetic engineering method for accurate and automated road/railway centerline geometry extraction based on the bearing diagram and fractal behavior. *IEEE Trans. Intell. Syst.*, Volume : 13, No.1 :115–126, Mar. 2012.
- Safety Regulation Group. *GPS integrity and potential impact on aviation safety.* Civil Aviation Authority, 2003.
- G.Seber et C.Wild. *Nonlinear regression.* Wiley-interscience, 1988.
- K. Hartwig, M. Grimm, M. Meyer zu Hörste, et K. Lemmer. Safety relevant positioning applications in rail traffic using the European satellite system "Galileo". In *14th International Symposium*, pages 183–191.
- K. Hartwig, M. Grimm, M. Meyer zu Hörste, et K. Lemmer. Requirements for safety relevant positioning applications in rail traffic - a demonstrator for a train borne navigation platform called "demoOrt". In *7th World Congress on Railway Research, WCRR*, 2006.
- S.D. Hodges et P.G. Moore. Data uncertainties and least squares regression. *JRSS, Series C (Applied Statistics)*, Volume : 21 :185–195, 1972.
- I. Illgen, G. Bikker, E. Schnieder, et M. Kaiser. Satnav-validation of a satellite based ground navigation system. In *Computers in Railways VII*, 2000.
- Marais Juliette. Impact du canal de propagation GNSS sur les performance de localisation en environnement constraint. 2011.
- H. Lacresse. *Détection de pannes en présence de paramètres de nuisance non-linéaires bornés.* PHD thesis, Université de Technologie de Troyes, 2004.
- H. Lacresse, A. Grall, et I. Nikiforov. Statistical fault detection with linear or nonlinear nuisance parameters. In *Safeprocess 2003, IFAC Conference*, pages 1–6, 2003.

H. Lacresse, A. Grall, et I. Nikiforov. Fault detection with nonlinear nuisance parameters and safe train navigation. In *Proc. 16th IFAC World Congress*, pages 1–6, 2005.

Martin Lindahl. *Track geometry for high-speed railways : a literature survey and simulation of dynamic vehicle response*. Royal Institutue of Technology, Stockholm, 2001.

Jiang Liu, Baigen Cai, Yunpeng Wang, et Jian Wang. A CKF based GNSS/INS train integrated positioning method. In *Proceedings of the 2010 IEEE International Conference on Mechatronics and Automation*, 2010.

Jiang Liu, Baigen Cai, Yunpeng Wang, Jian Wang, et Shangguan Wei. A GPS/Compass based train integrated positioning method for high-speed railways. In *Antennas and Propagation in Wireless Communications*, pages 1201–1204, 2012.

Katrin Lüddeken et Christian Rahmig. Evaluating multiple GNSS data in a multi-hypothesis based map-matching algorithm for train positioning. In *IEEE Intelligent Vehicles Symposium (IV)*, 2011.

M. Malvezzi, B. Allotta, M. Rinchi, M. Bruzzo, et P. De Bernardi. Distance and speed evaluation from odometric measurements. In *Proc. of World Congress on Railway Research*, 2001.

M. Malvezzi, B. Allotta, M. Rinchi, M. Bruzzo, et P. De Bernardi. Odometric estmation for automatic train protection and control systems. In *8th World Congres on Railway Research*, 2008.

M. Malvezzi, B. Allotta, M. Rinchi, M. Bruzzo, et P. De Bernardi. Odometric estmation for automatic train protection and control systems. *Vehicle System Dynamics*, Volume : 49, No.5 :723–739, 2011.

Pierre Mertens, Jean-Pierr Franckart, et Antonin Starck. A low cost train location and signalling systems for "low density" lines. In *Proceedings of World Congress on Railway Research*, 2003.

A. Mirabadi, N. Mort, et F. Schmid. Application of sensor fusion to railway systems. In *Proceedings of the IEEE/SICE/RSJ International Conference on Multisensor Fusion and Integration for Intelligent Systems*, pages 185–192, 1996.

- Pratap Misra et Per Enge. *Global Positioning System : Signals, Measurements, and Performance*. Ganga-Jamuna Press, 2011.
- Mo.S.SA. *Cubic parabola in railway applications*. The Mo.S.SA, Greece.
- J.S. Mundrey. *Railway track engineering*. Tata McGraw-Hill, 2007.
- I. Nikiforov. *Géo-localisation*. Université de Technologie de Troyes, 2013.
- I. Nikiforov et F. Choquette. Integrty equations for safe train positioning using GNSS. *Istituto Italiano di Navigazione*, Volume : 171 :52–77, 2003.
- W.Y. Ochieng, P.J. Shardlow, et G. Johnston. Advanced transport telematics positioning requirements : an assessment of GPS performance in greater london. *The Journal of Navigation*, pages 342–355, 1999.
- G.W. Oehlert. A note on the delta method. *American Statistician*, pages 27–29, 1992.
- V.A. Profiliidis. *Railway management and engineering*. Ashgate Publishing, Hampshire, England, 2006.
- Tsung-I Shen, Che-Hao Chang, Kuan-Yung Chang, et Cho-Chien Lu. A numerical study of cubic parabolas on railway transition curves. *Journal of Marine Science and Technology*, Volume : 21, No.2 :191–197, 2013.
- A. Simsky, F. Wilms, et J-P. Franckart. GNSS-based failsafe train positioning system for low-density traffic lines based on one-dimensional positioning algorithm. In *2nd ESA Workshop on Satellite Navigation User Equipment Technologies NAVITEC*, 8-10 Dec. 2004.
- V.B. Sood. *Notes on curves for railways*. Indian Railways Institute of Civil Engineering.
- Heqing Sun, Zhongsheng Hou, Lucio Foglia, et Tao Tang. An iterative learning approach for train trajectory tracking control. In *The 18th IFAC World Congress*, pages 1–6, 2011.
- Benee F. Swindel et David R. Bower. Rounding errors in the independent variables in a general linear model. *Technometrics*, Volume : 14, No. 1 :215–218, 1972.
- James Bao-Yen Tsui. *Fundamentals of Global Positioning System receivers : a software approach*. Tata McGraw-Hill, 2007.

- A. Urech, J. Pérez Diestro, et O. González. GADEROS, a Galileo deonstrator for railway operation system. In *Proceedings of World Congress on Railway Research*, 2003.
- G. Vettori, L. Pugi, A. Ridolfi, B. Allotta, et M. Malvezzi. Design and test of a pose estimation algorithm for railway vehicles based on odometers and INS. In *National Congress of Theoretical and Applied Mechanics*, 12-15 Sept. 2011.
- Hofmann-Wellenhof Lichtenegger Wasle. *GNSS-GPS,GLONASS, Galileo and more.* SpringerWienNewYork, 2007.
- Yuheng Zheng. *Integration of satellite positioning and a track database for safety-critical railway control systems.* PHD thesis, University College London, 2008.
- Yuheng Zheng. Improving accuracy and integrity in rail applications through the integration of GNSS with a digital route map. *GRAIL*, pages 1–24, 2007.
- Yuheng Zheng et Paul Cross. Integrated GNSS with different accuracy of track database for safety-critical railway control systems. *GPS Solution*, Volume : 16 :169–179, 2012.
- G. Zhu, L. Fillatre, et I. Nikiforov. Estimation of the train travelled distance, velocity and acceleration by using GPS signals. In *The European Navigation Conference*, 23-26 Apr. 2013.
- G. Zhu, L. Fillatre, et I. Nikiforov. Impact of the railway centerline geometry uncertainties on the train velocity estimation by GPS. In *5th International Conference on Personal Satellite Service*, 27-28 Jun. 2013.
- G. Zhu, L. Fillatre, et I. Nikiforov. Impact of the data uncertainties on the regression model :application to the trajectory-aided surface GNSS navigation. In *XXIVème Colloque Gretsi*, 3-6 Sept. 2013.
- G. Zhu, L. Fillatre, et I. Nikiforov. Improvement of trajectory-aided gnss land navigation : precision and integrity of train positioning. In *7th International Satellite Navigation Forum*, Apr. 2013.
- M.Meyer zu Hörste, K.Lemmer, A.Urech, et M.Jose. The GRAIL project : Galileo localisation for the european train control system. *Galileo 6th Framework Programme*, pages 1–19, 2008.

Guoliang ZHU
Doctorat : Optimisation et Sûreté des Systèmes
Année 2014

La navigation terrestre GNSS assistée par la trajectoire : application au positionnement du train

Au cours des dernières années, la technologie GNSS a beaucoup attiré l'attention et elle a été appliquée à de nombreux domaines. Par ailleurs, les systèmes avancés d'exploitation ferroviaire ont largement été utilisés pour garantir la sécurité, la sûreté et l'efficacité du réseau ferroviaire. L'efficacité de ces systèmes se fonde sur un positionnement fiable du train. L'utilisation de la technologie GNSS pour le positionnement des trains est un domaine de recherche très prometteur. Dans cette thèse, plusieurs algorithmes sont proposés pour le positionnement du train en utilisant des signaux GNSS et un modèle géométrique de la voie ferroviaire stocké dans la base de données à bord du train. Tout d'abord, la distance et la vitesse du train sont estimées en utilisant des signaux GNSS et un modèle géométrique "idéal" qui est composé de lignes droites, d'arcs de cercles et de courbes de transitions entre les deux. L'impact du rayon de courbure de la voie sur ces estimations est étudié. Ensuite, la distance et la vitesse du train sont estimées en utilisant des signaux GNSS et un modèle géométrique "non-idéal" de la voie ferroviaire qui est approchée par une ligne polygonale avec un certain niveau d'incertitude. L'impact du niveau d'incertitude sur ces estimations est étudié. Finalement, la distance et la vitesse du train sont estimées en se basant sur une intégration des mesures GNSS avec une base de données bruitées. L'impact des erreurs de mesures GNSS et de la base de données sur ces estimations est étudié.

Mots clés : transports ferroviaires - GPS - estimation, théorie de l' - analyse de régression - moindres carrés.

**Trajectory-aided GNSS Land Navigation:
Application to Train Positioning**

Over these years, GNSS technology has attracted many attentions around world and it has been widely applied in navigation for airplanes, ground vehicles and boats. On the other hand, advanced railway operating systems have been widely used to guarantee the safety and efficiency of the railway network. The efficiency of these systems is based on the availability of reliable train positioning. Hence, applying GNSS technology to the train positioning is a very promising research area, since it has such important benefits as lower initial costs and lower maintenance. In this thesis, several algorithms are proposed for train positioning by using GNSS signals and the railway centerline stored in the onboard computer database. At first, the train travelled distance, speed are estimated by using GNSS signals and an "ideal" railway centerline which is composed of straight line segments, transition curves and arcs of circles. The impact of the railroad curvature on these estimations is studied. Secondly, the train travelled distance, speed are estimated by using GNSS signals and a "non-ideal" railway centerline which is defined by a polygonal line with some level of uncertainty. The impact of the track geometric model imprecision on these estimations is studied. Finally, the train travelled distance, speed are estimated by integrating the GNSS measurements with a track database. The impact of the GNSS measurements and the track database errors on these estimations is studied.

Keywords: railroads - GPS - estimation theory - regression analysis – least square.

Thèse réalisée en partenariat entre :



Ecole Doctorale "Sciences et Technologies"